

University of Windsor

Scholarship at UWindor

Electronic Theses and Dissertations

Theses, Dissertations, and Major Papers

3-24-2019

Treatment of Aqueous Arylamine Contaminants by Enzyme-Catalyzed Oxidative Polymerization

Debjani Mukherjee
University of Windsor

Follow this and additional works at: <https://scholar.uwindsor.ca/etd>

Recommended Citation

Mukherjee, Debjani, "Treatment of Aqueous Arylamine Contaminants by Enzyme-Catalyzed Oxidative Polymerization" (2019). *Electronic Theses and Dissertations*. 7650.
<https://scholar.uwindsor.ca/etd/7650>

This online database contains the full-text of PhD dissertations and Masters' theses of University of Windsor students from 1954 forward. These documents are made available for personal study and research purposes only, in accordance with the Canadian Copyright Act and the Creative Commons license—CC BY-NC-ND (Attribution, Non-Commercial, No Derivative Works). Under this license, works must always be attributed to the copyright holder (original author), cannot be used for any commercial purposes, and may not be altered. Any other use would require the permission of the copyright holder. Students may inquire about withdrawing their dissertation and/or thesis from this database. For additional inquiries, please contact the repository administrator via email (scholarship@uwindsor.ca) or by telephone at 519-253-3000ext. 3208.

**Treatment of Aqueous Arylamine Contaminants by
Enzyme-Catalyzed Oxidative Polymerization**

By

Debjani Mukherjee

A Dissertation
Submitted to the Faculty of Graduate Studies
through the Department of Civil and Environmental Engineering
in Partial Fulfillment of the Requirements for
the Degree of Doctor of Philosophy
at the University of Windsor

Windsor, Ontario, Canada

2019

© 2019 Debjani Mukherjee

**Treatment of Aqueous Arylamine Contaminants by
Enzyme-Catalyzed Oxidative Polymerization**

by

Debjani Mukherjee

APPROVED BY:

G. Achari, External Examiner
University of Calgary

R. Riahi
Department of Mechanical, Automotive and Materials Engineering

J. K. Bewtra
Department of Civil and Environmental Engineering

R. Seth
Department of Civil and Environmental Engineering

N. Biswas, Co-Advisor
Department of Civil and Environmental Engineering

K. E. Taylor, Co-Advisor
Department of Chemistry and Biochemistry

January 16, 2019

DECLARATION OF ORIGINALITY

I hereby certify that I am the sole author of this thesis and that no part of this thesis has been published or submitted for publication.

I certify that, to the best of my knowledge, my thesis does not infringe upon anyone's copyright nor violate any proprietary rights and that any ideas, techniques, quotations, or any other material from the work of other people included in my thesis, published or otherwise, are fully acknowledged in accordance with the standard referencing practices. Furthermore, to the extent that I have included copyrighted material that surpasses the bounds of fair dealing within the meaning of the Canada Copyright Act, I certify that I have obtained a written permission from the copyright owner(s) to include such material(s) in my thesis and have included copies of such copyright clearances to my appendix.

I declare that this is a true copy of my thesis, including any final revisions, as approved by my thesis committee and the Graduate Studies office, and that this thesis has not been submitted for a higher degree to any other University or Institution.

ABSTRACT

Oxidative polymerization of hazardous aqueous pollutants that are suspected to be human carcinogens by U.S. EPA 2018, including poly-substituted monocyclic anilines (*p*-cresidine and 4-chloro-*o*-toluidine) and atom-bridged bis-anilines (4,4'-oxydianiline, 4,4'-methylenedianiline, 4,4'-thiodianiline and 4,4'-methylenebis(2-chlororaniline)), were catalyzed by a crude form of soybean peroxidase (SBP), isolated from soybean seed hulls, in the presence of hydrogen peroxide. In this work, harmful arylamines present in water were treated and removed for the first time using SBP. Firstly, experiments were conducted to achieve the optimal operating conditions with respect to *pH*, hydrogen peroxide-to-substrate concentration ratio and enzyme activity to achieve $\geq 95\%$ removal of these compounds from water in a 3-hour period monitored by a high-performance liquid chromatography system with ultraviolet detection capability (HPLC-UV). 4-Chloro-*o*-toluidine required the lowest enzyme activity (0.009 U/mL), whereas 4,4'-methylenedianiline required the highest enzyme activity (0.700 U/mL). The reaction time profiles, directly related to the economic consideration of the treatment process, were monitored from which the half-lives and rate constants for removal of the compounds were estimated. Investigation of these kinetic parameters is also expected to play an important role in the design of wastewater treatment plants. Secondly, a kinetic study involving pollutant removal was performed using the Michaelis-Menten model to determine the affinity of the enzyme for the substrates by investigating the Michaelis constant (K_M) and the maximum velocity of the reaction (V_{max}). Thirdly, an investigation was performed on the fate of the analytes by determining the products generated after the enzymatic treatment using mass spectrometry techniques. The results indicated

formation of product oligomers that could be removed in subsequent treatment processes. UV-VIS characteristics were used to confirm the formation of the azo products that were detected using mass spectrometry. And lastly, a *pro-forma* cost analysis for the feasibility of commercializing enzymatic treatment in comparison to other conventional treatment methods was performed. It was estimated that the total cost of enzymatic treatment of these pollutants was nearly 2 to 8 times less than that of the conventional treatment processes. It is recommended that enzymatic treatment could be employed to pretreat the effluent consisting of these toxic chemicals before they are released and/or mixed with wastewater from other industrial sources.

DEDICATION

This dissertation is dedicated to my late grandparents, Kalipada Chatterjee and Mayarani Chatterjee, my parents, Tapes K. Mukherjee and Jharna Mukherjee, my husband, Dr. Sandeep Bhattacharya, my sister, Debika Mukherjee, my parents-in-law, Kishore Bhattacharya and Anuroma Bhattacharya.

Appreciating the blessings by God

ACKNOWLEDGEMENTS

First and foremost, I offer my sincerest gratitude and appreciation to Dr. Niharendu Biswas and Dr. Keith E. Taylor for their support, guidance, continuous motivation and encouragement especially in the most challenging times of this journey. I am grateful to Dr. Jatinder K. Bewtra for his valuable suggestions and recommendations that helped me immensely in this research.

I would like to express my deep appreciation to my committee members, Dr. Rajesh Seth and Dr. Reza Riahi for their time and valuable suggestions. My sincere thanks to Dr. Gopal Achari for being the External Examiner of my committee and providing insightful comments.

I would like to thank Mr. Bill Middleton for his help and guidance with the instrumentation in the laboratory and helping me to learn troubleshooting the issues. I extend my gratitude to Dr. Janeen Auld for her guidance and suggestions with mass spectrometry, to Mr. Joe Lichaa for providing technical support in the laboratory.

I am thankful to the faculty and the staff at the Department of Civil and Environmental Engineering. A special thanks to Dr. Rajan Ray for his help especially during my coursework. Many thanks to the past and present colleagues in my research group and to all my volunteer students for their immense help.

Sincere thanks to the Natural Sciences and Engineering Research Council of Canada (NSERC), Ontario Graduate Scholarship, Sustainable Engineering Faculty Scholarship, and the University of Windsor Doctoral Entrance Scholarship for providing financial support.

My deepest gratitude to my parents, Tapesh K. and Jharna Mukherjee, since this journey would not have been possible without their love and support. Thank you

for believing in me and giving me the motivation to work hard. A special appreciation to my sister Debika Mukherjee, for her love, affection and moral support.

I owe my deepest indebtedness towards my husband, Dr.Sandeep Bhattacharya for his perpetual support and understanding of my goals and aspirations. His patience, love, sacrifice and help during my Ph.D. will be my inspiration throughout my life and without whom this achievement would not have been possible.

My affectionate regards and appreciation goes to my father-in-law, Kishore Bhattacharya, for helping me during my Ph.D. comprehensive preparations and in other aspects of my research, and to my mother-in-law, Anuroma Bhattacharya, for her unconditional love and moral support. I would also like to thank my uncle, Asit Chatterjee, and my late aunt, Chitrita Chatterjee, for loving and encouraging me always. My sincere thanks to my sisters-in-law, Sanjukta and Sudeshna Bhattacharya, brothers-in-law, Sougat Ray and Shaunak Daam for their love and affection.

I feel a deep sense of gratefulness for my late grandparents, Kalipada Chatterjee and Mayarani Chatterjee, who taught me the initial lessons of life that helped to create values in me including honesty, integrity, compassion, and perseverance.

Lastly, my appreciation goes to all my good friends in Canada and India.

TABLE OF CONTENTS

DECLARATION OF ORIGINALITY	iii
ABSTRACT.....	iv
DEDICATION.....	vi
ACKNOWLEDGEMENTS.....	vii
LIST OF TABLES.....	xii
LIST OF FIGURES	xiv
LIST OF APPENDICES.....	xxi
LIST OF ABBREVIATIONS/SYMBOLS.....	xxii
CHAPTER 1. INTRODUCTION	1
1.1. Aromatic Pollutants.....	1
1.1.1. Sources of arylamines.....	1
1.1.2. Arylamines in wastewater and their treatment	3
1.1.3. Enzyme-based water treatment.....	3
1.1.4. Uses of arylamine pollutants	4
1.2. Health Hazards	7
1.3. Environmental Fate of Pollutants.....	9
1.4. Research Objectives	12
1.5. Scope of Research	12
CHAPTER 2. LITERATURE SURVEY.....	14
2.1. Wastewater Treatment Methods.....	14
2.2. Peroxidases.....	15

2.3. Enzymatic Treatment	15
2.4. Peroxidase as an Enzyme	19
2.5. Peroxidase Mechanism.....	20
2.6. Soybean Peroxidase (SBP).....	21
2.6.1. Soybeans production in Canada	21
2.6.2. SBP extraction	21
2.6.3. SBP catalytic properties.....	22
2.6.4. Active site of SBP.....	24
2.7. Enzyme Inactivation.....	24
2.8. Kinetics of Enzyme-catalyzed Reaction	27
2.9. Background to Mass Spectrometry	32
2.9.1. Electrospray ionization (ESI) and atmospheric solids analysis probe (ASAP) mass spectrometry	33
2.9.2. Identification of aromatic amines by mass spectrometry	34
CHAPTER 3. EXPERIMENTAL PROCEDURE.....	36
3.1. Materials.....	36
3.1.1. Enzyme	36
3.1.2. Aromatic compounds.....	36
3.1.3. Reagents.....	36
3.1.4. Buffer and solvents.....	37
3.1.5. Other materials	37
3.2. Analytical Equipment.....	37
3.2.1. UV-VIS spectrophotometry.....	37
3.2.2. High performance liquid chromatography (HPLC).....	38
3.2.3. Electrospray ionization (ESI) and atmospheric solids analysis probe (ASAP) mass spectrometry	38
3.2.4. Total organic carbon (TOC) analysis	39
3.2.5. Centrifuge and <i>pH</i> meter	39
3.2.6. Other equipment	39
3.3. Analytical Methods	40
3.3.1. Colorimetric assay for SBP activity	40
3.3.2. Buffer preparation.....	41
3.3.3. Technical feasibility of substrate/SBP compatibility	41
3.3.4. Substrate/buffers compatibility tests in UV-VIS spectrophotometer	41
3.3.5. HPLC analysis	42

3.3.6. Enzyme stock solution preparation.....	42
3.3.7. Total organic carbon (TOC) analysis	42
3.4. Experimental Protocols	43
3.4.1. SBP-catalyzed polymerization of aromatic substrates	43
3.4.2. Preliminary product determination using mass spectrometry	44
3.4.3. Identification of azo-products using UV-VIS spectrophotometry	44
3.4.4. Kinetics study	44
3.4.5. TOC analysis	45
3.4.6. Sources of error	45
CHAPTER 4: RESULTS AND DISCUSSION.....	47
4.1. Optimization of <i>pH</i>	47
4.2. Optimum Hydrogen Peroxide-to-Substrate Concentration Ratio	54
4.3. Minimum SBP Concentrations Required for Treatment.....	61
4.4. Time Course of Reactions	67
4.5. Kinetics.....	73
4.6. Analyses of Mass Spectrometry (MS) Results.....	81
4.7. Product Identification using UV-VIS.....	123
4.8. TOC Analysis	128
4.9. Cost Analyses of Enzymatic Treatment of the Arylamines	128
4.9.1. General methodology for capital cost estimation	129
4.9.2. Estimation of chemical cost of enzymatic treatment.....	130
4.9.3. General summary of cost analyses	131
CHAPTER 5: GENERAL SUMMARY AND CONCLUSIONS	133
5.1. Summary	133
5.2. Conclusions	137
CHAPTER 6: FUTURE WORK	138
BIBLIOGRAPHY.....	140
APPENDICES	166
VITA AUCTORIS	183

LIST OF TABLES

Table 1.1. Chemical and physical properties of all aromatic pollutants considered in this study (Data obtained from The Pubchem Project website).....	6
Table 2.1. Summary of kinetic parameters from non-linear curve fit of initial rate data to the Michaelis-Menten equation for phenolic substrate using laccase enzyme (Steevensz 2008).....	31
Table 2.2. Summary of kinetic parameters fit to the Michaelis-Menten equation for azo-dyes, Crocein Orange G (COG), Acid Blue 113 (AB113) and Direct Black 38 (DB38), using SBP (Cordova Villegas 2017).....	31
Table 2.3. Aromatic amines studied and their MS/MS transitions (Sutthivaiyakit <i>et al.</i> 2005).....	35
Table 3.1. Summary of the mobile phase solvents, mobile phase ratio, column temperature and the absorbance detector wavelength for the aromatic pollutants.	42
Table 4.1. List of the optimized parameters of the chemicals.....	67
Table 4.2. List of rate constants and half-lives of the compounds as determined from the time course experiments.....	68
Table 4.3. List of the determined values of the Michaelis constant (K_M), the normalized maximum velocity (V_{max}), the catalytic efficiency (V_{max}/K_M) and the normalized V_{max}/K_M values for all compounds.	80
Table 4.4. Summary of mass spectrometry results consisting of m/z ratios, molecular formula, types of compounds/products and their nomenclature.....	123
Table 4.5. Estimated costs (in US\$) for enzymatic treatment of wastewater.	132

Table 4.6. Cost comparison (in US\$) for the treatment of wastewater by three types of treatment. *Estimates are based on conversion of costs as reported by Ibrahim *et al.* (2001) to a present-worth basis using compound interest and an average inflation rate of 3.27% in the USA (Trading Economics 2017) as indicated in the text.....132

LIST OF FIGURES

Figure 2.1. Global soybean production 2017 according to USDA (2018).	21
Figure 2.2. (a) The 3-D structure of SBP (generated by Jmol software from RCSB-Protein Data Base, category no. 1FHF, 2018) and (b) ferriprotoporphyrin IX prosthetic group (adopted from Van Rantwijk and Sheldon, 2000).	24
Figure 2.3. (a) Graphical plot of reaction rate v_o against substrate concentration $[S]$ according to Michaelis-Menten equation. The enzyme concentration is fixed. (b) Lineweaver-Burk plots of $1/v_o$ against $1/[S]$. K_M and V_{max} can be determined directly by the intersection on the x- and y-axis (Jiang 2013).	30
Figure 2.4. (a) Waters XEVO G2-XS Time-of-flight (Tof) mass spectrometer, and (b) a schematic showing the working principle of the spectrometer. Reprinted from Waters (2014).	33
Figure 4.1. Effect of pH on removal of p -cresidine	50
Figure 4.2. Effect of pH on removal of 4-COT.	51
Figure 4.3. Effect of pH on removal of ODA	52
Figure 4.4. Effect of pH on removal of MDA.	52
Figure 4.5. Effect of pH on removal of TDA.....	53
Figure 4.6. Effect of pH on removal of MOCA.....	53
Figure 4.7. Effect of hydrogen peroxide concentration on removal of p -cresidine.	55
Figure 4.8. Effect of hydrogen peroxide concentration on removal of 4-COT.	56
Figure 4.9. Effect of hydrogen peroxide concentration on removal of ODA	57
Figure 4.10. Effect of hydrogen peroxide concentration on removal of MDA.	58
Figure 4.11. Effect of hydrogen peroxide concentration on removal of TDA.....	59

Figure 4.12. Effect of hydrogen peroxide concentration on removal of MOCA...	59
Figure 4.13. SBP optimisation for the removal of <i>p</i> -cresidine	62
Figure 4.14. SBP optimisation for the removal of 4-COT.....	62
Figure 4.15. SBP optimisation for the removal of ODA.	64
Figure 4.16. SBP optimisation for the removal of MDA.....	64
Figure 4.17. SBP optimisation for the removal of TDA.....	65
Figure 4.18. SBP optimisation for the removal of MOCA	66
Figure 4.19. <i>p</i> -Cresidine removal with respect to time.....	69
Figure 4.20. 4-COT removal with respect to time	69
Figure 4.21. ODA removal with respect to time.....	70
Figure 4.22. MDA removal with respect to time	71
Figure 4.23. TDA removal with respect to time	72
Figure 4.24. MOCA removal with respect to time	72
Figure 4.25. Initial velocities for <i>p</i> -cresidine	74
Figure 4.26. Michaelis-Menten plot for <i>p</i> -cresidine	74
Figure 4.27. Initial velocities for 4-COT	75
Figure 4.28. Michaelis-Menten plot for 4-COT.....	75
Figure 4.29. Initial velocities for ODA	76
Figure 4.30. Michaelis-Menten plot for ODA	76
Figure 4.31. Initial velocities for MDA	77
Figure 4.32. Michaelis-Menten plot for MDA.....	77
Figure 4.33. Initial velocities for TDA	78
Figure 4.34. Michaelis-Menten plot for TDA.....	78
Figure 4.35. Initial velocities for MOCA.....	79

Figure 4.36. Michaelis-Menten plot for MOCA	79
Figure 4.37. ESI-MS (+) of <i>p</i> -cresidine standard. Molecular formula $C_8H_{12}NO$ ($m/z = 138.0917$) represents the protonated standard	83
Figure 4.38. ESI-MS (+) of <i>p</i> -cresidine enzymatic reaction precipitate. Molecular formula $C_{16}H_{19}N_2O_2$ ($m/z = 271.1447$ and 271.1442) represents the protonated azo-dimer	84
Figure 4.39. ESI-MS (+) of <i>p</i> -cresidine enzymatic reaction supernatant. Molecular formula $C_8H_{12}NO$ ($m/z = 138.0914$) represents the protonated residual monomer	85
Figure 4.40. ESI-MS (+) of <i>p</i> -cresidine enzymatic reaction precipitate. Molecular formula C_7H_9NO ($m/z = 123.0682$) represents the fragmentation product	86
Figure 4.41. ASAP-MS (+) of 4-COT standard. Molecular formula C_7H_9NCl ($m/z = 142.0418$) represents the protonated standard	88
Figure 4.42. ASAP-MS (+) of 4-COT cationic radical. Molecular formula C_7H_8NCl ($m/z = 141.0345$) represents the cationic radical	89
Figure 4.43. ASAP-MS (+) of 4-COT enzymatic reaction supernatant. Molecular formula $C_{14}H_{13}ClNO$ ($m/z = 246.0687$) represents the dimer ($M_2H-2-NH-Cl+O$)	90
Figure 4.44. ASAP-MS (+) of 4-COT enzymatic reaction supernatant. Molecular formula $C_{21}H_{19}Cl_2N_2O$ ($m/z = 385.0871$) represents the trimer ($M_3H-4-NH-Cl+O$)	91
Figure 4.45. ASAP-MS (+) of 4-COT enzymatic reaction supernatant. Molecular formula C_7H_9NCl ($m/z = 142.0420$) represents the protonated residual monomer	92

Figure 4.46. ESI-MS (+) of ODA standard. Molecular formula $C_{12}H_{13}N_2O$ ($m/z = 138.0917$) represents the protonated ODA standard	95
Figure 4.47. ESI-MS (+) of ODA enzymatic reaction precipitate. Molecular formula $C_{24}H_{21}N_4O_2$ ($m/z = 397.1659$) represents the protonated azo-dimer	96
Figure 4.48. ESI-MS (+) of ODA enzymatic reaction precipitate. Molecular formula $C_{36}H_{31}N_6O_3$ ($m/z = 595.2437$) represents the protonated mono-azo trimer.....	97
Figure 4.49. ESI-MS (+) of ODA enzymatic reaction precipitate. Molecular formula $C_{36}H_{29}N_6O_3$ ($m/z = 593.2279$) represents the protonated bis-azo trimer.....	98
Figure 4.50. ESI-MS (+) of ODA enzymatic reaction precipitate. Molecular formula $C_{48}H_{37}N_8O_4$ ($m/z = 789.2932$ and 789.2935) represents the protonated tris-azo tetramer	99
Figure 4.51. ESI-MS (+) of ODA enzymatic reaction supernatant. Molecular formula $C_{12}H_{13}N_2O$ ($m/z = 201.1028$ and 201.1022) represents the protonated residual monomer.....	100
Figure 4.52. ESI-MS (+) of ODA enzymatic reaction supernatant. Molecular formula $C_{24}H_{21}N_4O_2$ ($m/z = 397.1656$) represents the protonated azo-dimer	101
Figure 4.53. ESI-MS (+) of MDA standard. Molecular formula $C_{13}H_{15}N_2$ ($m/z = 199.1233$) represents the protonated standard	103
Figure 4.54. ESI-MS (+) of MDA enzymatic reaction precipitate. Molecular formula $C_{26}H_{25}N_4$ ($m/z = 393.2068$ and 393.2063) represents the protonated azo-dimer	104
Figure 4.55. ESI-MS (+) of MDA enzymatic reaction precipitate. Molecular formula $C_{39}H_{37}N_6$ ($m/z = 589.3063$) represents the protonated mono-azo trimer	105

Figure 4.56. ESI-MS (+) of MDA enzymatic reaction precipitate. Molecular formula $C_{39}H_{35}N_6$ ($m/z = 587.2911$) represents the protonated bis-azo trimer	106
Figure 4.57. ESI-MS (+) of MDA enzymatic reaction precipitate. Molecular formula $C_{52}H_{47}N_8$ ($m/z = 783.3887$) represents the protonated bis-azo tetramer..	107
Figure 4.58. ESI-MS (+) of MDA (a) enzymatic reaction precipitate. Molecular formula $C_{13}H_{15}N_2$ ($m/z = 199.1236$) represents the protonated residual monomer; and (b) enzymatic reaction supernatant. Molecular formula $C_{13}H_{15}N_2$ ($m/z = 199.1237$) represents the protonated residual monomer	108
Figure 4.59. ESI-MS (+) of MDA enzymatic reaction supernatant. Molecular formula $C_{26}H_{25}N_4$ ($m/z = 393.2088$) represents the protonated azo-dimer	109
Figure 4.60. ESI-MS (+) of TDA standard. Molecular formula $C_{12}H_{13}N_2S$ ($m/z = 217.0800$), $C_{12}H_{12}N_2S$ ($m/z = 216.0725$) and represents the protonated standard and cationic radical, respectively	111
Figure 4.61. ESI-MS (+) of TDA enzymatic reaction precipitate. Molecular formula $C_{24}H_{21}N_4S_2$ ($m/z = 429.1208$) represents the protonated azo-dimer	112
Figure 4.62. ESI-MS (+) of TDA enzymatic reaction precipitate. Molecular formula $C_{36}H_{31}N_6S_3$ ($m/z = 643.1759$), $C_{36}H_{29}N_6S_3$ ($m/z = 641.1610$) represents the protonated mono-azo and bis-azo trimers, respectively	113
Figure 4.63. ESI-MS (+) of TDA enzymatic reaction precipitate. Molecular formula $C_{48}H_{41}N_8S_4$ ($m/z = 857.2308$ and 857.2322) represents the protonated mono-azo tetramer	114
Figure 4.64. ESI-MS (+) of TDA enzymatic reaction supernatant. Molecular formula $C_{12}H_{13}N_2S$ ($m/z = 217.0797$) represents the protonated residual monomer	115

Figure 4.65. ESI-MS (+) of MOCA standard. Molecular formula $C_{13}H_{13}N_2Cl_2$ ($m/z = 267.0459$) represents the protonated standard	117
Figure 4.66. ESI-MS (+) of MOCA enzymatic reaction precipitate. Molecular formula $C_{26}H_{21}Cl_4N_4$ ($m/z = 529.0501$) represents the protonated azo-dimer.....	118
Figure 4.67. ESI-MS (+) of MOCA enzymatic reaction precipitate. Molecular formula $C_{39}H_{29}Cl_6N_6$ ($m/z = 791.0560$) represents the protonated bis-azo trimer.	119
Figure 4.68. ESI-MS (+) of MOCA enzymatic reaction supernatant. Molecular formula C_7H_7ClNO ($m/z = 156.0214$ and 156.0215) represents a MOCA fragmentation product.....	120
Figure 4.69. ESI-MS (+) of MOCA enzymatic reaction supernatant. Molecular formula $C_{13}H_{13}Cl_2N_2$ ($m/z = 267.0455$) represents the protonated residual monomer	121
Figure 4.70. VIS spectrum of <i>p</i> -cresidine batch reaction supernatant	125
Figure 4.71. UV-VIS spectrum of ODA batch reaction supernatant with (a) broad and (b) narrow ranges	126
Figure 4.72. UV spectrum of MDA batch reactions supernatant.....	127
Figure 4.73. UV-VIS spectrum of TDA batch reaction supernatant	127
Figure 4.74. UV-VIS spectrum of MOCA batch reaction supernatant.....	127
Figure A.1. 0.3 mM <i>p</i> -cresidine, extinction coefficient is $2947\text{ M}^{-1}\text{cm}^{-1}$	166
Figure A.2. 0.1 mM 4-COT, extinction coefficient is $1667\text{ M}^{-1}\text{cm}^{-1}$	166
Figure A.3. 0.1 mM ODA, extinction coefficient is $3383\text{ M}^{-1}\text{cm}^{-1}$	167
Figure A.4. 0.1 mM MDA, extinction coefficient is $2775\text{ M}^{-1}\text{cm}^{-1}$	167
Figure A.5. 0.01 mM TDA, extinction coefficient is $22658\text{ M}^{-1}\text{cm}^{-1}$	168

Figure A.6. 0.03 mM MOCA, extinction coefficient is $3875 \text{ M}^{-1}\text{cm}^{-1}$	168
Figure C.1. <i>p</i> -Cresidine standard curve at 287 nm	171
Figure C.2. 4-COT standard curve in <i>pH</i> 2.6 at 290 nm.....	172
Figure C.3. 4-COT standard curve in <i>pH</i> 3.0 at 290 nm.....	172
Figure C.4. 4-COT standard curve in <i>pH</i> 4.0 at 290 nm.....	173
Figure C.5. 4-COT standard curve in <i>pH</i> 5.0 at 290 nm.....	173
Figure C.6. 4-COT standard curve in <i>pH</i> 7.0 at 290 nm.....	174
Figure C.7. ODA standard curve in <i>pH</i> 2.6 at 271 nm	174
Figure C.8. ODA standard curve in <i>pH</i> 4.0 at 271 nm	175
Figure C.9. ODA standard curve in <i>pH</i> 7.0 at 293 nm	175
Figure C.10. ODA standard curve in <i>pH</i> 9.2 at 293 nm.	176
Figure C.11. MDA standard curve in <i>pH</i> 2.6 at 260 nm.....	176
Figure C.12. MDA standard curve in <i>pH</i> 3.0 at 260 nm.....	177
Figure C.13. MDA standard curve in <i>pH</i> 4.0 at 285 nm.....	177
Figure C.14. MDA standard curve in <i>pH</i> 5.0 at 285 nm.....	178
Figure C.15. MDA standard curve in <i>pH</i> 7.0 at 285 nm.....	178
Figure C.16. TDA standard curve in <i>pH</i> 3.0 at 253 nm.....	179
Figure C.17. TDA standard curve in <i>pH</i> 7.0 at 260 nm.....	179
Figure C.18. MOCA standard curve in <i>pH</i> 2.6 at 291 nm.....	180
Figure C.19. MOCA standard curve in <i>pH</i> 3.0 at 291 nm.....	180
Figure C.20. MOCA standard curve in <i>pH</i> 7.0 at 291 nm.....	181

LIST OF APPENDICES

Appendix A: Maximum Wavelength Absorbance Curves in UV-VIS.....	166
Appendix B: Colorimetric Assay for SBP Activity.....	169
Appendix C: HPLC Calibration Curves	171
Appendix D: Preparation of SBP and Catalase Stock Solutions	182

LIST OF ABBREVIATIONS/SYMBOLS

Abbreviations

4-AAP	4-Amino-antipyrine
4-COT	4-Chloro- <i>o</i> -toluidine
ACN	Acetonitrile
ARP	<i>Arthromyces ramosus</i> peroxidase
ASAP	Atmospheric solids analysis probe
EPA	Environmental Protection Agency
ESI	Electrospray ionization
HPLC	High-performance liquid chromatography
HRP	Horseradish peroxidase
M-M	Michaelis-Menten
MDA	4,4'-Methylenedianiline
MOCA	4,4'-Methylenebis(2-chlororanoline)
MS	Mass spectrometry
ODA	4,4'-Oxydianiline
<i>p</i> -Cresidine	<i>para</i> -Cresidine
SBP	Soybean peroxidase
TDA	4,4'-Thiodianiline
TOC	Total organic carbon
TRI	Toxic Release Inventory
UV-VIS	Ultraviolet-Visible

Symbols

Arg38	Arginine
H ₂ O ₂	Hydrogen peroxide
His42	Histidine
<i>k</i>	First-order rate constant
<i>k</i> _{cat}	Turnover number
K _M	Michaelis constant
m/z	Mass-to-charge ratio
<i>p</i> K _a	-log ₁₀ (K _a), where K _a = Acid dissociation constant
<i>t</i> _{0.5}	Half-life
V _{max}	Maximum velocity
V _{max} /K _M	Catalytic efficiency
λ _{max}	Maximum wavelength

CHAPTER 1. INTRODUCTION

1.1. Aromatic Pollutants

1.1.1. Sources of arylamines

Aromatic amines, or arylamines, consist of one or more benzene or other aromatic rings (carbocyclic or heterocyclic) with at least one amino group (primary, secondary, or tertiary) directly attached to the aromatic ring (Chung and Gadupudi 2010; Ćirić-Marjanović *et al.* 2017). They vary from parent aniline to highly complex molecules with conjugated aromatic or heterocyclic structures and multiple substituents. The main sources of these amines in the environment are from chemical industry such as oil refining, synthetic polymers, dyes, adhesives, rubbers, pharmaceuticals, pesticides and explosives (Pinheiro *et al.* 2004; Pollution inventory 2003). Non-industrial sources, which warrant investigation, due to their role in cancer development in humans, include hair dyes, automobile exhaust fumes, burning/pyrolysis of protein-rich vegetable matter and the cooking and subsequent consumption of meats (Pinheiro *et al.* 2004; Snyderwine *et al.* 2002). Aromatic amines also enter the aqueous environment as precursors from the synthesis of these compounds, via azo-dye and nitroaromatic compound reductions (Lizier and Zanoni 2012; Akyüz and Ata 2008; Lloret *et al.* 2002), diesel exhaust, combustion of wood chips and rubber, tobacco smoke and grilled meats and fish and have been identified as potential carcinogens (Possanzini and Palo 1990). Since they have been designated as high priority pollutants, their presence in the environment must be at concentration levels lower than 30 mg/L compatible with the limits allowed by regulations (Lizier and Zanoni 2012).

Arylamines can also be generated by reduction of nitrated polycyclic aromatic hydrocarbons (nitro-PAHs) by anaerobic bacteria of the human intestine (Rafii *et al.* 1991;

Fu *et al.* 1990; Richardson *et al.* 1998). Nitro-PAHs have been detected in carbon toners, urban air particulates, diesel fuel emissions, used motor oils, barbecued food, and tea leaves (Ohnishi *et al.* 1985; Rosenkranz *et al.* 1980; Rosenkranz *et al.* 1983; Tokiwa *et al.* 1987). Dinitrotoluene (DNT) can also act as a source of arylamines. DNT can be reduced by microorganisms to aromatic amines, which contaminate the groundwater. Stayner *et al.* (1993) reported that there was excess hepatobiliary cancer mortality among munition workers exposed to DNT. Numerous other arylamines can be generated endogenously, as the end products or intermediates of normal metabolism. However, under certain conditions, endogenous arylamines could accumulate in high concentrations through abnormal metabolism. For example, intake of excessive tryptophan-containing diet or deficiency of vitamin B6 (Chung and Gadupudi 2010; Rose *et al.* 1972; Bertazzo *et al.* 2001; Birt *et al.* 1987; Sidransky *et al.* 1997). Some of the tryptophan metabolites have been reported to be involved in cancer (Chung and Gadupudi 2010).

Most aromatic amines are toxic, and many are classified as carcinogenic or probable human carcinogens as per the toxic release inventory (TRI) list of the United States Environmental Protection Agency (2018). As early as the late 19th century, aromatic amine exposure was viewed as a concern in the dye manufacturing industry (Karim and Husain, 2009). They have been shown to biodegrade, however this process seems to be more complicated than the reduction of the azo linkage. In certain cases, specific microbial strains or co-cultures may be required (Pinheiro *et al.* 2004). Thus, a problem of bioaccumulation may arise, posing a further risk to aquatic life (Suzuki *et al.* 2001). Under certain situations, these aromatic amines can become mutagenic in mammals (Spadaro *et al.* 1992). Azo-dye linkages can possibly breakdown to aromatic amines during their use or disposal and thus are considered to be a health hazard (Pinheiro *et al.* 2004).

1.1.2. Arylamines in wastewater and their treatment

Arylamines, having high solubility in water, can easily enter through the soil and also into the water cycle in various forms, in the form of chemical effluents or via the breakdown products of herbicides. Their occurrence in ground waters or soil samples subjected to industrial, agricultural or urban pollution is a matter of concern. Therefore, it is important to monitor these amines in water in order to protect human health and environmental safety. There are conventional treatment processes for the removal of aromatic amines from industrial wastewaters that includes extraction, adsorption onto activated carbon, chemical oxidation, advanced oxidation, electrochemical techniques and irradiation. These methods suffer from problems like high costs, formation of hazardous by-products and low efficiency (Franciscon *et al.* 2010; Mondal *et al.* 2010). On the other hand, biological methods are more economic, energy efficient and environment-friendly (Rieger *et al.* 2002). However, they too have drawbacks like autoxidation once they are exposed to oxygen. Biodegradation with microorganisms, which requires the least energy input and generates minimal secondary pollution, emerges to be a promising process compared to others. Also, the microbial environment requires more sophisticated maintenance to sustain high removal efficiency and the biodegradation rate is influenced by the compound toxicity and resistance to breakdown. Therefore, it is more suitable for utilizing the same as a secondary treatment and is not optimal for rapid removal.

1.1.3. Enzyme-based water treatment

Enzyme-based water treatments provide a better defined system with simpler process control. The advantages of this kind of method over physical/chemical treatments are their ability to operate under less corrosive conditions, and removal of even trace level organic compounds that are not removed by conventional physical/chemical processes. It

operates with much lower consumption of oxidants as well as lower amounts of adsorbent material for disposal (Nicell 1991; Nicell *et al.* 1993). The enzymatic treatment method has several benefits over other treatment methods as a result of the specificity of the enzyme for the target pollutant, efficiency in removal of the pollutant, lower cost, ease of handling and storage. Another benefit of enzymatic treatment over conventional biological treatment is the ability of the enzyme to remove high concentrations of toxic compounds (Mousa Al-Ansari *et al.* 2011). In this way, enzymatic treatment created a new prospect for treating hazardous aromatic compounds.

1.1.4. Uses of arylamine pollutants

The arylamine pollutants considered in this study are listed in Table 1.1 along with their chemical and physical properties. *p*-Cresidine is used exclusively as a synthetic chemical intermediate to produce azo-dyes and pigments, such as FD&C Red no. 40 and C.I. Direct Black 17, Direct Blue 67, Direct Blue 126, Direct Green 26, Direct Orange 34, Direct Orange 83, Direct Red 79, Direct Violet 51, Direct Yellow 41, Disperse Black 2, Direct Orange 72, and Direct Violet 9 (Lloret *et al.* 2002, ROC for *p*-cresidine, Ed.14).

It has been reported that another mono-cyclic arylamine 4-chloro-*o*-toluidine (4-COT) and its hydrochloride salt have been used commercially to produce azo-dyes for cotton, silk, acetate, and nylon and as an intermediate in the production of Pigment Red 7 and Pigment Yellow 49. As an azoic diazo component, *p*-chloro-*o*-toluidine is used in the synthesis of some azoic dyes (IARC 1990, 2000a, 2000b; NCI 1979). 4-COT has also been identified in field samples of plant materials treated with chlordimeform, for e.g. young bean leaves at concentrations of less than 0.1-0.2 mg/L, in grape stems and berries at 0.02-0.05 ppm, and in prunes and apples at less than 0.04 ppm (HSDB 4-COT 2018). Occurrence was found in rice grains at 3-61 ppb in straw parts 42 days after the last of three treatments

with chlordimeform. Detectable traces were also found as a metabolic product of cotton plants, cargo rice and husks, cucumbers, and apples after treatment with chlordimeform (Chung and Gadupudi 2010).

4,4'-Oxydianiline (ODA), an atom-bridged bis-aniline, is considered as an environmentally hazardous degradation product of azo dyes (Ekici *et al.* 2001; Sánchez *et al.* 2014). ODA is also used in the production of polyimide and poly(ester)imide resins that are, in turn, used in the manufacture of temperature-resistant products such as wire enamels, coatings, film, adhesives, etc. It is also released in waste streams of the textile industry (Ekici *et al.* 2001).

Another atom-bridged bis-aniline, 4,4'-methylenedianiline (MDA) is primarily used to produce 4,4'-methylenedianiline diisocyanate and other polymeric isocyanates which are used to manufacture polyurethane foams (US EPA 1984; Merc Index 1989; ASTDR 1998). MDA is also used as a curing agent for epoxy resins and urethane elastomers, as a corrosion preventative for iron, as an antioxidant for lubricating oils, as a rubber processing chemical, as an intermediate in the manufacture of elastomeric fibers (e.g., Spandex), and in the preparation of azo-dyes (US EPA MDA 1984; Merc Index 1989; US EPA MDA Hazard summary 2016).

4,4'-thiodianiline (TDA) was used as a chemical intermediate in the production of three dyes: CI Mordant Yellow 16, Milling Red G, and Milling Red FR (OEHHA TDA 2018).

In contrast, 4,4'-methylenebis(2-chlororaniline) (MOCA) is used as a curing agent for liquid polyurethane elastomers. These elastomers have been used to produce shoe soles; rolls for postage stamp machines; cutting bars in plywood manufacturing; rolls and belt

drives in cameras, computers, and reproducing equipment; and pulleys for escalators and elevators (US EPA MOCA Hazard summary 2000; ATSDR 2009).

Table 1.1. Chemical and physical properties of all aromatic pollutants considered in this study (Data obtained from The Pubchem Project website).

Compound	4-Chloro-o-toluidine	4,4'-Oxydianiline	4,4'-Methylene dianiline	4,4'-Thiodianiline	4,4'-Methylenebis (2-chloroaniline)
Molecular structure					
Abbreviation used in thesis	<i>p</i> -Cresidine	ODA	MDA	TDA	MOCA
Molecular formula	C ₈ H ₁₁ NO	C ₁₂ H ₁₂ N ₂ O	C ₁₃ H ₁₄ N ₂	C ₁₂ H ₁₂ N ₂ S	C ₁₃ H ₁₂ Cl ₂ N ₂
Molecular Weight (g/mol)	137.182	200.241	198.269	216.302	267.153
Appearance	White to silver-gray odorless crystals	Colorless crystals	Colourless-to-pale-yellow flakes	Needles or brown powder	Tan-colored pellets or flakes
Density (g/cm³)	1.0 (20°C)	1.315 (20 °C)	1.070 (103 °C)	1.26	1.44
Melting point (°C)	51.5	189	92.5	108.5	110
Boiling Point (°C)	235	>300	398	464.8	202-214 (0.3 mm Hg, L)
Log K_{ow}	1.74	1.36	1.59	2.18	3.91
Water solubility (mg/mL)	2.81 (25°C)	> 0.1 at 15 °C	1 (25 °C)	310 (25 °C)	<1 (25 °C)
Vapor Pressure (mm Hg at 25°C)	2.52 × 10 ⁻²	2.5 × 10 ⁻⁶	2.03 × 10 ⁻⁷	1.1 × 10 ⁻⁵	3.9 × 10 ⁻⁶
pK_a (Sánchez et.al. 2014)	4.7	5.5	5.3	4.6	3.3
Henry's Constant (atm.m³/mole)	1.2 × 10 ⁻⁷	1.5 × 10 ⁻¹¹	5.30 × 10 ⁻¹¹	3.9 × 10 ⁻¹²	1.1 × 10 ⁻¹¹

1.2. Health Hazards

The poly-substituted monocyclic anilines and atom-bridged bis-anilines under investigation are classified in the US EPA TRI list of 2017 (US EPA 2017). *p*-Cresidine is classified under category, Group 2A, which is probably carcinogenic to humans, and 4-COT, ODA, MDA, TDA, are classified as 2B pollutants, that means they are possibly carcinogenic to humans. The compound MOCA is carcinogenic to humans and falls under the category of Group 1.

It is necessary to scrutinize *p*-cresidine as inhalation, ingestion or dermal contact of the same by human cause cancer. Due to the enhanced reactivity of the aromatic amine group, *p*-cresidine is also known to bind with the organic matter in soil, sediment, or suspended solids. It has been reported that around 5,897 kg (13,000 lb) of *p*-cresidine was released which mostly went to the air in 1988 as reported by Toxic Release Inventory and then in 2000 more than 5,443 kg (12,000 lb) of *p*-cresidine was released to an off-site waste broker. Thereafter, no data for *p*-cresidine release was reported between 2002 and 2004. After 2004, approximately 118 kg (260 lb) of *p*-cresidine was reported to have been released to surface water (TOXNET®).

Exposure to 4-COT could occur to workers involved in the manufacture of pesticide chlordimeform that contains 4-COT (IARC 1990). It is usually present in water from such workplaces because of the hydrolysis of chlordimeform of the intermediate N-formyl-4-chloro-*o*-toluidine. The microbial degradation of chlordimeform to 4-chloro-*o*-toluidine in soils by a number of bacterial species has been reported (Chung and Gadupudi 2010). Toxic effects from 4-COT could arise from inhalation, whose symptoms include macro or microscopic haematuria, dysuria and reduced bladder capacity. Also, acute or short-term

intoxication has been observed in workers in the chemical industry involved in the production and use of 4-COT (IARC 2000a).

For ODA, it is reported that 6,651 kg (14,663 lb) of the same was discharged to the environment in 2002, of which around 6,350 kg (14,000 lb) was released to an on-site landfill. Later, the amount of release was, however, decreased to 1,228 kg (2,708 lb) in 2007, of which 975 kg (2,149 lb) was released to landfills, 157 kg (346 lb) to the air and the remaining 97 kg (214 lb) was released to surface water (ROC for ODA, Ed. 14). The EU legislation prohibits the use of certain azo-dyes which form such arylamines upon reduction in the environment at concentrations above a threshold limit, which is 30 mg/kg (0.003 % by wt.) (Sánchez *et al.* 2014). Symptoms of acute ODA intoxication observed in animal studies include lowered body temperature, flaccid skeletal muscles, dyspnoea, cyanosis and lethargy. ODA also seems to directly affect the thyroid (MAK list 1987).

MDA is another harmful compound which causes liver damage in humans and animals upon acute (short-term) oral and dermal exposure (US EPA MDA 2000). It causes irritation to human skin and eyes. It has been seen that continuous exposure to the dihydrochloride salt of MDA in the drinking water of rats and mice statistically increases the probability of liver and thyroid tumors (US EPA MDA 2000). MDA is responsible for occurrence of a disease termed “Epping Jaundice”, which has symptoms including tender liver, general physical weakness, abdominal pain, nausea, vomiting, headache, fever, chills, and muscle pain in humans. The International Agency for Research on Cancer (IARC) has classified MDA as a Group 2B-type human carcinogen (US EPA MDA 2000).

Exposure to TDA causes respiratory tract irritation. It may lead to methemoglobinemia that causes dizziness, headache and weakness. It can also cause shortness of breath, causing collapse and even death (NCIt 2018). TDA induces reverse mutation when

tested for *Salmonella typhimurium* strains (IARC 1982). It showed adequate evidence of carcinogenicity in animals. It has been tested and shown to be carcinogenic in both rats and mice (Hasegawa *et al.* 1991).

Chronic oral exposure to MOCA has been reported to have a prominent role in the formation of tumors in the liver, lung, urinary bladder, kidney and mammary glands in animals. Hence EPA has also classified MOCA as a Group B2-type human carcinogen (US EPA MOCA 2000). Occupational exposure may occur in workers who work in factories that manufacture MOCA or use it to produce plastic products (ASTDR 1994). Short-term exposure to MOCA has also shown to cause gastrointestinal distress, transitory kidney damage, and burning face and eyes in humans (US EPA MOCA 2000).

1.3. Environmental Fate of Pollutants

Aromatic pollutants can have detrimental effects on humans as well as short and long-term effects on the environment that are irreversible.

Exposure summary of *p*-cresidine: *p*-Cresidine is known to be released to the environment by means of various waste streams during its production and use in dye industries. It has a vapor pressure of approximately 2.5×10^{-2} mm Hg at 25°C (HSDB *p*-cresidine 2018) if released in air. The high value of vapor pressure suggest that it will remain exclusively as a vapor in the ambient atmosphere. The estimated half-life reaction in air is 2 hours. It is degraded by photochemical reaction to generate hydroxyl radicals in the vapor phase. *p*-Cresidine has high mobility when released in soil as evident from the value of K_{oc} (organic carbon partition coefficient) which is 53. Aromatic amines are known to bind strongly to humus or organic matter in suspended solids and sediments due to the high reactivity of the aromatic amino group. Volatilization from moist soil surfaces would occur at a very low rate based on the compound's Henry's Law constant of 1.2×10^{-7} atm.m³/mole. When

released to water it binds strongly to humus and organic matter. The volatilization half-life assessed for a model river and lake were 23 and 169 days, respectively (HSDB *p*-cresidine 2018).

Exposure summary of 4-COT: 4-COT is known to be produced in the environment through the microbial/chemical degradation and photo-decomposition of various pesticides. Sunlight-induced degradation of the chemical in its vapor-phase causes generation of hydroxyl radicals with half-life of approximately 9 hours. It may also be subjected to photolysis at the soil surface (HSDB 4-COT 2018). Due to its K_{oc} value of 410, 4-COT has moderate mobility in soil (Lyman *et al.* 1990; HSDB 4-COT 2018). Experimental investigations revealed that almost 50% of this compound could bind very strongly to soil medium and the binding was attributed to interactions between the aromatic amine and humic/organic materials in the soil (Bollag 1978; Adrian *et al.* 1989). When released in water, volatilization of 4-COT is expected to be slow based on its Henry's Law constant of 2×10^{-6} atm.m³/mole, whereas sorption of this compound to the organic material in water is an important parameter (Bollag 1978; Adrian *et al.* 1989). Biodegradation of 4-COT in a soil system is expected to happen with 20% mineralization of the chemical over a time period of 6 weeks and is considered as the major fate of this compound in soil. 4-COT present in a petrochemical industrial process wastewater at an initial concentration of 110 mg/L with activated sludge as an inoculum and a one-day acclimation period have been shown to provide almost 16% removal by measuring COD (Mn) and 7% removal of TOC after a 24-hour period under aerobic conditions (Matsui *et al.* 1988).

Exposure summary of ODA: ODA is expected to have moderate-to-low mobility in soil depending on its composition. Considering its Henry's Law constant of 1.5×10^{-11} atm.m³/mole (calculated by means of a fragment constant estimation method), volatilization of

ODA from moist soil surfaces is not expected to be an important fate process (Meylan and Howard 1991). It is anticipated to be adsorbed to suspended solids and sediments because of its K_{oc} (= 450). With a vapor pressure of 2.5×10^{-6} mm Hg at 25°C, ODA may exist both in vapor and particulate phase in the ambient atmosphere (HSDB ODA 2018). Based on the value of $\log K_{ow}$ (n-octanol/water partition coefficient) of 1.36 (BioByte 1995) and also from a regression-derived equation (Meylan *et al.* 1999), it can be suggested that the possibility for ODA's bioconcentration in aquatic organisms is low (HSDB ODA 2018).

Exposure summary of MDA: MDA's mobility in the soil is almost negligible due to the value of K_{oc} ranging from 3825 to 5681 (Cowen *et al.* 1998) and it gets adsorbed to suspended solids and sediments. Its Henry's Law constant of 5.30×10^{-11} atm.m³/mole indicates that volatilization of MDA from moist soil surfaces may not be an important fate (Amini and Lowenkron 2005; Moore 1978). MDA can exist in both vapor and particulate phases in ambient conditions. Aromatic amines are known to react rapidly with photochemically produced hydroxyl radicals and peroxy radicals in sunlit natural water (Mill and Mabey 1985). Aromatic amines have been observed to undergo rapid and reversible covalent bonding with humic materials in aqueous solution. Here, the initial bonding is followed by a slower and nearly irreversible reaction thought to indicate the addition of the amine to quinoidal structures, which is followed by oxidation of the product resulting in an amino-substituted quinone. These processes represent pathways by which aromatic amines may be converted to latent forms in the biosphere (Parris 1980). In the vapor phase, MDA is degraded by photochemical reactions to generate hydroxyl radicals.

Exposure summary of TDA: TDA is adsorbed in suspended solids and sediment since the K_{oc} value of 2100 suggests that it has only slight mobility in soil. Volatilization from water surfaces is not expected (Lyman *et al.* 1990) based on the measured Henry's Law constant

of 3.9×10^{-12} atm.m³/mole calculated using a fragment constant estimation method (Meylan and Howard 1991). Like MDA, TDA is also degraded by photochemical reaction to generate hydroxyl radicals in the vapor phase. It also exists in both the vapor and particulate phases in ambient conditions. It is suggested that the particulate phase of TDA may be removed from the air by wet or dry deposition (HSDB TDA 2018).

Exposure summary of MOCA: Similar to MDA and TDA, MOCA is also expected to be adsorbed to suspended solids and sediment due to its K_{oc} value of 5700. Volatilization from water surfaces is not expected based upon its Henry's Law constant value of 1.1×10^{-11} atm.m³/mole, as calculated using a fragment constant estimation method (Meylan and Howard 1991). It has been suggested that MOCA's bioconcentration in aquatic organisms is high. Similar to aniline, the photodegradation of MOCA may be photosensitized by the presence of humic acids (Zepp *et al.* 1981) and algae (Suzuki *et al.* 1983).

1.4. Research Objectives

- Optimize the enzyme-catalyzed conversion of selected arylamines present in water.
- Perform reaction kinetics to determine SBP requirements for removal of the substrates.
- Conduct preliminary identification of the polymeric products by mass spectrometry techniques and further confirmation by UV-Visible (UV-VIS) spectrophotometry.
- Perform a *pro-forma* cost analysis for enzymatic treatment of the substrates.

1.5. Scope of Research

Part I: Optimization for Conversion of Substrates:

1. Determine the technical feasibility of using crude SBP to catalyze the removal of harmful pollutants: *p*-cresidine, 4-COT, ODA, MDA, TDA, and MOCA, from water through polymerization followed by chemical flocculation/precipitation.

2. Establish the optimal operating conditions to achieve at least 95% conversion of the substrate in a 3-hour reaction time.
3. Monitor the time course of substrate consumption by H_2O_2 and derive the apparent first-order rate constants and half-lives.

Part II: Reaction Kinetics:

Deduce a structure-function relationship for the foregoing relative SBP requirements for removal of the toxic substrates from the Michaelis-Menten model.

Part III: Preliminary Product Identification:

Apply mass spectrometry (MS) by electrospray ionization (ESI) and atmospheric solids analysis probe (ASAP) techniques to identify the soluble/insoluble polymeric products formed and characterization of the polymeric products in terms of their structure, and then further confirmation by UV-VIS spectrophotometry.

Part IV: Cost Analysis:

Perform a *pro-forma* cost analysis for the feasibility of commercializing enzymatic treatment in comparison to other conventional treatment methods.

CHAPTER 2. LITERATURE SURVEY

2.1. Wastewater Treatment Methods

The increasing concern for the environment has prompted implementation of innovative and sustainable methods for removing aromatic amines from wastewater. Current treatment methods are divided into three categories: chemical, physical, and biological. Physical and chemical methods include activated carbon, ozone oxidation, Fenton oxidation, photocatalytic oxidation, electrochemical oxidation, wet air oxidation and incineration (Gu *et al.* 2008; Singh *et al.* 2008). However, all these methods have some limitations such as: high costs (Chhabra *et al.* 2015), low efficiency (May *et al.* 2018), harsh reaction conditions, high energy demand (Oller *et al.* 2011), not applicable to concentrations > 300 mg/L (Wu *et al.* 1993; Steevensz *et al.* 2014), and/or formation of hazardous by-products (Oller *et al.* 2011). Incineration is appropriate for effluents with TOC > 100 g/L but is energy intensive and not very “green” (Suarez-Ojeda *et al.* 2008). Chemical oxidation is the most widely used treatment; however, it is dependent on the oxidant, amine structure and reaction conditions. In certain cases, the by-products of oxidation include quinoneimines, nitroso- and nitro-compounds, polymeric substances and azo-compounds (Saunders *et al.* 1964; Casero *et al.* 1997). Activated carbon and other adsorption techniques are very expensive (Busca *et al.* 2008; Laszlo 2005). Current biological treatment methods include activated sludge, bio-oxidation lagoons, aerated lagoons, oxidation ditch and rotating biological contactors (Wang *et al.* 2009). The use of different micro-organisms in biological treatment when treating wastewaters containing aromatic amines can lead to more specific conversions and hence results in complete mineralization (Pereira *et al.* 2015). However, the disadvantages to this include the high cost of microbes, which are normally substrate-specific, requiring additional alternate

carbon sources, and suffering from metabolic inhibition (Husain *et al.* 2009). Also, microorganisms require sufficient nutrients, oxygen and stable environmental conditions, including *pH*, salt content and temperature, in order to maintain optimum efficiency. Further, high-strength waste can kill the microorganisms due to shock-loading effect. Overall, biological methods are costly, require high energy and long reaction time (Klibanov *et al.* 1980; Nicell 1993; Mousa Al-Ansari *et al.* 2011).

2.2. Peroxidases

Peroxidases belong to the oxidoreductase class of enzymes. They are widely distributed in nature, abundant in microbial and plant sources but not so much in mammalian cells. The oligomerization of phenoxy radicals generated in the presence of peroxidases was characterized during 1940s, and later the mechanism was rationalized; further oxidation of this product to trimers and oligomers was also observed (Westerfeld, and Lowe 1942; Danner *et al.* 1973; Klibanov *et al.* 1980). They catalyze the oxidation of a wide range of substrates in the presence of hydrogen peroxide (Dunford and Stillman, 1976). Peroxidases are used in many industries and processes ranging from indicators in the food industry, protein engineering, recombinant protein expression and as catalysts for the removal of aromatics from wastewater (Flock *et al.* 1999; Ryan *et al.* 2006; Regalado *et al.* 2004). Their wide use is due to their high redox potential, and structural properties giving them relatively high thermal stability and wide distribution (Demarche *et al.* 2012; Regalado *et al.* 2004). Aromatic compounds, which are a major class of pollutants, can be removed by polymerization using peroxidases (Dunford and Stillman, 1976).

2.3. Enzymatic Treatment

An enzyme-based treatment method to remove organic compounds from aqueous wastewater was proposed by Klibanov *et al.* (1980). The proposed treatment method

employed the enzyme peroxidase from horseradish in the presence of hydrogen peroxide catalyzing the oxidation of over 30 different phenols and aromatic amines. During the same period, Bollag and co-workers started investigating the enzyme laccase catalyzing the oxidation of phenols by oxygen (Bollag *et al.* 1979; Bollag *et al.* 1988).

Peroxidases catalyze the oxidization of phenols and anilines to form aromatic radicals and these radicals diffuse from the active site of the enzyme into the solution, where coupling takes place non-enzymatically to form dimers, and with further enzymatic cycles, forms oligomers. A point is reached in the cyclic process where the polymer reaches its solubility limit and it precipitates out of the solution, which can be subsequently removed by filtration or sedimentation (Ćirić-Marjanović *et al.* 2017; Steevensz *et al.* 2014). The potential of other enzymes, *Coprinus cinereus* peroxidase (CCP), *Coprinus macrorhizus* peroxidase (CMP), *Arthromyces ramosus* peroxidase (ARP) and soybean peroxidase (SBP) have been investigated earlier (Patapas *et al.* 2007; Steevensz *et al.* 2008; Al-Kassim *et al.* 1993 and 1994; Caza *et al.* 1999; Ibrahim *et al.* 2001; Mantha *et al.* 2002; Ikehata *et al.* 2003).

The most investigated peroxidase is the horseradish peroxidase (HRP) (Dunford, 2016). However, it has been shown that HRP has a short catalytic lifetime due to enzyme inhibition and reaction temperature. It is active mainly between 5-55°C and is rapidly inactivated at temperatures above 65°C, and also is inhibited at low pH (Caza *et al.* 1999; Flock *et al.* 1999; Yu *et al.* 1994). The main disadvantage in the use of HRP is the high cost for extracting and purifying, limiting its availability in large quantities at a price that would be feasible for wastewater treatment (Bassi *et al.* 2004; Mousa Al-Ansari *et al.* 2009). These disadvantages paved the way for looking at other peroxidases such as soybean peroxidase (SBP).

Another oxidoreductase classes of enzymes that were studied were laccase and tyrosinase. They were investigated because of their ability to oxidize phenols and aromatic amines, analogous to peroxidases. Laccases are glycosylated multicopper oxidases found in most plants and fungi of which fungal laccases are more reactive than plant laccases. Laccases require molecular oxygen for their catalytic cycle in which four one-electron oxidations of aromatic substrates occur along with the irreversible four-electron reduction of molecular oxygen to water. The exact mechanism is not clear, but it is believed to follow a modified ping-pong mechanism (Mousa Al-Ansari 2008). Laccase was found to be an efficient peroxidase in removal of phenols and aromatic amines. However, they are less resistant to inactivation (Modaressi *et al.* 2005; Bollag *et al.* 1979; Bollag *et al.* 1988). Also, one downside of laccases is that they are slower than peroxidases and higher in cost. Tyrosinase is also a glycosylated multicopper oxidase found in most plants, bacteria and fungi. It follows a different mechanism for aromatic substrate oxidation. They catalyze the hydroxylation of various monophenols to the *o*-diphenols by the oxygenated form of the enzyme; the diphenols then can be oxidized to *o*-quinones. The quinones are highly reactive and nonenzymatically couple to intermediate products that slowly polymerize to form insoluble polyphenolic compounds (Dec *et al.* 1995; Wada *et al.* 1995; Ikehata *et al.* 2000).

SBP is considered to be a better alternative for enzymatic treatment than HRP for several reasons: (i) SBP has been shown to have decreased susceptibility to inactivation by its co-substrate H₂O₂ compared to other peroxidases used for wastewater treatment, such as HRP (Wright and Nicell, 1999) and *Arthromyces ramosus* peroxidase (ARP) (Patapas *et al.* 2007), resulting in more robust activity; (ii) SBP has high catalytic activity over a wide range of pH (Patapas *et al.* 2007; Caza *et al.* 1999; Kamal and Behere 2002; Wright

and Nicell 1999) and it has been shown to be a more effective peroxidase estimated by its specificity constant (k_{cat}/K_M) (Steevensz *et al.* 2014); (iii) SBP remains functional to catalyze oxidative reactions at relatively high temperatures (as high as 70°C) compared to other peroxidases (McEldoon and Dordick, 1996); and (iv) a crude SBP extract has been found to be more efficient than its corresponding purified form (Flock *et al.* 1999). These properties, along with SBP's potential low cost and widespread availability as a by-product of soybean processing, makes it suitable for wastewater treatment.

Increasingly, stringent environmental laws demand development and implementation of innovative, environmentally-friendly wastewater treatment methods to complement or replace existing technologies. There have been few recent modifications in the physico-chemical and biological processes that are presently used. The characteristics of these processes include: high costs (Robinson *et al.* 2001; Chhabra *et al.* 2015), low efficiency, harsh reaction conditions, high-energy demand (Oller *et al.* 2011), applicability only to low concentrations (Steevensz *et al.* 2014; Cordova Villegas *et al.* 2016) and/or formation of hazardous by-products (Oller *et al.* 2011). These reasons have prompted further investigation for alternative methods that are cheaper, faster and easier to maintain. One of the extensively demonstrated alternative methods, enzymatic treatment, combines aspects of both physico-chemical and biological processes since it uses the chemical reaction of a biological catalyst (Steevensz *et al.* 2014). The process is attractive due to its ease and simplicity of control, short contact time, applicability to many bio-refractory compounds, better tolerance to shock loading, reduction in sludge quantity and its effectiveness over broad pH, temperature and salinity ranges (Mousa Al-Ansari *et al.* 2009; Cordova Villegas *et al.* 2016).

2.4. Peroxidase as an Enzyme

Enzymes are biological catalysts, which increase chemical reaction rates that take place in living cells. They are proteins that are composed of polymers of amino acids arranged in a specific sequence and linked by peptide bonds. Enzymes are tightly regulated, highly specific and act under mild conditions of pressure, temperature and *pH*. The active site of an enzyme limits specificity to only one type of chemical group and the type of reaction. The substrate that binds to the enzyme interacts in a stereo-specific manner (fit) with high affinity. Also, the substrate must react either by forming or breaking bonds. The enzyme has an active site which consists of the catalytic site and the binding site. The catalytic site is where the reaction occurs, whereas the binding site is the area that holds the substrate in a proper conformation (Fersht 1977). Normally, an enzyme uses weak noncovalent interactions to hold the substrate in place.

Peroxidases were one of the first enzymes discovered in the 19th century and have been found in plants, animals, bacteria and fungi. They have been classified into three super families: plant, animal and catalase peroxidases. The classification was based on the amino acid sequence, three-dimensional structure and biological function (Dunford 2016).

The plant peroxidase superfamily was further subdivided into three families based on their sequence homologies. Class I peroxidases consist of prokaryotic origin such as yeast cytochrome *c*, chloroplast and ascorbate peroxidase. They have no calcium ions, cystine bridges, carbohydrate and no signal peptide for secretion. Class II peroxidases are secreted fungal peroxidases such as lignin, manganese and ARP. They have two calcium ions, cystine bridges (four conserved) and a signal peptide for secretion. Class III peroxidases consists of classical secretory plant enzymes such as horseradish, peanut and

soybean peroxidases. They have two calcium ions, cystine bridges (different location than class II), extra helices and a signal peptide for secretion (Everse *et al.* 1991).

On the other hand, the animal peroxidase superfamily is larger than plant peroxidase one with major differences in primary and tertiary structure. The animal peroxidases are similar to plant peroxidases in the helices that make up the heme (iron protoporphyrin IX molecule) binding pocket. Examples of animal peroxidases are lactoperoxidase, myeloperoxidase, and eosinophil peroxidase (Dunford 2016).

The catalase peroxidase superfamily has been classified as one of the peroxidase subfamilies as a result of catalases' ability to act as a peroxidase and the ability of Classes II and III plant peroxidases to act as catalases. Catalases scavenge hydrogen peroxide, converting it to water and oxygen via a two-step enzymatic cycle. Catalases have similar heme groups to that of peroxidase, but the catalases have different structure and primary sequence than those of animal and plant peroxidases (Dunford 1999 and 2016).

2.5. Peroxidase Mechanism

The peroxidase reaction cycle is a modified bi-bi ping-pong mechanism. The native form of the enzyme (E_N) reduces hydrogen peroxide to water and is converted to Compound I (E_1), an active form of the enzyme (Equation 1). Compound I is capable of oxidizing a reducing substrate (AH) such as phenols and arylamines by one electron, generating a free radical ($A\cdot$) and is converted to Compound II (E_2) of the enzyme (Equation 2). The Compound II is capable of oxidizing another reducing substrate, generating another free radical and returning the enzyme to its native form (Equation 3) (Dunford 1999).





2.6. Soybean Peroxidase (SBP)

2.6.1. Soybeans production in Canada

Global soybean production in 2017 was around 300 MT (Fig. 2.1). According to Agriculture and Agri-Food Canada, annual soybean exports are valued to over USD 1 billion. In recent times, annual production has been increasing steadily. Based on Statistics Canada's report in 2014, over 6 million tons of soybean were harvested, which was a 12.9% increase since 2013. In the same time period, land for soya production had increased to 5.5 million hectares. 80% of soybeans produced in Canada are grown in Ontario and Manitoba, and almost 50-70% of the total production is exported, either raw or processed, to the U.S, Japan, Europe, Southeast Asia, and the Middle East, collectively, according to Soy Canada (2018).

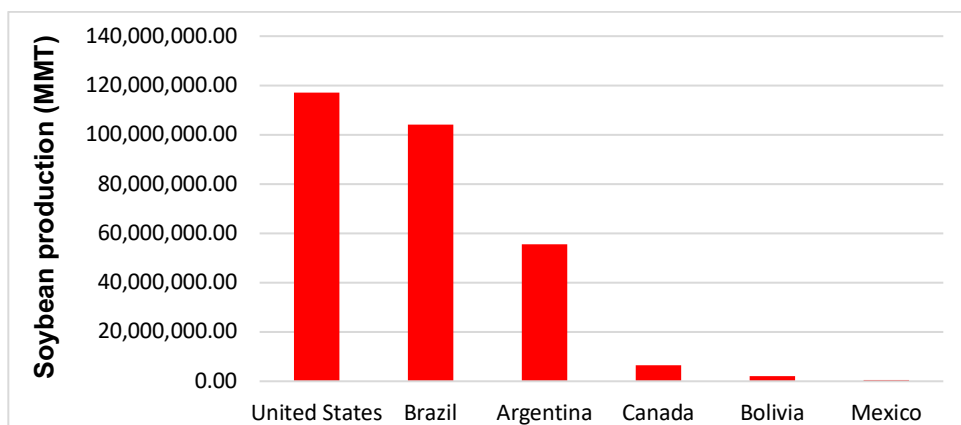


Figure 2.1. Global soybean production 2017 according to USDA (2018).

2.6.2. SBP extraction

The soybean seed coats (hulls) are a by-product from crushing operations that are used as animal feed. The dry soybean seed is soaked in water for (1-2 hours) till the seed coat/hull becomes softer and crumpled. After washing these hulls with water, SBP can be

extracted without compromising the feed value of the hulls. The activity of the SBP varies among the cultivars and seed coats (Steevensz *et al.* 2013; Buzzell and Buttery, 1968; Buzzell and Buttery, 1969; Gijzen *et al.* 1993; Gijzen 1997).

2.6.3. SBP catalytic properties

Soybean seed coat peroxidase (oxidoreductase), a member of Class III plant peroxidase superfamily, is a 37 kD glycoprotein, which can be found in the seed coat of soybeans (Henriksen *et al.* 2001). The seed coats of soybean are considered as waste products, their hulls provide an inexpensive and abundant source of enzyme that could be commercially used in wastewater treatment (Nicell 2003; Hailu *et al.* 2010). Even though HRP, extracted from horseradish root, has been the most widely studied peroxidase, SBP shows 57% amino acid sequence homology with HRP and has been receiving attention recently even in its crude form (Bassi *et al.* 2004; Henriksen *et al.* 2001; McEldoon and Dordick 1996). The strong heme-apo-protein interaction suggests an increased hydrophobic and ionic interaction at the heme-cavity of SBP that stabilizes its native state, which could be the major contributor to the conformational, thermal and kinetic stabilities being substantially higher than those of HRP (Kamal and Behere 2008). The optimal catalytic activity of SBP in a standard activity test with phenol and 4-AAP is at pH 7.4; more than 90% of the activity retained in the range of pH 5.7 to 7.0 (Wright and Nicell 1999). The high thermal stability allows SBP to retain its activity even at 70°C and after 12 hours of incubation. SBP also has a melting point of 90.5°C that is much higher than other peroxidases like HRP (81.5°C) and *Coprinus cinereus* peroxidase (CiP; 65°C) due to the changes in its secondary structure. SBP shows no change in the secondary structure at temperatures below 70°C (McEldoon and Dordick 1996). The k_{cat} (turnover number, see section 2.7) and catalytic efficiency values for SBP are much higher than HRP-C at two

different *pH* values, which suggests that SBP has a better catalytic performance. The k_{cat} value of SBP shows a bell-shaped curve over *pH* 3-10 and the maximum k_{cat} has been reported at *pH* between 5.0-5.5 for substrate 2,2'-azinobis-(3-ethylbenzthiazoline-6-sulphonic acid) (Kamal and Behere 2003).

Experiments were done to find the activity of SBP in the presence of different organic solvents like acetone, ethanol, methanol, and acetonitrile (Geng *et al.* 2001). It was observed that the enzyme exhibited its maximum activity in aqueous ethanol (16.67% w/v) followed by acetone, methanol and acetonitrile. The use of organic co-solvent is beneficial over aqueous phase alone as it renders the enzyme's ability to act against a variety of organic pollutants, which are highly soluble in and hydro-organic solvent mixtures. It has also been observed that mixture of benzene/acetone served as a good solvent system. The normalised activity of SBP was about 65% as observed by Geng *et al.* (2001) where the mixture of benzene/acetone used was 16.67% (w/v).

The catalytic and conformational stability of a peroxidase depends on numerous structural features in the active site of the enzyme such as the accessibility of the heme active site to hydrogen peroxide and reducing substrates, amino acid environment around the heme, electron transfer rate in the heme cavity, hydrogen bonding network in the active site, and the coordination and spin-state of the heme iron (Dunford 1999 and 2016; Filizola and Loew 2000; Henriksen *et al.* 2001; Kamal and Behere 2002 and 2003). However, these structural features in the active site of the enzyme can be affected by several environmental factors such as *pH*, temperature, solvent, etc. (Henriksen *et al.* 2001; Kamal and Behere 2002 and 2003; Geng *et al.* 2001). Also, the stability of SBP at low *pH* enables catalysis of halogenation reactions. It catalyzes the efficient bromination of veratryl alcohol and several other organic substrates under acidic conditions (Munir and Dordick 2000). The

use of SBP as a halogenation catalyst provides an environmentally friendly method for replacing the harsh bleach conditions used in chemical halogenations (Munir and Dordick 2000).

2.6.4. Active site of SBP

SBP has a molecular mass of 40660 Da, contains 17.7-18.2% carbohydrate; the secondary structure of the enzyme consists of 13 α -helices and 2 β -sheets (Henriksen *et al.* 2001; Welinder and Larsen 2004; Ryan *et al.* 2006). The active site of peroxidase bears an iron protoporphyrin IX molecule, also known as heme. The iron protoporphyrin IX molecule consists of four co-planar pyrrole rings joined by methane bridges (carbon atoms labeled α , β , γ and δ) with iron (III) complexed in the center. It carries eight side chains, four methyl groups, two vinyl groups and two propionate groups (Fig. 2.2) (Mousa Al-Ansari *et al.* 2011; Henriksen *et al.* 2001; Dunford 1999).

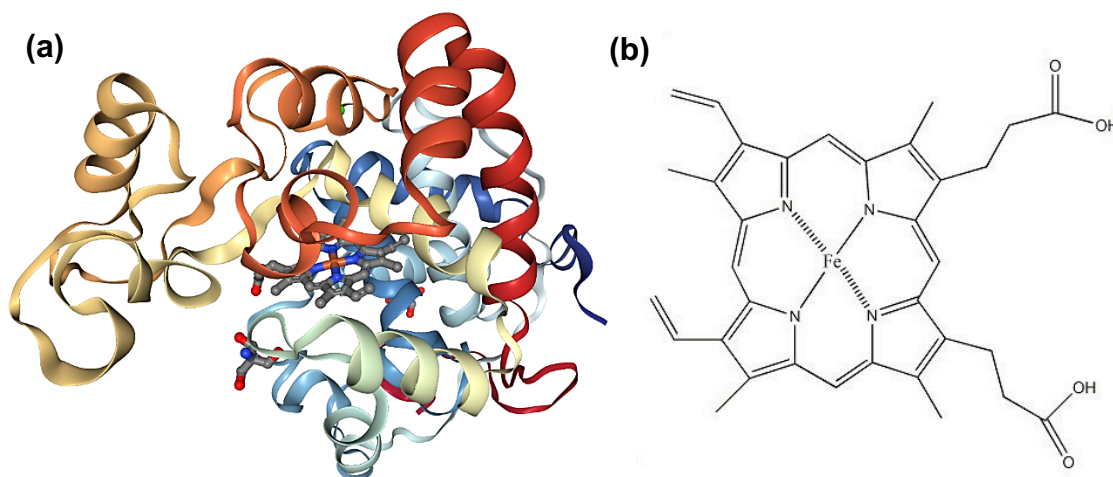
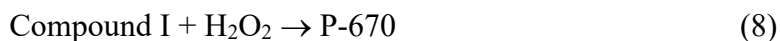
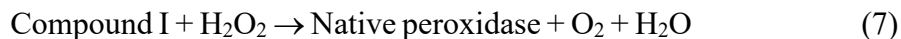


Figure 2.2. (a) The 3-D structure of SBP (generated by Jmol software from RCSB-Protein Data Base, category no. 1FHF, 2018) and (b) ferriprotoporphyrin IX prosthetic group (adopted from Van Rantwijk and Sheldon, 2000).

2.7. Enzyme Inactivation

Peroxidase inactivation is a downside in enzyme application (Mousa Al-Ansari *et al.* 2011). There are three likely pathways by which the enzyme is deactivated. First,

permanent inactivation can be by the generation of free radicals during the catalytic process. The free radicals can return to the active site of the enzyme and form a covalent bond that prevents further substrate molecules from accessing the active site due to proximity (Ortiz de Montellano *et al.* 1988). Second, inactivation can be by the end-product polymers formed during the catalytic process (Nakamoto and Machida 1992). It has been proposed that the polymeric product particles can adsorb the enzyme and co-precipitate it, resulting in a lower concentration of soluble enzyme. However, Feng *et al.* (2013) reported that this phenomenon, with phenol as substrate, is not inactivation, but immobilization in a form with lower specific activity. Third, inactivation can be by the excess hydrogen peroxide (Arnao *et al.* 1990; Baynton *et al.* 1994; Dunford, 1999). Thus, in the presence of excess hydrogen peroxide and absence of reducing substrate, or when reducing substrate concentrations are low, Compound II is oxidized to Compound III which is catalytically inactive, but its formation does not represent a terminal inactivation since it can slowly decompose back to the native form of the enzyme (Equations 4 and 5).



By means of a one-electron reduction, Compound III can also be reduced to Compound I. In this way a radical is generated from which Compound I can be oxidized back to the native enzyme, or, to the terminally inactive verdohemoprotein referred to as P-670 through a series of reactions (due to the shift in absorbance from 405 nm to 670 nm) (equations 4-8) (Arnao *et al.* 1990; Baynton *et al.* 1994; Dunford 1999).

There have been different efforts made to prevent peroxidase inactivation and increase the catalytic life. Different additives have been investigated for this purpose such as polyethylene glycol (PEG), gelatin and certain polyelectrolytes (Nakamoto and Machida 1992; Wu *et al.* 1997). Most of the additives studied were found to be effective in reducing peroxide inactivation, while the use of PEG was found to be better than other additives in terms of the practical additive dose range (PADR). There was no negative effect on the efficiency of the removal reaction, the additive easily separated from solution as co-precipitate with the enzymatic products formed, it was nontoxic and more competitive than others in terms of cost (Nakamoto and Machida 1992; Wu 1996; Wu *et al.* 1997; Harris 1992; Kinsley *et al.* 2000). The effectiveness of PEG in the protection of enzyme has been observed on various peroxidases such as HRP, ARP SBP and other enzymes such as laccase. PEG protection efficiency varies depending on the concentration and average molecular mass of PEG. The PEG act as a sacrificial polymer (Wu *et al.* 1998), thereby, prevents the free radical generated during the catalytic process from covalently binding to the active side or it prevents the adsorption of the enzyme into the polymeric products (Nakamoto and Machida 1992). There were other attempts to prevent peroxidase inactivation by hydrogen peroxide. It has been suggested that inactivation of peroxidases by excess hydrogen peroxide can be reduced by a step-feeding of hydrogen peroxide rather than single feed (Wu *et al.* 1994; Ibrahim *et al.* 2001) to keep the radical concentration low and reduce the possibility of SBP inactivation by excess hydrogen peroxide and/or radicals thus improving removal efficiency. Overcoming peroxidase inactivation can solve one of the main problems in the enzymatic treatment (Ibrahim *et al.* 2001).

Previous studies have also shown that use of additives can even reduce the amount of enzyme needed in the treatment (Mazloun *et al.* 2016). Different additives have been

used such as polyethylene glycol (PEG) or surfactants such as Triton X-100, Tween 20, sodium dodecyl sulfate (SDS) and NP-40 (Mazloun *et al.* 2016). It was first proposed by Nakamoto and Machida (1992) that with purified HRP, a 200-fold reduction of required peroxidase concentration can be achieved in the presence of PEG to suppress the adsorption of HRP by phenolic reaction end-product (Steevensz *et al.* 2012). Also, addition of PEG is known to enhance *Arthromyces ramosus* peroxidase treatment of phenol and laccase treatment of bisphenol-A. Other additives mentioned above were also effective during enzymatic treatment (Mazloun *et al.* 2016). However, it is noted that an additive could increase the carbon footprint of the process. Additive usage can be reduced or even avoided, by enhancing precipitate recycling in consecutive batch reactions, for removal of phenol. For example, the optimum SBP concentration for 1 mM phenol removal can be reduced by 2.4-fold due to precipitate recycling. Here, with no additive, the active enzyme that is absorbed by the precipitate during the reaction, and it has no secondary contribution of organic carbon compared to the processes where additives are used (Steevensz *et al.* 2014; Feng *et al.* 2013).

2.8. Kinetics of Enzyme-catalyzed Reaction

Enzyme kinetics is the branch of enzymology which deals with the factors that affect the rates of enzyme-catalyzed reactions (Jiang 2013). The first general rate equation for reactions involving enzymes was proposed by Henri in 1903 (Henri 1903) Based on Henri's experimental work, Michaelis and Menten presented the best known Michaelis-Menten (M-M) model of enzyme kinetics in 1913 (Michaelis and Menten 1913). It defines the rate of enzyme-catalyzed reactions by relating the reaction rate to the concentration of the substrate. The simple form of the reaction involves one substrate and one enzyme featuring one catalytic site. In this process the enzyme (E) and substrate (S) associate to

form an enzyme-substrate complex (ES), which can then subsequently dissociate back to the substrate and enzyme again or rearrange and form the product (P) of the reaction and release enzyme again. When the initial rate of reaction is measured the equilibrium is assumed to be not disturbed by product formation.



The rate constants for the individual steps are depicted with k_1 , k_{-1} and k_2 which are used for the definition of Michaelis constant, K_M :

$$K_M = \frac{k_{-1} + k_2}{k_1} \quad (10)$$

Assuming that the enzyme-substrate complex is in rapid equilibrium with the reactants, enzyme and substrate, which means that the equilibrium takes place on a much faster time-scale than the product is formed, the M-M equation is obtained as follows:

$$v_o = \frac{v_{max}[S]}{K_M + [S]} \quad (11)$$

In this equation, the initial reaction rate v_o correlates to the substrate concentration $[S]$ and the maximum rate of the reaction is V_{max} where (Cornish-Bowden 1976):

$$V_{max} = k_2 [E] \quad (12)$$

Quasi-steady state approximation or pseudo-steady state, an alternative approach examined by Briggs and Haldane (1925), where they assumed that concentration of ES does not change with time during product formation. Mathematically it can be written as,

$$k_f [E][S] = k_r [ES] + k_{cat}[ES] \quad (13)$$

According to enzyme conservation law:

$$[E] = [E]_o - [ES] \quad (14)$$

(13) and (14) gives:

$$(k_r + k_{cat})[ES] = k_f [S]([E]_o - [ES]) = k_f [S][E]_o - k_f [S][ES] \quad (15)$$

$$[ES] = \frac{k_f [S][E]_o}{(k_r + k_{cat}) + k_f [S]} = \frac{[S][E]_o}{\left(\frac{k_r + k_{cat}}{k_f}\right) + [S]} = \frac{[S][E]_o}{K_M + [S]} \quad (16)$$

where, $K_M = \frac{k_r + k_{cat}}{k_f}$ is known as the Michaelis constant, k_r , k_{cat} , and k_f being the constants for substrate unbinding, conversion to product, and binding to the enzyme, respectively. Hence the velocity v of the reaction is:

$$v = \frac{d[P]}{dt} = k_{cat}[ES] = \frac{V_{max}[S]}{K_M + [S]} \quad (17)$$

where, $V_{max} = k_{cat}[E]_o$

The plot of the reaction rate and the substrate concentration in the enzyme-catalyzed reaction defines a hyperbolic curve as shown in Fig.2.3 (a). The K_M value is obtained from the graph as seen in left of figure when the substrate concentration is the half of V_{max} . The same parameters can also be obtained from Lineweaver-Burk equation (Equation 18):

$$\frac{1}{v_o} = \left(\frac{K_M}{V_{max}}\right) \left(\frac{1}{[S]} + \frac{1}{V_{max}}\right) \quad (18)$$

This can be obtained as well by linearizing the M-M equation, by taking the reciprocal of both sides of the equation. The parameters V_{max} and K_M can be determined directly from this representation by checking the intercept on the y axis and the slope of the plot, shown in Fig.2.3 (b).

V_{max} is the maximum rate of enzyme activity and usually has the unit of mM/s, whereas, K_M has the unit of mM and is defined as the concentration of substrate at which the rate (V_o) is a half of V_{max} (Ranaldi *et al.* 1999). Other parameters that are widely used

to compare enzymes are the turnover number, k_{cat} , and catalytic efficiency or specificity constants, which combines both aspects, recognition (binding) and reactivity (catalysis).

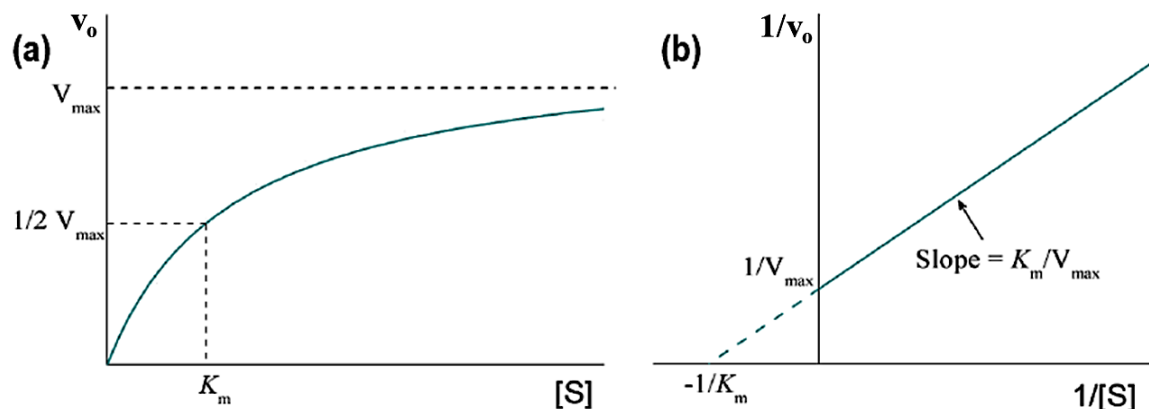


Figure 2.3. (a) Graphical plot of reaction rate v_o against substrate concentration $[S]$ according to Michaelis-Menten equation. The enzyme concentration is fixed. (b) Lineweaver-Burk plots of $1/v_o$ against $1/[S]$. K_M and V_{max} can be determined directly by the intersection on the x- and y-axis (Jiang 2013).

The reciprocal of k_{cat} can be defined as the time needed to convert one molecule of substrate into product by one enzyme. Catalytic efficiency, also known as specificity constant, is the measure of efficiency of an enzyme to convert its substrates. Catalytic efficiency is an important way for measuring the efficiency of an enzyme in converting two or more substrates (Sutiono 2016). Catalytic efficiency, however, not to be used for comparing two enzymes acting on the same substrates (Eisenthal *et al.* 2007). Even though many enzymes obey the M-M model, however some enzymes show a deviation. There are many factors for this deviation. The M-M model is based on the assumption that the amount of substrate used is very large compared to the amount of enzyme. Another assumption of this model is that the initial rate of enzyme is the initial rate where substrate and product inhibition have yet to occur. However, some enzymes may be inhibited by their substrates or products. Substrate and product inhibition of enzymes is important, and a common mechanism by which cells control their metabolism (Nelson and Cox 2008). Inhibition in general can be classified into two types, reversible and irreversible inhibition.

Previous studies with laccase have been done where kinetic parameters K_M and V_{max} have been determined for conditions with and without PEG. Table 2.1 shows a list of kinetic parameters from non-linear curve fits of initial-rate data to the M-M equation for phenolic substrates using laccase (Steevensz 2008). Since laccase is a multi-substrate enzyme, focus has been on the removal of reducing substrate which has been documented as being the rate-determining step in catalysis. It has been proven that PEG helps in extending the catalytic lifespan of enzyme. If the increased conversion is only due to extended lifespan of enzyme then it is expected that the initial velocities, before significant inactivation has occurred and should produce almost identical apparent kinetic parameters. But if there is an increase in oxidation rate in combined to extended catalytic life span of enzyme then varying apparent kinetic parameter is expected to be seen (Steevensz 2008). Similar studies for removal of azo-dyes with SBP have also been performed and kinetic parameters K_M and V_{max} for a M-M model that were obtained are listed in Table 2.2 (Cordova Villegas 2017).

Table 2.1. Summary of kinetic parameters from non-linear curve fit of initial rate data to the Michaelis-Menten equation for phenolic substrate using laccase enzyme (Steevensz 2008).

Kinetic parameters	<i>o</i> -Cresol		<i>m</i> -Cresol	<i>p</i> -Cresol	
	No PEG	PEG	No PEG	No PEG	PEG
K_M (mM)	1.144±0.111	2.294±0.042	201.702 ± 34.570	2.258 ± 0.153	1.582 ±0.088
V_{max} (mM/min)	0.074±0.003	0.135±0.014	0.688 ± 0.08	0.054 ± 0.002	0.045 ± 0.001
V_{max}/K_M (/min)	0.065	0.059	0.003	0.024	0.028

Table 2.2. Summary of kinetic parameters fit to the Michaelis-Menten equation for azo-dyes, Crocein Orange G (COG), Acid Blue 113 (AB113) and Direct Black 38 (DB38), using SBP (Cordova Villegas 2017).

Kinetic parameters	Azo-dyes		
	COG	AB113	DB38
K_M (μM)	4.7 ± 0.45	21 ± 2.8	36 ± 4.3
V_{max} (μm/s)	0.014 ± 0.00045	0.11 ± 0.00550	0.19 ± 0.0090
V_{max}/K_M (/s)	0.0030 ± 0.0003	0.0053 ± 0.00074	0.0053 ± 0.00067

2.9. Background to Mass Spectrometry

Mass spectrometry (MS) is an analytical technique that was used for the first time by Sir J.J. Thomson in 1912 (Griffiths 1997). The first study on the electrospray process was conducted by Zeleny in 1917 who observed the electrohydrodynamic pulsation of a charged liquid surface. Dole *et al.* (1968) used electrospray ionization to determine the molecular weight of a dilute polymer solution. That was the first article where electrospray ionization was used for mass analysis. Yamashita and Fenn (1984) for the first time coupled an electrospray source to a mass spectrometer. Aleksandrov *et al.* (1985) investigated inorganic ions by ESI-MS. This showed that ESI-MS is a useful tool in the fields of inorganic and organometallic chemistry. Figure 2.4. (a) shows a Waters XEVO G2-XS Time-of-flight (ToF) mass spectrometer, and the schematic of the working principle of the spectrometer is shown in Fig.2.4 (b). The instrument comprises of an ion source, a mass analyzer and a detector. As the name suggests, ions are generated in the ion source. The ions are separated by their mass-to-charge ratio (m/z) in the analyzer, and the ions are detected in the detector by their m/z and abundance.

Atmospheric solids analysis probe (ASAP) mass spectrometry is considered as a direct analysis and ambient ionization technique (McEwen *et al.* 2005; Smith *et al.* 2012) of MS and is promising for the analysis of polymers that exhibit poor electrospray ionization (ESI) efficiency (McEwen *et al.* 2005; Barrère *et al.* 2012). It is suitable for analyzing volatile and semi-volatile chemical compounds in both solid and liquid forms. ASAP analysis has helped to overcome the solubility issues of many compounds used for MS which is a very common problem when dealing with synthetic polymers. The main instrumentation parameter includes an ion source and when the desolvation temperature is

set at 60°C, it is capable of vaporizing the heavier polymers for ionization (Smith *et al.* 2012).

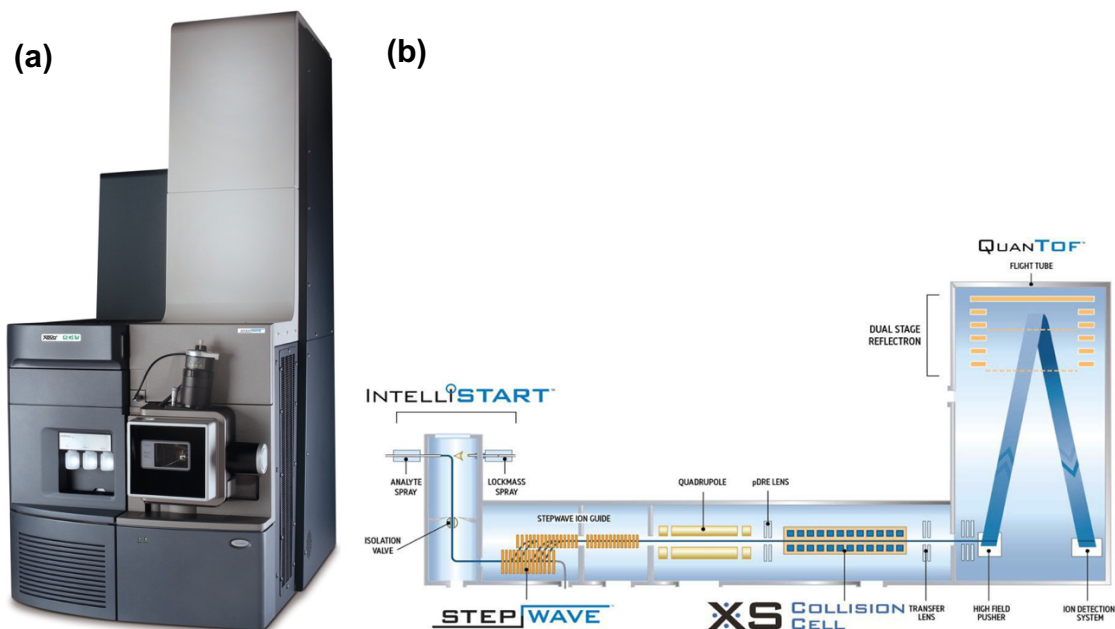


Figure 2.4. (a) Waters XEVO G2-XS Time-of-flight (ToF) mass spectrometer, and (b) a schematic showing the working principle of the spectrometer. Reprinted from Waters (2014).

2.9.1. Electrospray ionization (ESI) and atmospheric solids analysis probe (ASAP) mass spectrometry

In ESI technique, a high voltage is applied to a capillary through which a solution of the analyte is pumped. Highly charged mist droplets are sprayed from the tip of the capillary and the small droplets evaporate. The evaporation process is supported by heating and a nebulizing gas, generally nitrogen, is used to assist this. The gas-phase ions then enter the mass spectrometer for separation and detection based on their mass-to-charge ratios (m/z) (Mann and Wilm 1995). ESI is known as “soft ionization” technique because only a small amount of internal energy is imparted to the analyte (Mann and Wilm 1995; Cole 2000). The availability of the ESI technique has largely proliferated the application of mass spectrometry in research areas such as water quality, proteomics, biomarker discovery, drug discovery, combinatorial chemistry, pharmacokinetics, drug metabolism, clinical

drug testing, forensics, the analysis of food/herbal nutrients/toxins, food contamination, and the study of petrofuel/biofuel compositions (Smyth *et al.* 2004; Zuehlke *et al.* 2007; Smyth *et al.* 2007; Eide *et al.* 2007; Su 2008).

The ASAP technique provides quick and simple way for the analysis of a range of low molecular weight pharmaceutical compounds which had suffered a great challenge when analyzed by ESI due to the signal suppression by the solvents (Petucci and Diffendal 2008). ASAP is useful in detecting of compounds with molecular weight as high as 2000 Da (McEwen *et al.* 2005).

2.9.2. Identification of aromatic amines by mass spectrometry

Sutthivaiyakit *et al.* 2005 studied different aromatic amines after they were cleaved from the azo dyes by high-performance liquid chromatography/tandem mass spectrometry with atmospheric-pressure chemical ionization. A liquid chromatography (LC)-MS/MS method was developed for aromatic amines that were separated by HPLC followed by tandem mass spectrometry. Tandem mass spectrometry, also known as MS/MS, is a method involving at least two stages of mass analysis either in conjunction with a dissociation process, or with a chemical reaction that causes a change in the mass or charge of an ion (Cooks *et al.* 1973; McLafferty 1983; McLuckey 1988). Ionization was obtained in the positive ion mode, by atmospheric-pressure chemical ionization and the identification was done by using two typical daughter ions of the molecular ion, respectively. The precursor ions of aromatic amines mostly the $[M+H]^+$ ion were identified from 50 up to 100 amu above their respective molecular weights. The MS/MS transitions of a few of the aromatic compounds studied are summarized in Table 2.3. The MH^+ of 201, 217 and 142 were detected for ODA, TDA and 4-COT, respectively (Sutthivaiyakit *et al.* 2005).

Another investigation of primary aromatic amines (PAA) in mainstream water pipe smoke using liquid chromatography-electrospray ionization tandem mass spectrometry was done by Schubert *et al.* in 2011. An HPLC system coupled with an API 4000 Q TRAP mass spectrometer was used for quantification of precursor and product ions. The Precursor ions of each PAA identified were of type $[M+H]^+$. A few of the PAA studied were ODA, 4-COT and *p*-cresidine, benzidine, aniline, *para*-anisidine, etc.

Table 2.3. Aromatic amines studied and their MS/MS transitions (Sutthivaiyakit *et al.* 2005).

Chemical name	MS/MS Transition
ODA	$201([M+H]^+) \rightarrow 108([M+H-C_6H_7N]^+)$
MDA	$199([M+H]^+) \rightarrow 182([M+H-NH_3]^+)$
<i>p</i> -Cresidine	$138([M+H]^+) \rightarrow 123([M+H-CH_3]^+)$
TDA	$217([M+H]^+) \rightarrow 200([M+H-NH_3]^+)$
MOCA	$267([M+H]^+) \rightarrow 231([M+H-Cl]^+)$

CHAPTER 3. EXPERIMENTAL PROCEDURE

3.1. Materials

3.1.1. Enzyme

Crude dry solid SBP (E.C. 1.11.1.7, Industrial Grade lot #18541NX, $RZ = 0.75 \pm 0.10$, activity ≈ 5 U/mg) was obtained from Organic Technologies (Coshocton, OH). Dry solid bovine liver catalase (E.C. 1.11.1.6, lot #120H7060, activity $\approx 19,900$ U/mg) was purchased from Sigma Aldrich Chemical Company Inc. (Oakville, ON). Both the enzymes were stored at -15°C , although the aqueous stock solutions prepared were stored at 4°C .

3.1.2. Aromatic compounds

p-Cresidine (99% pure), 4,4'-oxydianiline (ODA) (97% pure) and 4-chloro-*o*-toluidine (4-COT) (98% pure) were purchased from Sigma-Aldrich Chemical Company (Oakville, ON). The other compounds: 4,4'-thiodianiline (TDA) purity $>98.0\%$, 4,4'-methylenedianiline (MDA) purity $>98.0\%$, 4,4' methylene-bis (2-chloroaniline) (MOCA) $>90.0\%$ pure were obtained from the Tokyo Chemical Industry (TCI America), (Woodrush Way, Portland). These chemicals were stored at room temperature.

3.1.3. Reagents

4-Amino-antipyrine (AAP) was obtained from BDH Inc. (Toronto, ON), ammonium acetate HPLC-grade was purchased from Fluka Analytical (Oakville, ON) and were also stored at room temperature. Hydrogen peroxide (30% w/v) was purchased from ACP Chemicals Inc. (Montreal, QC) and stored at 4°C .

3.1.4. Buffer and solvents

Analytical grade monobasic and dibasic sodium phosphate, sodium bicarbonate, and ethanol were purchased from ACP Chemicals Inc. Citric acid and sodium carbonate were purchased from Sigma-Aldrich Chemical Company. HPLC-grade water was obtained from BDH and HPLC-grade acetonitrile (ACN) was obtained from Fisher Scientific Company (Ottawa, ON). HPLC-grade formic acid was purchased from ACP Chemicals Inc.

3.1.5. Other materials

Syringe filters (0.2 μm , non-sterile) were purchased from Sarstedt (Montreal, QC). The 10 ml syringes were purchased from Fisher Scientific Company. 1 mL screw-top HPLC vials were purchased from Waters Corporation (Mississauga, ON). Magnetic stir bars in different sizes were obtained from Fisher Scientific Company. Corning 15 mL and 50 mL graduated plastic centrifuge tubes were purchased from Sarstedt, Inc. Pipette tips (100-1000 μL) were purchased from VWR International Inc. (Mississauga, ON) and 5 mL tips were purchased from Sarstedt. Pipetman adjustable volume pipettes (200 μL , 1000 μL , 5 mL) were purchased from Mandel Scientific (Guelph, ON). All other chemicals used in this study were analytical grade and purchased either from Sigma-Aldrich Chemical Company (Oakville, ON) or BDH Inc. (Toronto, ON).

3.2. Analytical Equipment

3.2.1. UV-VIS spectrophotometry

An Agilent (Mississauga, ON) 8453 UV-Visible spectrophotometer (λ range of 190-1100 nm and 1 nm resolution) controlled by a Hewlett Packard Vectra ES/12 computer was used to measure the absorbance of the sample and also the enzyme activity. Quartz

spectrometer cuvettes with 10 cm path length type 104-QS were purchased from Hellma (Concord, ON). The maximum wavelength (λ_{max}) of each substrate was monitored in UV-VIS spectrophotometer and the spectra is available in Appendix A.

3.2.2. High performance liquid chromatography (HPLC)

Aromatic compound concentrations were analyzed using a high-performance liquid chromatography (HPLC) system (Model 2487), from Waters Corporation (Oakville, ON), with a dual-wavelength absorbance detector, binary HPLC pump (model 1525) and autosampler (model 717) operated by Breeze 3.3 software. A Waters Symmetry C18 (reversed-phase mode) column (5 μm , 4.6 \times 150 mm) was used.

3.2.3. Electrospray ionization (ESI) and atmospheric solids analysis probe (ASAP) mass spectrometry

The MS experiments were conducted by means of a XEVO G2-XS Time-of-flight (ToF) mass spectrometer obtained from Waters (Oakville, ON) equipped with an ion source. For both techniques, high purity nitrogen was used as a nebulizer gas. The capillary voltage of the ESI probe was set at 3.00 kV and the acquisition range was 50-1200 m/z. The measurements were done in positive ion full-scan mode. All measurements were in the form of a 1 μL injection into a sample loop with a constant flow of 50:50 water:ACN with 0.1% formic acid at 5 $\mu\text{L}/\text{min}$. For ASAP, the measurements were also done in positive ion full-scan mode but with an ASAP probe with mass acquisition range same as ESI as stated above. The corona current was 1.0 μA and the desolvation gas flow was 600 L/h. The instrument was operated by the MassLynx software (version 4.1).

3.2.4. Total organic carbon (TOC) analysis

Carbon content of solutions was determined by a Shimadzu model TOC-L CPH Total Carbon Analyzer purchased from Shimadzu Scientific Instruments (Columbia, MD). The total organic carbon was calculated from the difference of total carbon (TC) and inorganic carbon (IC). Both TC and IC were detected by a non-dispersive infrared spectrophotometer. Before injection, the samples were micro-filtered. Standard curves for both TC and IC were selected from the database of the instrument.

3.2.5. Centrifuge and *pH* meter

All the centrifugation was performed using a Corning LSE™ Compact Centrifuge (Tewksbury, MA) with 6×50 mL and 6×15 mL centrifuge tubes and a maximum speed of 6000 rpm. The centrifuge conditions are specified in the respective experimental protocols. The *pH* meter used was an Oakton PC 700 benchtop meter (*pH* range 0.00 to 14.00, *pH* resolution 0.01, ±0.01 *pH* accuracy), with an Orion *pH* probe (9110DJWP, Ag/AgCl double junction, glass body) (Vernon Hills, IL). Calibration buffers at 4.00, 7.00 and 10.00 were purchased from ACP Chemicals Inc. whereas, a calibration buffer at *pH* 1.68 was purchased from Hanna Instruments (Laval, QC).

3.2.6. Other equipment

Model K-550-G vortex mixer (50/60Hz, 0.5 Amps, 120 volts) was purchased from Scientific Industries, Inc (Bohemia, NY). VWR magnetic stirrers VS-C10 (50-60 Hz, 30Watts) were purchased from VWR International Inc.

3.3. Analytical Methods

3.3.1. Colorimetric assay for SBP activity

A colorimetric assay was used to determine the enzyme activity in this study. The enzyme activity can be determined by monitoring the initial rate of color formation resulting from the oxidative coupling of phenol and 4-AAP in the presence of hydrogen peroxide using SBP as a catalyst. The product of such reaction is a pink chromophore with an absorption maximum at 510 nm and an extinction coefficient of 6000 M⁻¹cm⁻¹ relative to hydrogen peroxide (Ibrahim *et al.* 2001).



The reaction mixture consisted of 0.025 g of AAP, 100 µL of 100 mM hydrogen peroxide; 5 mL solution consisting of 100 mM phenol in 0.5 M sodium phosphate buffer of pH 7.4 (Caza *et al.* 1999) and was made up to 47.5 mL in a volumetric flask. The sample was added to the cuvette first, followed by quick addition of reagent to provide mixing power and start the reaction. The regular assay was to mix a 50 µL approximately diluted enzyme sample with 950 µL of reagent and monitor the absorbance change for 30 s, which had a detection limit around 0.1 U/mL. The absorbance was measured at 510 nm with run time of 30 seconds and cycle time of 5 seconds. The rate was calculated by the zero-order kinetics feature available in the instrument software. Enzyme catalytic activity in ‘units’ (U) is defined as the number of micromoles of hydrogen peroxide converted per minute at pH 7.4 and 23°C in a standard ‘Trinder-type’ assay described previously by Wu *et al.* 1998. One unit by this assay corresponds to 8 U as determined by Mousa Al-Ansari (unpublished) by the standard guaiacol activity assay (Sessa and Anderson 1981). Additional information is provided in Appendix B.

3.3.2. Buffer preparation

The buffers were prepared according to Gomori (1955). Citrate-phosphate buffer was used in the *pH* range of 2.6-5.0. Monobasic-dibasic sodium phosphate buffer was used for the *pH* range of 6.0-8.0, and for higher *pH* (9.2 and 10.0), sodium bicarbonate-sodium carbonate buffer was used.

3.3.3. Technical feasibility of substrate/SBP compatibility

A preliminary study was conducted to verify if the selected arylamines were substrates for SBP. For this, individual batch reactors with appropriate concentrations of substrate, buffer, SBP and H₂O₂ were stirred thoroughly for 3 hours to observe possible changes in colour or formation of precipitates. Reactions were then stopped by adding catalase, microfiltered and analyzed for the residual concentration by UV-VIS and HPLC. UV-VIS and HPLC were also used to study the standards of the respective substrates with the same initial concentration. The occurrences of conversion of the substrates were confirmed when there was a decrease in the concentrations, hence establishing that the arylamines would act as a substrate for SBP.

3.3.4. Substrate/buffers compatibility tests in UV-VIS spectrophotometer

The aromatic pollutants MDA, TDA, ODA, 4-COT, MOCA were tested against each buffer (citrate-phosphate, phosphate, carbonate-bicarbonate) from *pH* range of 2.6-10.0 to check the compatibility of the substrate in each buffer in spectrophotometer. It was observed that the aromatic pollutants showed different absorbance and wavelength when dissolved in different buffers of the same concentration. Therefore, it was decided that a separate calibration curve was needed for each substrate in the respective buffer where such changes were observed. Calibration curves for each aromatic pollutant in the respective buffers, measured by HPLC, are given in Appendix C.

3.3.5. HPLC analysis

The residual concentrations of the substrates after enzymatic treatment were analyzed with an HPLC System. Elutions were isocratic and injection volume was 10 μ L for all the substrates. The UV-detector was adjusted according to the predetermined λ_{max} obtained by the spectrophotometer. Table 3.1 summarizes the HPLC conditions for the aromatic pollutants.

Table 3.1. Summary of the mobile phase solvents, mobile phase ratio, column temperature and the absorbance detector wavelength for the aromatic pollutants.

Aromatic compound	Mobile phase solvents		Ratio of solvent in mobile phase (%)		pH	Wavelength (nm)	Column temperature (°C)
	Pump A	Pump B	Pump A	Pump B			
<i>p</i> -Cresidine	Formic acid (0.1%)	Acetonitrile (ACN)	80	20	-	287	35
4-COT	Ammonium acetate (5 mM) <i>pH</i> 6.8		40	60	2.6-5.0, 7.0	290	30
ODA			70	30	2.6-4.0	271	
					5.0-10.0	293	
MDA			55	45	2.6-3.0	260	
					4.0-10.0	285	
TDA			50	50	2.6-3.0	253	
	5.0-10.0	260					
MOCA		30	70	2.6, 3.0, 7.0	291		

3.3.6. Enzyme stock solution preparation

SBP stock solution was prepared by weighing 1.4 g solid enzyme and mixing with 100 mL distilled water for 24 hours; then the mixture was centrifuged for 25 min. at 4000 rpm. The supernatant was stored at 4°C. Catalase stock was prepared as 0.5 g/100 mL mixing for 4 hours and stored at 4°C. Additional information is provided in Appendix D.

3.3.7. Total organic carbon (TOC) analysis

TOC analysis was done for MDA samples collected from batch reactor experiments run under the optimum conditions for enzymatic treatment. 20 mL samples were micro-

filtered before injecting in to the instrument. The machine was allowed to start up and run with 3 Milli-Q water injections to make sure the system was properly purged. Each sample was then measured for both TOC and IC (inorganic carbon). The TOC was obtained by subtracting the IC from the TC (total carbon). Three injections were used for each reading and the average was recorded.

3.4. Experimental Protocols

3.4.1. SBP-catalyzed polymerization of aromatic substrates

All experiments were run in triplicates, unless otherwise stated, at room temperature and standard deviations were calculated and denoted by error bars. The first part of this study was to optimize the reaction conditions for the removal of aromatic substrate in the presence of SBP and peroxide. For initiating the reaction, batch reactors in 30 mL vials were used that consisted of a mixture of aromatic substrate, 40 mM of citrate-phosphate, phosphate or carbonate-bicarbonate buffer, SBP and hydrogen peroxide of appropriate concentrations. The solutions were mixed in open vials appropriately using teflon-coated magnetic stirrer bars on magnetic stirring plates for a 3-hour reaction time at an ambient temperature of $22\pm3^{\circ}\text{C}$. At the end of 3 hours, the reactions were stopped by quenching with excess catalase of 50 U/mL concentration to consume any residual hydrogen peroxide. The samples were then micro-filtered followed by analysis of the residual substrate concentrations by the HPLC-UV system. Separate controls were also run with no hydrogen peroxide and no SBP. The study was carried out to achieve enzymatic removal of at least 95% of the parent substrate, by optimization of *pH*, hydrogen peroxide and enzyme concentrations. Analogous experiments were also conducted to monitor the substrate consumption over time and apparent first-order rate constants and half-lives of the pollutants were derived.

3.4.2. Preliminary product determination using mass spectrometry

For MS samples, batch reactions were performed under the optimized conditions established for each substrate. The buffers created interferences with the product peak in MS; therefore, the concentration of 40 mM as used during batch optimization was reduced to 10 mM for MS samples. The batch reactors were run for 3 h and the reaction was stopped by adding catalase of 50 U/mL concentration to consume any residual hydrogen peroxide. These aliquots were centrifuged at 3500 rcf. The supernatant and precipitate were both analyzed by electrospray ionization mass spectrometry (ESI-MS). However, 4-COT samples were analyzed by the ASAP technique because ESI did not give significant signals. The precipitates were rinsed with water several times to wash out as much buffer as possible to avoid the interferences with the product peak. All MS experiments were run in positive-ion mode consisting of treated, appropriate blanks and standard samples. The standard samples were prepared in the appropriate buffer solutions for better and easier discrimination of the product peaks.

3.4.3. Identification of azo-products using UV-VIS spectrophotometry

Since mass spectra showed the presence of azo-products in some of the cases, such azo-coupled products were further characterized by UV-VIS spectrophotometry. After the completion of the batch experiments, the aliquots were centrifuged at 3500 rcf. The supernatant was diluted as required and checked for the presence of any peak at a wavelength range of 300-320 nm (*trans*-form), and near 440 nm (*cis*-form), which is the range for azobenzene (Michail *et al.* 2013; Beharry and Andrew 2011).

3.4.4. Kinetics study

Initial velocity for the conversion of *p*-cresidine, 4-COT, MDA, TDA, ODA, MOCA were monitored by keeping the SBP and H₂O₂ concentrations constant and varying

substrate concentration until adequate conversion was obtained to estimate an apparent single-substrate kinetic parameters (K_M and V_{max}). Individual 10 mL batch reactors were run with 40 mM buffer at optimum pH for each substrate. Samples were catalase-quenched at 0, 30, 60, 90, 120, 150, and 180 s, microfiltered and analyzed by UV-VIS. Origin 8.0 was used to plot the initial rate of the reaction as a function of the initial substrate concentration. The plotted data were fitted to the Michaelis-Menten equation to provide the Michaelis constant (K_M), the maximum velocity (V_{max}) and the catalytic efficiency (V_{max}/K_M).

3.4.5. TOC analysis

TOC analyses were done using experiments run under the optimum conditions with MDA for 3 hours. Individual batch reactors consisted of treated, untreated and standards samples were then microfiltered and analyzed in the analyzer. The stock solution for the other aromatic substrates in this study had an organic solvent of approximately $\leq 10\%$, therefore, TOC analysis was not possible.

3.4.6. Sources of error

In every experiment, the combination of systematic and random errors can affect the accuracy and reliability of the results. Systematic errors are due to analytical techniques and instruments, whereas random errors are caused by normal variability of measurement that can be minimised, not avoided. All pipettes, scales and other measuring instruments were calibrated before use to minimize the systematic errors. Random errors were minimized by conducting experiments in triplicates and sensitive experiments were repeated on different days to determine the reproducibility. All graphs show the standard deviation as error bars, which were obtained from the average of the triplicate experiments. Experimental protocol and procedure were carefully followed and compounds that can

easily degrade, for example MOCA were prepared as fresh solution for each experiment. SBP activity is sensitive to the change in room temperature, reagent age and mixing conditions. Therefore, to minimize the error, SBP stock activity was checked every day before starting an experiment. Room temperature was tracked on regular basis to conduct all activity tests at $22\pm 3^{\circ}\text{C}$. All the analytical instruments were monitored on time to time basis and proper maintenance was followed.

CHAPTER 4: RESULTS AND DISCUSSION

4.1. Optimization of *pH*

Enzymes are biological catalysts, proteins with dynamic polymeric structures containing characteristic ionizable side chains of amino acid residues liable for structural and catalytic functions. In addition to being catalysts of the living world, their excellent properties render them also exploitable in many applications that range from industrial catalysis to therapeutics (Saha *et al.* 2009). *pH* changes can lead to perturbations in structural geometry by varying the charge state of these ionizable side chains, denaturing the enzyme, or diminishing its catalytic activity (Xu 1997). The relative activity of SBP at 25°C in different *pH* buffers ranging from 2.0-10.0 was investigated by Geng *et al.* (2001) to find that SBP was active over an extensive range of *pH* in case of tetra-guaiacol formation showing its maximum activity between *pH* 5.5 and 6.0. More than 95% of enzyme activity was observed at *pH* 5.0, about 90% at *pH* 6.5, and >50% between *pH* 3.0 and 7.0. About 25 and 32% enzyme activity was observed at *pH* 2.2 and 8, respectively. Later on, Nicell and Wright (1997) reported similar results with some variation in *pH* for SBP activity with phenol. These results gave an indication that SBP from seed hulls have significant activity over a wide *pH* range which enable it to oxidise a wide range of substrates.

The catalytic mechanism is dependent on two key residues conserved through plant peroxidases, the distal histidine-42, that acts as a proton acceptor from hydrogen peroxide, and the distal arginine-38 acting as a charge stabilizer (Dunford 1999). It is supposed that SBP has less chance of inactivation due to the low pK_a (3.2) of the distal histidine side chain (Dunford 1999; Nisum *et al.* 2001). The catalytic activity of a specific enzyme-substrate complex is dependent on *pH*, which suggests that acid-base catalysis plays a vital

role in enzymatic reaction. Protein denaturation can occur at high pH and the extent of ionization of a few of the amino acid side chains could affect the enzyme activity. Catalytic efficiency is affected by the protonation state of the active site residues. The distal histidine (His42) should be in its deprotonated form while the arginine (Arg38) in its protonated form in order to perform their functions as a catalytic base and as a charge stabilizer, respectively. The optimum pH is a value that optimally satisfies both the amino acids ionization state condition and the value that provides the best conformational state of the enzyme for the catalysis (Henriksen *et al.* 2001; Kamal and Behere 2002).

The different substrates were studied in different buffers, pH range 2.6-10.0, in the UV-VIS spectrophotometer. For 4-COT, the maximum absorbance was determined at 290 nm irrespective of the buffers used but the extinction coefficient varied in different buffers. Hence, separate calibration curves for pH s 2.6-5.0 and 7.0 were necessary to determine the concentration of 4-COT remaining in the pH optimization experiments. For ODA, it was observed that the maximum wavelength (λ_{max}) was not the same in different buffers. For pH 2.6 to 4.0 the wavelength was 271 nm and from pH 5.0-10.0 the wavelength determined was 293 nm. The extinction coefficient of the compound also varied in different buffers. Therefore, a separate calibration curve was made at pH 2.6, 4.0, 7.0 and 9.2 in the HPLC for determining ODA concentrations in batch reactors and, thence, the optimum pH for the enzymatic reaction. MDA showed a maximum wavelength of 285 nm for all buffers except for pH 2.6-3.0 which was 260 nm and the extinction coefficients in different buffers were dissimilar, therefore, separate calibration curves were determined for pH s 2.6-5.0 and for pH 7.0. For TDA, reactions in the pH range 2.6-3.0 were read at 253 nm and while those in the pH range 4.0-10.0 were read at 260 nm. Separate calibration curves were made in pH 3.0 and pH 7.0 buffers to get the remaining TDA concentrations after the treatment.

The MOCA spectrum showed a maximum wavelength at 291 nm, independent of the buffers used, but the extinction coefficient was not same in all buffers, thus, separate calibration curves were established for those *pH*s where such differences were observed. Calibration curves were made for *pH*s 2.6, 3.0 and 7.0. All calibration curves for each of the substrates were obtained on the HPLC instrument and are shown in Appendix D.

During the preliminary feasibility study of substrate/SBP compatibility, there was reduction in the HPLC peak areas and heights after treatment compared to the standard run under the same conditions. There was also decrease in the absorbance of the treated samples compared to their respective standards in UV-VIS, which confirmed that the studied arylamines were substrates for SBP.

By means of HPLC, the effect of *pH* for conversion of the substrates, was studied in the *pH* range 2-10, both under “stressed” (stringent) conditions, *i.e.* where enzyme concentration was the limiting factor leading to incomplete removal within a 3-h reaction period, in order to establish clearer and easier discrimination of the *pH* effects, as seen in Figs. 4.1-4.6. The atom bridged bis-anilines studied had a concentration of 0.5 mM, except MOCA with the initial concentration of 0.1 mM, whereas, the monocyclic anilines had an initial concentration of 1.0 mM in the batch reactors. For all substrates, three separate control experiments were performed, the first one was without SBP, the second one was without H₂O₂ and, lastly, one without SBP and H₂O₂ and it was observed that there was no conversion of the substrate in any of these cases. The H₂O₂ concentration was maintained at a sufficient level for the enzymatic reaction. All experiments were run in triplicate at 22±3°C. The error bars denote respective standard deviations. The error bars are not visible for some of the symbols as the latter concealed the bars.

p-Cresidine showed an optimum *pH* of 4.6 as shown in Fig. 4.1 and the value is close to the pK_a of the compound, which is 4.7 (Sánchez *et al.* 2014). The optimum *pH* for the other monocyclic aromatic amine, 4-COT, was determined to be 4.4 as shown in Fig. 4.2, and the pK_a of the substrate being 3.8 (Sánchez *et al.* 2014). Earlier, SBP and anilino compounds had shown similar trends exhibiting optima at *pH* 5.2 (Patapas *et al.* 2007), *pH* 5.0 (Malik Altahir *et al.* 2015) and *pH* 4.5-5.6 (Mousa Al-Ansari *et al.* 2009). In Fig. 4.2, it can be seen that 4-COT was sensitive in the *pH* range of 3.4-3.8 and 4.4-5.0. At *pH* > 7.0 there was almost no removal. Increasing the SBP concentration by two-fold also did not show any changes with varying *pH*.

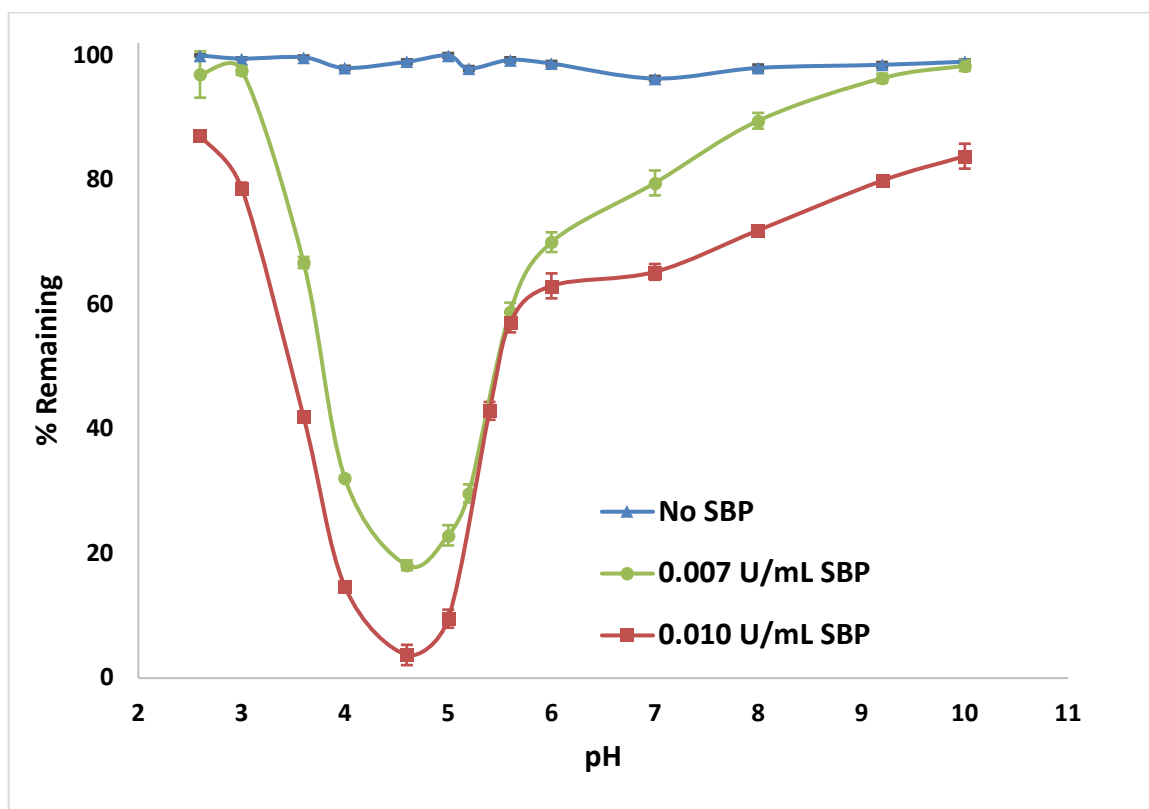


Figure 4.1. Effect of *pH* on removal of *p*-cresidine. Conditions: 1.0 mM *p*-cresidine; 0.000, 0.007 and 0.010 U/mL SBP; 1.5 mM hydrogen peroxide; 40.0 mM buffers; and 3-h reaction.

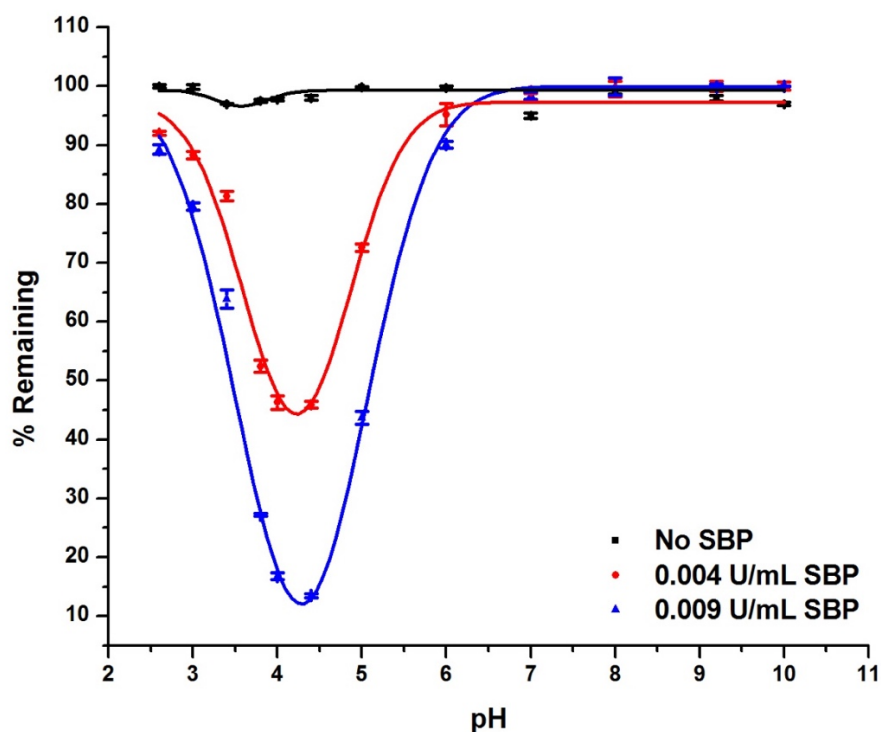


Figure 4.2. Effect of pH on removal of 4-COT. Conditions: 1.0 mM 4-COT; 0.000, 0.004 and 0.009 U/mL SBP; 1.5 mM hydrogen peroxide; 40.0 mM buffers; and 3-h reaction.

In contrast, the optimum pH obtained for the atom-bridged bis-anilines ODA, MDA, TDA was 6.0, close to neutral pH , as seen in Figs. 4.3-4.5. The pK_{as} of ODA, MDA and TDA were 5.5, 5.3 and 4.6, respectively (Sánchez *et al.* 2014). In previous work, similar pH optima, were observed, such as for benzenediols (6.5-8.0), except for hydroquinone, which was between pH 4.0-6.5 (Mousa Al-Ansari *et al.* 2009). For 2-mercaptobenzothiazole, the optimum pH was from 6.0 to 8.0 (Mousa Al-Ansari *et al.* 2010). Aniline and toluidines (*o*-, *m*- and *p*-), also showed similar results, which had optima in the pH range of 5.0-8.0 (Mantha *et al.* 2002). As seen in Fig. 4.4, for MDA, doubling the concentration of SBP showed more percent conversion of substrate and it was consistent across the pH range. Similarly, for MOCA, pK_a 3.3 (Sánchez *et al.* 2014), the optimum pH determined was 4.2, which is in the acidic region as shown in Fig. 4.6. When

the SBP concentrations were increased, from 0.04 to 0.05 U/mL, higher percent conversion was achieved.

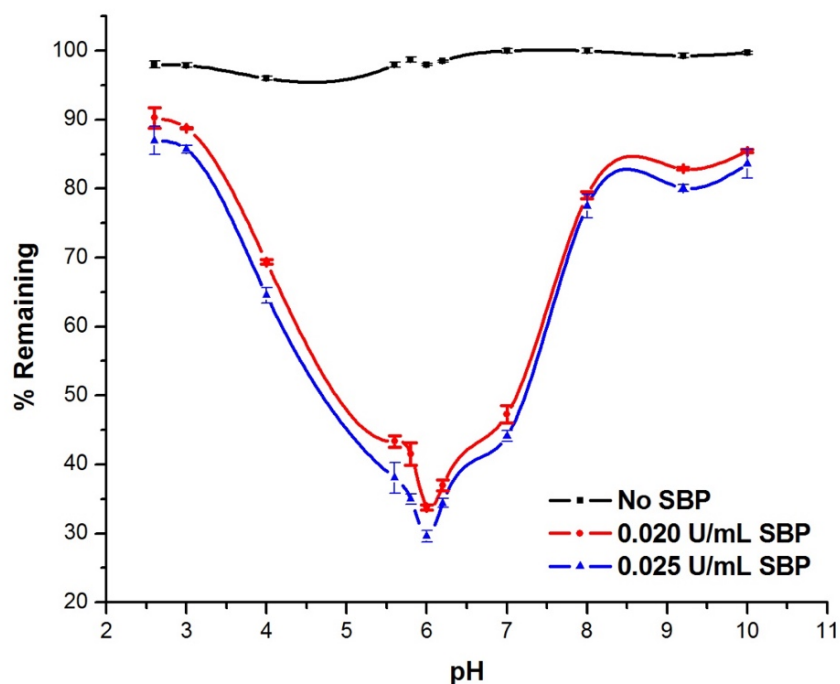


Figure 4.3. Effect of *pH* on removal of ODA. Conditions: 0.5 mM ODA; 0.000, 0.020 and 0.025 U/mL SBP; 0.75 mM hydrogen peroxide; 40.0 mM buffers; and 3-h reaction.

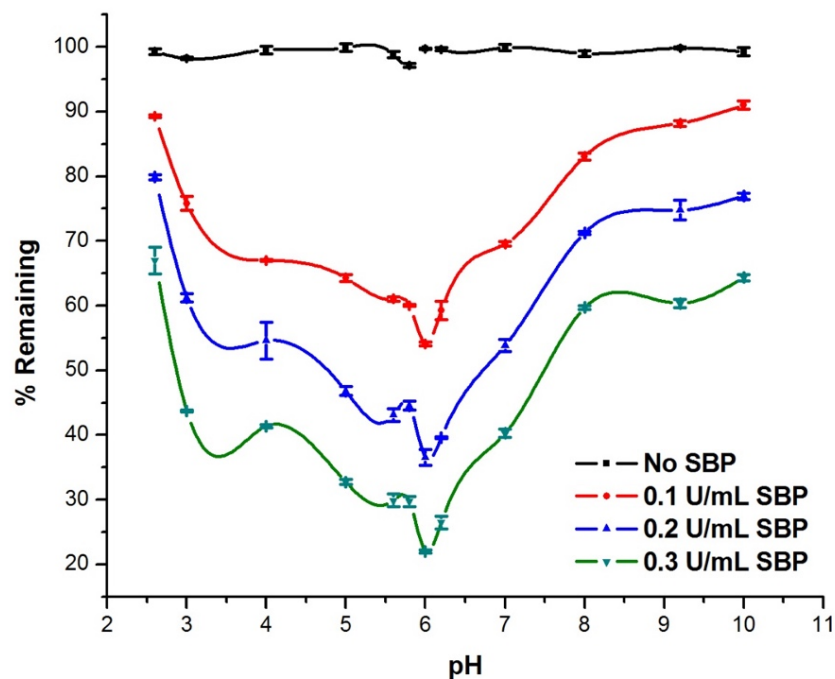


Figure 4.4. Effect of *pH* on removal of MDA. Conditions: 0.5 mM MDA; 0.0, 0.1, 0.2 and 0.3 U/mL SBP; 0.75 mM hydrogen peroxide; 40.0 mM buffers; and 3-h reaction.

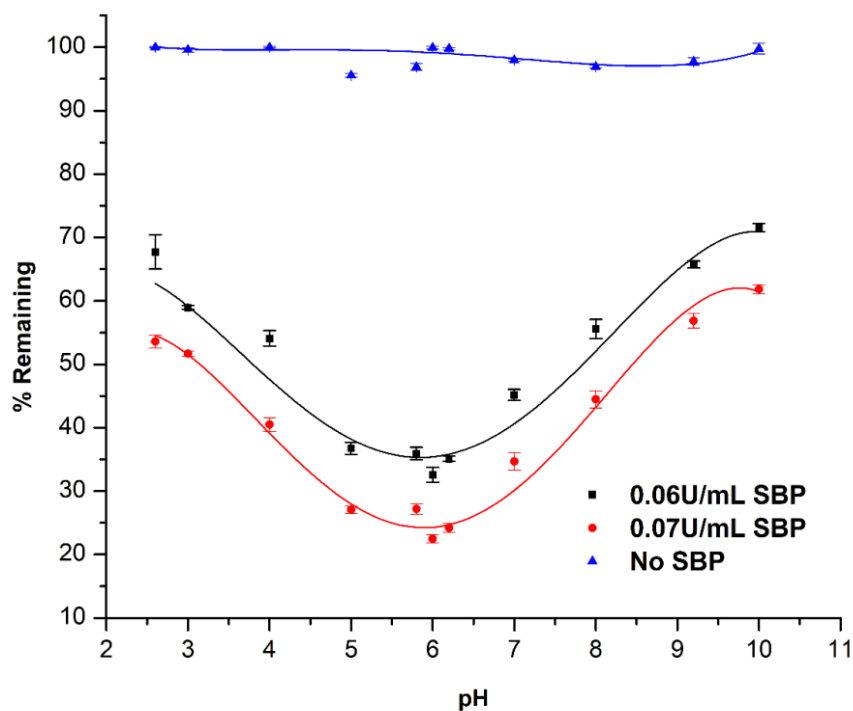


Figure 4.5. Effect of *pH* on removal of TDA. Conditions: 0.5 mM TDA; 0.00, 0.06, and 0.07 U/mL SBP; 0.75 mM hydrogen peroxide; 40.0 mM buffers; and 3-h reaction.

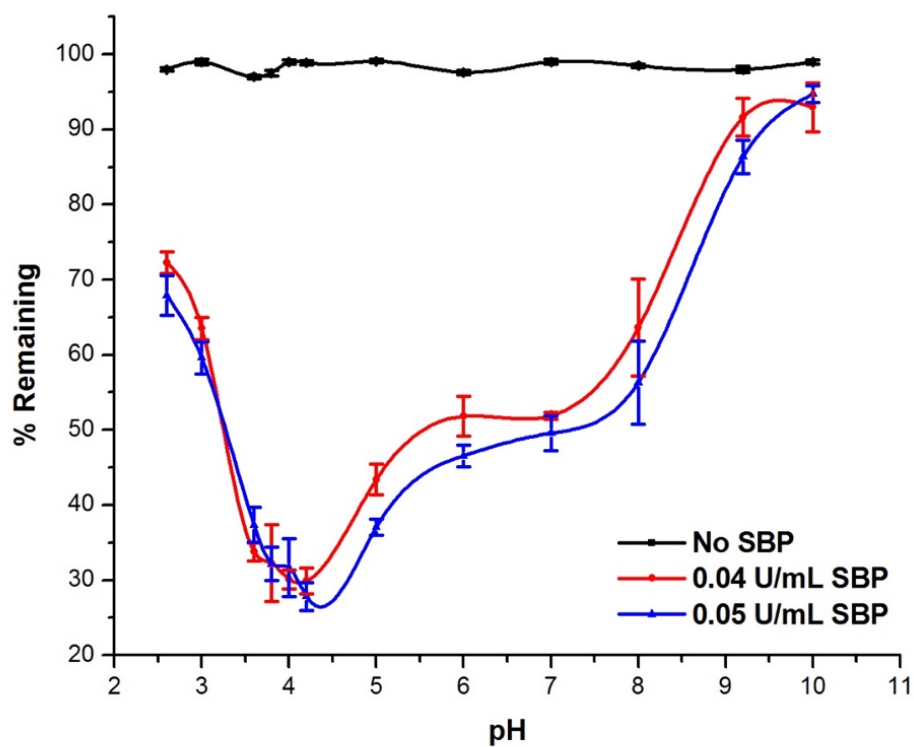


Figure 4.6. Effect of *pH* on removal of MOCA. Conditions: 0.1 mM MOCA; 0.00, 0.04 and 0.05 U/mL SBP; 0.15 mM hydrogen peroxide; 40.0 mM buffers; and 3-h reaction.

In the above figures, drastic reduction in percentage conversion was seen at pH s on either side of the respective optima. This decrease could be due to the lower stability of the Compound I form of SBP in a neutral solution (Patapas *et al.* 2007). Another possibility for such sensitivity of the percentage conversion to pH , when pH was higher than 4.0, as seen in Figs. 4.1-4.6, might be due to the changes in ionization of catalytic residues of the enzyme at this pH or higher. A bell-shaped pH dependence indicates that at least two ionizable groups of enzyme and/or substrate are involved (Kamal and Behere 2003). Figures 4.1-4.6 exhibit inverted bell-shaped pH curves.

A few conclusions that can be drawn from the pH optima for the studied compounds are that SBP can tolerate an acidic region better than a basic region, which has been observed by others (Mousa Al-Ansari *et al.* 2009 and 2011); and that the optimum pH not only is dependent on proper ionization state of the catalytic residues but also on the type of aromatic compound being treated by enzymatic process and its pK_a . The concentrations of SBP needed to be increased beyond the stringent level to achieve $\geq 95\%$ conversion of the substrates, and that is when the enzyme becomes less sensitive to the pH changes. This could be of great advantage during the application of SBP in treating industrial wastewaters compared to other enzymes, such as laccases, which require a specific pH to be effective (Bodalo *et al.* 2006). The pH optima found here were used for optimising other parameters in the following experiments.

4.2. Optimum Hydrogen Peroxide-to-Substrate Concentration Ratio

Hydrogen peroxide is a major factor in the enzymatic reaction, since it is a co-substrate that initiates the enzymatic process. If the concentration of H_2O_2 is in excess in the reaction it can cause enzyme inhibition whereas low concentration, can make it a

limiting factor (Dunford 1999). For this reason, it was important to check the effect of H_2O_2 concentration on the reaction and how it affected the required SBP concentration.

The peroxide mechanism dictates that for every mole of H_2O_2 consumed, 2 moles of aromatic amine would be converted to free radicals. However, with radical coupling and subsequent enzymatic cycles producing higher oligomers, the peroxide:arylamine stoichiometry would approach a limit of 1.0 (Mousa Al-Ansari *et al.* 2010).

Experiments were designed for optimising the hydrogen peroxide-to-substrate molar concentration ratio. H_2O_2 was varied between 0.50 mM and 2.00 mM with optimum *pH* established in Section 4.1 for reaction of 1.0 mM *p*-cresidine as in Fig. 4.7, whereas, for 1.0 mM 4-COT at optimum *pH*, the concentration of H_2O_2 was varied from 0.09 to 1.0 mM (Fig. 4.8). Thus, *p*-cresidine and 4-COT needed around 1.25 and 0.50 mM of H_2O_2 , respectively, for conversion of $\geq 95\%$ in a 3-hour reaction period.

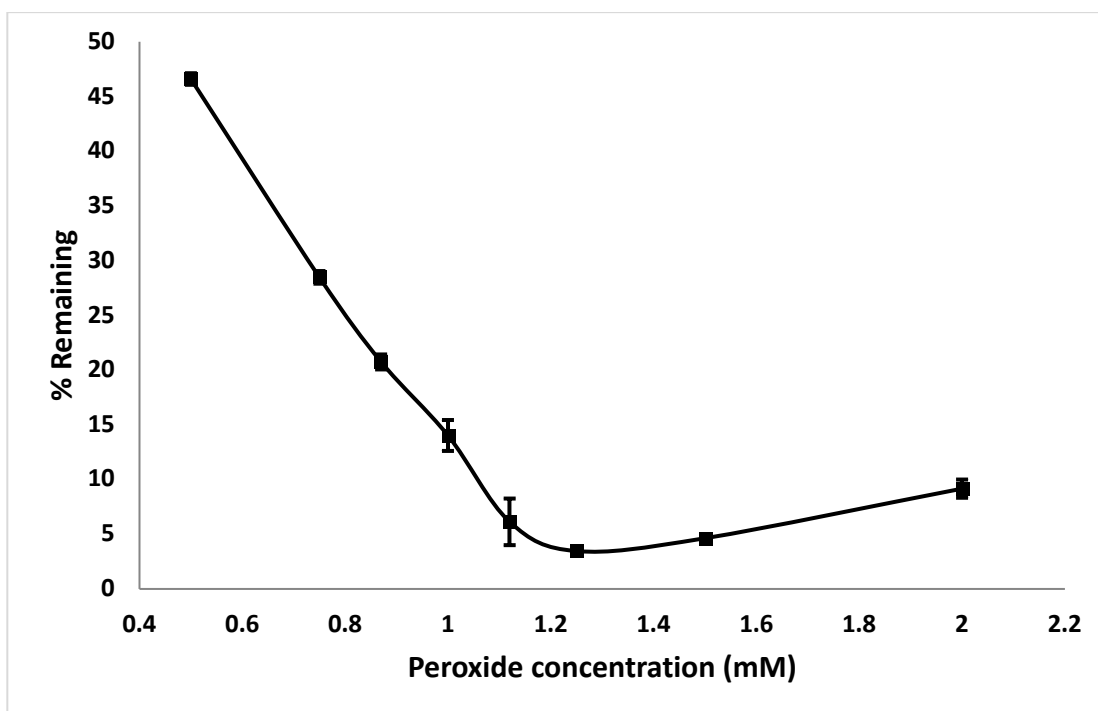


Figure 4.7. Effect of hydrogen peroxide concentration on removal of *p*-cresidine. Conditions: 1.0 mM *p*-cresidine; 0.010 U/mL SBP; 40 mM *pH* 4.6 buffer; and 3-h reaction.

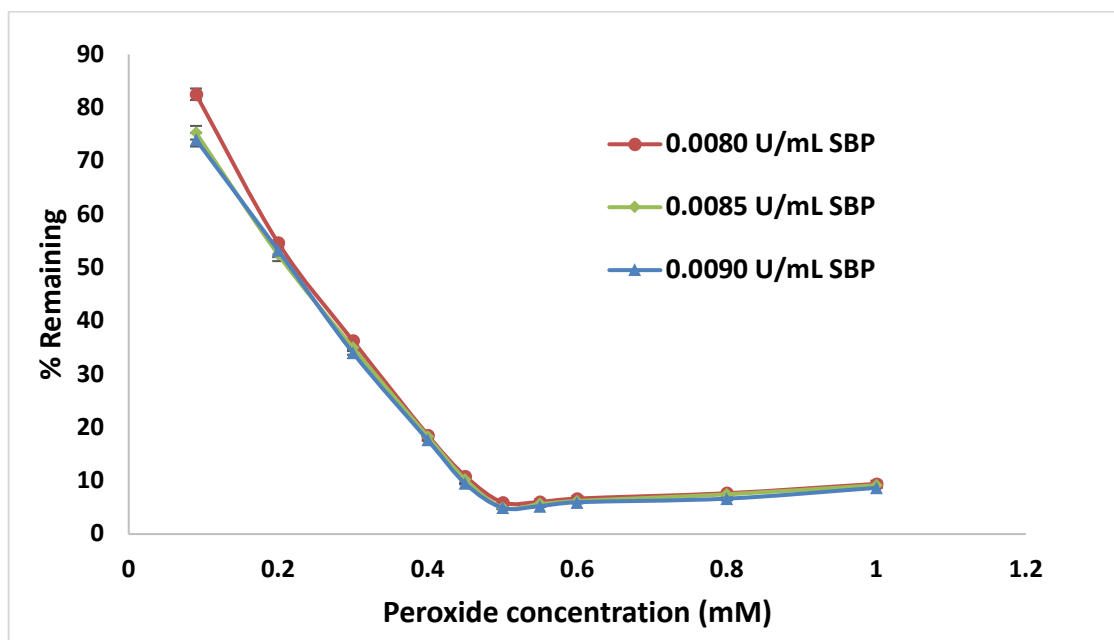


Figure 4.8. Effect of hydrogen peroxide concentration on removal of 4-COT. Conditions: 1.0 mM 4-COT; 0.0080, 0.0085 and 0.0090 U/mL SBP; 40 mM pH 4.4 buffer; and 3-h reaction.

The ratio of $[H_2O_2]/[p\text{-cresidine}]$ was found to be 1.25. Thus, it can be seen that although a demand of 1 mole of H_2O_2 per two anilines is theoretically needed for conversion, an additional consumption of H_2O_2 over that requirement is observed and attributed to its consumption by dimeric and polymeric compounds produced in the reaction, as observed by Yu *et al.* (1994). In addition, according to Dunford (2016), this increase in demand over a peroxide-to-substrate ratio of 1 could be a result of catalase activity that is found in all plant peroxidases, including SBP. Catalase decomposes H_2O_2 to oxygen and water. Another possibility for such increase in demand could be due to the result of H_2O_2 oxidation of organic matter present in the crude enzyme mixture (Biswas 1999). The result obtained for *p*-cresidine can be compared with the previous work with *o*-anisidine (Mazloun *et al.* 2016) where optimal treatment of 1.0 mM of substrate using 0.012 U/mL of SBP was also achieved at 1.25 mM H_2O_2 concentration. Another preceding work, with the model compound diphenylamine (DPA), showed similar kind of results. Its

optimum requirement per functional group was 1.0 to 1.2 mM of H_2O_2 for a substrate concentration of 0.2 mM with *Arthromyces ramosus* peroxidase, ARP (Biswas *et al.* 2007).

For 4-COT, the ratio between peroxide and substrate concentration was 0.5 mM, very close to the theoretical value. It can be observed in Fig. 4.8 that increasing the concentrations of SBP from 0.0080 to 0.0090 U/mL, there was negligible improvement in the conversion of the substrate.

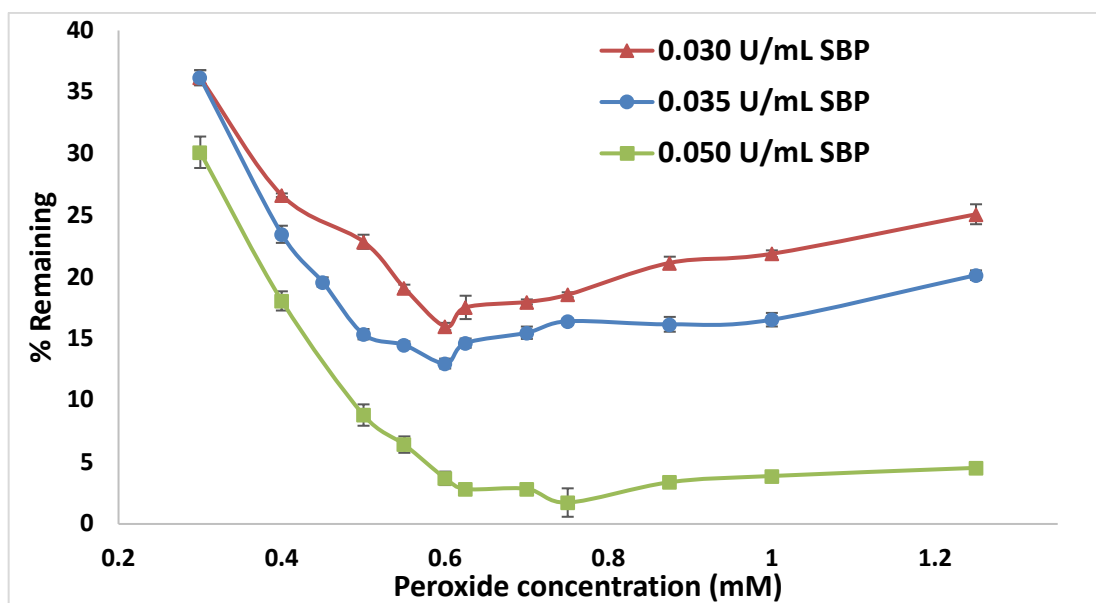


Figure 4.9. Effect of hydrogen peroxide concentration on removal of ODA. Conditions: 0.5 mM ODA; 0.030, 0.035 and 0.050 U/mL SBP; 40 mM pH 6.0 buffer; and 3-h reaction.

For the bis-aniline, ODA, H_2O_2 was varied between 0.30 and 1.25 mM. The enzyme concentration was also varied as shown in Fig. 4.9. ODA required 0.60 mM H_2O_2 for $\geq 95\%$ conversion of 0.50 mM substrate. MDA was studied between 0.3-2.0 mM peroxide concentrations. In Fig. 4.10, it can be observed that increasing the SBP concentration from 0.40 to 0.45 U/mL did not make much difference in the H_2O_2 consumption. Hence, the reaction was further conducted at a higher SBP concentration, 0.55 U/mL, for 3 and 6 h to observe if there was any improvement in H_2O_2 demand. It

exhibited some improvement in the percent conversion of the substrate but did not reach the goal of $\geq 95\%$ removal. Hence, SBP concentration was increased to 0.65 U/mL, and 0.5 mM of MDA required 0.7 mM of H_2O_2 to achieve $\geq 95\%$ conversion, as seen in Fig. 4.10.

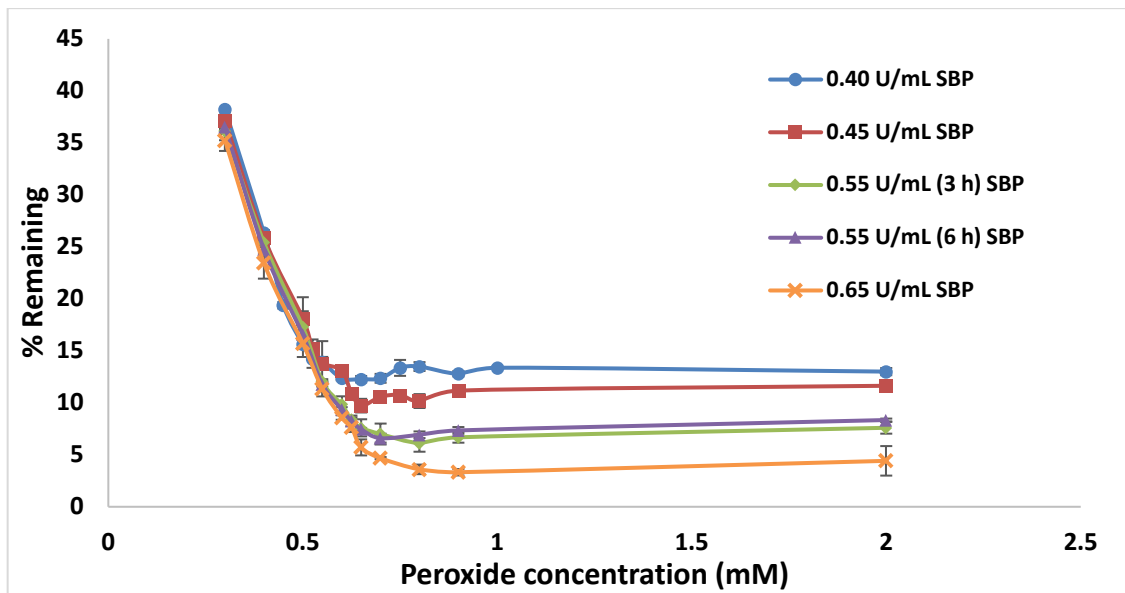


Figure 4.10. Effect of hydrogen peroxide concentration on removal of MDA. Conditions: 0.5 mM MDA; 0.40, 0.45, 0.55 (3 h), 0.55 (6 h) and 0.65 U/mL SBP; 40 mM pH 6.0 buffer; and 3-h reaction.

Similarly, H_2O_2 was varied between 0.30 and 1.25 mM with the previously established optimum pH (6.0) for reaction of 0.5 mM TDA. The SBP concentrations were varied from stress conditions to sufficient level to achieve 95% conversion as seen in Fig. 4.11. The TDA took almost 0.55 mM H_2O_2 for $\geq 95\%$ conversion. The concentration of H_2O_2 studied was in the range 0.09-0.20 mM for conversion of 0.1 mM MOCA. The optimum H_2O_2 concentration was 0.15 mM in the presence of sufficient SBP to achieve at least 95% conversion of the MOCA in a 3-hour reaction period, Fig. 4.12.

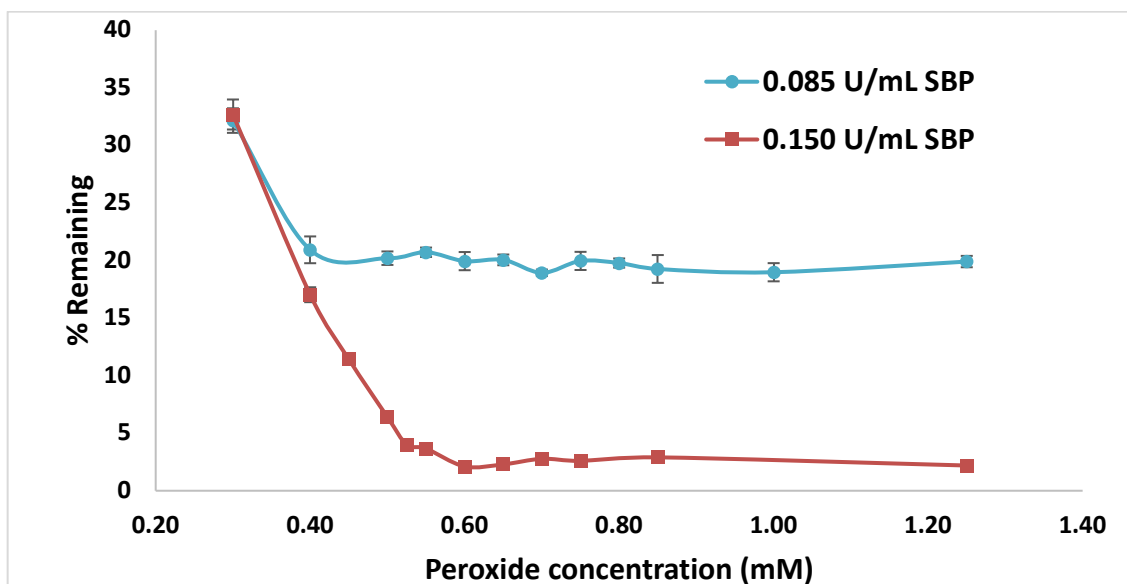


Figure 4.11. Effect of hydrogen peroxide concentration on removal of TDA. Conditions: 0.5 mM TDA; 0.085 and 0.150 U/mL SBP; 40 mM pH 6.0 buffer; and 3-h reaction.

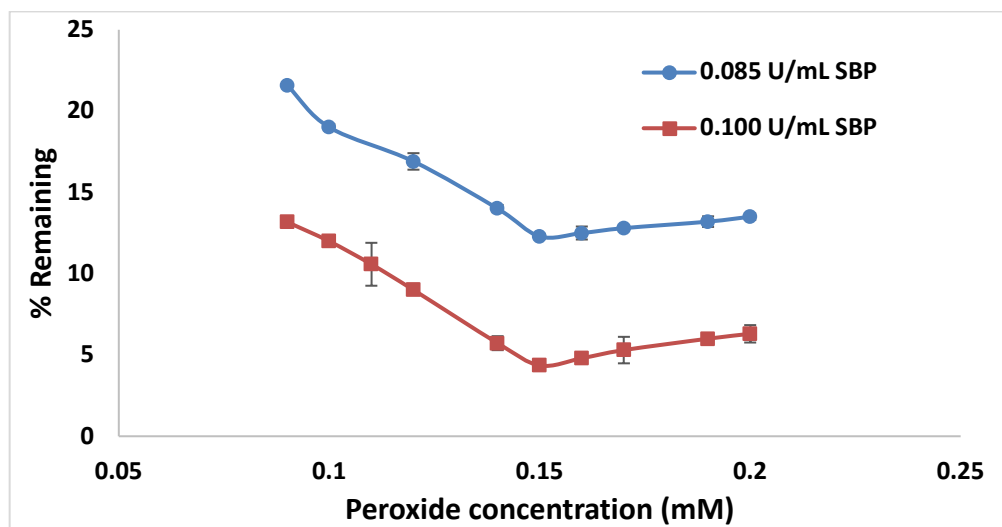


Figure 4.12. Effect of hydrogen peroxide concentration on removal of MOCA. Conditions: 0.1 mM MOCA; 0.085 and 0.100 U/mL SBP; 40 mM pH 4.2 buffer; and 3-h reaction.

As the hydrogen peroxide-to-substrate ratio increased beyond the optimum value, presented in Figs. 4.7 to 4.10 and Fig. 4.12, all the substrates showed a decrease in conversion, which could be due to peroxide inactivation of the enzyme. This could be due to the transformation of an active form of enzyme (Compound II) to an inactive form

(Compound III) (Mousa Al-Ansari *et al.* 2009; Dunford 1999). Another reason might be the formation of an inactive form of enzyme due to the release of free radicals from Compound I and Compound II of the peroxidase that have the possibility to react back with the active site (Dunford 1999). However, TDA in Fig. 4.11 was an exception and did not show any decrease in the percent of substrate conversion at peroxide concentrations beyond the optimum.

It is to be noted that due to the presence of two aniline functional groups in the bis-anilines (ODA, TDA, and MDA) the substrate concentration was selected as 0.5 mM. This made it comparable to the 1.0 mM concentration of the mono-anilines *p*-cresidine and 4-COT. In this study, for example, the molar ratio of the concentrations H_2O_2 /(ODA amino groups) was $0.60/(2 \times 0.5) = 0.60$, whereas the ratio of H_2O_2 /(*p*-cresidine amino group) was $1.25/(1 \times 1.00) = 1.25$. Thus, for the bifunctional molecule, MOCA, the ratio of the concentrations H_2O_2 /(MOCA amino groups) was $0.15/(2 \times 0.1) = 0.75$. The optimum seen in Fig. 4.12 is somewhat less than the theoretical peroxide requirement of 0.1 mM, which is an indication that not both ends of every MOCA must be coupled to achieve conversion and hence removal.

It is evident that the H_2O_2 consumption of bifunctional anilino groups are very near to the theoretical stoichiometric value, i.e. $(\text{H}_2\text{O}_2)/(\text{substrate}) \leq 1$, in contrast to the mono-functional arylamines which have the ratio greater than 1. A different trend was observed with 4-COT. Previous work with phenylenediamines, which are also bis-anilines (Mousa Al-Ansari *et al.* 2009), reported consumption of H_2O_2 in the concentration range of 1.5-2.0 mM for $\geq 95\%$ conversion of 1.0 mM substrate.

4.3. Minimum SBP Concentrations Required for Treatment

The cost of enzyme in an enzymatic treatment can be one of the drawbacks in the application to real wastewater (Steevensz *et al.* 2009). Therefore, determining the minimum SBP concentration needed at optimum conditions is an important parameter in enzymatic treatment. The minimum SBP concentrations required for the 95% conversion of the aromatic substrates were investigated in the following set of experiments. The reaction time was 3 hours at the previously established optimal *p*Hs and H₂O₂ concentrations obtained in Sections 4.1 and 4.2, respectively. The SBP concentrations were varied to determine the minimum effective concentration.

The SBP concentration ranges studied for 1.0 mM *p*-cresidine and 4-COT, were 0.007-0.010 and 0.006-0.030 U/mL, respectively, to find the minimum concentration of enzyme needed to achieve $\geq 95\%$ conversion of the aromatic substrate. The results showed that 0.010 U/mL and 0.009 U/mL of enzyme were needed for *p*-cresidine (Fig. 4.13) and 4-COT (Fig. 4.14), respectively. In Fig. 4.13, no major change on percent conversion of *p*-cresidine was observed by increasing the SBP concentration beyond the required minimum, whereas in Fig. 4.14, it is observed that beyond the minimum SBP concentration, there was a slight increase in the percent conversion of 4-COT. The value of 0.010 U/mL of SBP for 1.0 mM *p*-cresidine can be compared with 0.012 U/mL of SBP for 1.0 mM *o*-anisidine, the structure of *o*-anisidine being very similar to *p*-cresidine (Mazloun *et al.* 2016). The minimum SBP concentration required for 4-COT (0.009 U/mL) can be compared with 0.002, 0.010, and 0.005 U/mL of SBP for 1.0 mM phenylenediamines (*o*-, *m*- and *p*-) (Mousa Al-Ansari *et al.* 2009), respectively.

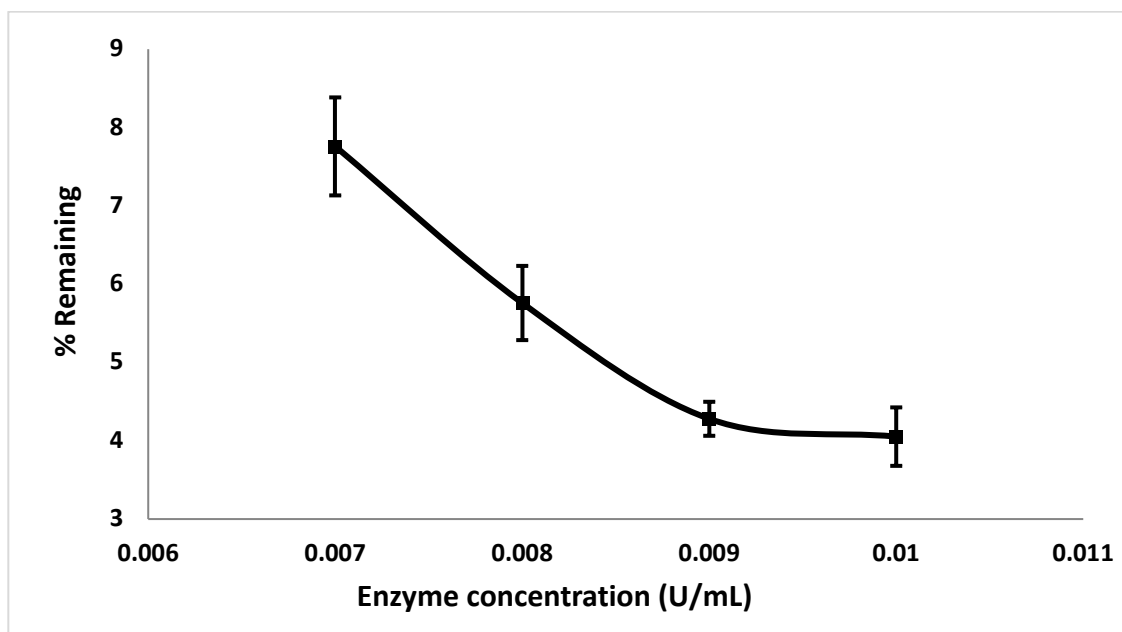


Figure 4.13. SBP optimisation for the removal of *p*-cresidine. Conditions: 1.0 mM *p*-cresidine; 1.25 mM hydrogen peroxide; 40 mM pH 4.6 buffer; and 3-h reaction.

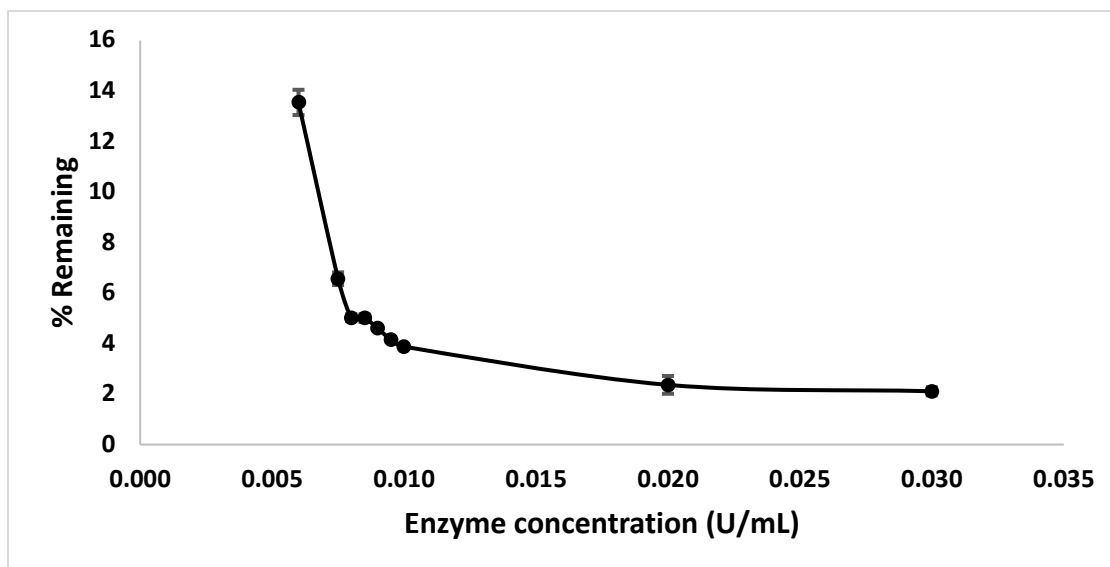


Figure 4.14. SBP optimisation for the removal of 4-COT. Conditions: 1.0 mM 4-COT; 0.50 mM hydrogen peroxide; 40 mM pH 4.4 buffer; and 3-h reaction.

The SBP concentration range studied for 0.5 mM of the bis-anilines, ODA, MDA, TDA were 0.009-0.050, 0.3-2.0 and 0.085-0.250 U/mL, respectively. TDA was run both

under stressed as well as with optimum H_2O_2 concentrations. MDA was also studied with limited H_2O_2 concentration and it demanded higher SBP concentration for 95% removal. This resulted in higher demand of H_2O_2 , as seen in Fig. 4.16. The results showed that 0.04, 0.70 and 0.15 U/mL of enzyme were needed to remove $\geq 95\%$ ODA, MDA and TDA, respectively, in Figs. 4.15, 4.16 and 4.17. In Fig. 4.15, for 0.6 mM H_2O_2 , a significant change was observed in the region of 0.009-0.025 U/mL of enzyme, and negligible change occurred between 0.025-0.050 U/mL. The minimum SBP concentrations required can be qualitatively compared with 0.002, 0.010, and 0.005 U/mL of SBP for 1.0 mM phenylenediamines (*o*-, *m*- and *p*-) (Mousa Al-Ansari *et al.* 2009), respectively. Also, an important observation in Fig. 4.15 was that as the concentration of H_2O_2 was increased to 0.75 mM the percent conversion of ODA for 95% removal become worse. This could be due to SBP inactivation caused due to excess H_2O_2 (Arnao *et al.* 1990; Baynton *et al.* 1994). For MDA, Fig 4.16, with 0.7 mM H_2O_2 a significant change in the percent conversion was seen in SBP concentration range between 0.3-0.5 U/mL, while increasing the SBP concentrations beyond 0.8 U/mL made no significant change in the conversion. When the stress conditions of H_2O_2 , 0.45 and 0.50 mM were used for TDA, Fig. 4.17, there was no substantial change in the percent conversion of the substrate by SBP in the range 0.10-0.25 U/mL. However, increasing the H_2O_2 concentration to the optimum condition, 0.55 mM leads to a significant change in the percent conversion of TDA over the same SBP range.

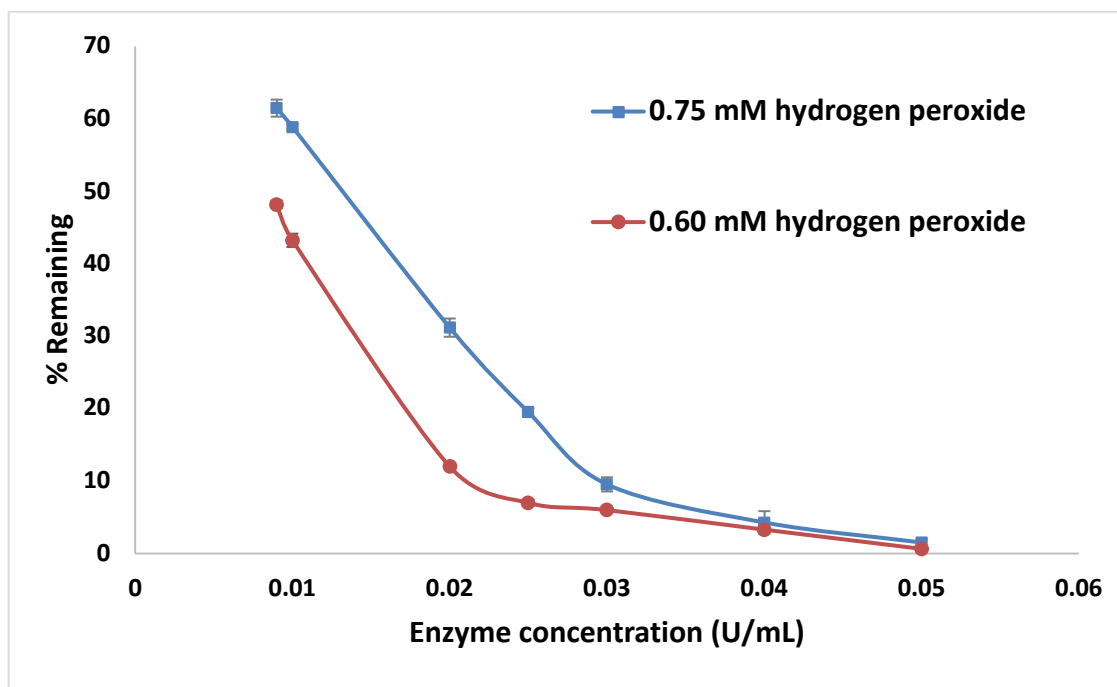


Figure 4.15. SBP optimisation for the removal of ODA. Conditions: 0.5 mM ODA; 0.60 and 0.75 mM hydrogen peroxide; 40 mM pH 6.0 buffer; and 3-h reaction.

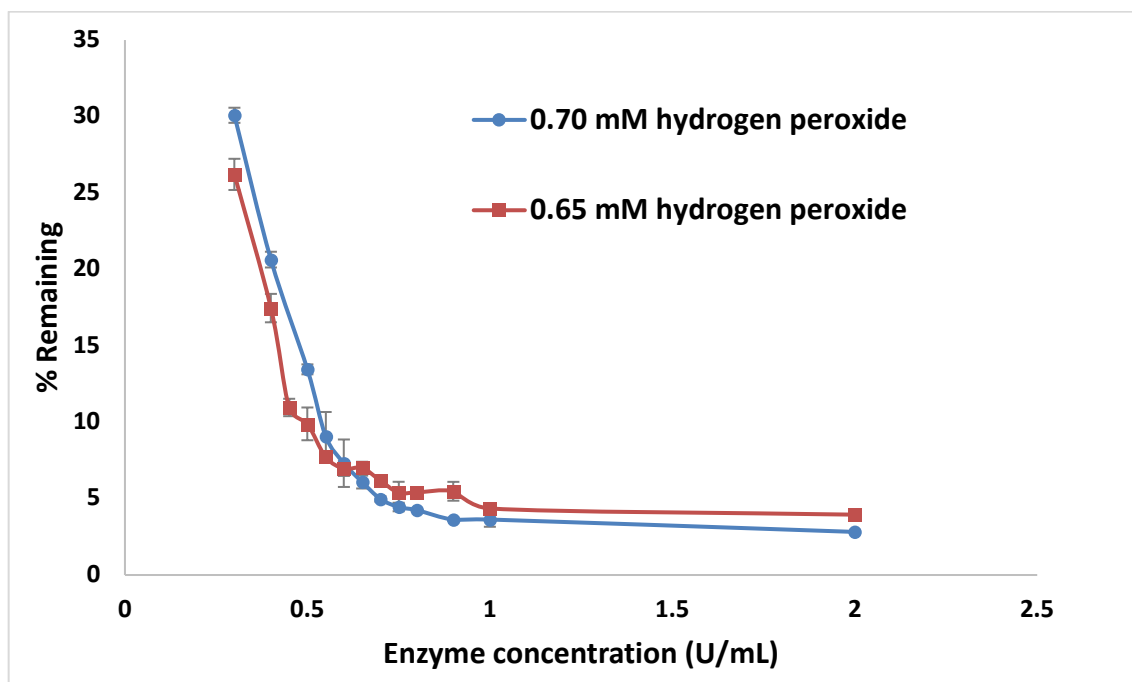


Figure 4.16. SBP optimisation for the removal of MDA. Conditions: 0.5 mM MDA; 0.65 and 0.70 mM hydrogen peroxide; 40 mM pH 6.0 buffer; and 3-h reaction.

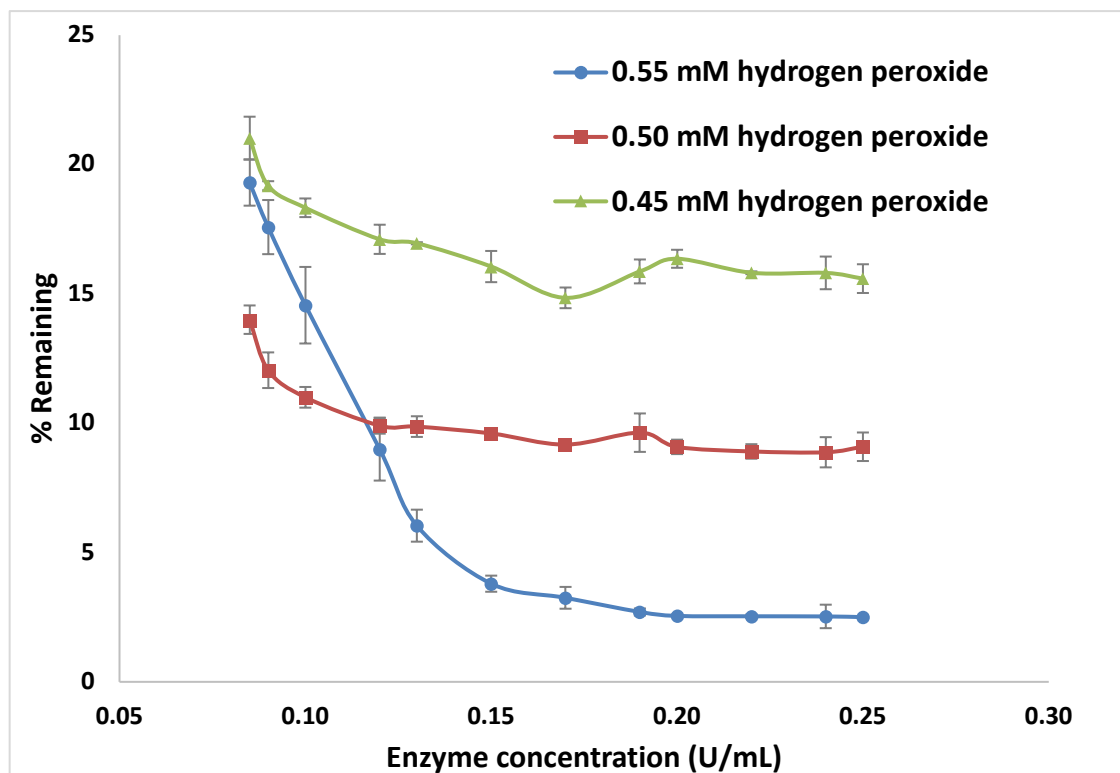


Figure 4.17. SBP optimisation for the removal of TDA. Conditions: 0.5 mM TDA; 0.45, 0.50 and 0.55 mM hydrogen peroxide; 40 mM pH 6.0 buffer; and 3-h reaction.

MOCA, also a bi-functional anilino compound, enzyme concentration was varied at the established optimal pH and H₂O₂ so as to achieve $\geq 95\%$ conversion of 0.1 mM of MOCA. Figure 4.18 shows that MOCA required 0.1 U/mL of enzyme. There was not much change in the removal efficiency of the substrate when the SBP concentration was increased beyond 0.1 U/mL. This SBP requirement may be qualitatively compared with that observed during SBP optimization using 0.1 mM of benzidine where the changes occurred at 0.43×10^{-3} U/mL of SBP (Malik Altahir *et al.* 2015).

During comparison of the quantity of enzyme requirement for 95% removal of the monocyclic anilines (*p*-cresidine, 4-COT) and the atom-bridged bis-anilines (ODA, MDA, TDA), except MOCA, it is to be noted that important structural analysis was performed. *p*-Cresidine and 4-COT consist of one anilino group, whereas ODA, MDA and TDA consist

of two anilines as a functional group on their respective structures. Therefore, the concentrations of substrate that were to be removed by the enzyme were equivalent, which helps us to differentiate them based on SBP requirement. Thus, ODA needed four times more enzyme based on per anilino functional group than *p*-cresidine and 4-COT for 95% conversion of the substrate. Among all the substrates, MDA required the highest SBP concentration of 0.7 U/mL while 4-COT required the lowest (0.009 U/mL) for $\geq 95\%$ removal. The optimized parameters for the removal of each of the chemicals are summarized in Table 4.1.

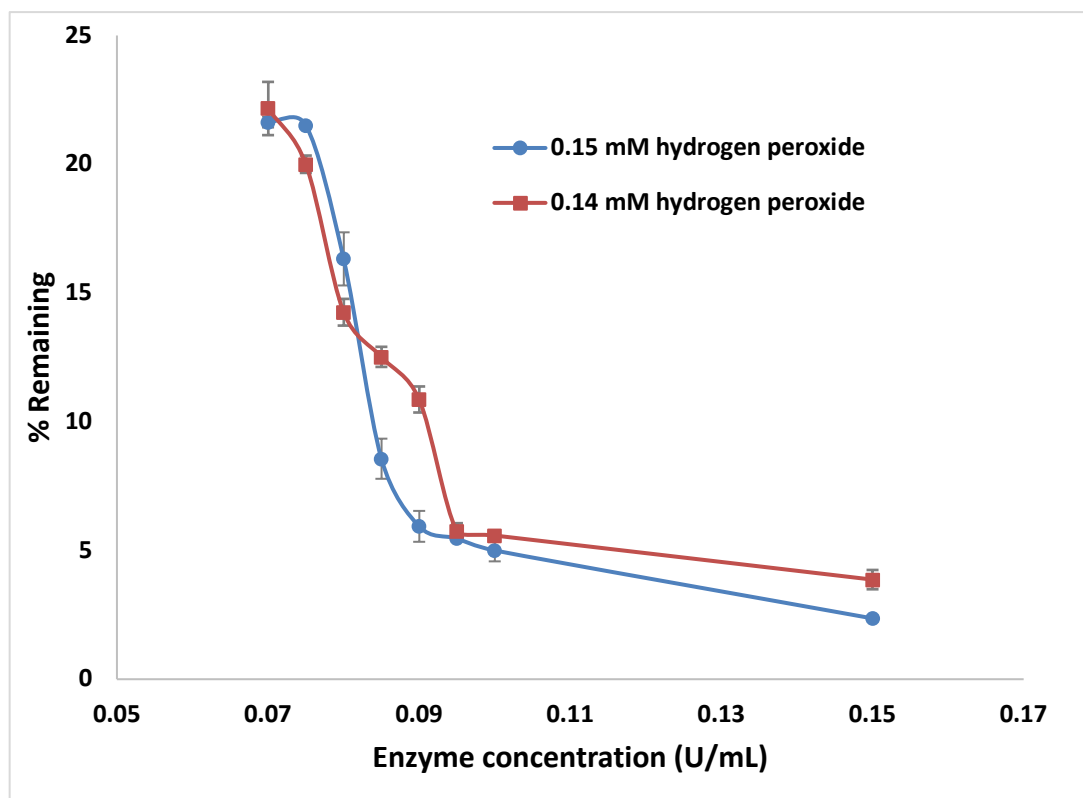


Figure 4.18. SBP optimisation for the removal of MOCA. Conditions: 0.1 mM MOCA; 0.14 and 0.15 mM hydrogen peroxide; 40 mM pH 4.2 buffer; and 3-h reaction.

Table 4.1. List of the optimized parameters of the chemicals.

Compound	Substrate concentration (mM)	Optimized parameters		
		pH	H ₂ O ₂ (mM)	SBP (U/mL)
<i>p</i> -Cresidine	1.0	4.6	1.25	0.010
4-COT	1.0	4.4	0.50	0.009
ODA	0.5	6.0	0.60	0.040
MDA	0.5	6.0	0.70	0.700
TDA	0.5	6.0	0.55	0.150
MOCA	0.1	4.2	0.15	0.100

4.4. Time Course of Reactions

The reaction time chosen for these studies was 3 hours, which was an arbitrary time period used to compare enzymes and substrates being studied. Reaction time is considered one of the main and vital parameters when designing a treatment plant because it directly relates to the reactor size, which is one of the major economic limitations. Since retention time of a reactor dictates the reactor volume, it is useful to know the minimum time needed for ≥ 95 % conversion of the aromatic pollutants. Substrate consumption was monitored with respect to time interval using batch reactors run under optimal operating conditions as established in Sections 4.1 to 4.3. Aliquots withdrawn at various time intervals were quenched with catalase then micro-filtered and analysed by HPLC. The rate constants and half-lives were derived from the plots. Half-life of a substrate is the time at which the substrate concentrations decreases to half of the original concentration, and can be calculated using the first-order reaction model. The half-life ($t_{0.5}$) for all substrates were calculated using the following relationship:

$$t_{0.5} = \frac{0.693}{k} \quad (20)$$

where, k is the first-order rate constant. As seen in Fig. 4.19 (*p*-cresidine), Fig. 4.20 (4-COT), Fig. 4.21 (ODA), Fig.4.22 (MDA), Fig.4.23 (TDA) and Fig. 4.24 (MOCA), SBP's

catalytic reaction proceeded rapidly at the start and then it slowed down. The removal of all the substrates by SBP were fitted as a first-order process to the initial part of the progress curves. The rate constants and their half-lives were normalized with their respective enzyme activities for comparison. Table 4.2 summarizes the rate constants and half-lives for the substrates as determined from the progress curves along with their corresponding normalized values. As seen in the table, the reaction of ODA progressed the fastest with k being 9.63 ± 0.5 /min, and the slowest rate was observed for MOCA ($k = 1.70 \pm 0.22$ /min). Accordingly, the $t_{0.5}$ for ODA was the lowest at 0.072 ± 0.0006 min, whereas MOCA had the highest $t_{0.5}$ (0.4076 ± 0.002 min). Based on the normalized rate constant values, the ranking of the substrates was done from fastest to slowest reaction rates as: ODA > TDA > 4-COT > *p*-cresidine > MDA > MOCA (Table 4.2).

Table 4.2. List of rate constants and half-lives of the compounds as determined from the time course experiments.

Compound	Rate constant, k (/min)	Half-life, $t_{0.5}$ (min)	Normalized rate constant, k (/min)	Normalized half-life, $t_{0.5}$ (min)
<i>p</i> -Cresidine	0.0562 ± 0.013	12.40 ± 0.009	5.62 ± 1.3	0.124 ± 0.0001
4-COT	0.0601 ± 0.0002	11.5 ± 0.0001	6.68 ± 0.02	0.1035 ± 0.00001
ODA	0.385 ± 0.02	1.80 ± 0.02	9.63 ± 0.5	0.072 ± 0.0006
MDA	1.20 ± 0.15	0.578 ± 0.1	1.72 ± 0.2	0.4046 ± 0.07
TDA	1.35 ± 0.01	0.513 ± 0.007	9.00 ± 0.06	0.0770 ± 0.001
MOCA	0.170 ± 0.022	4.076 ± 0.02	1.70 ± 0.22	0.4076 ± 0.002

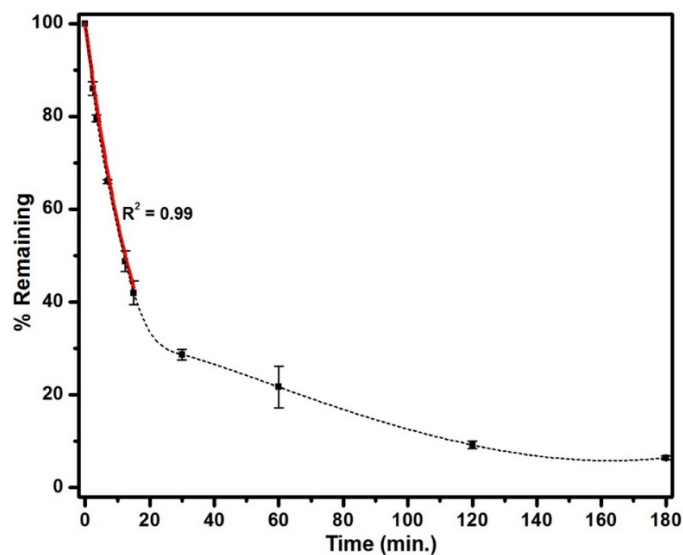


Figure 4.19. *p*-Cresidine removal with respect to time. Optimal conditions: 1.0 mM *p*-cresidine; 40 mM pH 4.6 buffer; 1.25 mM hydrogen peroxide; and 0.01 U/mL SBP. The solid line drawn is from direct fitting by non-linear regression of the first 15 minute's data using the first-order decay model, percentage remaining = (initial percentage) e^{-kt} , where $k = 0.0562 \pm 0.013 \text{ min}^{-1}$, is the apparent first-order rate constant, initial percentage = $100.0 \pm 0.2\%$. The dashed line represents smooth interpolation from point-to-point with no mechanistic assumptions.

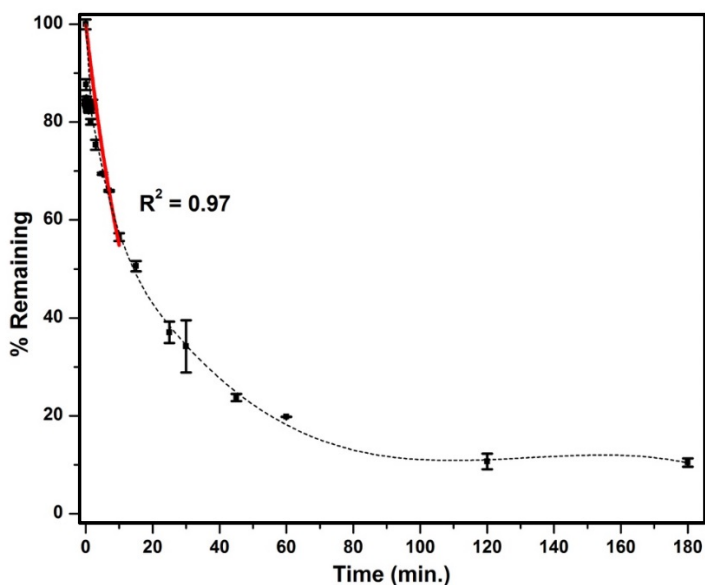


Figure 4.20. 4-COT removal with respect to time. Optimal conditions: 1.0 mM 4-COT; 40 mM pH 4.4 buffer; 0.5 mM hydrogen peroxide; and 0.009 U/mL SBP. The solid line drawn is from direct fitting by non-linear regression of the first 10 minute's data using the first-order decay model, percentage remaining = (initial percentage) e^{-kt} , where $k = 0.06010 \pm 0.0002 \text{ min}^{-1}$, is the apparent first-order rate constant, initial percentage = $100.0 \pm 0.5\%$. The dashed line represents smooth interpolation from point-to-point with no mechanistic assumptions.

There could be several reasons for the fast-catalytic reaction observed at the beginning, such as, competitive conversion of dimers and higher oligomers and/or enzyme inactivation caused by the reactive radicals or end-product oligomers (Nakamoto and Machida 1992; Mousa Al-Ansari *et al.* 2009; Malik Altahir *et al.* 2015; Feng *et al.* 2013; Wu *et al.* 1998). The rate of the reaction must be directly proportional to the active concentration of the enzyme (Dunford 1999; Mousa Al-Ansari *et al.* 2009), hence, the reaction will imperceptibly slow down as the activity of the enzyme loses over the time course.

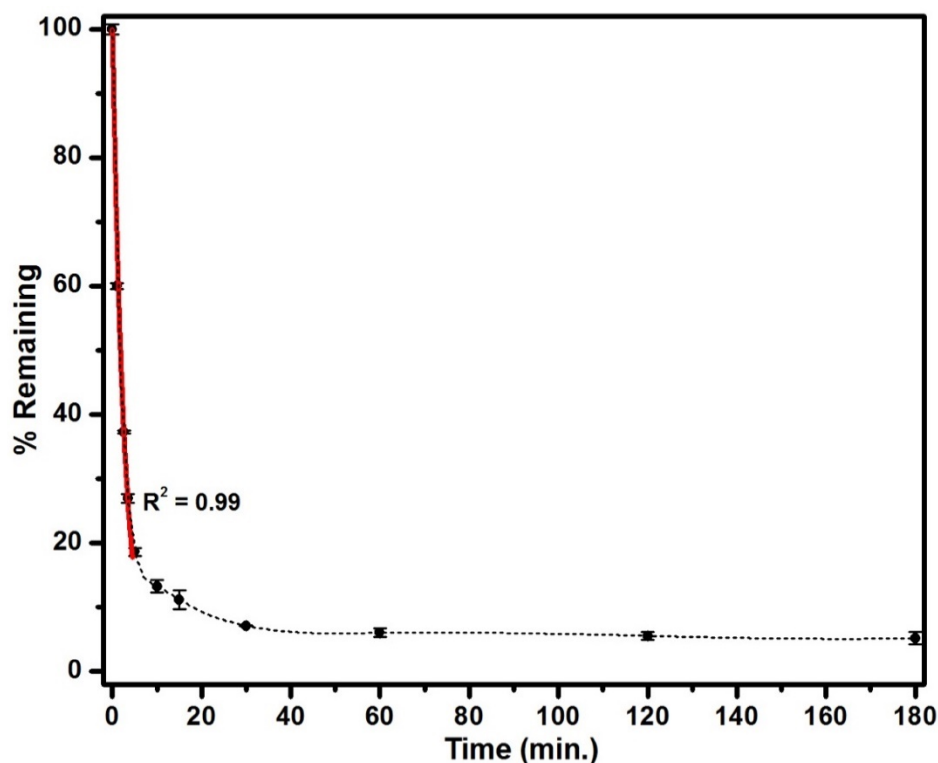


Figure 4.21. ODA removal with respect to time. Optimal conditions: 0.5 mM ODA; 40 mM pH 6.0 buffer; 0.6 mM hydrogen peroxide; and 0.04 U/mL SBP. The solid line drawn is from direct fitting by non-linear regression of the first 5 minute's data using the first-order decay model, percentage remaining = (initial percentage) e^{-kt} , where $k = 0.385 \pm 0.02 \text{ min}^{-1}$, is the apparent first-order rate constant, initial percentage = $100.0 \pm 0.7\%$. The dashed line represents smooth interpolation from point-to-point with no mechanistic assumptions.

Previous studies with 0.1 mM benzidine treated with SBP showed an estimated rate constant, k of 0.039 min^{-1} (Malik Altahir *et al.* 2015). A similar trend was also observed in previous research where, approximately 65-95% of the phenylenediamines were converted during the first 15 min of the reaction when treated with SBP and then the rate of reaction declined (Mousa Al-Ansari *et al.* 2009).

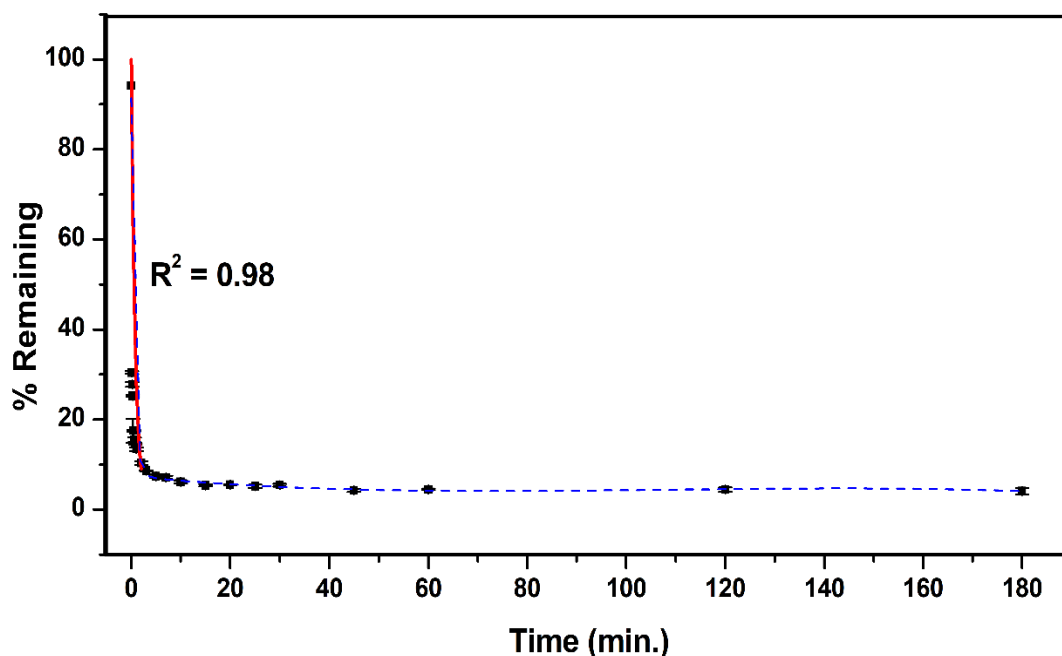


Figure 4.22. MDA removal with respect to time. Optimal conditions: 0.5 mM MDA; 40 mM pH 6.0 buffer; 0.7 mM hydrogen peroxide; and 0.7 U/mL SBP. The solid line drawn is from direct fitting by non-linear regression of the first 2 minute's data using the first-order decay model, percentage remaining = (initial percentage) e^{-kt} , where $k = 1.20 \pm 0.15 \text{ min}^{-1}$, is the apparent first-order rate constant, initial percentage = $100.0 \pm 0.2\%$. The dashed line represents smooth interpolation from point-to-point with no mechanistic assumptions.

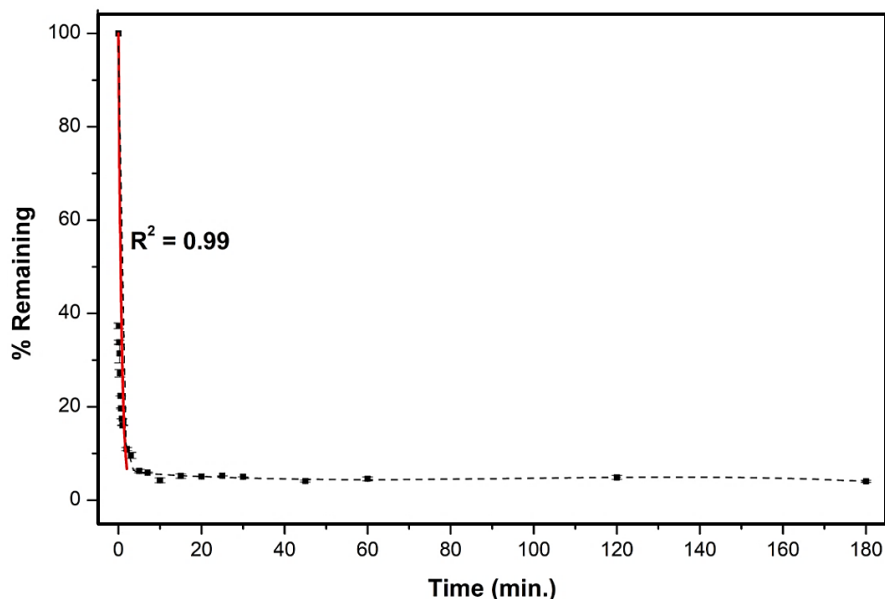


Figure 4.23. TDA removal with respect to time. Optimal conditions: 0.5 mM TDA; 40 mM pH 6.0 buffer; 0.55 mM hydrogen peroxide; and 0.15 U/mL SBP. The solid line drawn is from direct fitting by non-linear regression of the first 2 minute's data using the first-order decay model, percentage remaining = (initial percentage) e^{-kt} , where $k = 1.35 \pm 0.01 \text{ min}^{-1}$, is the apparent first-order rate constant, initial percentage = $100.0 \pm 0.2\%$. The dashed line represents smooth interpolation from point-to-point with no mechanistic assumptions.

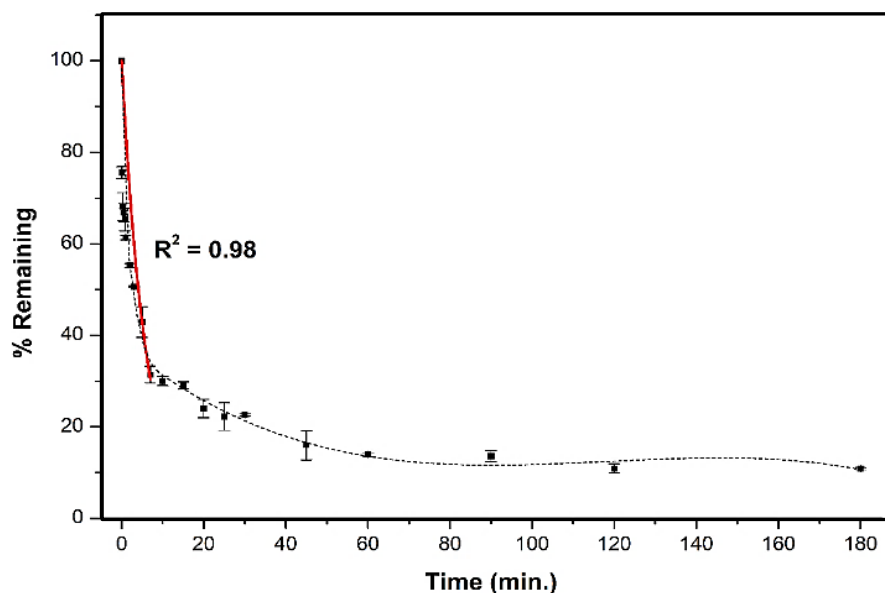


Figure 4.24. MOCA removal with respect to time. Optimal conditions: 0.1 mM MOCA; 40 mM pH 4.2 buffer; 0.15 mM hydrogen peroxide; and 0.1 U/mL SBP. The solid red line drawn is from direct fitting by non-linear regression of the first 7 minute's data using the first-order decay model, percentage remaining = (initial percentage) e^{-kt} , where $k = 0.170 \pm 0.022 \text{ min}^{-1}$, is the apparent first-order rate constant, initial percentage = $100.0 \pm 0.2\%$. The dashed line represents smooth interpolation from point-to-point with no mechanistic assumptions.

4.5. Kinetics

During consideration of reactor design constraints, kinetic parameters are usually an asset in giving a guide to the general affinity and reactivity that a particular enzyme may have for various substrates. Generally, in the reactors there are a series of competing reactions which make the analysis difficult. The Michaelis constant, K_M , equivalent to the dissociation constant, is an indicator of the affinity of enzyme for a substrate (lower value means higher affinity, better recognition). Also, higher the V_{max} , faster is the reaction. The quotient, V_{max}/K_M , known as catalytic efficiency combines both affinity and reactivity. The catalytic efficiency was further normalized by the respective enzyme activities of the substrates.

Initial rates were determined from the second-order polynomial fits obtained by plotting the initial substrate concentration versus time in Fig. 4.25 (*p*-cresidine), Fig. 4.27 (4-COT), Fig. 4.29 (ODA), Fig. 4.31 (MDA), Fig. 4.33 (TDA) and Fig. 4.35 (MOCA). The initial rates of the reaction taken from the first-power coefficients, were plotted against the initial substrate concentration in the Michaelis-Menten model (M-M), Eq.11, in Fig. 4.26 (*p*-cresidine), Fig. 4.28 (4-COT), Fig. 4.30 (ODA), Fig. 4.32 (MDA), Fig. 4.34 (TDA) and Fig. 4.36 (MOCA) to obtain the apparent kinetic parameters K_M and V_{max} using Origin 8.0. Reactions were formulated with 40 mM buffer at the optimum *pH* values obtained in Section 4.1. The substrate concentrations were varied while maintaining H_2O_2 and SBP concentrations constant. Reactions were stopped each time at intervals of 30 s, for a total period of 180 s, by quenching with catalase. It was then micro-filtered and analyzed for residual substrate concentrations by UV-VIS at their respective wavelength maxima as discussed in Section 4.1. The desired M-M parameters are shown in Table 4.3.

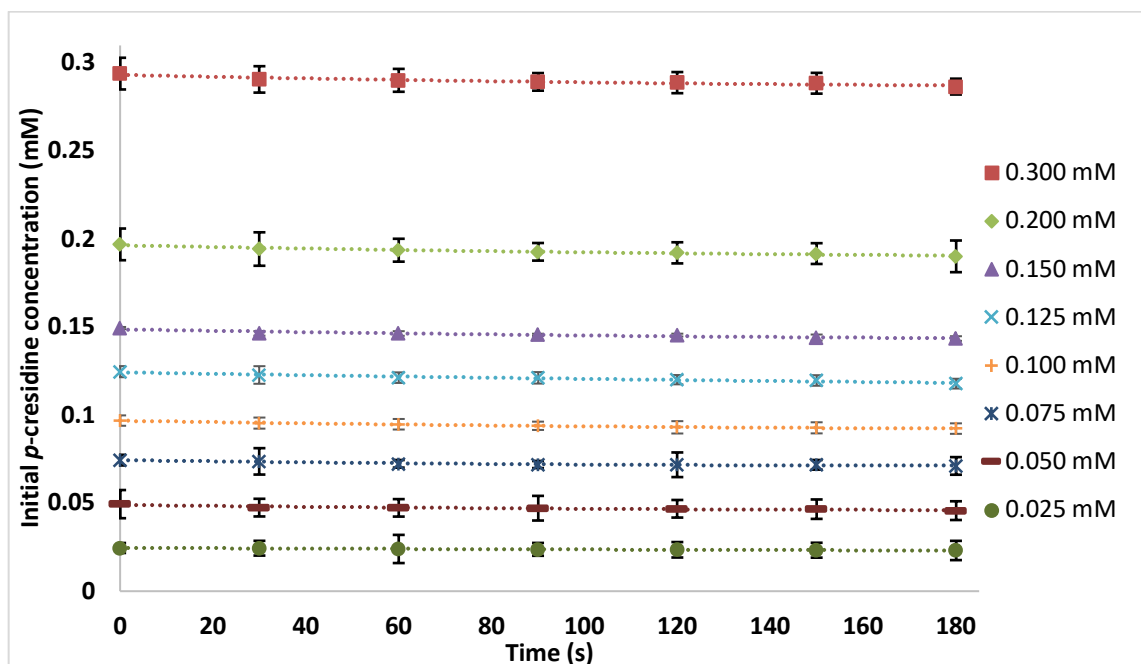


Figure 4.25. Initial velocities for *p*-cresidine. Conditions: 0.0006 U/mL SBP; 40 mM pH 4.6 buffer; 0.1 mM hydrogen peroxide; and wavelength at 287 nm. Second-order polynomial fits had $R^2 \geq 0.95$.

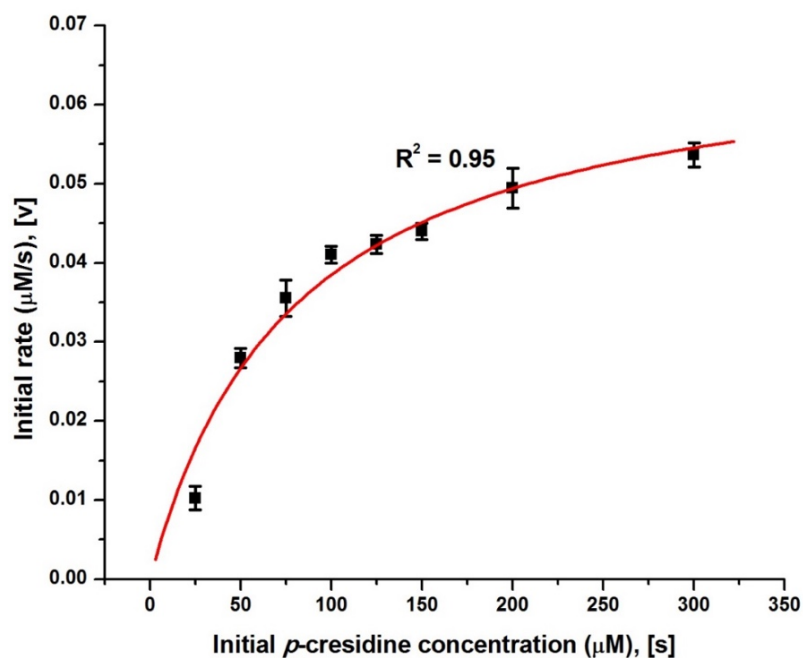


Figure 4.26. Michaelis-Menten plot for *p*-cresidine. Data from Figure 4.25. Calculated $K_M = 79.1 \pm 1.0$ (μM), $V_{\max} = 0.0690 \pm 0.006$ ($\mu\text{M/s}$). Conditions: 0.0006 U/mL SBP; 40 mM pH 4.6 buffer; 0.1 mM hydrogen peroxide; and wavelength at 287 nm.

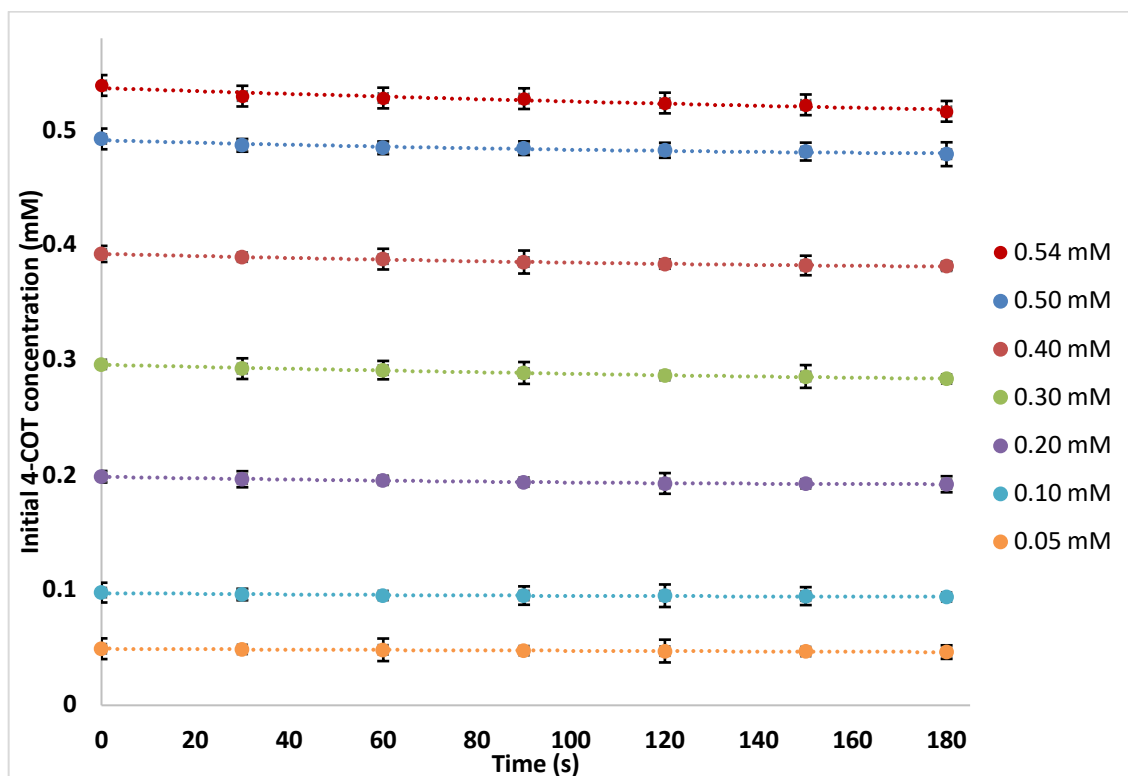


Figure 4.27. Initial velocities for 4-COT. Conditions: 0.0006 U/mL SBP; 40 mM pH 4.4 buffer; 0.1 mM hydrogen peroxide; and wavelength at 290 nm. Second-order polynomial fits had $R^2 \geq 0.96$.

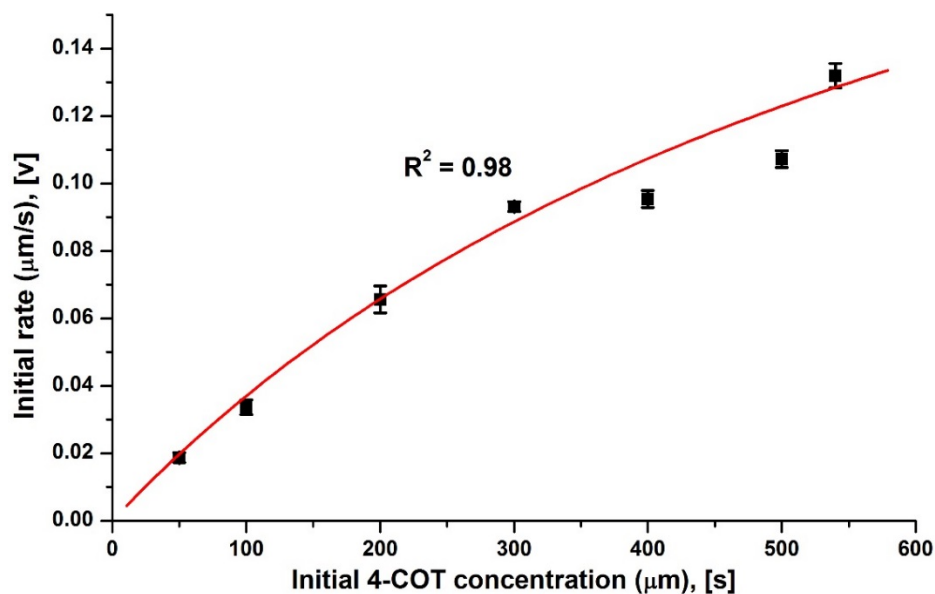


Figure 4.28. Michaelis-Menten plot for 4-COT. Data from Figure 4.27. Calculated $K_M = 691.0 \pm 53.0$ (μM), $V_{\max} = 0.293 \pm 0.070$ ($\mu\text{M/s}$). Conditions: 0.0006 U/mL SBP; 40 mM pH 4.4 buffer; 0.1 mM hydrogen peroxide; and wavelength at 290 nm.

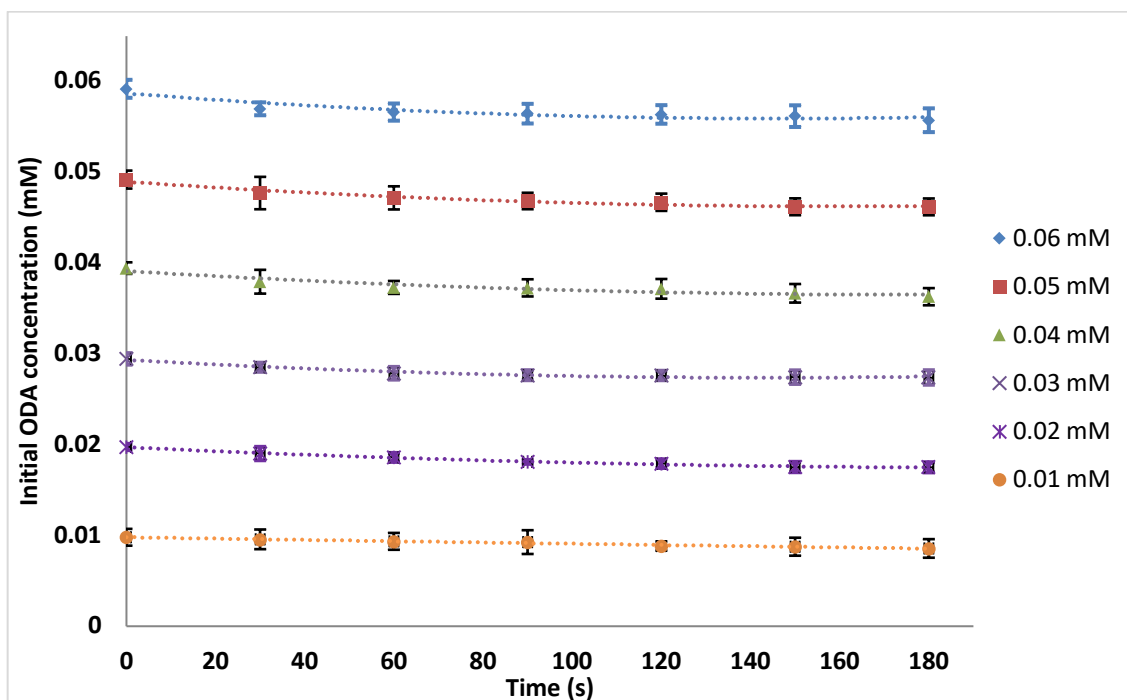


Figure 4.29. Initial velocities for ODA. Conditions: 0.0002 U/mL SBP; 40 mM pH 6.0 buffer; 0.6 mM hydrogen peroxide; and wavelength at 293 nm. Second-order polynomial fits had $R^2 \geq 0.95$.

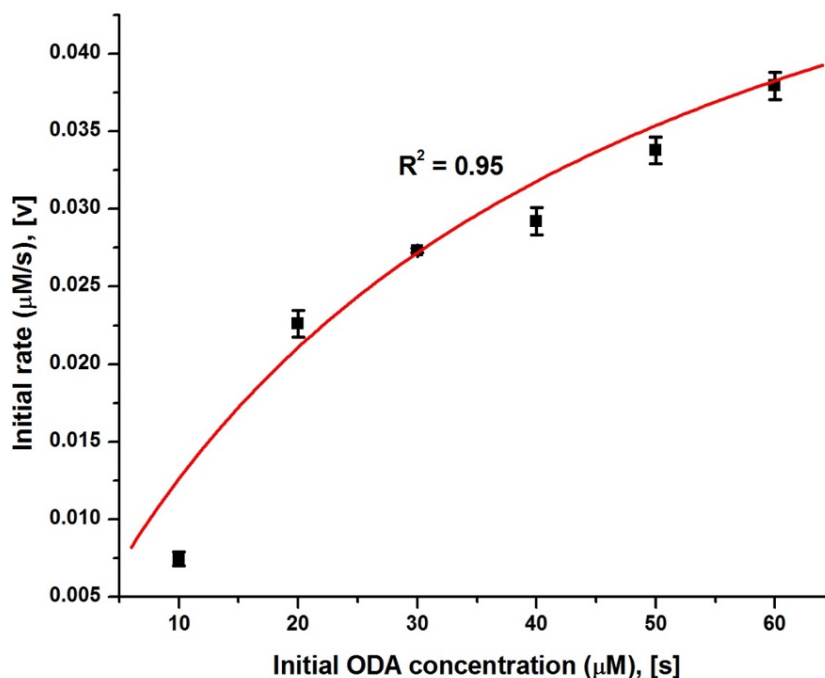


Figure 4.30. Michaelis-Menten plot for ODA. Data from Figure 4.29. Calculated $K_M = 41.5 \pm 5.8$ (μM), $V_{\max} = 0.0647 \pm 0.010$ ($\mu\text{M/s}$). Conditions: 0.0002 U/mL SBP; 40 mM pH 6.0 buffer; 0.6 mM hydrogen peroxide; and wavelength at 293 nm.

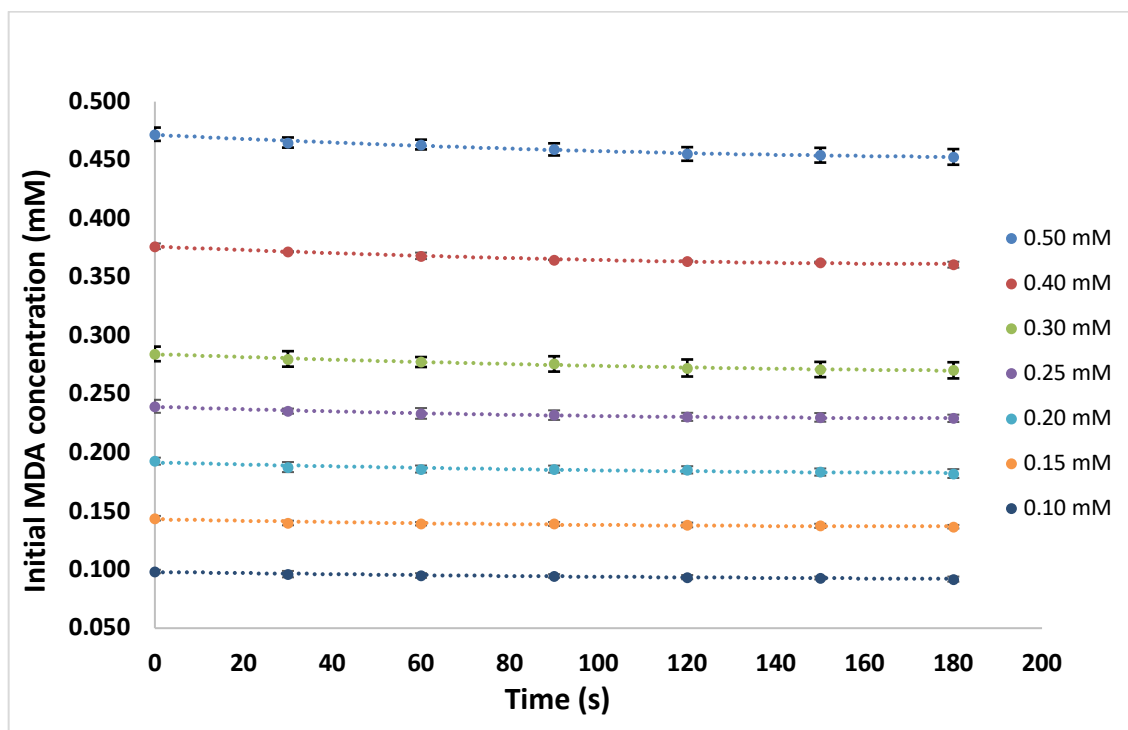


Figure 4.31. Initial velocities for MDA. Conditions: 0.01 U/mL SBP; 40 mM pH 6.0 buffer; 0.1 mM hydrogen peroxide; and wavelength at 285 nm. Second-order polynomial fits had $R^2 \geq 0.97$.

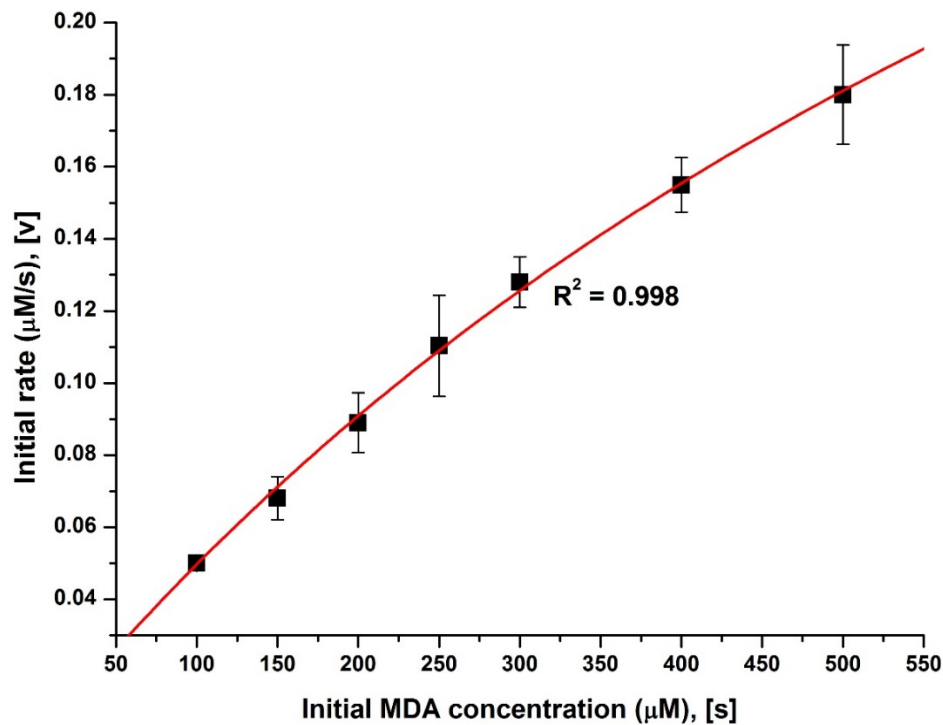


Figure 4.32. Michaelis-Menten plot for MDA. Data from Figure 4.31. Calculated $K_M = 979.0 \pm 80.0$ (μM), $V_{\max} = 0.536 \pm 0.030$ ($\mu\text{M/s}$). Conditions: 0.01 U/mL SBP; 40 mM pH 6.0 buffer; 0.1 mM hydrogen peroxide; and wavelength at 285 nm.

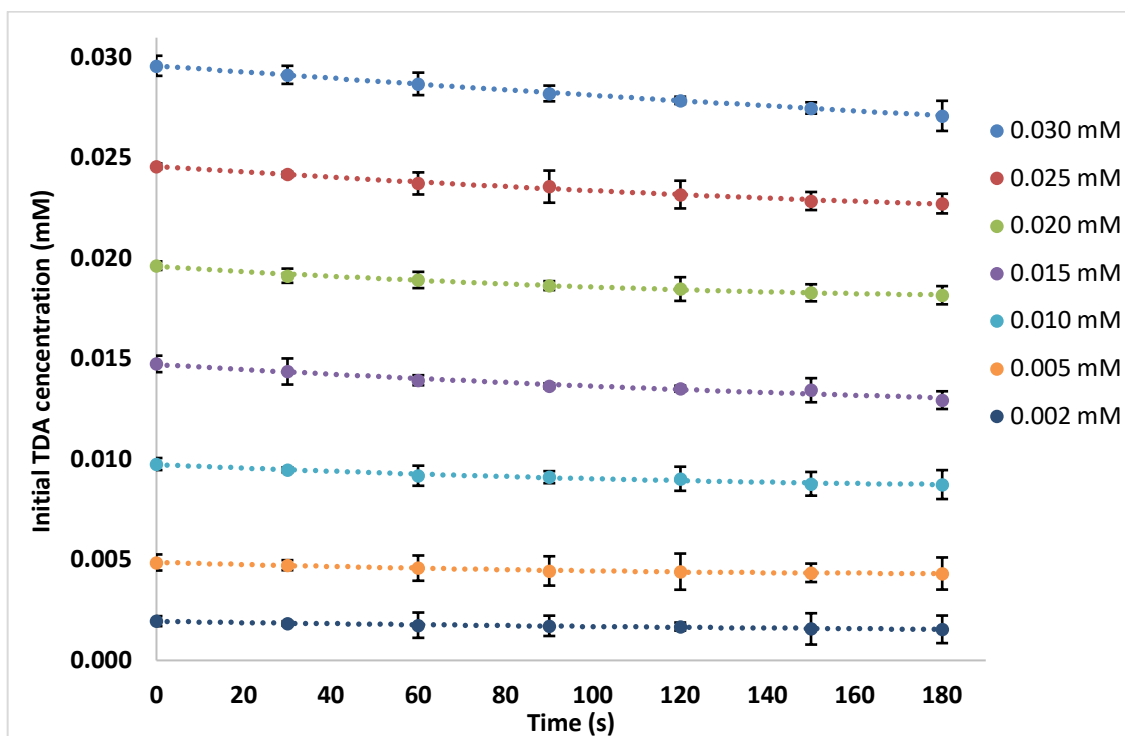


Figure 4.33. Initial velocities for TDA. Conditions: 0.00009 U/mL SBP; 40 mM pH 6.0 buffer; 0.55 mM hydrogen peroxide; and wavelength at 260 nm. Second-order polynomial fits had $R^2 \geq 0.96$.

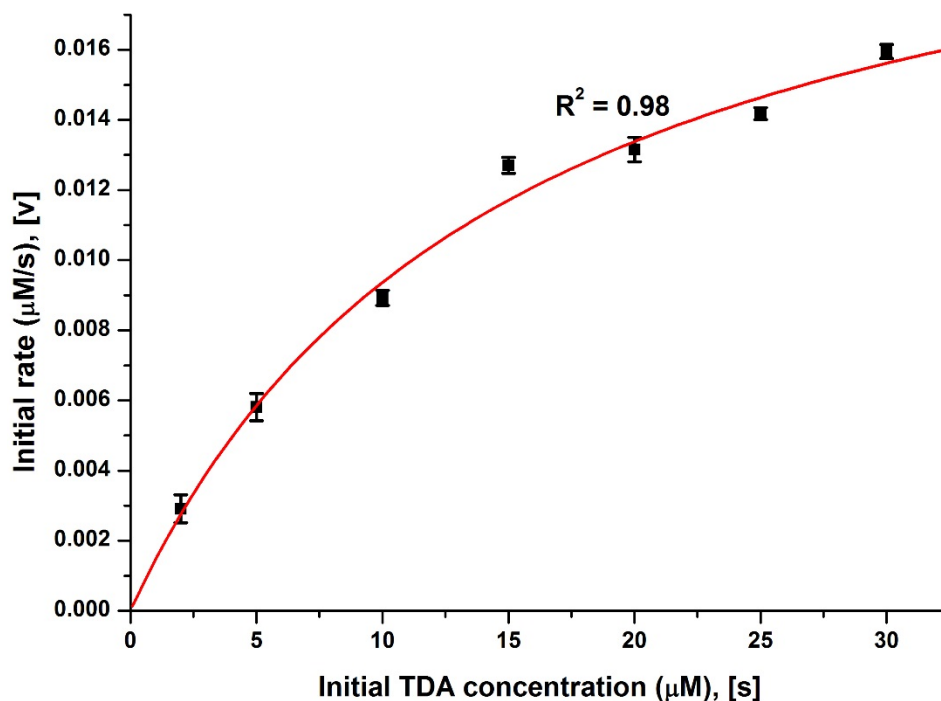


Figure 4.34. Michaelis-Menten plot for TDA. Data from Figure 4.33. Calculated $K_M = 15.02 \pm 3.0$ (μM), $V_{\max} = 0.0234 \pm 0.002$ ($\mu\text{M/s}$). Conditions: 0.00009 U/mL SBP; 40 mM pH 6.0 buffer; 0.55 mM hydrogen peroxide; and wavelength at 260 nm.

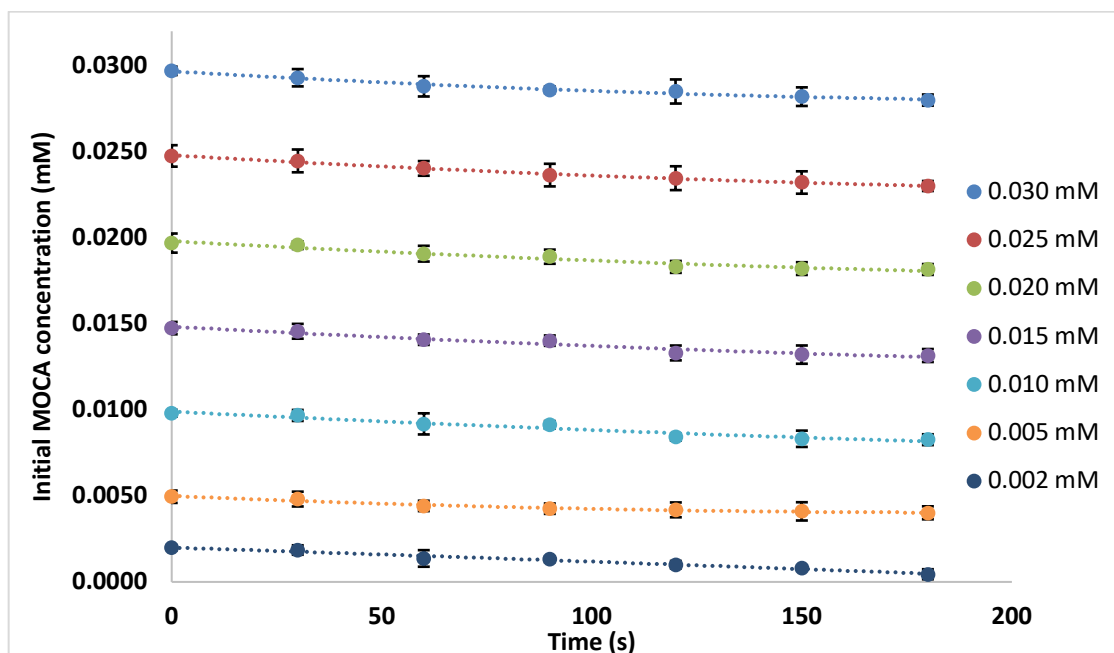


Figure 4.35. Initial velocities for MOCA. Conditions: 0.0002 U/mL SBP; 40 mM pH 4.2 buffer; 0.1 mM hydrogen peroxide; and wavelength at 291 nm. Second-order polynomial fits had $R^2 \geq 0.96$.

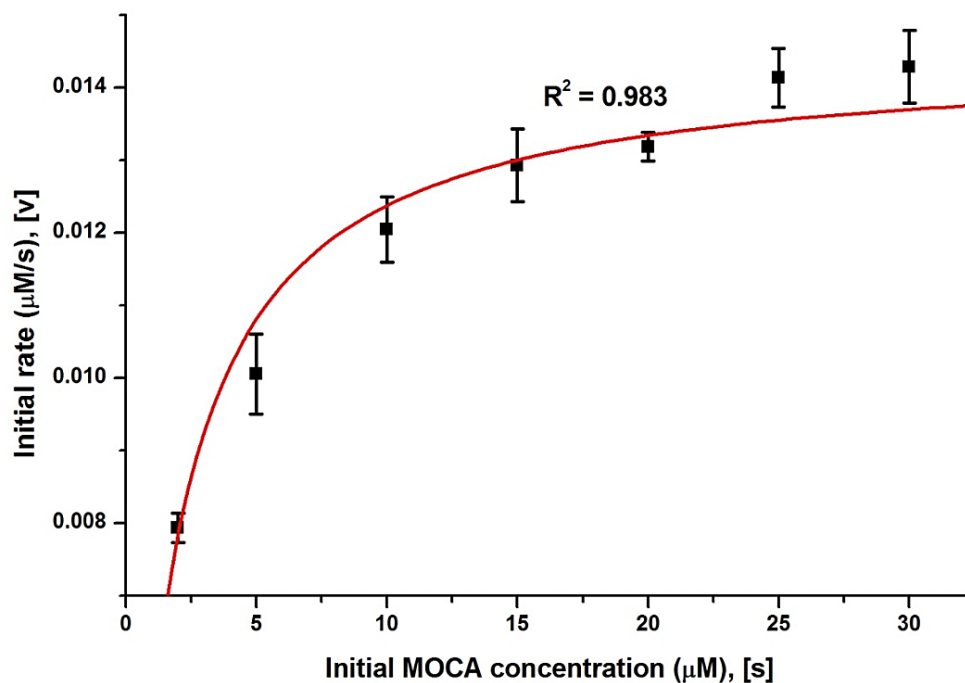


Figure 4.36. Michaelis-Menten plot for MOCA. Data from Figure 4.35. Calculated $K_M = 1.70 \pm 0.14$ (μM), $V_{\max} = 0.0145 \pm 0.0004$ ($\mu\text{M/s}$). Conditions: 0.0002 U/mL SBP; 40 mM pH 4.2 buffer; 0.1 mM hydrogen peroxide; and wavelength at 291 nm.

Table 4.3. List of the determined values of the Michaelis constant (K_M), the normalized maximum velocity (V_{max}), the catalytic efficiency (V_{max}/K_M) and the normalized V_{max}/K_M values for all compounds.

Compound	Michaelis constant, K_M (μM)	Normalized maximum velocity, V_{max} ($\mu M/s$)	Catalytic efficiency, V_{max}/K_M (/s)	Normalized catalytic efficiency, V_{max}/K_M (/s)
<i>p</i> -Cresidine	79.1 \pm 1.0	115 \pm 10	0.000872 \pm 0.00001	1.45 \pm 0.145
4-COT	691.0 \pm 53.0	488 \pm 116	0.000424 \pm 0.0001	0.7066 \pm 0.223
ODA	41.5 \pm 5.8	323.5 \pm 50	0.00156 \pm 0.0005	7.80 \pm 2.29
MDA	979.0 \pm 80.0	53.6 \pm 3.0	0.000548 \pm 0.00008	0.055 \pm 0.008
TDA	15.02 \pm 3.0	260 \pm 22.2	0.00156 \pm 0.0004	17.3 \pm 4.95
MOCA	1.70 \pm 0.14	72.5 \pm 2.0	0.00855 \pm 0.0009	42.8 \pm 4.71

By comparing the K_M values for all the aromatic pollutants from the M-M model as shown in Table 4.3, it can be seen that MOCA has the lowest K_M , 1.70 \pm 0.14 μM , followed by TDA < ODA < *p*-cresidine < 4-COT < MDA; MDA had the highest K_M of 979.0 \pm 80.0 μM . By normalizing these with the respective enzyme activities, it was observed that 4-COT had the maximum velocity of 488 \pm 116 $\mu M/s$ followed by ODA > TDA > *p*-cresidine > MOCA > MDA. The MDA showed the slowest reaction rate of 53.6 \pm 3.0 $\mu M/s$ among all. MOCA displayed the highest normalized catalytic efficiency as 42.8 \pm 4.71 /s and MDA the minimum (0.055 \pm 0.008 /s) as shown in Table 4.3.

A previous study with crude laccase, from *C. unicolor* with substrate Reactive Blue 81, showed the kinetic constant K_M of 79 μM (Michniewicz *et al.* 2008). In another study, *p*-cresol, catalyzed by multi-walled carbon nanotubes-SBP, followed the classical M-M model. It had K_M of 7.2 \pm 0.8 mM (Asuri *et al.* 2006). Bhunia *et al.* (2001) determined the kinetic parameters for dye, Remazol Blue with HRP and the K_M value was 0.04 mmol L⁻¹. They also determined the kinetic constants for another dye, Crystal Violet, and its K_M value was nearly five-fold lower than the preceding one, concluding that enzyme binding may

be superior for the latter substrate. The activities of aniline dioxygenase, catechol 2,3-dioxygenase and other enzymes involved in degradation of aniline were determined by Liu *et al.* (2002). The K_M of aniline dioxygenase and catechol 2,3-dioxygenase for catechol were 0.290 and 0.016 mM, respectively. Kinetic parameters were also obtained in a previous work on the treatment of cresols (*o*-, *m*- and *p*-) treated with laccase where the K_M values were determined as 1.144, 201.702 and 2.258 mM, respectively (Steevensz 2008). Similarly, removal of azo-dyes with SBP investigated by Cordova Villegas (2017) showed that the K_M values for substrates COG, AB113 and DB38 were 4.7, 21 and 36 μ M, respectively.

4.6. Analyses of Mass Spectrometry (MS) Results

The MS analysis was done by the ESI technique in positive-ion full-scan mode for all compounds, except for 4-COT, which was analyzed by the ASAP technique because the peak signals were weak in the ESI technique. Enzymatic reactions were conducted for 3 hours at the previously established optimal conditions (Table 4.1) for *p*-cresidine, 4-COT, ODA, MDA, TDA, and MOCA. Mass spectra were taken of standards, treated samples (both supernatants and precipitates) and blanks. Spectral mass-to-charge (m/z) ratios were matched to molecular formulae within 5 ppm by the MassLynx software.

The enzymatic reaction produces substrate free radicals and the stable products are the results of radical coupling. During coupling of resonance-stabilized anilinium cation-radical, coupling can occur as N-C, C-C and N-N with *ortho*- and *para*-orientation. N-N coupling forms a hydrazine and there is some literature evidence that these readily oxidize to form azo-compounds (ATSDR 2009; Zhu and Shi 2013). The products generally observed in this section were in the form of oxidative dimers and trimers that might be further oxidized, deaminated, dechlorinated and/or oxygenated. Occasionally m/z peaks in

the MS were observed for standard molecular ions and product molecular ions, but most commonly these were protonated. Symbolism has been used to denote structures as follows: M, standard (as its radical cation); MH, protonated standard; ^{13}C -MH, protonated natural abundance ^{13}C -isomer of standard; ^{37}Cl -MH, protonated natural abundance ^{37}Cl -isomer of standard; ^{34}S -MH, protonated natural abundance of ^{34}S -isomer of standard; $\text{M}_2\text{H}-2$, protonated oxidative dimer; $\text{M}_2\text{H}-4$, protonated oxidized oxidative dimer (most commonly, an azo-dimer). Deamination, dechlorination and oxygenation are denoted here by -NH, -Cl and +O, respectively. Thus, $\text{M}_3\text{H}-4\text{-NH-Cl+O}$ denotes an oxidative trimer that was deaminated, dechlorinated and oxygenated. If one of the couplings were oxidized to an azo-link, the same product would be denoted $\text{M}_3\text{H}-6\text{-NH-Cl+O}$; the same syntax will be used for all proposed structures.

The m/z value of 138.0917 in Fig. 4.37 shows the mass spectrum of the protonated *p*-cresidine (MH) in a standard reaction solution showing only the molecular formula of $\text{C}_8\text{H}_{12}\text{NO}$ and the m/z value of 139.0944 denotes its ^{13}C isotope. A product with formula $\text{C}_{16}\text{H}_{19}\text{N}_2\text{O}_2$ and m/z value of 271.1447 seen in Fig. 4.38 was identified in the precipitates after the treatment which is consistent with the protonated azo-coupled dimer ($\text{M}_2\text{H}-4$), confirmed by the ^{13}C isotope at m/z value of 272.1473, though the height of isotope was relatively high. This might be due to the overlapping of products, and as a result peaks were not separated properly. There was no evidence of higher oligomer formation. Similarly, a product with m/z value of 138.0914 and molecular formula $\text{C}_8\text{H}_{12}\text{NO}$ showing the ^{13}C isotopic peak at m/z value of 139.0947, was identified in the reaction supernatant of *p*-cresidine shown in Fig. 4.39. The molecular formula corresponds to the protonated residual monomer (MH). There was also a fragmentation ion (MH-CH_2) detected with m/z value of 123.0682 in the precipitates with molecular formula $\text{C}_7\text{H}_9\text{NO}$ as seen in Fig. 4.40.

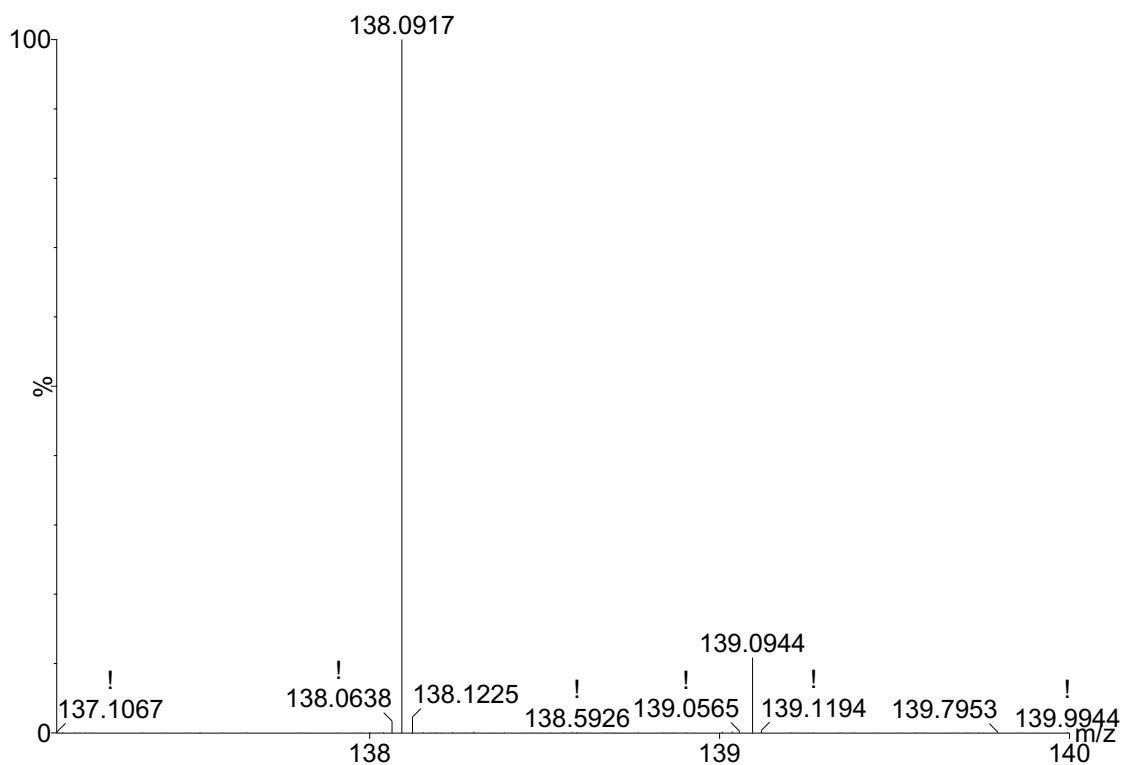


Figure 4.37. ESI-MS (+) of *p*-cresidine standard. Molecular formula $C_8H_{12}NO$ ($m/z = 138.0917$) represents the protonated standard. Conditions: 1.0 mM *p*-cresidine, 10 mM pH 4.6 buffer and 3-h incubation.

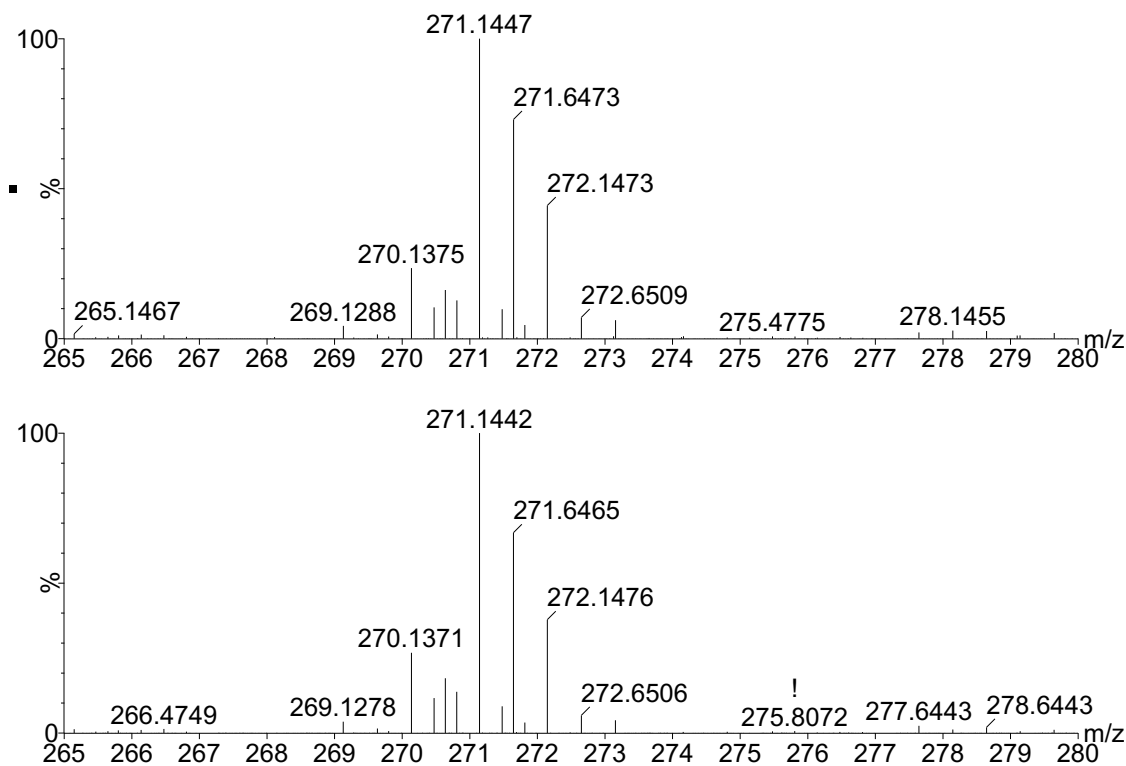


Figure 4.38. ESI-MS (+) of *p*-cresidine enzymatic reaction precipitate. Molecular formula $C_{16}H_{19}N_2O_2$ ($m/z = 271.1447$ and 271.1442) represents the protonated azo-dimer. Conditions: 1.0 mM *p*-cresidine, 1.25 mM hydrogen peroxide, 0.01 U/mL SBP, 10 mM pH 4.6 buffer and 3-h reaction. The two panels represent different acquisition numbers run at different time intervals.

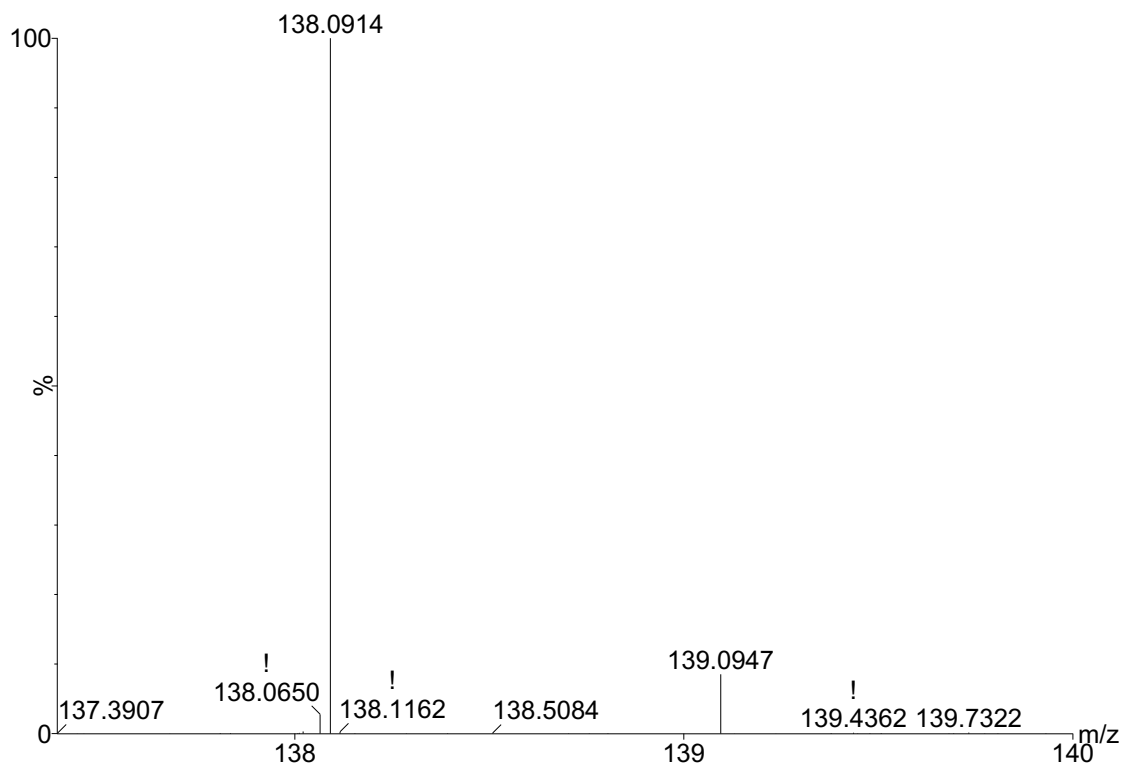


Figure 4.39. ESI-MS (+) of *p*-cresidine enzymatic reaction supernatant. Molecular formula $C_8H_{12}NO$ ($m/z = 138.0914$) represents the protonated residual monomer. Conditions: 1.0 mM *p*-cresidine, 1.25 mM hydrogen peroxide, 0.01 U/mL SBP, 10 mM pH 4.6 buffer and 3-h reaction.

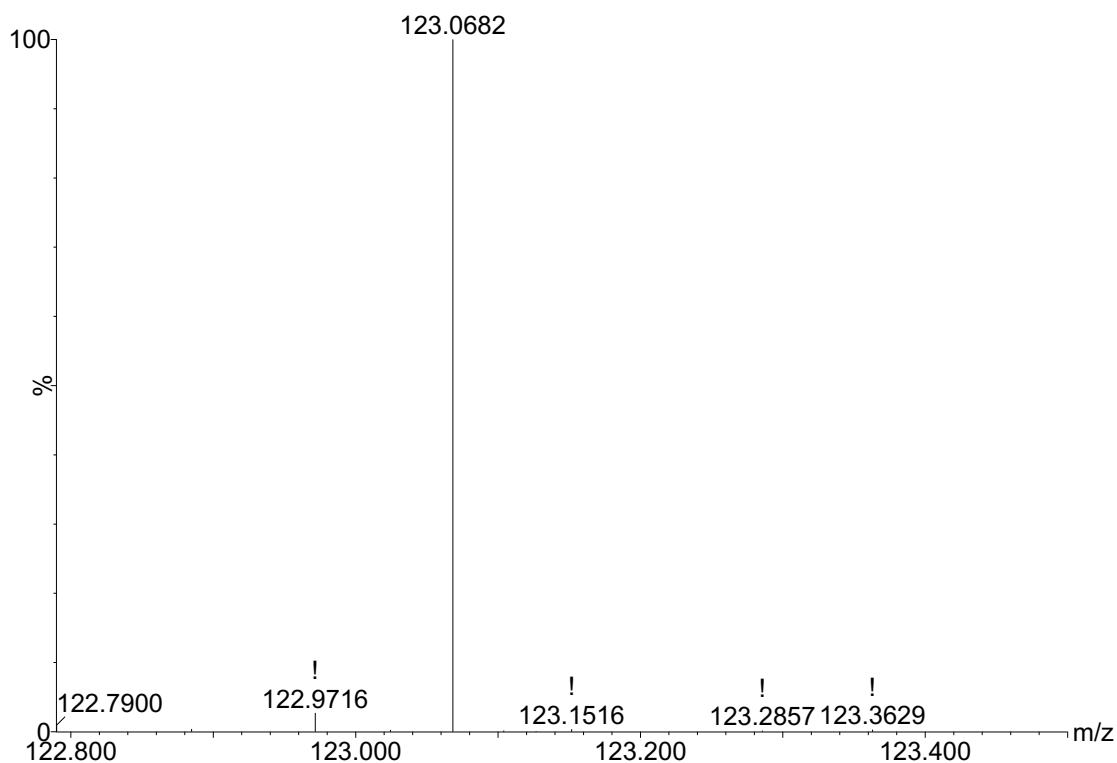


Figure 4.40. ESI-MS (+) of *p*-cresidine enzymatic reaction precipitate. Molecular formula C_7H_9NO ($m/z = 123.0682$) represents the fragmentation product. Conditions: 1.0 mM *p*-cresidine, 1.25 mM hydrogen peroxide, 0.01 U/mL SBP, 10 mM pH 4.6 buffer and 3-h reaction.

Figure 4.41 shows the mass spectrum of protonated 4-COT (MH) in a standard solution showing the molecular formula of C_7H_9NCl with m/z value of 142.0418. The m/z values of 143.0441 and 144.0388 signify its ^{13}C and ^{37}Cl isotope peaks, respectively (^{13}C -MH, ^{37}Cl -MH). Figure 4.42 shows the cationic radical (M) of 4-COT in a standard solution at m/z value of 141.0345 with molecular formula, C_7H_8NCl . In the higher mass range, Fig. 4.43 shows a product with m/z value of 246.0687 in the 4-COT supernatant corresponding to the molecular formula $C_{14}H_{13}ClNO$ consistent with protonated oxidative dimer that was further deaminated, dechlorinated and oxygenated (M_2H -2-NH-Cl+O). Similarly, in Fig. 4.44 a product in the supernatant with m/z value of 385.0871 ($C_{21}H_{19}Cl_2N_2O$) matches the protonated oxidative trimer which also endured deamination, dechlorination and oxygenation (M_3H -4-NH-Cl+O). The m/z values of 248.0660 and 387.0845 in Figs. 4.43 and 4.44 meant the ^{37}Cl isotopic peak of the dimer and trimer, respectively (^{37}Cl - M_2H -2-NH-Cl+O, ^{37}Cl - M_3H -4-NH-Cl+O). The m/z values of 247.0713 and 386.0901 in Figs. 4.43 and 4.44 signify the ^{13}C - M_2H -2-NH-Cl+O and ^{13}C - M_3H -4-NH-Cl+O, respectively. The oxygenation process was not due to MS condition. It must have occurred during the enzymatic reaction process since the standard does not show any oxygenation in the MS analysis. For the 4-COT reaction supernatant, the m/z value of 142.0420 in Fig. 4.45 corresponds to the protonated residual monomer (MH) with molecular formula C_7H_9NCl and the m/z values of 143.0441 and 144.0390 denoted its ^{13}C and ^{37}Cl isotope peaks, respectively.

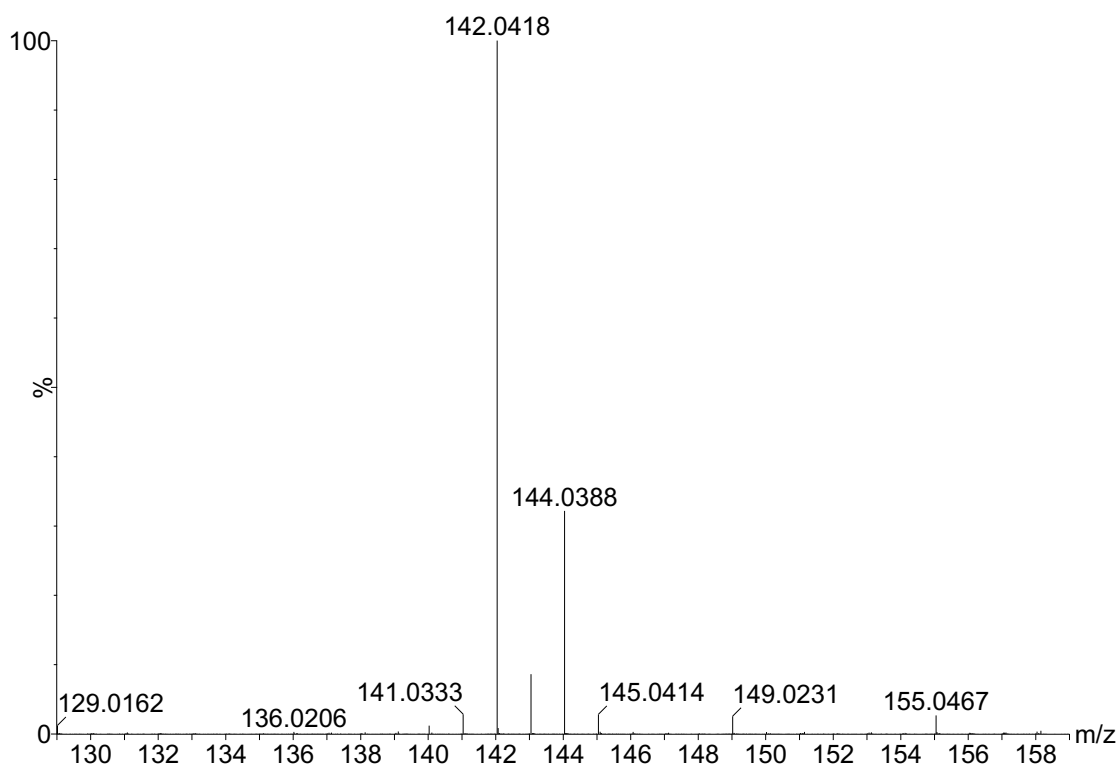


Figure 4.41. ASAP-MS (+) of 4-COT standard. Molecular formula C_7H_9NCl ($m/z = 142.0418$) represents the protonated standard. Conditions: 1.0 mM 4-COT, 10 mM pH 4.4 buffer and 3-h incubation.

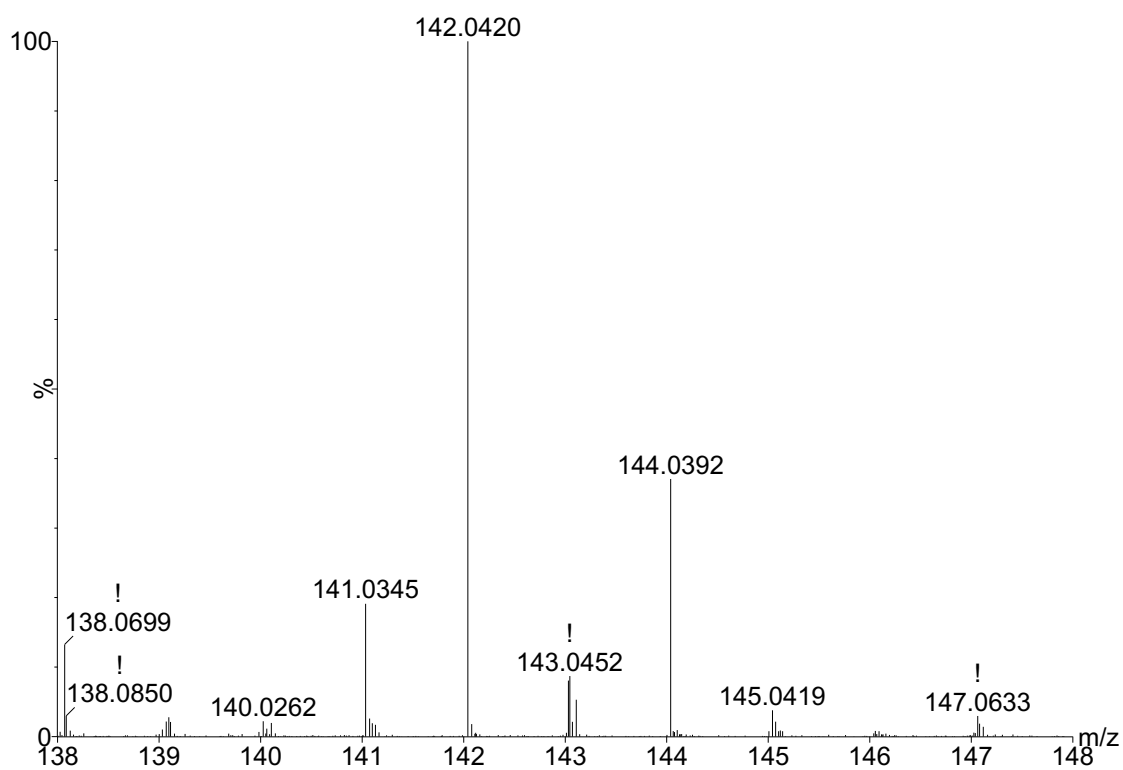


Figure 4.42. ASAP-MS (+) of 4-COT cationic radical. Molecular formula C_7H_8NCl ($m/z = 141.0345$) represents the cationic radical. Conditions: 1.0 mM 4-COT, 10 mM pH 4.4 buffer and 3-h incubation.

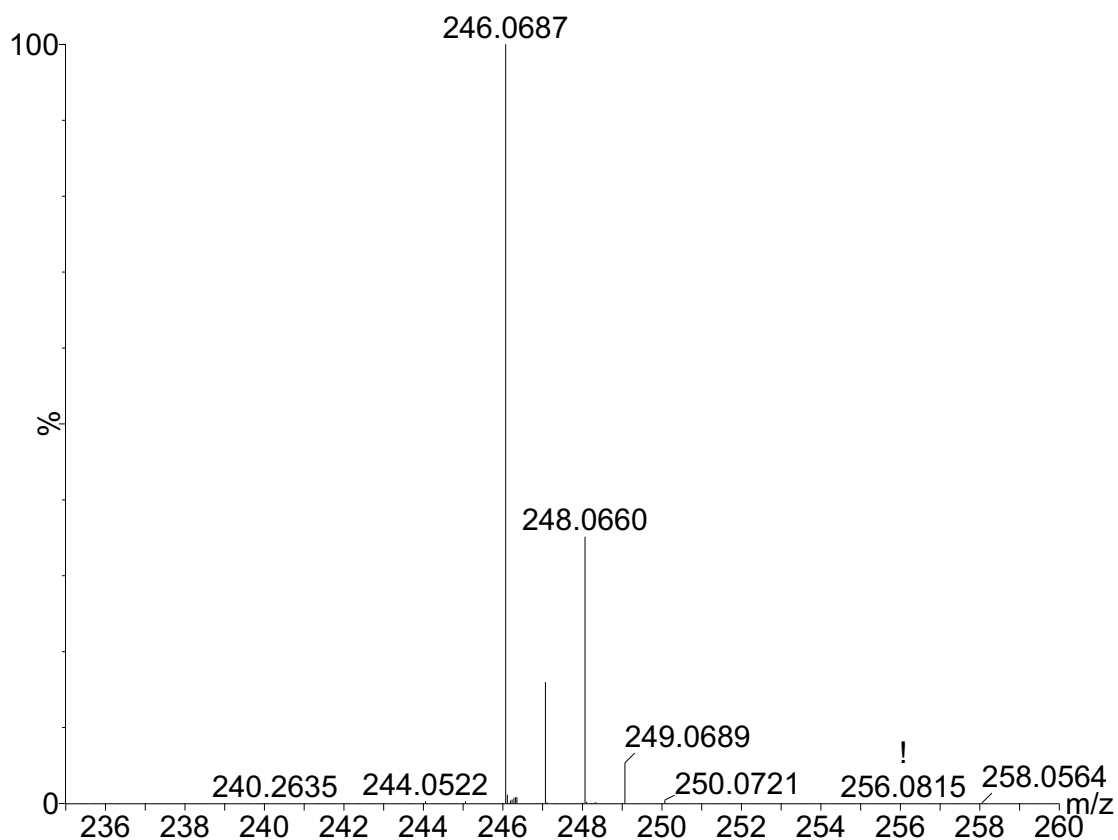


Figure 4.43. ASAP-MS (+) of 4-COT enzymatic reaction supernatant. Molecular formula $C_{14}H_{13}ClNO$ ($m/z = 246.0687$) represents the dimer ($M_2H-2-NH-Cl+O$). Conditions: 1.0 mM 4-COT, 0.5 mM hydrogen peroxide, 0.009 U/mL SBP, 10 mM pH 4.4 buffer and 3-h reaction.

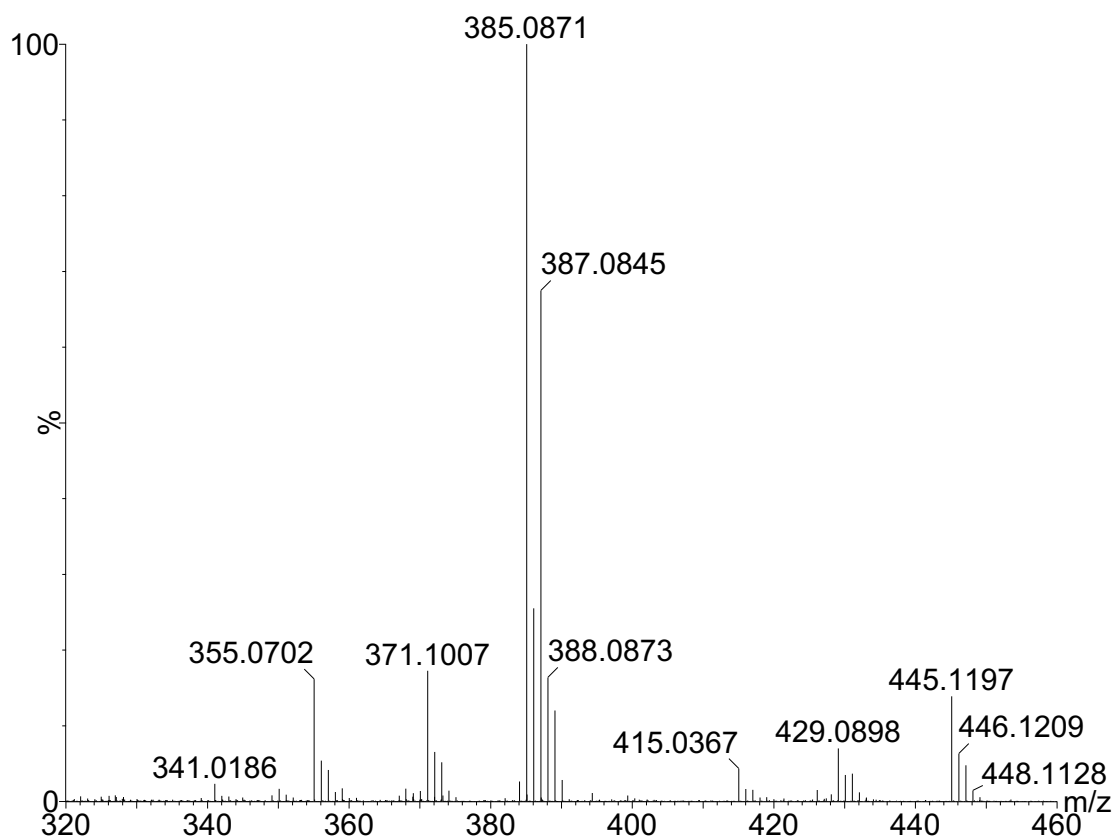


Figure 4.44. ASAP-MS (+) of 4-COT enzymatic reaction supernatant. Molecular formula $C_{21}H_{19}Cl_2N_2O$ ($m/z = 385.0871$) represents the trimer ($M_3H-4-NH-Cl+O$). Conditions: 1.0 mM 4-COT, 0.5 mM hydrogen peroxide, 0.009 U/mL SBP, 10 mM pH 4.4 buffer and 3-h reaction.

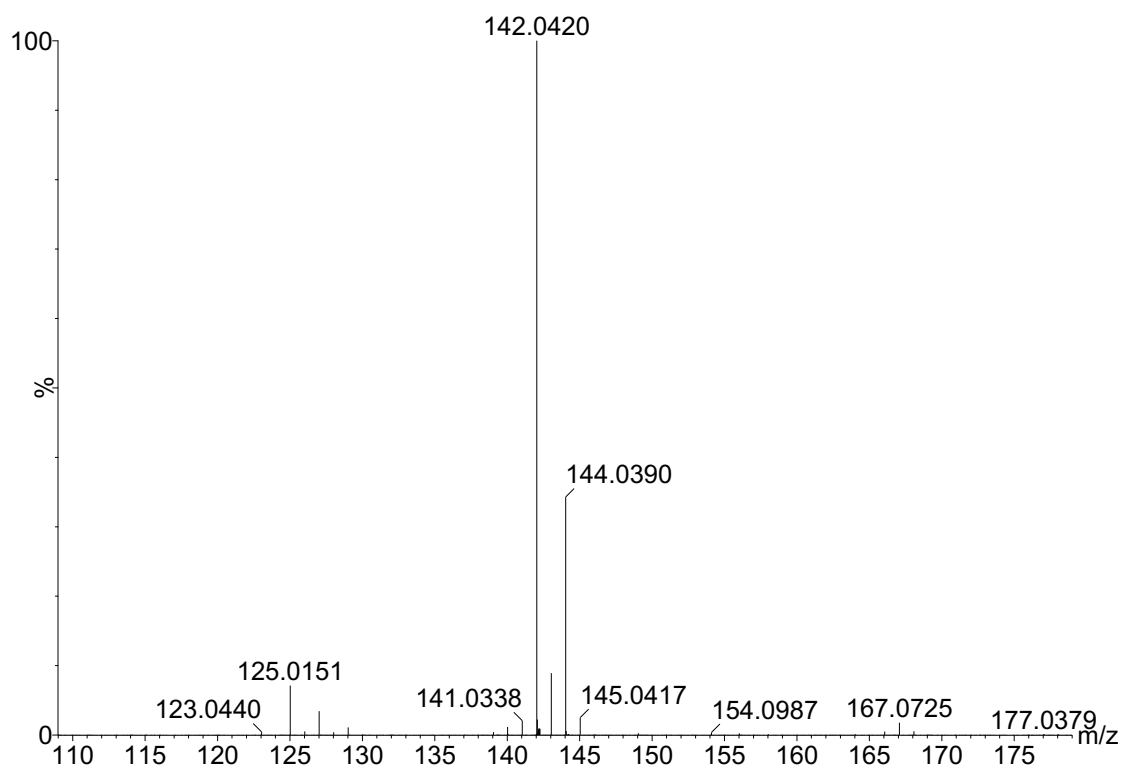


Figure 4.45. ASAP-MS (+) of 4-COT enzymatic reaction supernatant. Molecular formula C_7H_9NCl ($m/z = 142.0420$) represents the protonated residual monomer. Conditions: 1.0 mM 4-COT, 0.5 mM hydrogen peroxide, 0.009 U/mL SBP, 10 mM pH 4.4 buffer and 3-h reaction.

Similar loss of chlorine was reported by Wu *et al.* in 1993 during enzymatic polymerization, firstly for chlorinated phenols and secondly for their binding to humic acid. Dec and Bollag (1994) also reported enzymatic processes involving oxidative coupling with dehalogenation of chlorinated substrates. If the *ortho*- or *para*-positions carry a chlorine atom, then the coupling of such a radical can lead to dehalogenation. Minard *et al.* (1981) reported mass spectral evidence for the loss of chlorine atoms from 2,4-dichlorophenol during incubation with a laccase from the fungus *Rhizoctonia praticola*.

Other researchers, Lyr (1963) and Hammel and Tardone (1988), also investigated dehalogenation of pentachlorophenol and 2,4,6-trichlorophenol in the presence of a *Trametes versicolor* laccase and a peroxidase from *Phanerochaete chrysosporium*. Dec and Bollag (1994) described the release of chloride ions to the oxidative coupling reaction.

Therefore, it can be concluded that for 4-COT, the loss of Cl occurred during the oxidative coupling as the position of Cl on the ring was on the *para*-position relative to the amino functional group and which was very prone to such a dehalogenation event. Deamination was observed too which was due to MS fragmentation. In another study, the positively charged amino group detachment from the parent molecule though a rare event was observed for amino acid molecules (Romanova *et al.* 2015).

Figure 4.46 shows the mass spectrum of protonated standard solution of ODA with m/z value of 201.1029, molecular formula $C_{12}H_{13}N_2O$, and m/z value of 202.1066, corresponding to MH and ^{13}C -MH, respectively. Figure 4.47 shows a product in the precipitates after enzymatic reaction with molecular formula $C_{24}H_{21}N_4O_2$, suggesting formation of protonated azo-dimer of ODA (M_2H-4) with m/z value at 397.1659 and its ^{13}C isotope at m/z value at 398.1693. There might be occurrence of only N-N coupling to form the oxidized oxidative dimer (azo-dimer), since there was no MS evidence that

corresponds to formation of an oxidative dimer (M_2H-2) formed by C-C or N-C coupling during the enzymatic reaction. In the higher mass range, Fig. 4.48 shows a product with molecular formula $C_{36}H_{31}N_6O_3$ found in the precipitates after the reaction that resembles protonated trimer of an azo compound (M_3H-6) with m/z value of 595.2437, consistent with a mono-azo trimer. The relative height of ^{13}C - M_3H-6 was high due to overlapping of isotopic peaks. The coupling that must have occurred for formation of M_3H-6 is N-N and N-C or C-C. However, the mass spectrum in Fig. 4.49 with molecular formula $C_{36}H_{29}N_6O_3$ represents a protonated bis-azo trimer (M_3H-8) in the precipitates with m/z value of 593.2279. The N-N coupling leads to such product formation during the polymerization reaction. However, the peak was of low confidence of acceptance and there was overlapping of the isotopic peaks. The mass spectrum in Fig. 4.50 represents an oxidized oxidative product formed in the precipitates with molecular formula $C_{48}H_{37}N_8O_4$, which was consistent with protonated tris-azo tetramer (M_4H-12) with m/z value of 789.2935, the relative height of its ^{13}C isotope at m/z value of 790.2963 was minutely high. There were no signals in the mass spectrum corresponding to tetramers having some C-C or N-C coupling (M_4H-6 , M_4H-8 or M_4H-10). In the reaction supernatant, Fig. 4.51, a product with molecular formula $C_{12}H_{13}N_2O$, with m/z value of 201.1028 signifies the protonated monomer (MH) remaining after the reaction and its ^{13}C -MH isotope at m/z value of 202.1057. In the higher mass range, for the reaction supernatant, Fig. 4.52 shows a product with molecular formula $C_{24}H_{21}N_4O_2$ with m/z value at 397.1656 corresponding to the protonated azo-dimer of ODA (M_2H-4). The signal of the peak was weak and, thus, could not be confirmed by its ^{13}C -isotope. The weak presence of the dimer, and absence of higher oligomers, in the reaction supernatant is indicative of completeness of removal, in contrast to the mono-aromatic compound 4-COT.

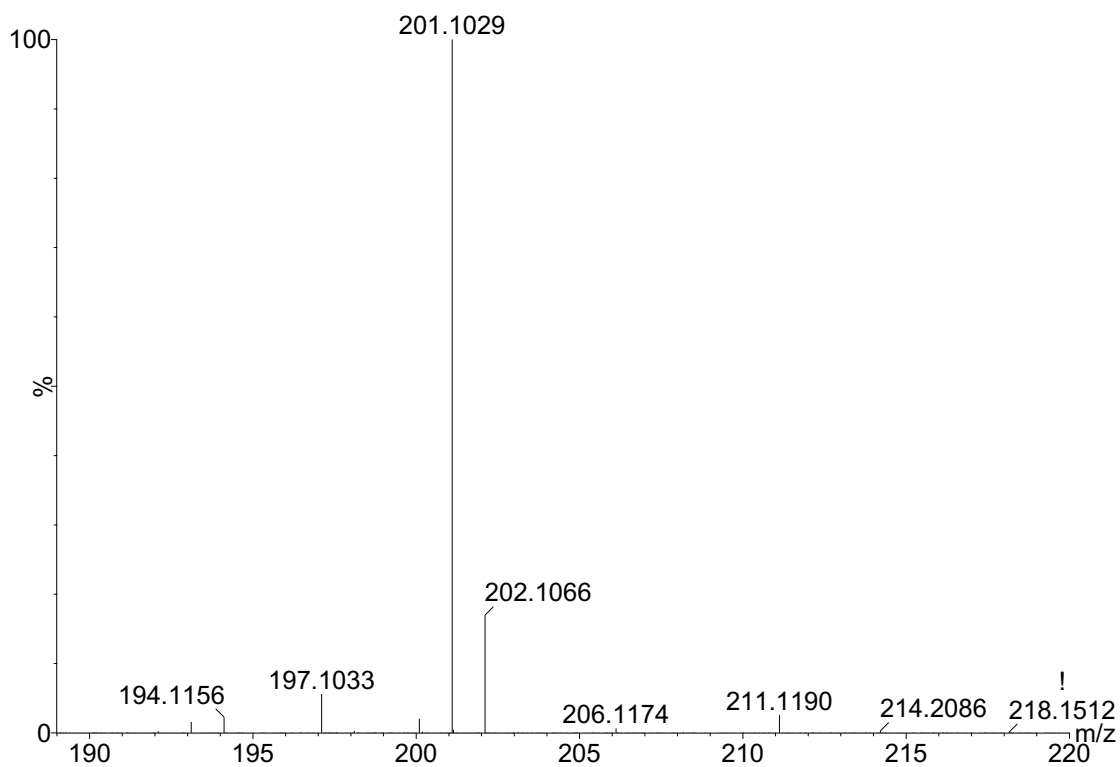


Figure 4.46. ESI-MS (+) of ODA standard. Molecular formula $C_{12}H_{13}N_2O$ ($m/z = 138.0917$) represents the protonated ODA standard. Conditions: 0.5 mM ODA, 10 mM pH 6.0 buffer and 3-h incubation.

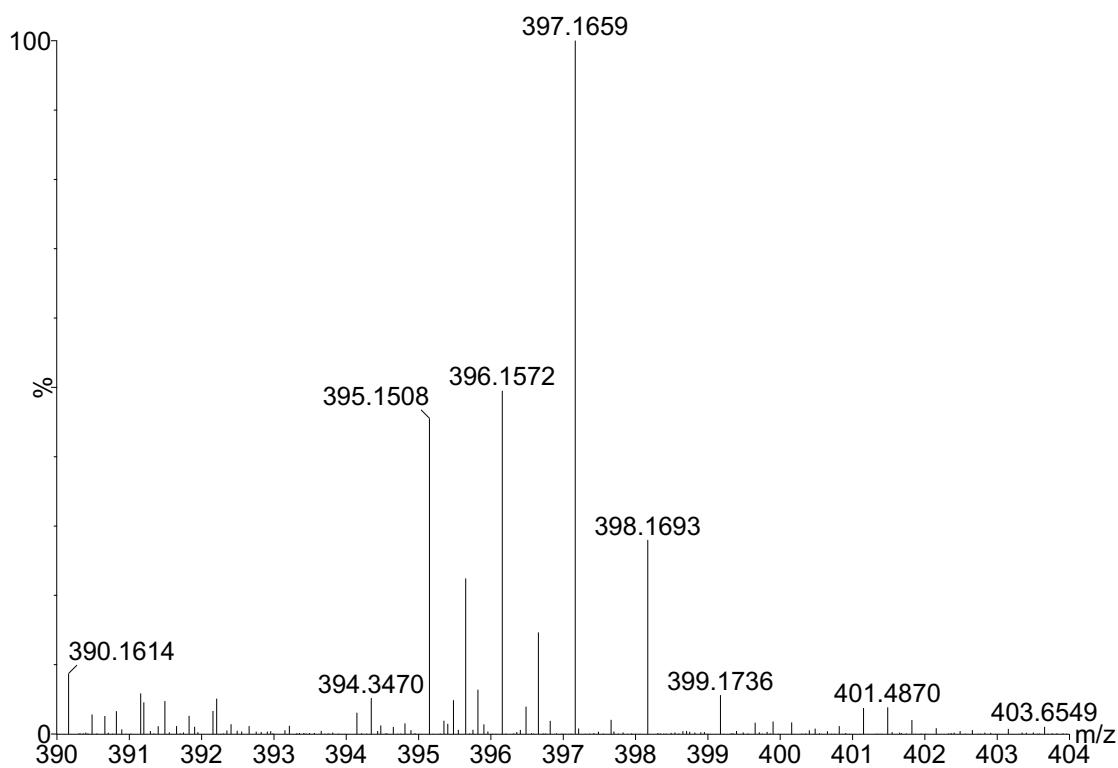


Figure 4.47. ESI-MS (+) of ODA enzymatic reaction precipitate. Molecular formula $C_{24}H_{21}N_4O_2$ ($m/z = 397.1659$) represents the protonated azo-dimer. Conditions: 0.5 mM ODA, 0.6 mM hydrogen peroxide, 0.04 U/mL SBP, 10 mM pH 6.0 buffer and 3-h reaction.

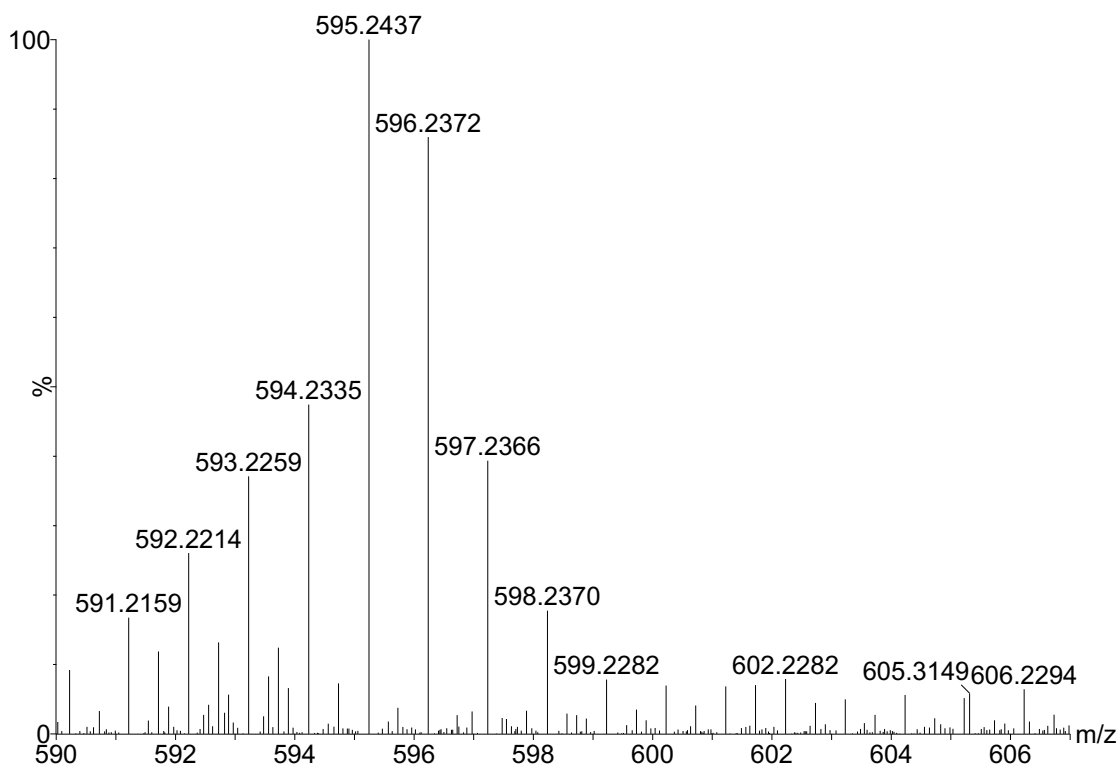


Figure 4.48. ESI-MS (+) of ODA enzymatic reaction precipitate. Molecular formula $C_{36}H_{31}N_6O_3$ ($m/z = 595.2437$) represents the protonated mono-azo trimer. Conditions: 0.5 mM ODA, 0.6 mM hydrogen peroxide, 0.04 U/mL SBP, 10 mM pH 6.0 buffer and 3-h reaction.

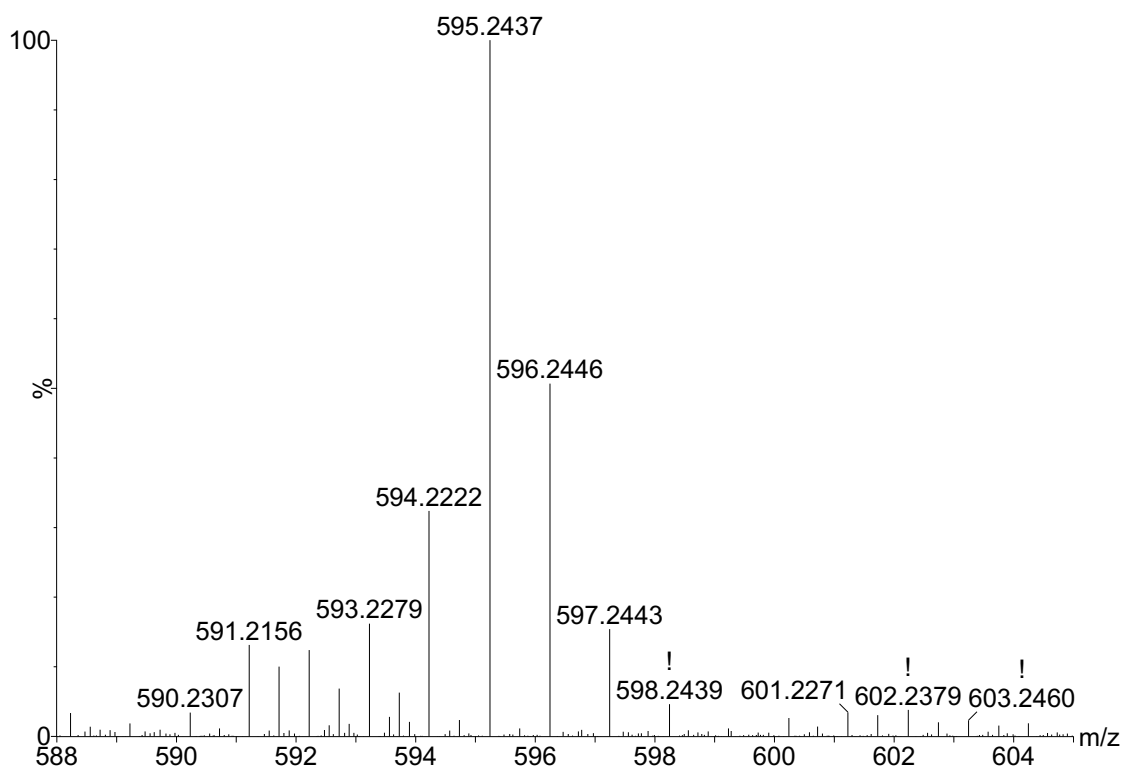


Figure 4.49. ESI-MS (+) of ODA enzymatic reaction precipitate. Molecular formula $C_{36}H_{29}N_6O_3$ ($m/z=593.2279$) represents the protonated bis-azo trimer. Conditions: 0.5 mM ODA, 0.6 mM hydrogen peroxide, 0.04 U/mL SBP, 10 mM pH 6.0 buffer and 3-h reaction.

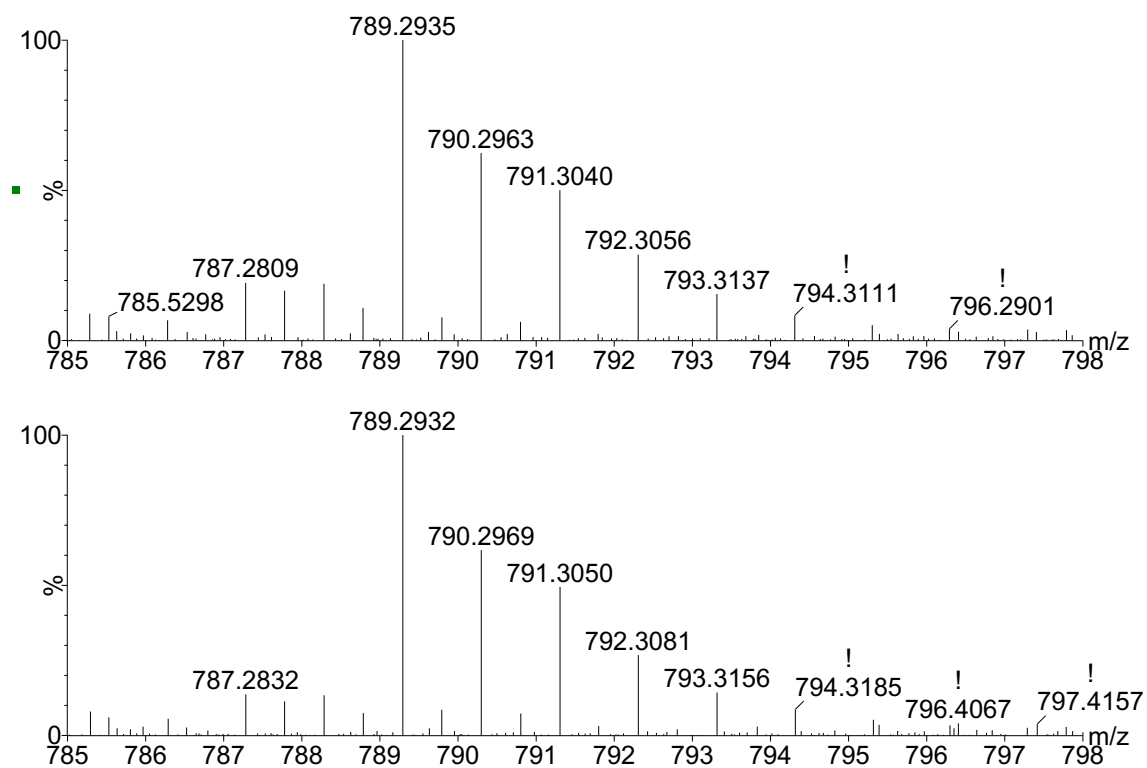


Figure 4.50. ESI-MS (+) of ODA enzymatic reaction precipitate. Molecular formula $C_{48}H_{37}N_8O_4$ ($m/z = 789.2932$ and 789.2935) represents the protonated tris-azo tetramer. Conditions: 0.5 mM ODA, 0.6 mM hydrogen peroxide, 0.04 U/mL SBP, 10 mM pH 6.0 buffer and 3-h reaction. The two panels represent different acquisition numbers run at different time intervals.

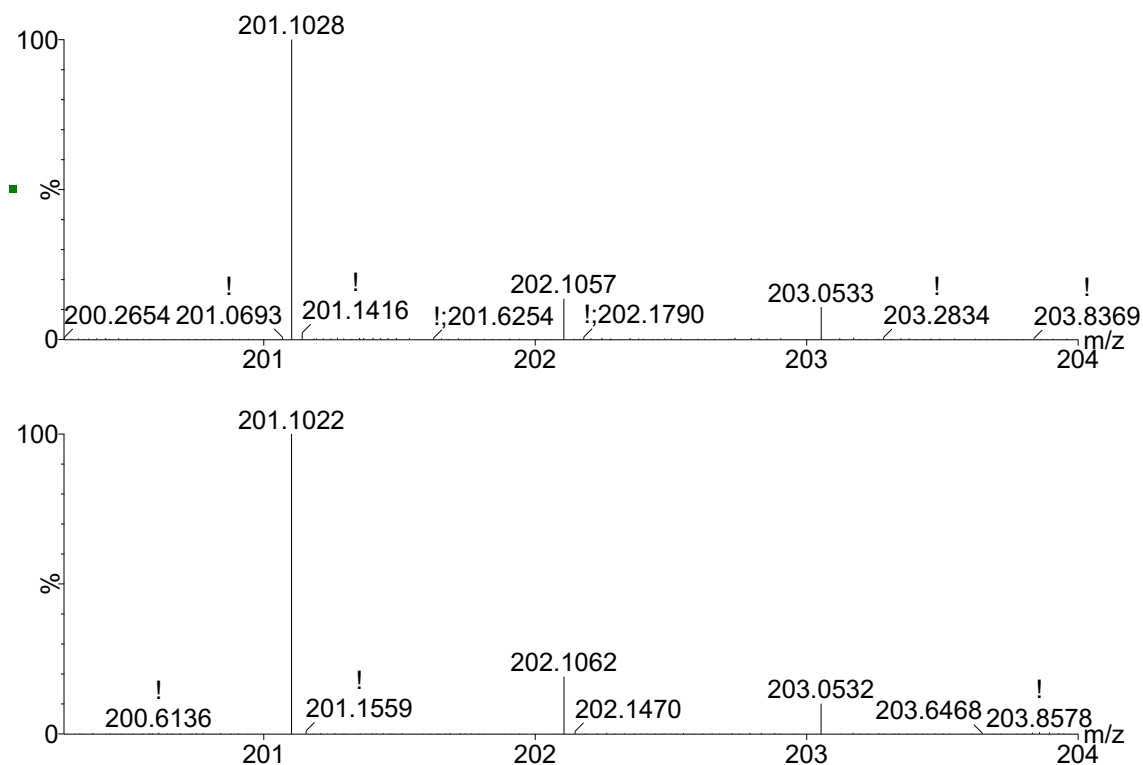


Figure 4.51. ESI-MS (+) of ODA enzymatic reaction supernatant. Molecular formula $C_{12}H_{13}N_2O$ ($m/z = 201.1028$ and 201.1022) represents the protonated residual monomer. Conditions: 0.5 mM ODA, 0.6 mM hydrogen peroxide, 0.04 U/mL SBP, 10 mM pH 6.0 buffer and 3-h reaction. The two panels represent different acquisition numbers run at different time intervals.

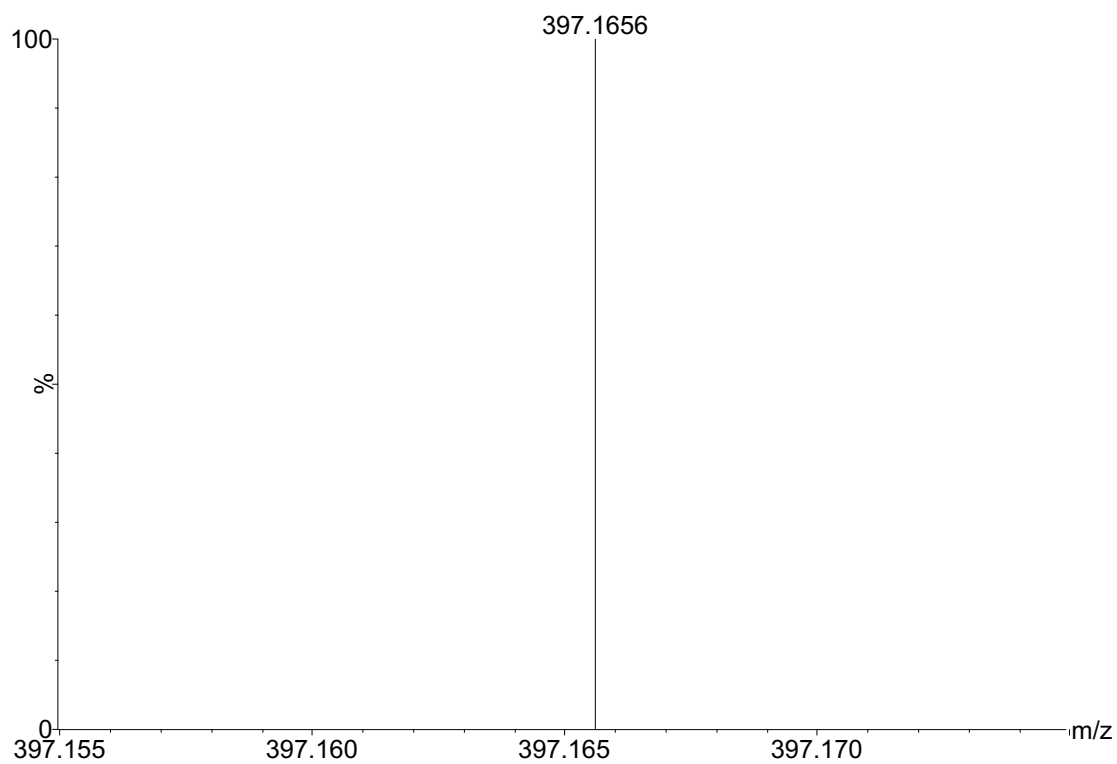


Figure 4.52. ESI-MS (+) of ODA enzymatic reaction supernatant. Molecular formula $C_{24}H_{21}N_4O_2$ ($m/z = 397.1656$) represents the protonated azo-dimer. Conditions: 0.5 mM ODA, 0.6 mM hydrogen peroxide, 0.04 U/mL SBP, 10 mM *pH* 6.0 buffer and 3-h reaction.

Figure 4.53 shows the mass spectrum of the standard solution of MDA with m/z value of 199.1233, molecular formula $C_{13}H_{15}N_2$, and m/z value of 200.1264, corresponding to MH and ^{13}C -MH, respectively. In the higher mass range, Fig. 4.54 shows a product with m/z value of 393.2068 in the MDA reaction precipitates corresponding to molecular formula $C_{26}H_{25}N_4$ consistent with protonated azo-dimer (M_2H-4) confirmed by ^{13}C -isotope, m/z value at 394.2094. There was also mass spectral evidence that corresponds to a protonated mono-azo-trimer (M_3H-6) in the precipitates shown in Fig. 4.55, the m/z value of 589.3063 corresponds to molecular formula $C_{39}H_{37}N_6$. The m/z value of 590.3106 denotes its ^{13}C -isotope peak (^{13}C - M_3H-6), the high relative height of the peak might be due to overlapping of products and isotope patterns, therefore peaks were not separated properly. The coupling reaction that might have occurred was N-N and N-C or C-C, whereas the mass spectrum with m/z value of 587.2911 corresponding to the molecular formula $C_{39}H_{35}N_6$ in Fig. 4.56 shows a protonated bis-azo trimer (M_3H-8) formed due to N-N coupling reaction. The signal of the peak was weak. In the higher mass range, for the reaction precipitates, Fig. 4.57 shows a product with m/z value of 783.3887, molecular formula, $C_{52}H_{47}N_8$ was consistent with a protonated bis-azo tetramer (M_4H-10). The signal of the peak was weak and, thus, could not be confirmed by its ^{13}C -isotope. The coupling that must have occurred for formation of (M_4H-10) is N-N and N-C or C-C. Products with m/z values of 199.1236 and 199.1237 were determined both in the precipitates and supernatant, respectively, with molecular formula $C_{13}H_{15}N_2$ as shown in Figs. 4.58.a-4.58.b which correspond to protonated residual monomer (MH), and the m/z value of 200.1271 denoted ^{13}C -MH. A product with m/z value of 393.2088 in the reaction supernatant as shown in Fig. 4.59 was consistent with protonated azo-dimer (M_2H-4), molecular formula ($C_{26}H_{25}N_4$) confirmed by its ^{13}C -isotope peak at m/z value of 394.2116.

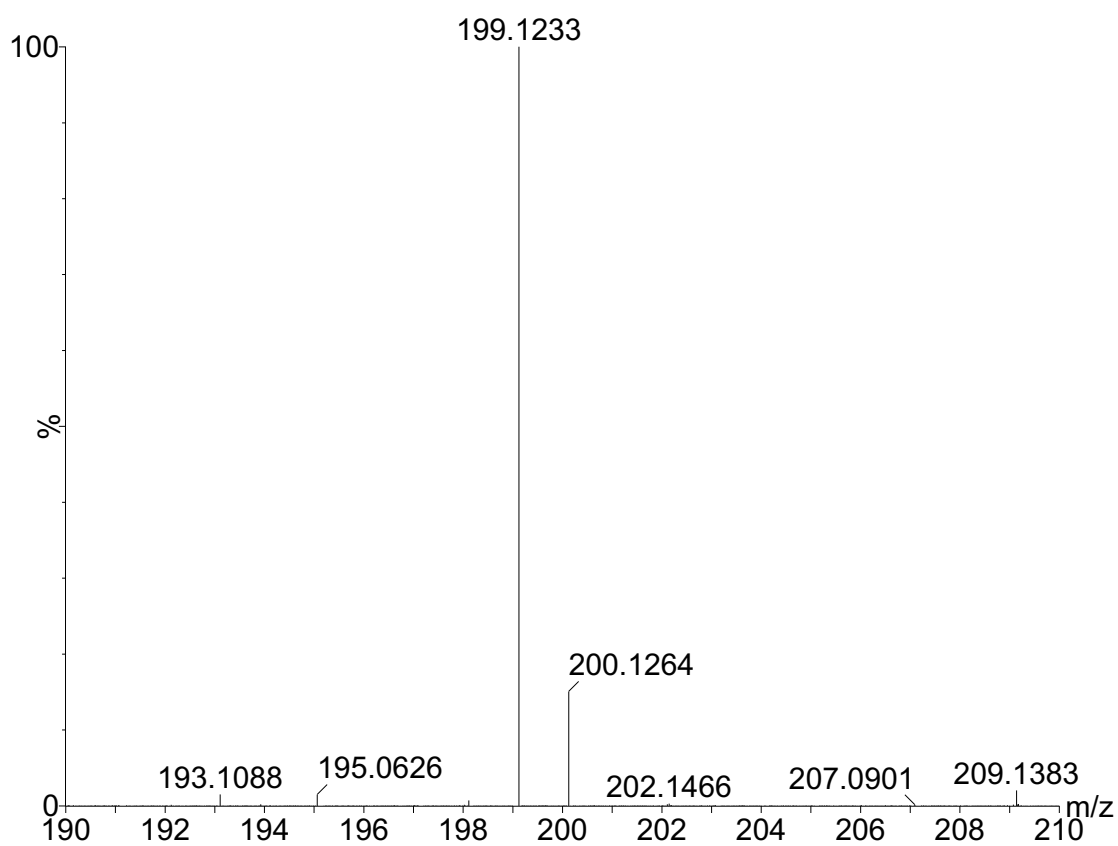


Figure 4.53. ESI-MS (+) of MDA standard. Molecular formula $C_{13}H_{15}N_2$ ($m/z = 199.1233$) represents the protonated standard. Conditions: 0.5 mM MDA, 10 mM pH 6.0 buffer and 3-h incubation.

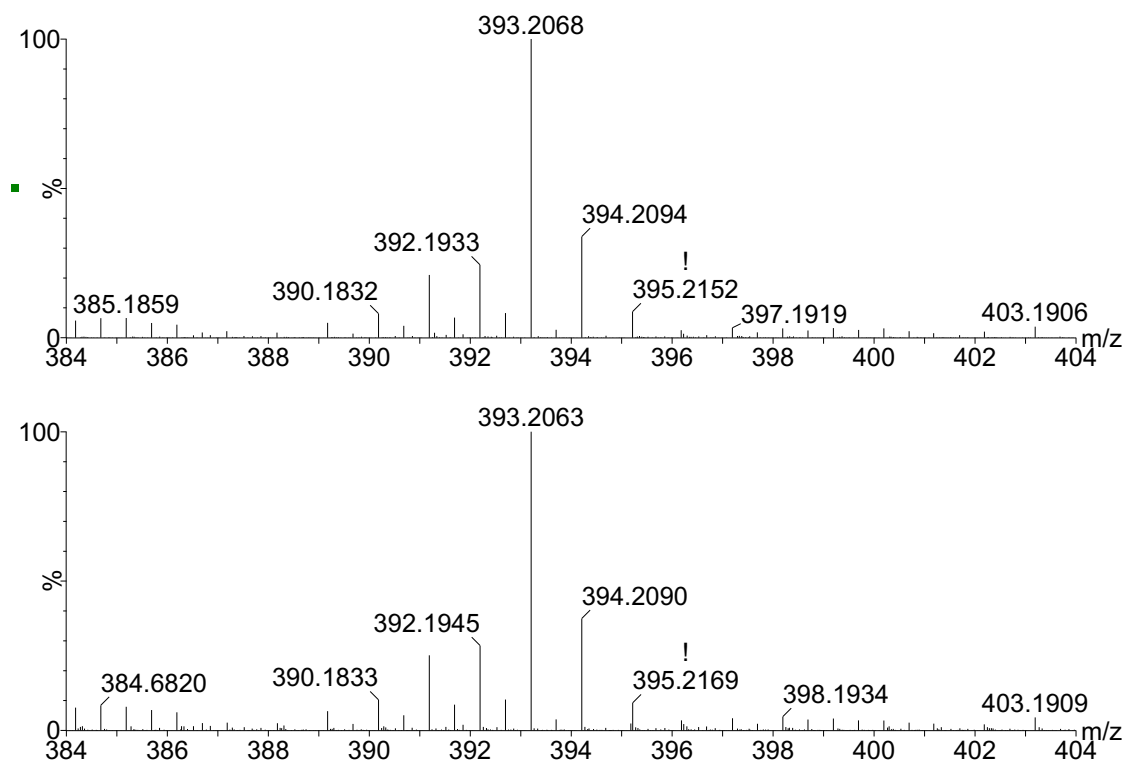


Figure 4.54. ESI-MS (+) of MDA enzymatic reaction precipitate. Molecular formula $C_{26}H_{25}N_4$ (m/z = 393.2068 and 393.2063) represents the protonated azo-dimer. Conditions: 0.5 mM MDA, 0.7 mM hydrogen peroxide, 0.7 U/mL SBP, 10 mM pH 6.0 buffer and 3-h reaction. The two panels represent different acquisition numbers run at different time interval.

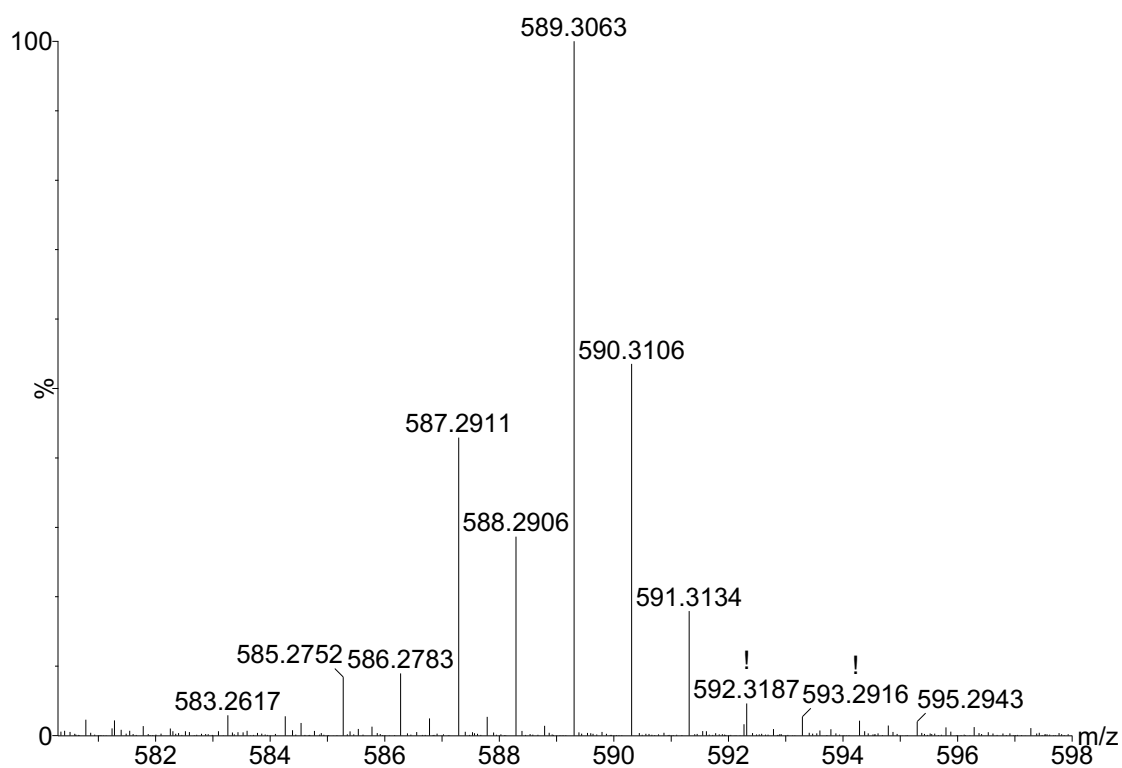


Figure 4.55. ESI-MS (+) of MDA enzymatic reaction precipitate. Molecular formula $C_{39}H_{37}N_6$ ($m/z = 589.3063$) represents the protonated mono-azo trimer. Conditions: 0.5 mM MDA, 0.7 mM hydrogen peroxide, 0.7 U/mL SBP, 10 mM pH 6.0 buffer and 3-h reaction.

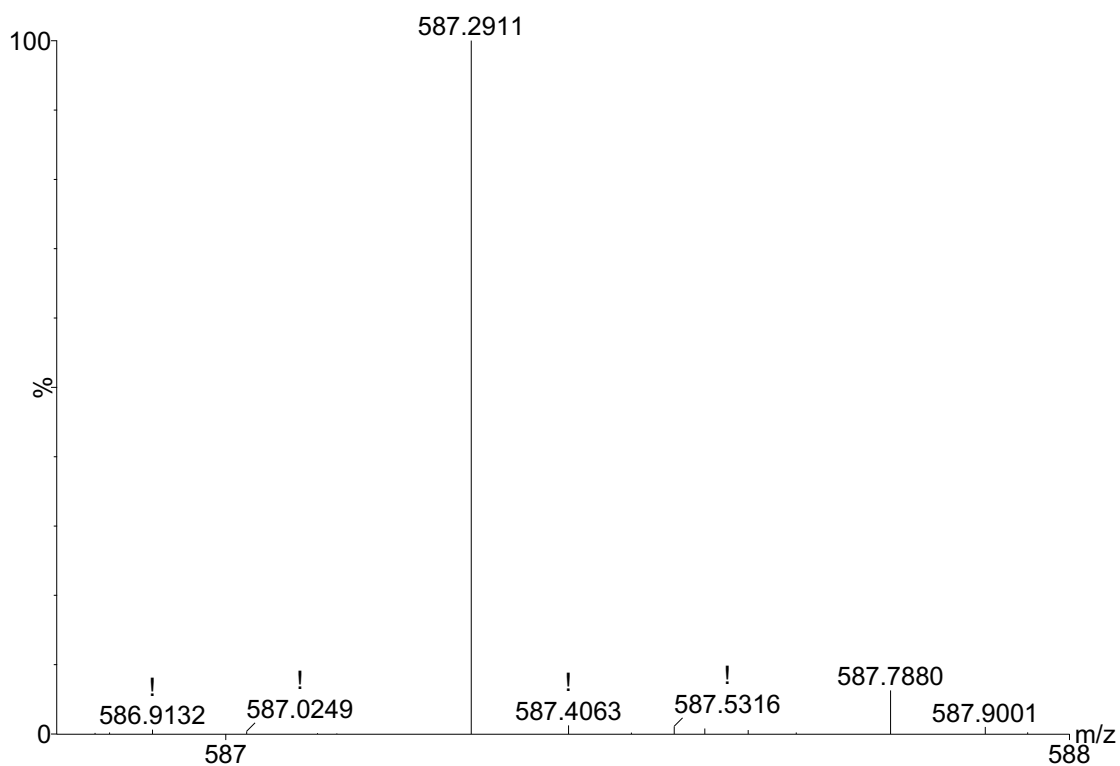


Figure 4.56. ESI-MS (+) of MDA enzymatic reaction precipitate. Molecular formula $C_{39}H_{35}N_6$ ($m/z = 587.2911$) represents the protonated bis-azo trimer. Conditions: 0.5 mM MDA, 0.7 mM hydrogen peroxide, 0.7 U/mL SBP, 10 mM pH 6.0 buffer and 3-h reaction.

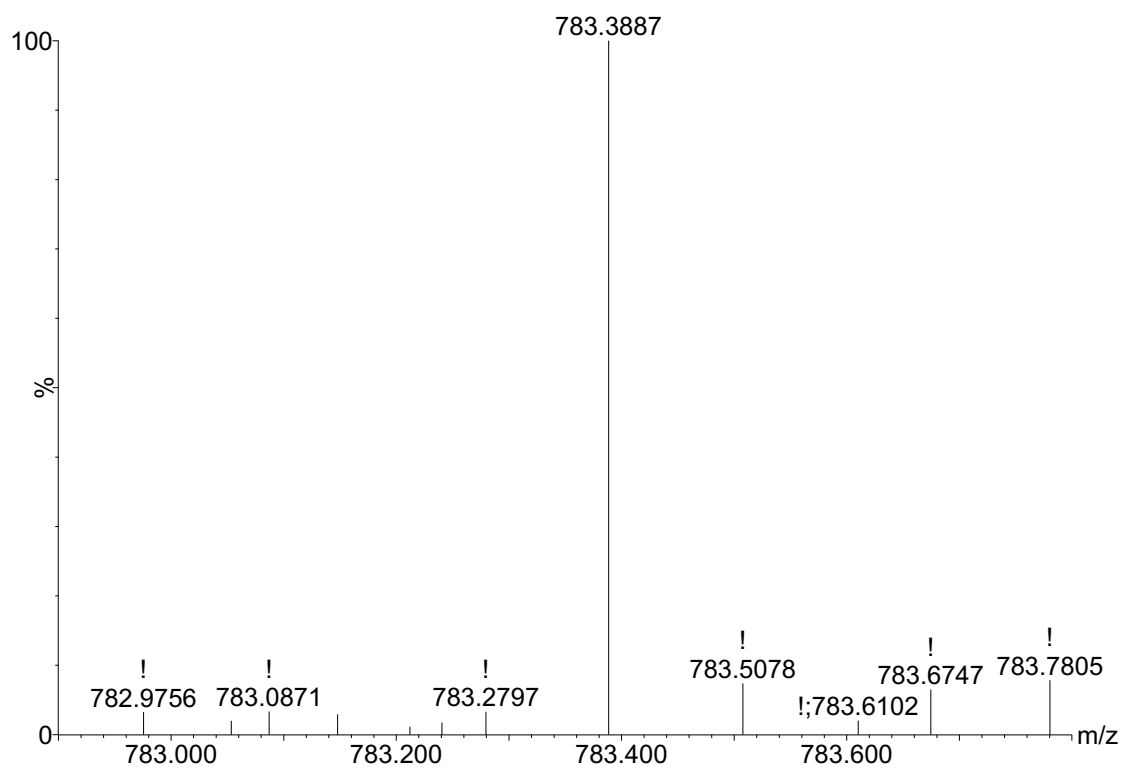


Figure 4.57. ESI-MS (+) of MDA enzymatic reaction precipitate. Molecular formula $C_{52}H_{47}N_8$ ($m/z = 783.3887$) represents the protonated bis-azo tetramer. Conditions: 0.5 mM MDA, 0.7 mM hydrogen peroxide, 0.7 U/mL SBP, 10 mM pH 6.0 buffer and 3-h reaction.

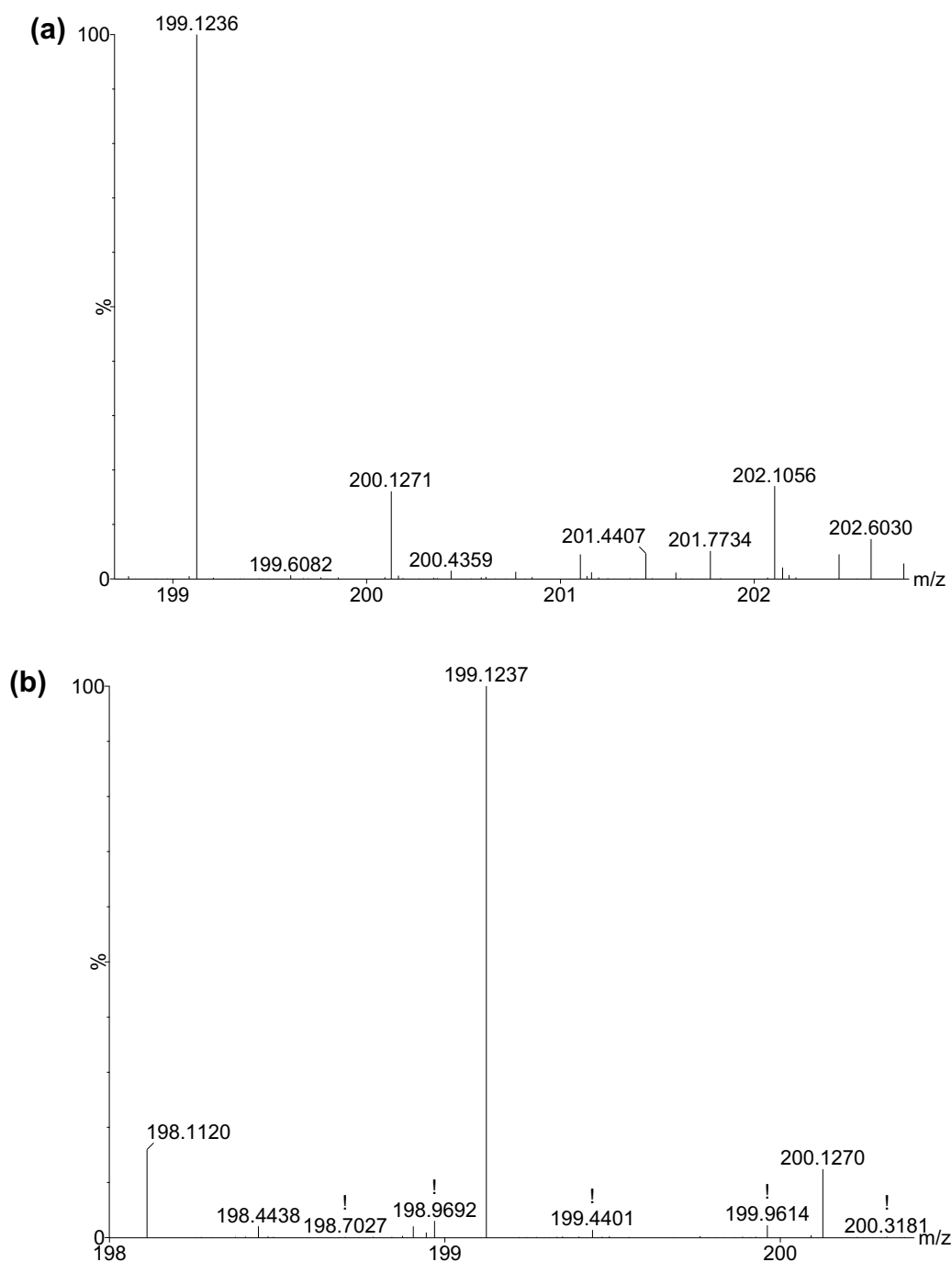


Figure 4.58. ESI-MS (+) of MDA (a) enzymatic reaction precipitate. Molecular formula $C_{13}H_{15}N_2$ ($m/z = 199.1236$) represents the protonated residual monomer. Conditions: 0.5 mM MDA, 0.7 mM hydrogen peroxide, 0.7 U/mL SBP, 10 mM pH 6.0 buffer and 3-h reaction; and (b) enzymatic reaction supernatant. Molecular formula $C_{13}H_{15}N_2$ ($m/z = 199.1237$) represents the protonated residual monomer. Conditions: 0.5 mM MDA, 0.7 mM hydrogen peroxide, 0.7 U/mL SBP, 10 mM pH 6.0 buffer and 3-h reaction.

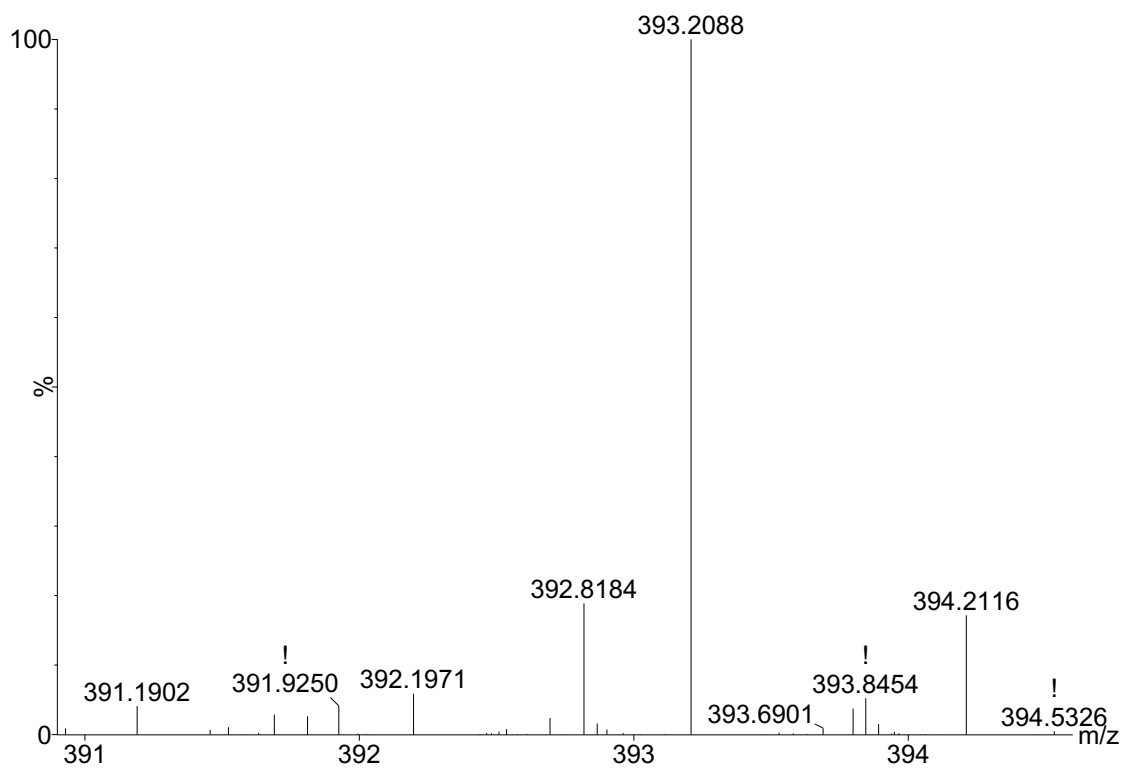


Figure 4.59. ESI-MS (+) of MDA enzymatic reaction supernatant. Molecular formula $C_{26}H_{25}N_4$ ($m/z = 393.2088$) represents the protonated azo-dimer. Conditions: 0.5 mM MDA, 0.7 mM hydrogen peroxide, 0.7 U/mL SBP, 10 mM pH 6.0 buffer and 3-h reaction.

Figure 4.60 shows the mass spectrum of protonated TDA (MH) in a standard solution with m/z value of 217.0800, molecular formula, $C_{12}H_{13}N_2S$. The m/z values of 218.0829 and 219.0733 signified its ^{13}C (^{13}C -MH) and ^{34}S (^{34}S -MH) isotope peaks, respectively. The m/z value of 216.0725 denoted radical cation (M), molecular formula, $C_{12}H_{12}N_2S$. In the higher mass range, for the reaction precipitates, Fig. 4.61 shows an oxidized oxidative dimer with m/z value of 429.1208 corresponding to molecular formula $C_{24}H_{21}N_4S_2$ was consistent with a protonated azo-dimer (M_2H -4). The m/z values of 430.1228 and 431.1190 denoted its ^{13}C - M_2H -4 and ^{34}S - M_2H -4 peaks, respectively.

Figure 4.62 shows evidence of a protonated mono-azo trimeric (M_3H -6) product in the precipitates with m/z value of 643.1759, molecular formula, $C_{36}H_{31}N_6S_3$ confirmed by its ^{13}C - M_3H -6 at m/z value of 644.1801 and ^{34}S - M_3H -6 at m/z value of 645.1780. The relative height was marginally high which could be due to overlapping of the isotopic peaks of the two products. The m/z value of 641.1610, molecular formula, $C_{36}H_{29}N_6S_3$ in Fig. 4.62, matches a product (M_3H -8). The m/z value is the same as a protonated bis-azo trimer though with lower confidence in identification due to a weak signal which, therefore, could not be confirmed by its isotopes. In the higher mass range, for the reaction precipitates, Fig. 4.63 shows a product with molecular formula $C_{48}H_{41}N_8S_4$ and m/z value at 857.2308 consistent with a protonated mono-azo tetramer of TDA (M_4H -8) confirmed by its ^{13}C - M_4H -8 and ^{34}S - M_4H -8 peaks. N-N and N-C or C-C coupling could lead to such product formation during the polymerization reaction. The m/z value of 217.0797 with molecular formula $C_{12}H_{13}N_2S$ corresponding to the protonated residual monomer (MH) in the reaction supernatant as shown in Fig. 4.64. The m/z values of 218.0808 and 219.0829 denote its ^{13}C -MH and ^{34}S -MH peaks, respectively.

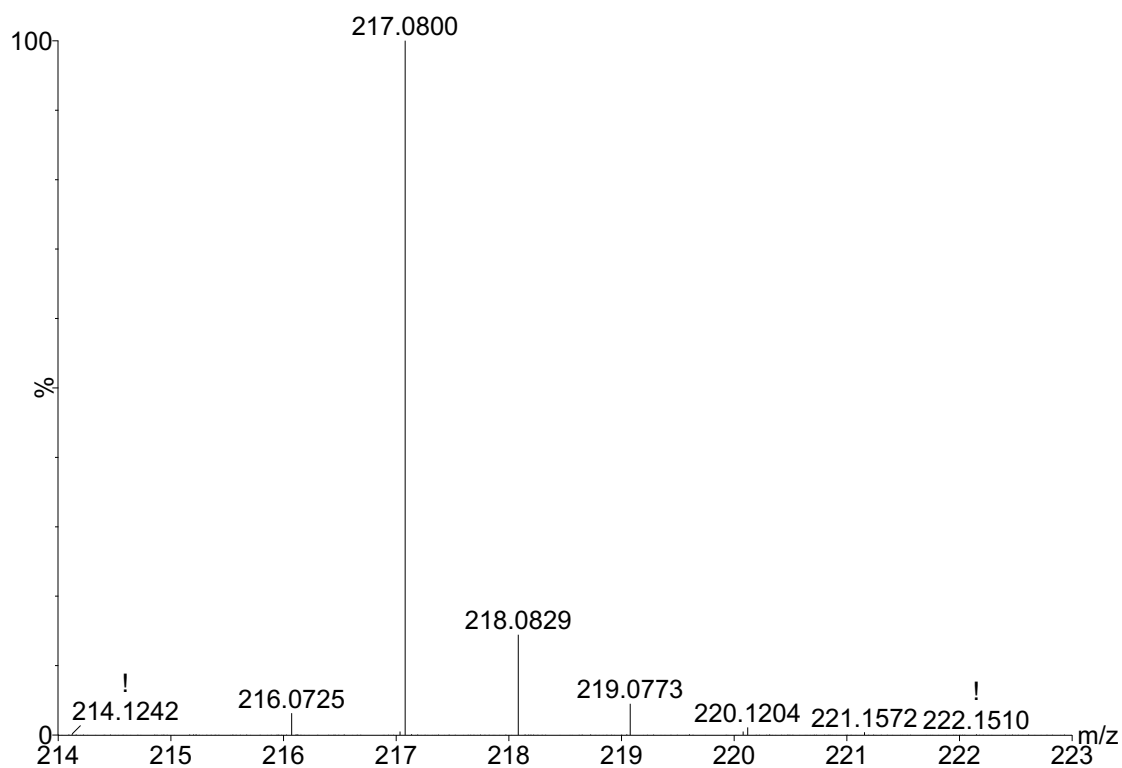


Figure 4.60. ESI-MS (+) of TDA standard. Molecular formula $C_{12}H_{13}N_2S$ ($m/z = 217.0800$), $C_{12}H_{12}N_2S$ ($m/z = 216.0725$) and represents the protonated standard and cationic radical, respectively. Conditions: 0.5 mM TDA, 10 mM pH 6.0 buffer and 3-h incubation.

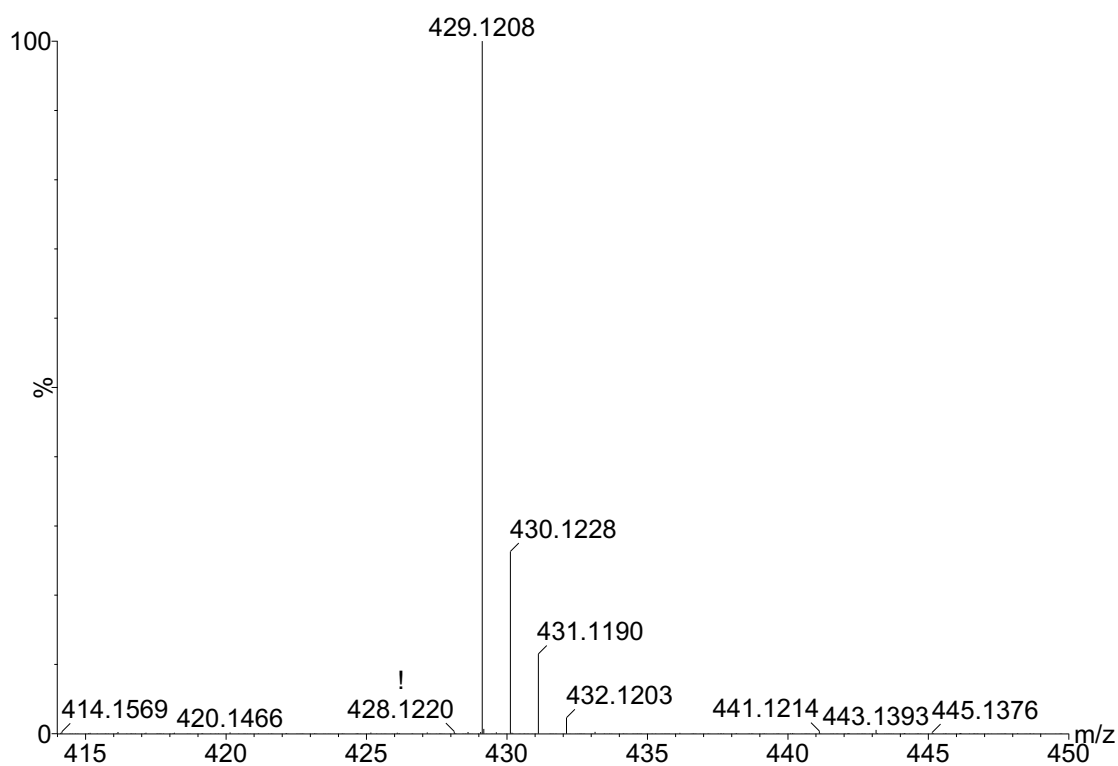


Figure 4.61. ESI-MS (+) of TDA enzymatic reaction precipitate. Molecular formula $C_{24}H_{21}N_4S_2$ ($m/z = 429.1208$) represents the protonated azo-dimer. Conditions: 0.5 mM TDA, 0.55 mM hydrogen peroxide, 0.15 U/mL SBP, 10 mM pH 6.0 buffer and 3-h reaction.

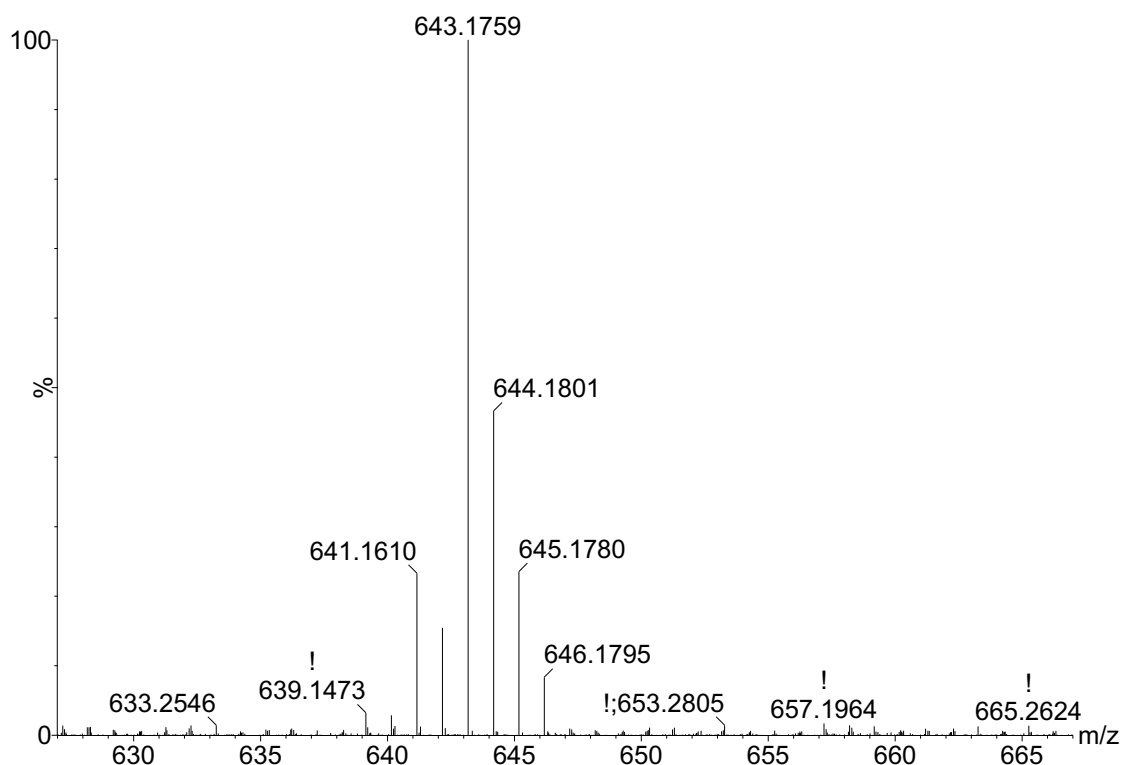


Figure 4.62. ESI-MS (+) of TDA enzymatic reaction precipitate. Molecular formula $C_{36}H_{31}N_6S_3$ ($m/z = 643.1759$), $C_{36}H_{29}N_6S_3$ ($m/z = 641.1610$) represents the protonated mono-azo and bis-azo trimers, respectively. The peak at $m/z = 641.1610$ represent weak signal with low confidence in identification. Conditions: 0.5 mM TDA, 0.55 mM hydrogen peroxide, 0.15 U/mL SBP, 10 mM pH 6.0 buffer and 3-h reaction.

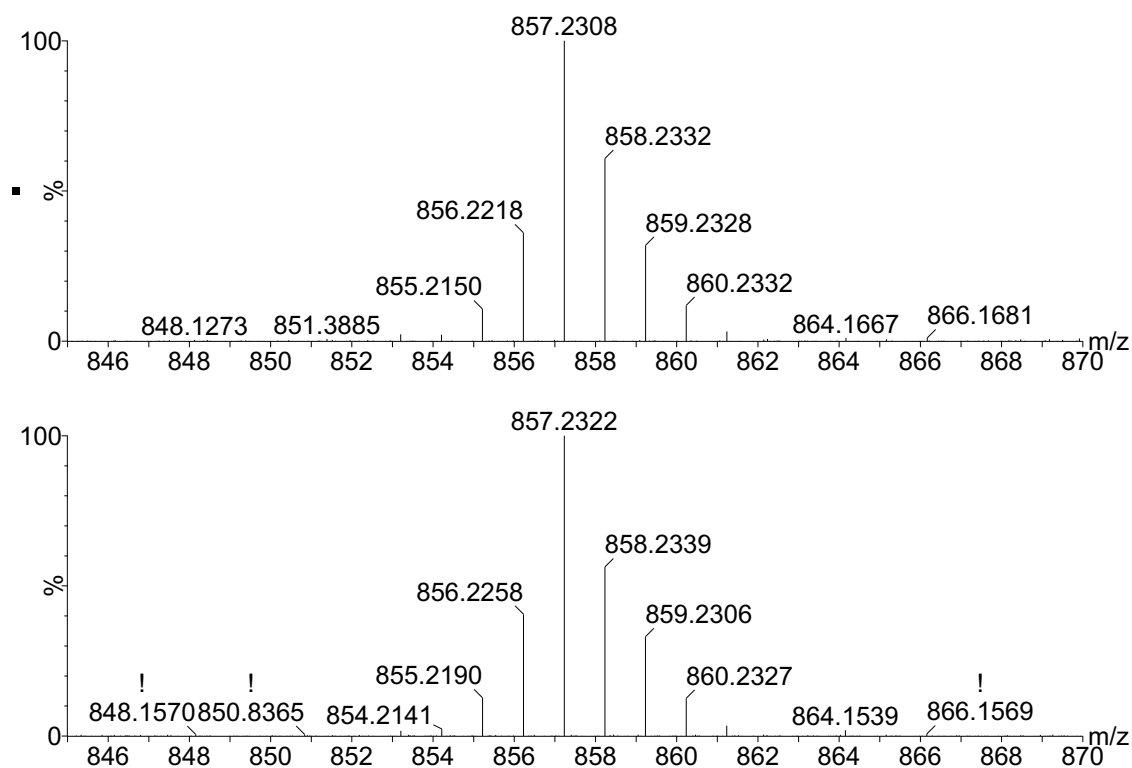


Figure 4.63. ESI-MS (+) of TDA enzymatic reaction precipitate. Molecular formula C₄₈H₄₁N₈S₄ (m/z = 857.2308 and 857.2322) represents the protonated mono-azo tetramer. Conditions: 0.5 mM TDA, 0.55 mM hydrogen peroxide, 0.15 U/mL SBP, 10 mM pH 6.0 buffer and 3-h reaction. The two panels represent different acquisition number run at different time interval.

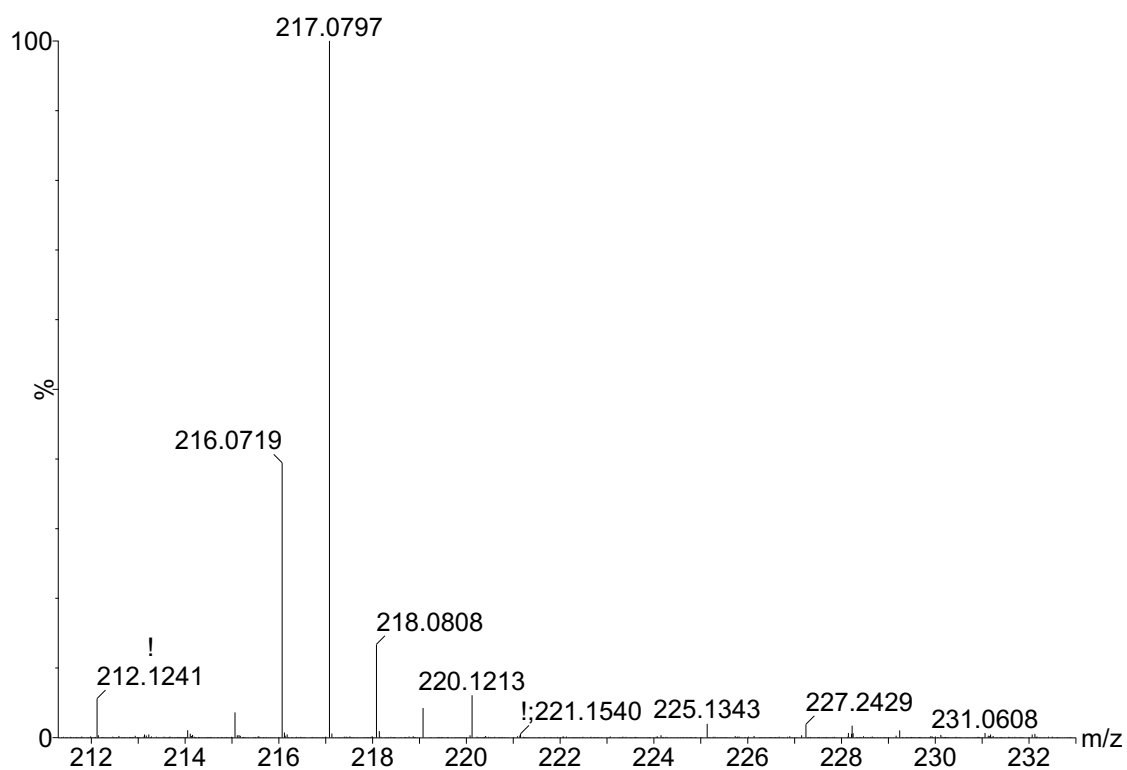


Figure 4.64. ESI-MS (+) of TDA enzymatic reaction supernatant. Molecular formula $C_{12}H_{13}N_2S$ ($m/z = 217.0797$) represents the protonated residual monomer. Conditions: 0.5 mM TDA, 0.55 mM hydrogen peroxide, 0.15 U/mL SBP, 10 mM pH 6.0 buffer and 3-h reaction.

Figure 4.65 shows the mass spectrum of MOCA (MH) in a standard solution with m/z value of 267.0459 and molecular formula $C_{13}H_{13}N_2Cl_2$. The m/z values of 268.0482 (^{13}C -MH) and 269.0422 (^{37}Cl -MH) signify its ^{13}C and ^{37}Cl peaks, respectively. A product with formula $C_{26}H_{21}Cl_4N_4$ and m/z value of 529.0501 shown in Fig. 4.66 was identified in the reaction precipitates, which was consistent with the protonated azo-dimer (M_2H-4), confirmed by its ^{13}C and ^{37}Cl isotope peaks at m/z values of 530.0522 and 531.0485, respectively. A product with m/z value of 791.0560 in the precipitates, corresponding to molecular formula $C_{39}H_{29}Cl_6N_6$ in Fig. 4.67, was consistent with protonated bis-azo trimer (M_3H-8) and its ^{37}Cl - M_3H-8 peak at m/z value of 793.0582. Figure 4.68 shows a MOCA fragmentation product ion in the reaction supernatant with m/z value of 156.0214 and molecular formula C_7H_7ClNO ($M-C_6H_5NCl+O$). There was evidence of dechlorination and oxygenation in the fragmentation product, similar to the result obtained for 4-COT described earlier. The loss of Cl was consistent with the results from 4-COT although loss of chlorine and addition of oxygen was not detected in the higher m/z ranges for MOCA as was seen in 4-COT. The product with m/z value of 267.0455 and molecular formula $C_{13}H_{13}Cl_2N_2$ in Fig. 4.69 is consistent with protonated residual monomer of MOCA (MH) in the supernatant confirmed by its corresponding ^{13}C -MH and ^{37}Cl -MH at m/z values of 268.0494 and 269.0432, respectively.

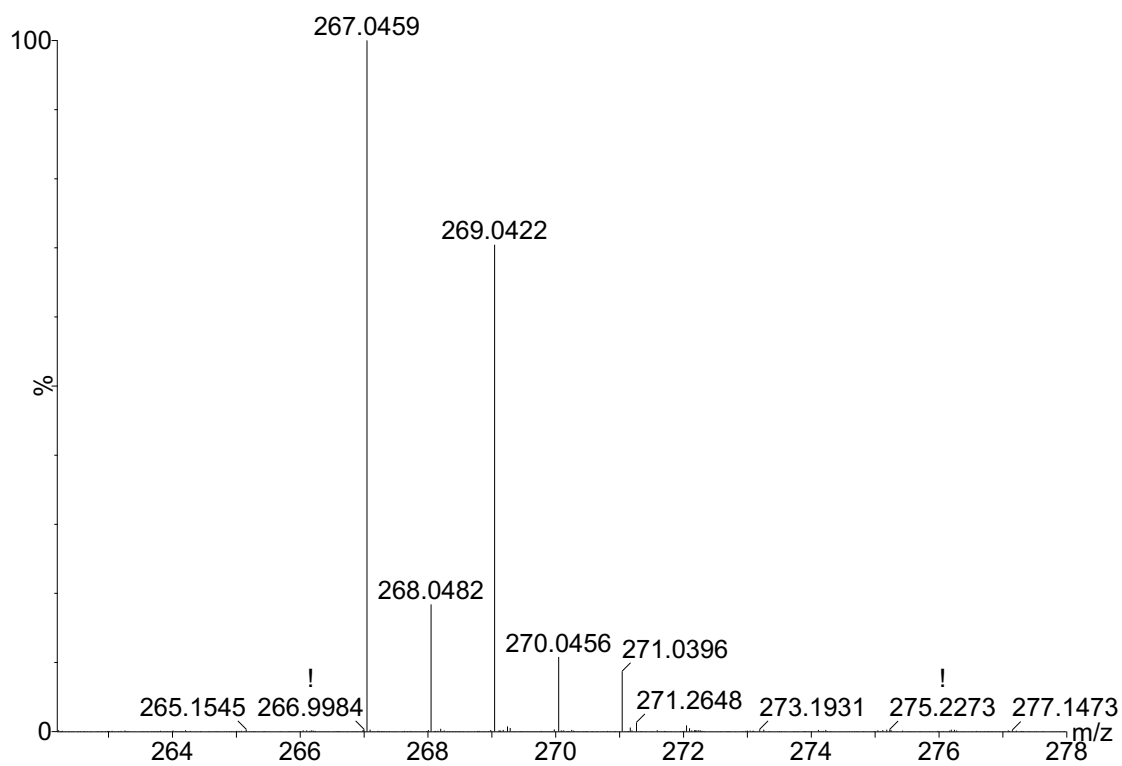


Figure 4.65. ESI-MS (+) of MOCA standard. Molecular formula $C_{13}H_{13}N_2Cl_2$ ($m/z = 267.0459$) represents the protonated standard. Conditions: 0.1 mM MOCA, 10 mM pH 4.2 buffer and 3-h incubation.

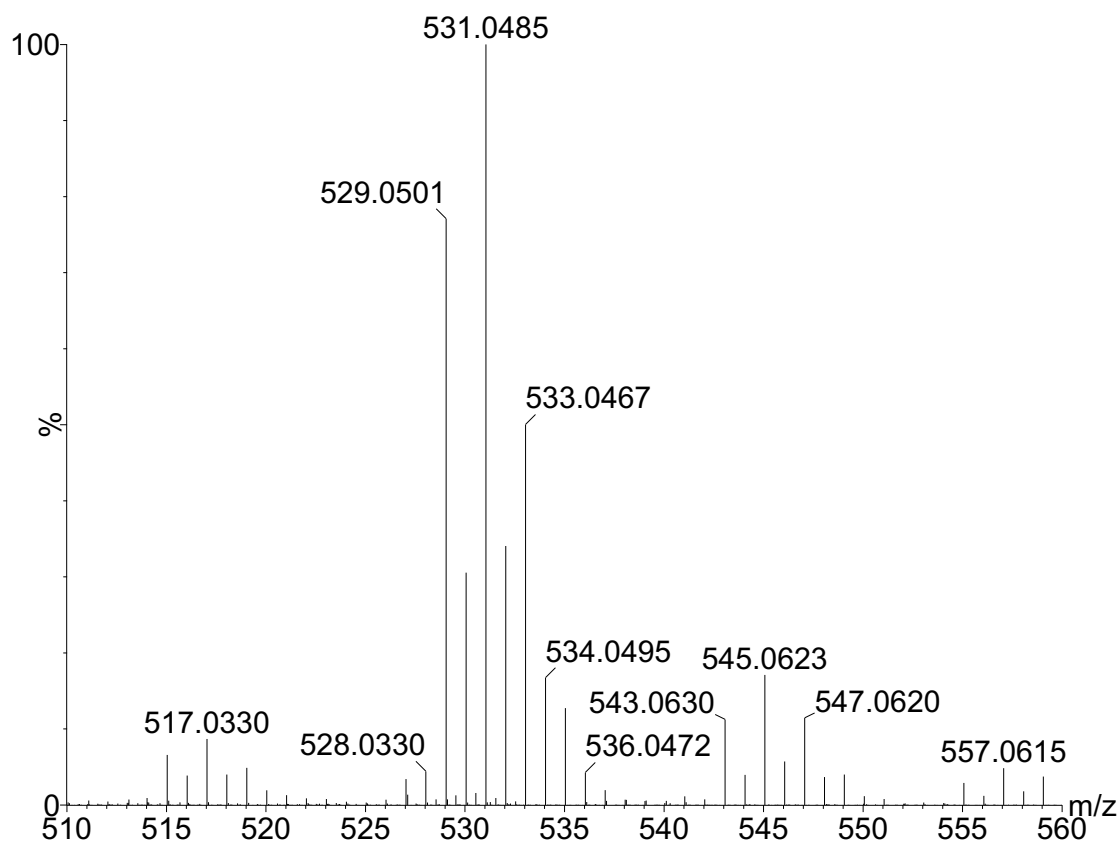


Figure 4.66. ESI-MS (+) of MOCA enzymatic reaction precipitate. Molecular formula $C_{26}H_{21}Cl_4N_4$ ($m/z = 529.0501$) represents the protonated azo-dimer. Conditions: 0.1 mM MOCA, 0.15 mM hydrogen peroxide, 0.1 U/mL SBP, 10 mM pH 4.2 buffer and 3-h reaction.

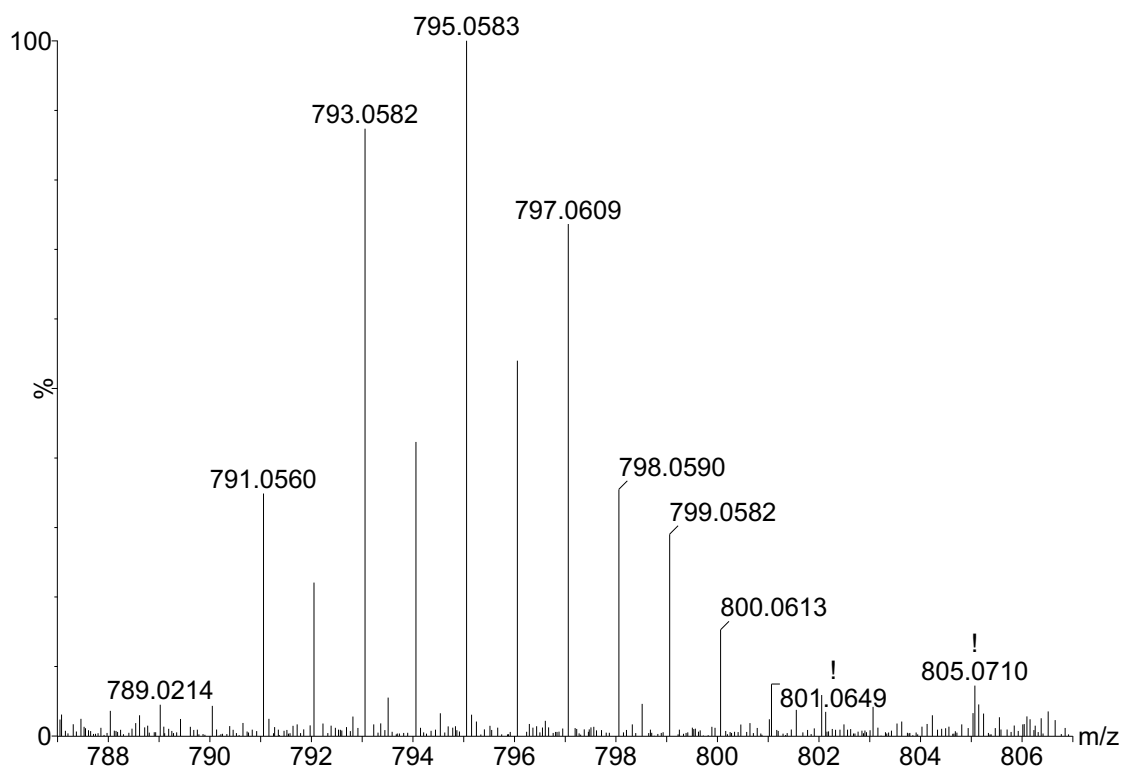


Figure 4.67. ESI-MS (+) of MOCA enzymatic reaction precipitate. Molecular formula $C_{39}H_{29}Cl_6N_6$ ($m/z = 791.0560$) represents the protonated bis-azo trimer. Conditions: 0.1mM MOCA, 0.15 mM hydrogen peroxide, 0.1 U/mL SBP, 10 mM pH 4.2 buffer and 3-h reaction.

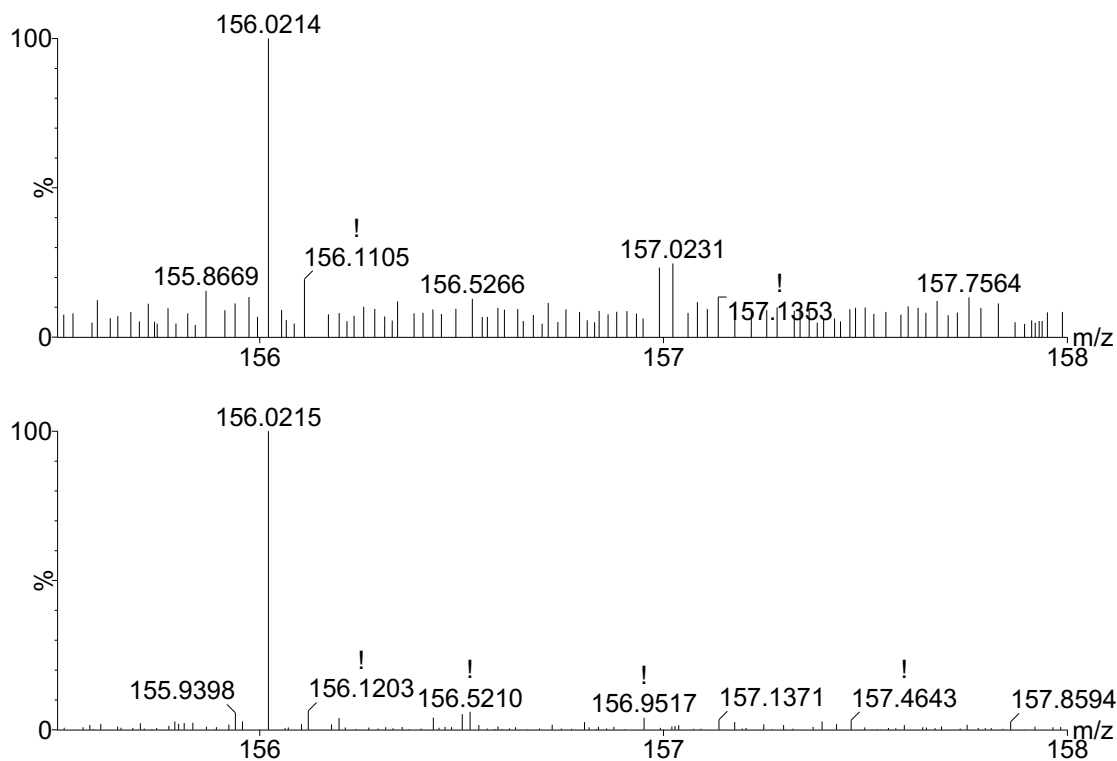


Figure 4.68. ESI-MS (+) of MOCA enzymatic reaction supernatant. Molecular formula C_7H_7ClNO ($m/z = 156.0214$ and 156.0215) represents a MOCA fragmentation product. Conditions: 0.1 mM MOCA, 0.15 mM hydrogen peroxide, 0.1 U/mL SBP, 10 mM pH 4.2 buffer and 3-h reaction. The two panels represent different acquisition number run at different time intervals.

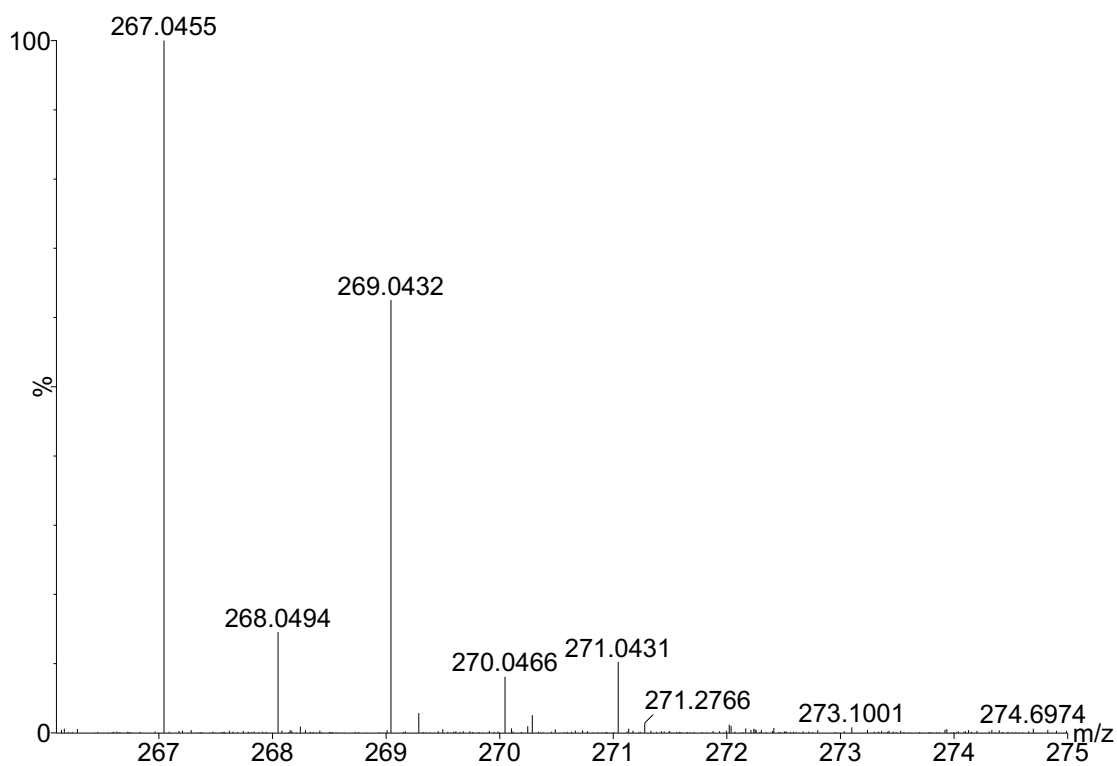


Figure 4.69. ESI-MS (+) of MOCA enzymatic reaction supernatant. Molecular formula $C_{13}H_{13}Cl_2N_2$ ($m/z = 267.0455$) represents the protonated residual monomer. Conditions: 0.1 mM MOCA, 0.15 mM hydrogen peroxide, 0.1 U/mL SBP, 10 mM pH 4.2 buffer and 3-h reaction.

The formation of azo-products that were investigated in this study occurred as a result of radical N-N-coupling after the enzymatic reaction that leads to formation of a hydrazine, which further reacted with H_2O_2 and/or air to form the corresponding azo compounds (ATSDR 2009). This is in agreement with the results of Zhu and Shi (2013) where they established a method of oxidative coupling of anilines using CuBr as catalyst and di-tert-butyl diaziridinone as oxidant, and it was shown that it is possible to couple various primary and secondary anilines under mild conditions to provide the corresponding hydrazines and, therefore, results in azo compounds in high yields. Another group of researchers have investigated that the monomer of N-aniline during peroxidase-catalyzed polymerization reaction with HRP leads to formation of azo-benzene. The formation of azobenzene, the dimerization product of N-N-coupled aniline radicals was identified using GC-MS analysis (gas chromatography-mass spectrometry) (Michail *et al.* 2013). The researchers studied the azobenzene standard by GC and the retention time of the polymerized product of the aromatic amine was same as that of the standard azo benzene thus, confirming the product as azo benzene formed after the enzymatic reaction with the HRP/ H_2O_2 system. Similar types of products were generated when the arylamines studied here were polymerized by SBP/ H_2O_2 catalyzed reaction.

The MS measurements presented in this study reflect preliminary evidence for the nature of products formed by enzymatic treatment. The MS results obtained consisting of m/z ratios, molecular formula, types of compounds/products and their symbolism are summarized in Table 4.4. However, it is suggested that employment of a substitute techniques such as MS-MS or HPLC/MS, as well as other spectroscopic techniques such as NMR and IR, should be used for further characterization of the products in terms of their

size and structure. The use of UV-VIS for more evidence of the azo-products formed is described in Section 4.7.

Table 4.4. Summary of mass spectrometry results consisting of m/z ratios, molecular formula, types of compounds/products and their nomenclature.

m/z ratio	Molecular formula	Types of compounds	Nomenclature
138.0917	C ₈ H ₁₂ NO	<i>p</i> -cresidine protonated standard	MH
271.1447	C ₁₆ H ₁₉ N ₂ O ₂	<i>p</i> -cresidine protonated azo-dimer	M ₂ H-4
138.0914	C ₈ H ₁₂ NO	<i>p</i> -cresidine protonated residual monomer	MH
123.0682	C ₇ H ₉ NO	<i>p</i> -cresidine fragmentation product	MH-CH ₂
142.0418	C ₇ H ₉ NCl	4-COT protonated standard	MH
141.0345	C ₇ H ₈ NCl	4-COT cationic radical	M
246.0687	C ₁₄ H ₁₃ ClNO	4-COT dimer/deaminated/dechlorinated/oxygenated	M ₂ H-2-NH-Cl+O
385.0871	C ₂₁ H ₁₉ Cl ₂ N ₂ O	4-COT trimer/deaminated/dechlorinated/oxygenated	M ₃ H-4-NH-Cl+O
142.0420	C ₇ H ₉ NCl	4-COT protonated residual monomer	MH
138.0917	C ₁₂ H ₁₃ N ₂ O	ODA protonated standard	MH
397.1659	C ₂₄ H ₂₁ N ₄ O ₂	ODA protonated azo-dimer precipitate	M ₂ H-4
595.2437	C ₃₆ H ₃₁ N ₆ O ₃	ODA protonated mono-azo trimer	M ₃ H-6
593.2279	C ₃₆ H ₂₉ N ₆ O ₃	ODA protonated bis-azo trimer	M ₃ H-8
789.2935	C ₄₈ H ₃₇ N ₈ O ₄	ODA protonated tris-azo tetramer	M ₄ H-12
201.1028	C ₁₂ H ₁₃ N ₂ O	ODA protonated residual monomer	MH
397.1656	C ₂₄ H ₂₁ N ₄ O ₂	ODA protonated azo-dimer in supernatant	M ₂ H-4
199.1233	C ₁₃ H ₁₅ N ₂	MDA protonated standard	MH
393.2068	C ₂₆ H ₂₅ N ₄	MDA protonated azo-dimer in precipitate	M ₂ H-4
589.3063	C ₃₉ H ₃₇ N ₆	MDA protonated mono-azo trimer	M ₃ H-6
587.2911	C ₃₉ H ₃₅ N ₆	MDA protonated bis-azo trimer	M ₃ H-8
783.3887	C ₅₂ H ₄₇ N ₈	MDA protonated bis-azo tetramer	M ₄ H-10
199.1236	C ₁₃ H ₁₅ N ₂	MDA protonated residual monomer in precipitate	MH
199.1237	C ₁₃ H ₁₅ N ₂	MDA protonated residual monomer in supernatant	MH
393.2088	C ₂₆ H ₂₅ N ₄	MDA protonated azo-dimer in supernatant	M ₂ H-4
217.0800	C ₁₂ H ₁₃ N ₂ S	TDA protonated standard	MH
216.0725	C ₁₂ H ₁₂ N ₂ S	TDA cationic radical	M
429.1208	C ₂₄ H ₂₁ N ₄ S ₂	TDA protonated azo-dimer in precipitate	M ₂ H-4
643.1759	C ₃₆ H ₃₁ N ₆ S ₃	TDA protonated mono-azo trimer	M ₃ H-6
641.1610	C ₃₆ H ₂₉ N ₆ S ₃	TDA protonated bis-azo trimer	M ₃ H-8
857.2308	C ₄₈ H ₄₁ N ₈ S ₄	TDA protonated mono-azo tetramer	M ₄ H-8
217.0797	C ₁₂ H ₁₃ N ₂ S	TDA protonated residual monomer in supernatant	MH
267.0459	C ₁₃ H ₁₃ N ₂ Cl ₂	MOCA protonated standard	MH
529.0501	C ₂₆ H ₂₁ Cl ₄ N ₄	MOCA protonated azo-dimer	M ₂ H-4
791.0560	C ₃₉ H ₂₉ Cl ₆ N ₆	MOCA protonated bis-azo trimer	M ₃ H-8
156.0214	C ₇ H ₇ ClNO	MOCA fragmentation product	M-C ₆ H ₅ NCl+O
267.0455	C ₁₃ H ₁₃ Cl ₂ N ₂	MOCA protonated residual monomer	MH

4.7. Product Identification using UV-VIS

To proceed further with the verification of the azo-products formed after enzyme catalysed reaction, UV spectrophotometric analysis was performed. As described by

Beharry and Woolley (2011), *trans*-form of azobenzene shows a weak $n\text{-}\pi^*$ band near 440 nm and a strong $\pi\text{-}\pi$ band near to 320 nm, whereas, for the *cis*-form the band is stronger near 440 nm and the short wavelength bands at 280 and 250 nm. The substituents on the phenyl rings may strongly impact the position and shapes of azoaromatic absorption bands. For example, amino groups at the *ortho*- or *para*-positions can red-shift the spectrum dramatically (Beharry and Woolley 2011).

Considering this fact, the supernatants after the enzyme catalysed reaction were read in the UV-VIS to check for the presence of azoaromatic bands. The *p*-cresidine showed a peak around 496 nm after the enzymatic treatment as seen in Fig. 4.70. The azoaromatic may exhibit substituent effects on the ring and therefore, the shift in peak observed. Similar findings of wavelength by Siewertsen *et al.* (2011) showed a photo-switching dynamics of dihydrodibenzodiazocine, a bridged azobenzene with its absorption maximum around ($\lambda = 490$ nm). Another finding reported by Siewertsen *et al.* (2009) where the $n\text{-}\pi^*$ band of *trans*-isomer occurs at 490 nm and *cis*-isomer at 404 nm. 4-COT exhibited no peak corresponding to azo-bands, which was consistent and supported by the MS results since no product was identified that resembled the azo-compound. For ODA, a peak was observed around 510 nm, in Figs. 4.71 (a) and (b), whereas, MDA exhibited a Gaussian peak at 321 nm (Fig. 4.72). This supports the presence of formation of azo-coupled product that was detected in MS analysis. Similarly, for TDA, the peak was observed around 510 nm as can be seen in Fig. 4.73. MOCA also showed a peak at 321 nm as seen in Fig. 4.74 that supports the results obtained in MS analysis. It might be due to the *trans*-azobenzene, which shows a strong band at 320 nm. As reported by Beharry *et al.* (2011) in bridged azoaromatics the magnitude of the $n\text{-}\pi^*$ separation is larger, therefore, more complete

switching is possible. The following diagrams show UV, VIS and UV-VIS ranges, wherever applicable, focussing mainly on the peak of interest.

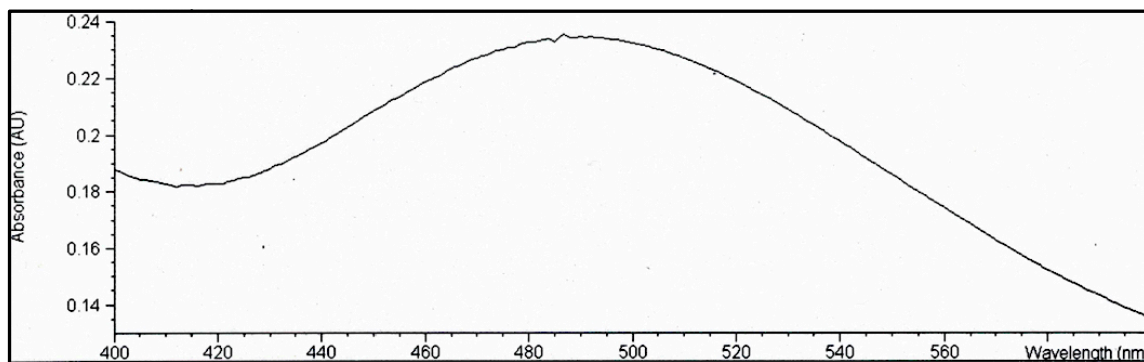


Figure 4.70. VIS spectrum of *p*-cresidine batch reaction supernatant. Conditions: 1.0 mM *p*-cresidine; 1.25 mM hydrogen peroxide, 0.01 U/mL SBP, 10 mM pH 4.6 buffer and 3-h reaction.

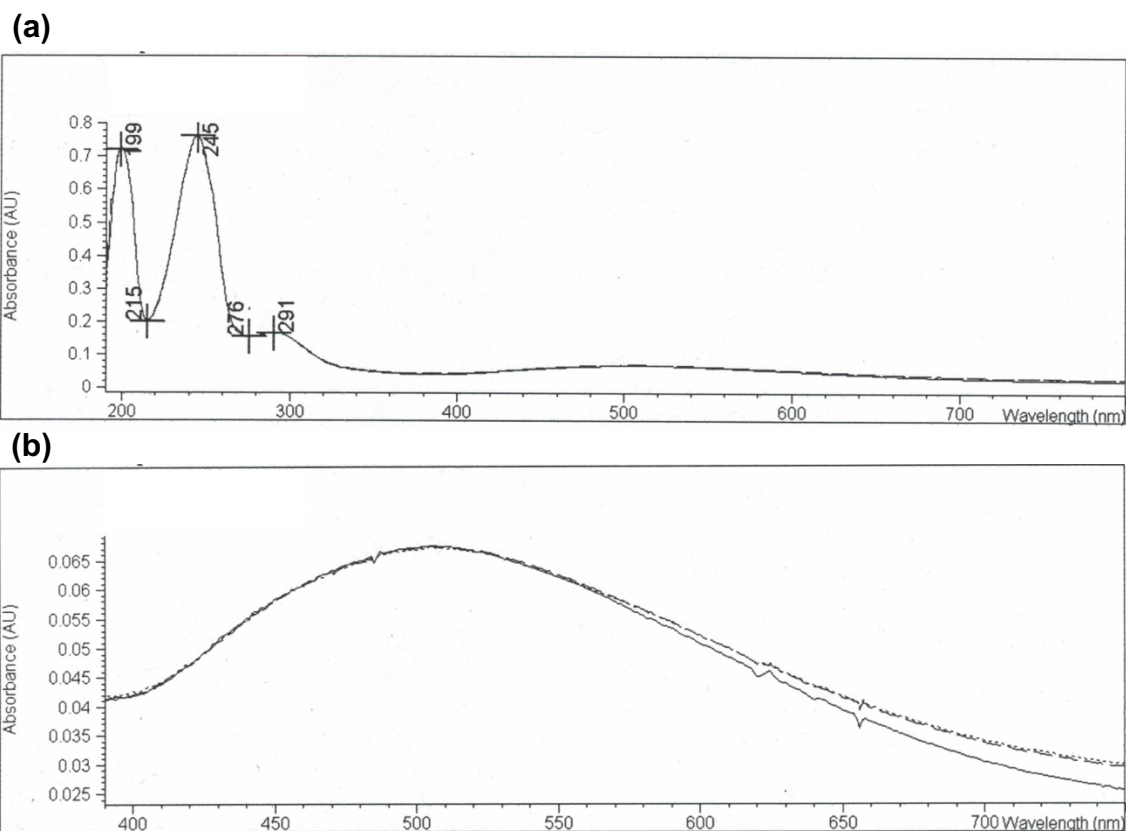


Figure 4.71. UV-VIS spectrum of ODA batch reaction supernatant with (a) broad and (b) narrow ranges. Conditions: 0.5 mM ODA, 0.6 mM hydrogen peroxide, 0.04 U/mL SBP, 10 mM pH 6.0 buffer and 3-h reaction.

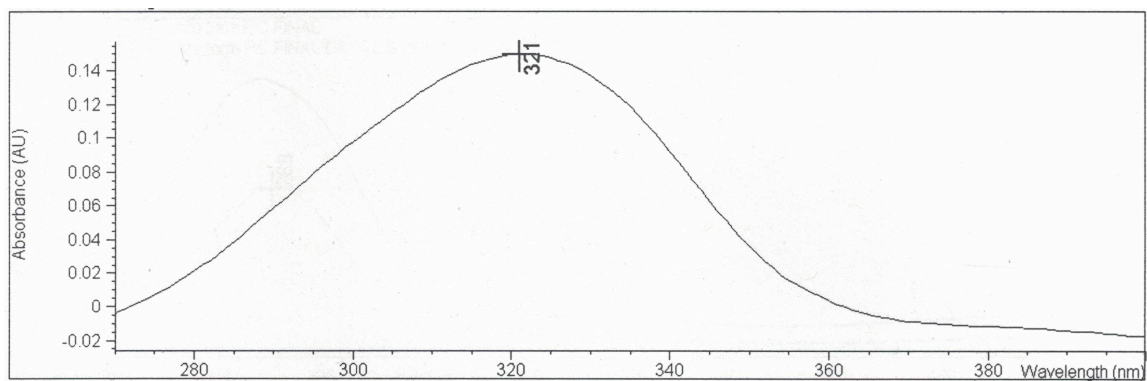


Figure 4.72. UV spectrum of MDA batch reactions supernatant. Conditions: 0.5 mM MDA, 0.7 mM hydrogen peroxide, 0.7 U/mL SBP, 10 mM pH 6.0 buffer and 3-h reaction.

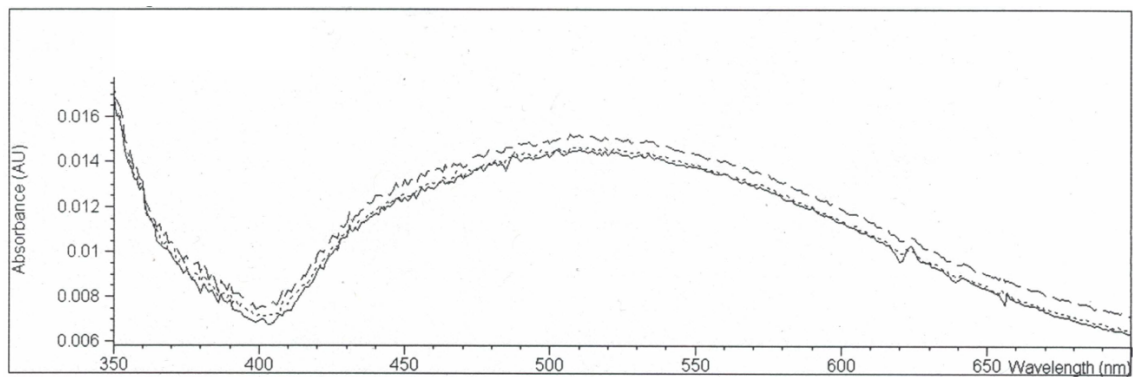


Figure 4.73. UV-VIS spectrum of TDA batch reaction supernatant. Conditions: 0.5 mM TDA, 0.55 mM hydrogen peroxide, 0.15 U/mL SBP, 10 mM pH 6.0 buffer and 3-h reaction.

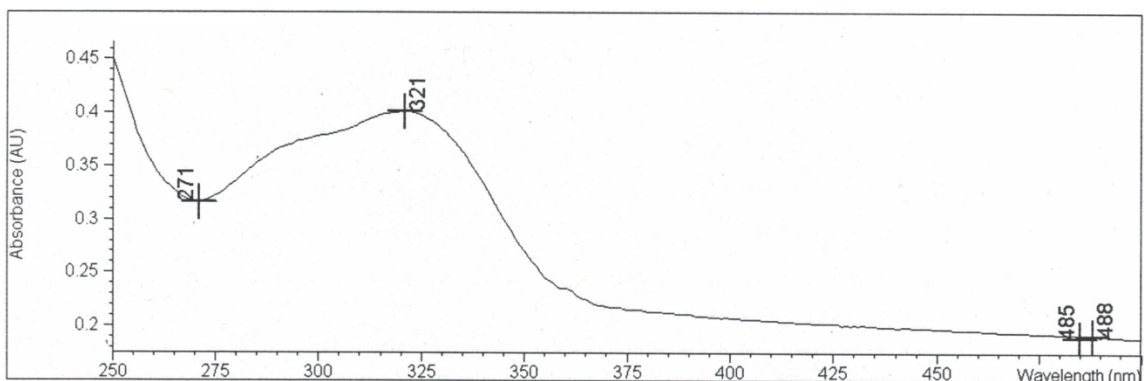


Figure 4.74. UV-VIS spectrum of MOCA batch reaction supernatant. Conditions: 0.1 mM MOCA, 0.15 mM hydrogen peroxide, 0.1 U/mL SBP, 10 mM pH 4.2 buffer and 3-h reaction.

4.8. TOC Analysis

The TOC analysis for MDA was performed on samples from a batch reactor run under the optimum conditions shown in Table 4.1. The TOC for both SBP and catalase (at the respective concentrations used for the batch reaction) were used to correct the carbon balance. The TOC of the batch reactor content was 130 mg/L without enzymatic treatment as determined from the analyzer, whereas, after the 3-h reaction, the TOC value obtained was 22.9 mg/L (TOC corrected for both SBP and catalase). The theoretical 0.5 mM TOC of MDA was calculated as 78.0 mg/L, close to the experimental value of 84.8 mg/L. This difference can be attributed to the impurity of MDA and experimental uncertainty. The calculated TOC from the HPLC conversion was 4.0 mg/L and the experimental was 22.9 mg/L. This difference is indicative of residual carbon in the reaction, which could be dimers or higher oligomers. Also, the experimental uncertainty, to some extent, might have attributed for such differences.

4.9. Cost Analyses of Enzymatic Treatment of the Arylamines

An important parameter that makes a technology suitable for use in industry is economic feasibility. Cost analysis is known to measure the economic burden incurred by a wastewater treatment method. Growth of population, industrialization and urbanization have caused mixing of contaminants into potable water without monitoring the proper limits of discharge, which is a major concern with effluents from industries. Different industrial sectors are improving the economic welfare of a country, but at the same time also contributing to polluting the waterbodies by discharging their wastewater in which the studied aromatic pollutants are present. It may not be possible to treat these pollutants by the conventional wastewater treatment methods. Therefore, their discharge is raising a great concern to public health, economics and aesthetic values of a country and increases

the need to implement a sustainable treatment method such as that developed in this study to treat these pollutants and improve the environment. The cost of treatment could be approximated based on laboratory-scale investigations. However, this estimated value could increase substantially when a real wastewater matrix from an industry is considered. It is also accepted that the treatment of wastewater provides benefits to the environment; however, in most cases, it is difficult to quantify the environmental benefits due to the absence of ‘market value’ of the benefits accrued. The enzymatic treatment is a viable option in terms of treatment of certain types of industrial wastewater. However, there is a need for the economic evaluation and justification and the feasibility of conventional industrial wastewater treatment against enzymatic treatment. The following sections present the general methodology used for performing a *pro-forma* cost analysis, along with capital and chemical costs for conventional as well as enzymatic treatment methods for comparison, both at a laboratory and pilot-plant scale.

4.9.1. General methodology for capital cost estimation

A general procedure for a *pro forma* calculation of the capital and chemical costs for enzymatic treatment is provided in this section. The time required for 95% removal, $t_{95\%}$ (Mahamuni and Adewuyi 2010), can be calculated using the first-order model, Equation 21 (Fogler 2004) for degradation of the pollutants based on the first-order rate constants, k , of the chemicals shown in Table 4.2:

$$\ln\left(\frac{C}{C_o}\right) = -kt \quad (21)$$

Therefore for 95% degradation ($C/C_o = 0.05$), Equation 21 can be formulated as:

$$t_{95\%} = \frac{2.996}{k} \quad (22)$$

If it is assumed that the design flow rate of a continuous-flow reactor is $1 \text{ m}^3/\text{min}$ and the energy density is $E \text{ watt/m}^3$, the cost of the reactor will be $\$(E \times t_{95\%})$, which will help to obtain the capital cost of the equipment. Ibrahim *et al.* in 2001 calculated the capital cost for enzymatic treatment in USD as approximately $\$0.14/\text{m}^3$. For obtaining the present cost, the capital cost reported in 2001 was converted to a present-worth basis using compound interest and the average inflation rate of 3.27% in the United States (Trading Economics 2017). In this way, the capital cost for enzymatic treatment in 2018 is calculated to be approximately $\$0.23/\text{m}^3$. Similarly, the total cost (capital and chemical) of conventional water treatment methods that were reported by Ibrahim *et al.* in 2001 were also converted. Thus, the present values become $\$1.75/\text{m}^3$ for activated sludge treatment, and $\$2.19/\text{m}^3$ for treatment by adsorption using activated carbon. The following section shows the methodology for estimating the chemical costs (SBP and H_2O_2) for the removal of the pollutants based on their optimized parameters shown in Table 4.1.

4.9.2. Estimation of chemical cost of enzymatic treatment

Expenses for bulk purchases of SBP and H_2O_2 required for the enzyme-catalyzed processes are assessed in this section. The cost of crude SBP was considered assuming the use of ground hulls to provide the minimum enzyme concentration that was required for at least 95% removal of the substrates. Detailed calculations of chemical costs for *p*-cresidine are explained in the text below and the same methodology was used to estimate the chemical costs of the other substrates that are summarized in Tables 4.5 and 4.6. For treating 1.0 mM *p*-cresidine, 0.01 U/mL , *i.e.*, 10 kU/m^3 of SBP was necessary, as previously seen in Section 4.3. In this analysis, it is assumed that soybean hulls having an activity of 68.1 U/g (Steevensz *et al.* 2013) were added to the reactor to achieve the desired levels. The cost of SBP hulls was found to be $\$125/\text{T}$ (New Balance Commodities,

Nodaway, IA). Using these values, the cost of enzyme for treating *p*-cresidine was calculated as \$0.018/m³. In a similar way, the costs of SBP for treating the other pollutants were calculated and the results are tabulated in Table 4.5. As expected, based on SBP requirement, the enzyme cost for treating of MDA was the highest, at \$1.285/m³, whereas the cost was lowest for 4-COT (\$0.017/m³).

The H₂O₂ concentration needed to treat 1.0 mM *p*-cresidine, was 1.25 mM, i.e., 42.5 g/m³. The cost of 35% w/w H₂O₂ was considered to be \$0.84/kg (Kencro Chemicals, Oakville, ON), from which the H₂O₂ costs for treating *p*-cresidine was calculated as \$0.036/m³. Similarly, the cost of H₂O₂ for the treatment process of the other substrates were calculated and the results are presented in Table 4.5. Thereafter, the total cost for enzymatic treatment was obtained by adding the capital costs to the chemical costs. This preliminary analysis shows that the total cost was highest for MDA at \$1.535/m³ and lowest for 4-COT at \$0.261/m³. For comparison, the total cost for enzymatic treatment of 1.0 mM phenol (Ibrahim *et al.* 2001) has also been provided in Table 4.6.

4.9.3. General summary of cost analyses

In order to compare the total value of the present-day costs of enzymatic treatment to the conventional wastewater treatment processes, the treatment methods along with their respective expenses are shown in Table 4.6. It can be seen that the total cost of enzymatic treatment of the chemical pollutants was almost 2 to 8 times less than that of the conventional treatment processes. It is to be noted that the capital cost of the three types of methods, and the chemical costs of the conventional methods, were in fact calculated considering the treatment of phenolic wastewater by Ibrahim *et al.* 2001. The purpose of the calculation presented here is not a direct cost comparison but only a preliminary estimate to show the feasibility since the conventional methods are also known to remove

solids, organic/inorganic matter, BOD, heavy metals, *etc.* associated with the wastewater. Also, the handling of the precipitates and other unit operations have not been considered.

It is suggested that enzymatic treatment could be specifically employed to pre-treat the effluent from an industry in which the specific pollutants are released, before it is mixed with other wastewater streams within the industrial facility. The pre-treated effluent could then be mixed with other streams for further treatment – including BOD contributed by the soybean hulls – and their disposal. Therefore, enzymatic pre-treatment could present a 10-15% surcharge on conventional treatment, but this may also be alleviated by lessening the burden that recalcitrant aromatics pose on a conventional wastewater treatment plant.

Table 4.5. Estimated costs (in US\$) for enzymatic treatment of wastewater.

Substrates	Substrate concentration (mM)	SBP			H ₂ O ₂			Capital cost (\$/m ³)	Total cost (\$/m ³)
		SBP requirement (U/mL)	SBP requirement (kU/m ³)	Enzyme cost (\$/m ³)	H ₂ O ₂ requirement (mM)	H ₂ O ₂ requirement (g/m ³)	H ₂ O ₂ cost (\$/m ³)		
<i>p</i> -Cresidine	1.00	0.010	10.0	0.018	1.25	42.5	0.0360	0.230	0.284
4-COT	1.00	0.009	9.00	0.017	0.500	17.0	0.0140	0.230	0.261
ODA	0.500	0.040	40.0	0.073	0.600	20.4	0.0170	0.230	0.321
MDA	0.500	0.700	700	1.285	0.700	23.8	0.020	0.230	1.535
TDA	0.500	0.150	150	0.275	0.550	18.7	0.0160	0.230	0.521
MOCA	0.100	0.100	100	0.184	0.150	5.10	0.0040	0.230	0.418

Table 4.6. Cost comparison (in US\$) for the treatment of wastewater by three types of treatment. *Estimates are based on conversion of costs as reported by Ibrahim *et al.* (2001) to a present-worth basis using compound interest and an average inflation rate of 3.27% in the USA (Trading Economics 2017) as indicated in the text.

Treatment method	Substrates	Total cost (\$/m ³)
Enzymatic	<i>p</i> -Cresidine	0.284
	4-COT	0.261
	ODA	0.321
	MDA	1.535
	TDA	0.521
	MOCA	0.418
	Phenol	1.950*
Activated sludge		1.750*
Activated carbon		2.190*

CHAPTER 5: GENERAL SUMMARY AND CONCLUSIONS

5.1. Summary

This research investigated the enzyme catalyzed oxidative polymerization and precipitation/co-precipitation of two hazardous monocyclic- (*p*-cresidine, 4-COT) and four atom-bridged bis-anilines (ODA, MDA, TDA, MOCA), hazardous pollutants present in water. Crude SBP has been shown to be a competent enzyme for removal of the toxic pollutants from water by a sustainable approach. The general summary is given in the following paragraphs:

1. Among the six substrates (pollutants) examined in this study all exhibited *pH* optima in the acidic range, 4.2-6.0, close to their respective *pK_a*s. Interestingly, the optimum *pH* for ODA, MDA and TDA were the same, 6.0. The results exhibited inverted bell-shaped *pH*-dependence curves. There was a steep reduction in percentage conversion of the substrates on either side of the optimum *pH* value possibly due to variations in ionization of catalytic residues of the enzyme and also the substrate since the optimum was near the *pK_a*s. The maximum conversion of these substrates was dependent on the optimal conditions which were substrate-specific.
2. Although a demand of 1 mole of H₂O₂ per two anilines is theoretically needed for conversion, additional consumption of H₂O₂ over the theoretical stoichiometric requirement was observed for *p*-cresidine. In contrast, the H₂O₂ consumption for anilino groups in the bifunctional compounds, and for 4-COT, were very near to the theoretical stoichiometric value, i.e. (H₂O₂)/(substrate functional group) ≤ 1.
3. In terms of SBP requirements, 4-COT required the least amount of enzyme, 0.009 U/mL, for removal of 1.0 mM of the substrate, in contrast to MDA which required

approximately 80 times more enzyme at 0.7 U/mL for removal of 0.5 mM of the substrate by $\geq 95\%$. The mono-cyclic compounds consisted of one anilino group unlike the bis-anilines, therefore the functional-group concentrations of substrate that were treated by the enzyme were equivalent, except for MOCA where 0.1 U/mL of SBP was required for 95% conversion of 0.1 mM MOCA. The concentrations of enzyme required for removal of these substrates were less than those reported for simple anilines in previous research, with the exception of MDA.

4. Substrate consumption was examined as a function of time using batch reactors run under optimal operating conditions. The rate constants and their half-lives were normalized with their respective enzyme activities for comparison. From the progress curves it was seen that SBP's catalytic reaction progressed rapidly at the start then slowed down. The removals of all the substrates by SBP were fitted as a first-order process to the initial part of the progress curves. The reaction of ODA progressed the fastest with k being 9.63 ± 0.5 /min, and the slowest rate was observed for MOCA ($k = 1.70 \pm 0.22$ /min). Accordingly, the $t_{0.5}$ for ODA was the lowest at 0.0720 ± 0.0006 min, whereas MOCA had the highest $t_{0.5}$ (0.4076 ± 0.002 min). Using the normalized rate constant values, the substrates were ranked based on fastest to slowest reaction rates as: ODA > TDA > 4-COT > *p*-cresidine > MDA > MOCA.
5. Kinetic parameters K_M and V_{max} were derived from the Michaelis-Menten model based on initial rates from progress curves for the substrates run at different concentrations. The Michaelis constant, K_M , is an indicator of the affinity of enzyme for a substrate (lower value means higher affinity). The quotient, V_{max}/K_M , known as catalytic efficiency combines both affinity and reactivity characteristics

of an enzyme reaction. MOCA depicted the lowest K_M , $1.70 \pm 0.14 \mu\text{M}$, followed by $\text{TDA} < \text{ODA} < p\text{-cresidine} < 4\text{-COT} < \text{MDA}$; MDA had the highest K_M , $979 \pm 80 \mu\text{M}$. By normalizing with their respective enzyme activities, 4-COT had the highest maximum velocity (V_{max}) of $488 \pm 116 \mu\text{M/s}$ followed by $\text{ODA} > \text{TDA} > p\text{-cresidine} > \text{MOCA} > \text{MDA}$. MDA showed the lowest V_{max} of $53.6 \pm 3.0 \mu\text{M/s}$. MOCA displayed the highest normalized catalytic efficiency (V_{max}/K_M), $42.8 \pm 4.71 /s$, and MDA the lowest at $0.055 \pm 0.008 /s$.

6. Product determination after enzymatic treatment was done by mass spectrometry (MS) using the ESI technique in positive-ion full-scan mode for all substrates except 4-COT, that was done by the ASAP technique. Protonation occurs under mass spectral conditions. Oxidized oxidative-coupling products, mostly azo-compounds such as azo-dimer ($\text{M}_2\text{H-4}$), mono-azo and bis-azo trimers ($\text{M}_3\text{H-6}$, $\text{M}_3\text{H-8}$, respectively), tris-azo tetramer ($\text{M}_4\text{H-12}$) were commonly detected by MS analysis after the enzymatic treatment except for 4-COT, where generation of oxidative dimer and trimer ($\text{M}_2\text{H-2-NH-Cl+O}$, $\text{M}_3\text{H-4-NH-Cl+O}$) were seen. In most cases, strong peak were confirmed by natural-abundance isotope peaks. A fragmentation product, MH-CH_2 , was seen in the mass spectrum of *p*-cresidine in the reaction precipitates. The oxygenation that occurred in 4-COT reaction supernatant was not a result of MS conditions that was confirmed by scrutinizing the standard which had no evidence of oxygenation. The loss of chlorine in 4-COT mass spectrum occurred during the oxidative coupling as the position of Cl on the ring was on the *para*-position relative to the amino functional group and which was very likely to get dehalogenated, and the deamination was due to MS fragmentation. MOCA, though it possess Cl as its functional group did not present

similar trends to 4-COT in terms of dehalogenation of product ions, however, a fragmentation ion ($M-C_6H_5NCl+O$) in the supernatant underwent dehalogenation and oxygenation. Different types of radical coupling reaction, N-N, N-C or C-C could be deduced from such products. In addition, N-N coupling can occur to form hydrazines which readily oxidize to form azo-compounds, which were observed frequently. It is recommended that employment of an alternative techniques such as MS-MS or HPLC/MS, NMR and IR, should be used for further characterization of the products in terms of their size and structure.

7. Occurrence of azo-products was further confirmed by UV-VIS analysis. MDA and MOCA showed a Gaussian peak at 320 nm confirming the azo-coupled products formed by MS. *p*-Cresidine, ODA and TDA showed peaks around 496-510 nm similar to a bridged azobenzene in previous research by Siewertsen *et al.* (2011). 4-COT did not show any peaks of azo-products consistent with the findings in MS.
8. TOC analysis for MDA showed a reduction in TOC after the enzymatic treatment that was not consistent with the conversion indicated by HPLC, if removal to the same extent is assumed. The discrepancy between calculated residual MDA and supernatant carbon content suggests the presence of soluble oligomers in the solution.
9. A *pro forma* calculation of the capital and chemical costs for enzymatic treatment of the pollutants was also performed and comparison of the total value of the present-day costs of enzymatic treatment to the conventional wastewater treatment processes was also presented. It was seen that the total cost of enzymatic treatment of the chemical pollutants was almost 2 to 8 times less than that of the conventional

treatment processes. The removal of $\geq 95\%$ of MDA requires highest cost of \$1.535/m³ and 4-COT the lowest at \$0.261/m³.

5.2. Conclusions

In conclusion, crude SBP isolated from soybean seed coat was proficient in catalyzing the oxidation of the hazardous pollutants in an ecologically friendly and sustainable manner. With SBP's availability in massive quantity from a by-product of commodity processing of the world's largest seed crop, SBP-based treatment of selected aromatics in this study provides a cost-effective alternative to conventional treatment processes for removing toxic aromatic pollutants from wastewaters. The SBP and H₂O₂ requirements for $\geq 95\%$ removal of these aromatics were much less compared those for simple anilines studied previously. Surprisingly, mono-cyclic anilines required much less SBP than the bis-anilines for removal of the same concentrations of substrates. From kinetic parameters MOCA showed the lowest K_M value indicating its highest affinity for SBP compared to others. ESI-MS and ASAP-MS were useful techniques for determination of oligomeric products arising from the enzymatic treatment. Azo-coupled oligomers seen in MS were further detected in UV-VIS. *Pro forma* cost analysis in this study finds the capital and chemical costs for enzymatic treatment of the harmful pollutants lower than conventional treatments and, thus, will aid in evaluation of the lab-scale process on real wastewater and subsequently the feasibility of commercializing enzymatic treatment.

CHAPTER 6: FUTURE WORK

The results in this study validate the use of SBP, to catalyze the removal of monocyclic and atom-bridged bis-anilines from wastewater. To implement the enzymatic treatment method to full-scale industrial application, several aspects need to be evaluated:

1. Implementation of the enzymatic treatment in a continuous-flow reactor to evaluate its feasibility in industrial scale is recommended.
2. Toxicity study for the soluble and insoluble polymeric products that are formed after the enzymatic treatment is suggested. In addition, an environmental impact assessment needs to be conducted to determine the fate and toxicity of these polymeric products formed.
3. Feasibility of recycling the polymeric products that are generated after the enzymatic treatment needs to be explored to minimise the disposal when dealing in industrial scale.
4. Additionally, some research is needed on the settling characteristics of the precipitates formed in the enzyme catalyzed reactions and the optimal flocculant requirements should be determined.
5. The matrix effect of real wastewater should be studied by re-optimizing the different parameters. More emphasis is commended on effluents consisting of mixtures of multiple substrates and their interactions, it is exceptional to have any effluents consisting only one type of contaminant.
6. A detailed study on kinetic modelling of the enzyme-catalyzed reaction is recommended to determining the rate of inactivation of enzyme. Selection of a reactor system operating in the most efficient mode determines the success of the process and this can be achieved by mathematical modelling, which aids in

selection and designing of a reactor system. The mathematical modelling will assist in selection, designing and optimization of a system for treatment of wastewater by enzymatic treatment. Both steady-state and transient-state models of the soybean peroxidase system should be done, and then further model validation is also recommended to be performed. Application of this model should be incorporated not only to batch systems but also to other reactor configurations such as semi-batch, continuously stirred tank and plug-flow reactors.

7. Structural determination of the products being generated after the enzymatic treatment needs to be completed by means of nuclear magnetic resonance (NMR) spectroscopy.
8. A more realistic cost estimation is recommended for commercializing the enzymatic method in large scale process for treatment of wastewater including the risk assessment parameters. In addition, cost-benefit analysis (CBA), one of the widely accepted rational and systematic decision-making support tools is also suggested.
9. Additive study can be conducted on the enzymatic treatment process that may economize the SBP requirement for removal of the substrates, hence improving the overall efficiency of the treatment method.

BIBLIOGRAPHY

- Adrian P. Andreux, F., Viswanathan, R., Freitag, D., Scheunert, I. (1989). Fate of anilines and related compounds in the environment. A review, *Toxicological & Environmental Chemistry*, 20-21: 109-120.
- Agency for Toxic Substances and Disease Registry Division of Toxicology and Environmental Medicine, ATSDR. (2009). Addendum to the toxicological profile for 1,2-diphenylhydrazine, 1-9.
- Agency for Toxic Substances and Disease Registry, ATSDR. (1994). Toxicological profile for 4,4'-methylenebis (2-chloroaniline). Public Health Service, U.S. Department of Health and Human Services, Atlanta, GA.
- Agency for Toxic Substances and Disease Registry, ATSDR. (1998). Toxicological profile for methylenedianiline. Public Health Service, U.S. Department of Health and Human Services, Atlanta, GA.
- Akyüz, M., Ata, S. (2008). Determination of aromatic amines in hair dye and henna samples by ion-pair extraction and gas chromatography–mass spectrometry. *Journal of Pharmaceutical and Biomedical Analysis*, 47: 68-80.
- Aleksandrov, M.L., Gall, L.N., Krasnov, N.V., Nikolaev, V.I., Shkurov, V.A. (1985). Mass spectrometric analysis of low-volatility thermally unstable substances based on extraction of ions from solution at atmospheric pressure, *Zhurnal Analiticheskoi Khimii*, 40: 1570-1580.
- Al-Kassim, L., Taylor, K.E., Bewtra, J.K., Biswas, N. (1993). Evaluation of the removal of aromatic and halogenated unsaturated hydrocarbons from synthetic wastewater by enzyme catalyzed polymerization, *Proceedings of the 48th Industrial Waste Conference Purdue University, West Lafayette, Indiana, US*, pp. 413-420.

- Al-Kassim, L., Taylor, K.E., Nicell, J.A., Bewtra, J.K., Biswas, N. (1994). Enzymatic removal of selected aromatic contaminants from wastewater by a fungal peroxidase from *Coprinus macrorhizus* in batch reactors, *Journal of Chemical Technology and Biotechnology*, 61: 179-182.
- Amini, B., Lowenkron, S. (2005). Aniline and its derivatives, *Kirk-Othmer Encyclopedia of Chemical Technology*, John Wiley & Sons, NY, USA.
- Arnao, M.B., Acosta, M., Del- Rio, J.A., Varon, R., Garcia-Canovas, F. (1990). A kinetic study on the suicide inactivation of peroxidase by hydrogen peroxide, *Biochimica et Biophysica Acta (BBA) - Protein Structure and Molecular Enzymology*, 1041: 43-47.
- Asuri, P., Karajanagi, S.S., Sellitto, E., Kim, D.Y., Kane, R.S., Dordick, J.S. (2006). Water-soluble carbon nanotube-enzyme conjugates as functional biocatalytic formulations, *Biotechnology and Bioengineering*, 95(5): 804-811.
- Baird, R., Carmona, L., Jenkins, R. L. (1977). Behavior of benzidine and other aromatic amines in aerobic wastewater treatment, *Journal (Water Pollution Control Federation)*, 49(7): 1609-1615.
- Barrère, C., Maire, F., Afonso, C., Giusti, P. (2012). Atmospheric solid analysis probe- ion mobility mass spectrometry of polypropylene, *Analytical Chemistry*, 84: 9349-9354.
- Bassi, A., Geng, Z., Gijzen, M. (2004). Enzymatic removal of phenol and chlorophenols using soybean seed hulls, *Engineering in Life Science*, 4(2): 125-130.
- Baynton, K.T., Bewtra, J.K., Biswas, N., Taylor, K.E. (1994). Inactivation of horseradish peroxidase by phenol and hydrogen peroxide: a kinetic investigation, *Biochimica et Biophysica Acta (BBA) - Protein Structure and Molecular Enzymology*, 1206: 272-278.

- Beharry, A.A., Oleg Sadowski, O., Woolley, G.A. (2011). Azobenzene photoswitching without ultraviolet light, *Journal of the American Chemical Society*, 133 (49): 19684-19687.
- Beharry, A.A., Woolley, G.A. (2011). Azobenzene photoswitches for biomolecules, *Chemical Society Reviews*, 40: 4422-4437.
- Bertazzo, A., Ragazzi, E., Biasiolo, M., Costa, C.V.L., Allegri, A. (2001). Enzymes activities involved in tryptophan metabolism along kynurenine pathway in rabbit, *Biochimica et Biophysica Acta (BBA) – General Subjects*, 1527: 167-175.
- Bhunja, A., Durani, S., Wangikar P.P. (2001). Horseradish peroxidase catalyzed degradation of industrially important dyes, *Biotechnology and Bioengineering*, 72: 562-567.
- BioByte. (1995). ClogP for Windows Program, BioByte Corp., Claremont, CA.
- Birt, D.F., Julius A.D., Hasegawa, R., St. John M., Cohen, S.M. (1987). Effect of L-tryptophan excess and vitamin B6 deficiency on rat urinary bladder cancer promotion, *Cancer Research*, 47: 1244-1245.
- Biswas, K. (1999). Removal of cresols from synthetic wastewater using crude soybean peroxidase, M.A.Sc. thesis, University of Windsor, Ontario, Canada.
- Biswas, M.M., Taylor, K.E., Bewtra, J.K., Biswas, N. (2007). Enzymatic treatment of sulfonated aromatic amines generated from reductive degradation of reactive azo dyes, *Water Environment Research*, 79(4): 351-356.
- Bodalo, A., Gomez, J.L., Gomez, E., Bastida, J., Maximo, M.F. (2006). Comparison of commercial peroxidases for removing phenol from water solutions, *Chemosphere*, 63, 626-632.

- Bollag, J.M., Blattmann, P., Laanio, T. (1978). Adsorption and transformation of four substituted anilines in soil, *Journal of Agricultural and Food Chemistry*, 26: 1302-1306.
- Bollag, J.M., Shuttleworth, K.L., Anderson, D.H. (1988). Laccase-mediated detoxification of phenolic compounds, *Applied and Environmental Microbiology*, 54: 3086-3091.
- Bollag, J.M., Sjöblad, R.D., Liu, S.Y. (1979). Characterization of an enzyme from *Rhizoctonia praticola* which polymerizes phenolic compounds, *Canadian Journal of Microbiology*, 24: 229-233.
- Briggs, G.E., Haldane, J.B.S. (1925). A note on the kinetics of enzyme action, *Biochemical Journal*, 19 (2): 338-339.
- Buzzell, R.I., Buttery B.R. (1968). Peroxidase activity in seeds of soybean varieties, *Crop Science*, 8(6): 722-725.
- Buzzell, R.I., Buttery B.R. (1969). Inheritance of peroxidase activity in soybean seed coats, *Crop Science*, 9(3): 387-388.
- Casero, I., Sicilia, D., Rubio, S., Perez-Bendito, D. (1997). Chemical degradation of aromatic amines by fenton's reagent, *Water Research*, 31(8): 1985-1995.
- Caza, N., Bewtra, J.K., Biswas, N., Taylor, K. E. (1999). Removal of phenolic compounds from synthetic wastewater using soybean peroxidase, *Water Research*, 33(13): 3012-3018.
- Chhabra, M., Mishra, S., Sreekrishnan, T.R. (2015). Combination of chemical and enzymatic treatment for efficient decolorization/degradation of textile effluent, *Biochemical Engineering Journal*, 93: 17-24.
- Chung, K.-T., Gadupudi, G.S. (2010). Possible roles of excess tryptophan metabolites in cancer, *Environmental and Molecular Mutagenesis*, 52: 81-104.

- Ćirić-Marjanović, G., Milojević-Rakić, M., Janošević-Ležaić, A., Luginbühl, S., Walde, P. (2017). Enzymatic oligomerization and polymerization of arylamines: state of the art and perspectives, *Chemical Papers*, 71: 199-242.
- Cole, R.B. (2000). Some tenets pertaining to electrospray ionization mass spectrometry, *Journal of Mass Spectrometry*, 35: 763-772.
- Cooks, R.G., Beynon, J.H., Caprioli, R.M., Lester, G.R. (1973). *Metastable Ions*, Elsevier, Amsterdam.
- Cordova Villegas, L.G. (2017). Enzymatic treatment of azo-dyes with soybean peroxidase, PhD dissertation, University of Windsor, Ontario, Canada.
- Cordova Villegas, L.G., Mashhadi, N., Chen, M., Mukherjee, D., Taylor, K.E., Biswas, N. (2016). A short review of techniques for phenol removal from wastewater, *Current Pollution Reports*, 2: 157-67.
- Cornish-Bowden, A. (1976). *Principles of Enzyme Kinetics*, Butterworths, London-Boston.
- Cowen, W.F., Gastinger, A.M., Spanier, C.E., Buckel, J.R., Bailey, R.E. (1998). Sorption and microbial degradation of toluenediamines and methylenedianiline in soil under aerobic and anaerobic conditions, *Environmental Science and Technology*, 32: 598-603.
- Danner, D.J., Brignac, P.J., Arceneaux, D., Patel, V. (1973). The oxidation of phenol and its reaction product by horseradish peroxidase and hydrogen peroxide, *Archives of Biochemistry and Biophysics*, 166: 759-763.
- Dec, J., Bollag, J.M. (1994). Dehalogenation of chlorinated phenols during oxidative coupling, *Environmental Science and Technology*, 28: 484-490.

- Dec, J., Bollag, J.-M. (1995). Effect of various factors on dehalogenation of chlorinated phenols and anilines during oxidative coupling, *Environmental Science and Technology*, 29: 657-663.
- Demarche, P., Junghanns, C., Nair, R.R., Agathos, S.N. (2012). Harnessing the power of enzymes for environmental stewardship, *Biotechnology Advances*, 30(5): 933-953.
- Dole, M., Mack, L.L., Hines, R.L., Mobley, R.C., Ferguson, L.D., Alice, M.B. (1968). Molecular beams of macroions, *The Journal of Chemical Physics*, 49: 2240-2249.
- Dunford, H.B. (1999). *Heme Peroxidases*, John Wiley & Sons, NY, USA, Ch.1, 3, 4, 5, 6, 18, pp. 1-36, 33-57, 58-91, 92-131, 270-319, 414-454.
- Dunford, H.B., Stillman, J.S. (1976). On the function and mechanism of action of peroxidases, *Coordination Chemistry Reviews*, 19: 187-251.
- Eide, I., Zahlsen, K. (2007). Chemical fingerprinting of biodiesel using electrospray mass spectrometry and chemometrics: characterization, discrimination, identification, and quantification in petrodiesel, *Energy and Fuels*, 21(6): 3702-3708.
- Eisenthal, R., Danson, M.J., Hough, D.W. (2007). Catalytic efficiency and k_{cat}/K_M : a useful comparator?, *Trends in Biotechnology*, 25(6): 247-249.
- Ekici, P., Leupold, G., Parlar, H. (2001). Degradability of selected azo dye metabolites in activated sludge systems, *Chemosphere*, 44: 721-728.
- Everse, J., Everse, K.E., Grisham, M.B. (1991). *Peroxidases in Chemistry and Biology*, CRC Press, Boca Raton, FL, USA, Vol. 2, pp. 1-50, 139-154, 219-238.
- Feng, W., Taylor, K.E., Biswas, N., Bewtra, J.K. (2013). Soybean peroxidase trapped in product precipitate during phenol polymerization retains activity and may be recycled, *Journal of Chemical Technology and Biotechnology*, 88(8): 1429-1435.

- Fersht, A. (1977). *Enzyme Structure and Mechanism*, W.H. Freeman & Co, Edition 2, pp. 1-271.
- Filizola, M., Loew, G.H. (2000). Role of protein environment in horseradish peroxidase compound I formation: Molecular dynamics simulations of horseradish peroxidase-HOOH complex, *Journal of the American Chemical Society*, 122: 18-25.
- Flock, C., Bassi, A., Gizen, M. (1999). Removal of aqueous phenol and 2-chlorophenol with purified soybean peroxidase and raw soybean hulls, *Journal of Chemical Technology Biotechnology*, 74(4): 303-309.
- Fogler, H.S. (2004). *Elements of Chemical Reaction Engineering*, Prentice Hall Publications, NJ.
- Franciscon, E., Piubeli, F., Fantinatti-Garboggini, F., Menezes, C.R., Silva, I.S., Cavaco-Paulo, A., Grossman, M.J., Durrant, L.R. (2010). Polymerization study of the aromatic amines generated by the biodegradation of azo dyes using the laccase enzyme, *Enzyme and Microbial Technology*, 46: 360-365.
- Fu, P.P. (1990). Metabolism of nitro-polycyclic aromatic hydrocarbon, *Drug Metabolism Reviews*, 22: 209-268.
- Geng, Z., Rao, J., Bassi, A.S., Gijzen, M., Krishnamoorthy, N. (2001). Investigation of biocatalytic properties of soybean seed hull peroxidase, *Catalysis Today*, 64: 233-238.
- Gijzen, M. (1997). A deletion mutation at the ep locus causes low seed coat peroxidase activity in soybean. *Plant Journal*, 12(5), 991-998.
- Gijzen, M., van Huystee, R., Buzzell, R.I. (1993). Soybean seed coat peroxidase (a comparison of high-activity and low-activity genotypes), *Plant physiology*, 103(4): 1061-1066.

- Gomori, G. (1955). Preparation of buffers for use in enzyme studies, *Methods in Enzymology* (1), Academic Press, NY, USA.
- Griffiths, I.W. (1997). J.J. Thomson—The centenary of his discovery of the electron and of his invention of mass spectrometry, *Rapid Communications in Mass Spectrometry*, 11 (1): 3-16.
- Gu, X., Zhou, J., Zhang, A., Wang, P., Xiao, M., Guangfei, L. (2008). Feasibility study of the treatment of aniline hypersaline wastewater with a combined adsorption/bio-regeneration system, *Desalination*, 227: 139-149.
- Hailu, G., Weersink, A., Cahlik, F. (2010). Examining the prospects for commercialization of soybean peroxidase, *AgBioForum*, 13(3): 263-273.
- Hammel, K.E., Tardone, P.J. (1988). The oxidative 4-dechlorination of polychlorinated phenols is catalyzed by extracellular fungal lignin peroxidases, *Biochemistry*, 27(17): 6563-6568.
- Harris, J.M. (1992). Introduction to biotechnical and biomedical application of poly(ethylene glycol), In: *Poly(Ethylene Glycol) Chemistry-Biotechnical and Biomedical Applications*, Ed. Harris, J.M., Plenum Press, NY, USA, pp. 1-14.
- Hasegawa, R., Shirai, T., Hakoi, K., Wada, S., Yamaguchi, K., Takayama, S. (1991). Synergistic enhancement of thyroid tumor induction by 2,4-diaminoanisoie sulfate, N,N'-diethylthiourea and 4,4'-thiodianiline in male F344 rats, *Carcinogenesis*, 12(8): 1515-1518.
- Hauri, U., Lutolf, B., Schlegel, U., Hohl, C. (2005). Determination of carcinogenic aromatic amines in dyes, cosmetics, finger paints and inks for pens and tattoos with LC/MS, *Mitteilungen Aus Lebensmitteluntersuchung und Hygeine*, 96 (5): 321-335.

Hazardous Substances Data Bank, HSDB, 4,4'-Methylenebis(2-chloroaniline)/MOCA.

(2018). Weblink: [https://toxnet.nlm.nih.gov/cgi-](https://toxnet.nlm.nih.gov/cgi-bin/sis/search/r?dbs+hsdb:@term+@rn+@rel+101-14-4)

[bin/sis/search/r?dbs+hsdb:@term+@rn+@rel+101-14-4](https://toxnet.nlm.nih.gov/cgi-bin/sis/search/r?dbs+hsdb:@term+@rn+@rel+101-14-4). Accessed: November 2018.

Hazardous Substances Data Bank, HSDB, 4,4'-Thiobisbenzenamine/TDA. (2018).

Weblink: [https://toxnet.nlm.nih.gov/cgi-](https://toxnet.nlm.nih.gov/cgi-bin/sis/search/r?dbs+hsdb:@term+@rn+@rel+139-65-1)

[bin/sis/search/r?dbs+hsdb:@term+@rn+@rel+139-65-1](https://toxnet.nlm.nih.gov/cgi-bin/sis/search/r?dbs+hsdb:@term+@rn+@rel+139-65-1). Accessed: November 2018.

Hazardous Substances Data Bank, HSDB, 4-Chloro-o-toluidine/4-COT. (2018). Weblink:

<https://toxnet.nlm.nih.gov/cgi-bin/sis/search/r?dbs+hsdb:@term+@rn+@rel+95-69-2>. Accessed: November 2018.

Hazardous Substances Data Bank, HSDB, Bis(4-Aminophenyl) Ether/ODA. (2018).

Weblink: [https://toxnet.nlm.nih.gov/cgi-](https://toxnet.nlm.nih.gov/cgi-bin/sis/search/r?dbs+hsdb:@term+@rn+@rel+139-65-1)

[bin/sis/search/r?dbs+hsdb:@term+@rn+@rel+139-65-1](https://toxnet.nlm.nih.gov/cgi-bin/sis/search/r?dbs+hsdb:@term+@rn+@rel+139-65-1).

Hazardous Substances Data Bank, HSDB, p-Cresidine. (2018). Weblink:

<https://toxnet.nlm.nih.gov/cgi-bin/sis/search/r?dbs+hsdb:@term+@rn+@rel+120-71-8>. Accessed: November 2018.

Henri, V. (1903). *Lois Générales de l'Action des Diastases*, Librairie Scientifique A. Hermann, Paris.

Henriksen, A., Mirza, O., Indiani, C., Teilum, K., Smulevich, G., Welinder, K.G., Gajhede, M. (2001). Structure of soybean seed coat peroxidase: A plant peroxidase with unusual stability and haem-apoprotein interactions, *Protein Science*, 10(1): 108-115.

- Husain, Q., Husain, M., Kulshrestha, Y. (2009). Remediation and treatment of organopollutants mediated by peroxidases: a review, *Critical Reviews in Biotechnology*, 29(2): 94-119.
- Ibrahim, M.S., Ali, H.I., Taylor, K.E., Biswas, N., Bewtra, J.K. (1997). Removal of phenol from industrial wastewaters using *Arthromyces ramosus* peroxidase in a continuous flow system, *Proceedings of the 1997 52nd Industrial Waste Conference*, 271-277.
- Ibrahim, M.S., Ali, H.I., Taylor, K.E., Biswas, N., Bewtra, J.K. (2001). Enzyme catalyzed removal of phenol from refinery wastewater: Feasibility studies, *Water Environment Research*, 73(2): 165-172.
- Ikehata, K., Buchanan, I.D., Smith, D.W. (2003). Treatments of oil refinery wastewater using crude *coprinus cinereus* peroxidase and hydrogen peroxide, *Journal of Environmental Engineering Society*, 2: 463-472.
- Ikehata, K., Nicell, J.A. (2000). Characterization of tyrosinase for the treatment of aqueous phenols, *Bioresource Technology*, 74: 191-199.
- International Agency for Research on Cancer, IARC. (1982). Monographs on the evaluation of the carcinogenic risk of chemicals to humans. Geneva: World Health Organization, International Agency for Research on Cancer, 1972-present. (Multivolume work). Weblink: <http://monographs.iarc.fr/ENG/Classification/index.php>, p. V27 151. Accessed: November 2018.
- International Agency for Research on Cancer, IARC. (1990). Some flame retardants and textile chemicals, and exposure in the textile manufacturing industry, *IARC Monographs on the Evaluation of Carcinogenic Risks to Humans*, 48: 1-278.

International Agency for Research on Cancer, IARC. (2000b). Monographs, 4-chloro-*ortho*-toluidine, Weblink:

<https://monographs.iarc.fr/ENG/Monographs/vol77/mono77-12.pdf>. Accessed: November 2018.

International Agency for Research on Cancer, IARC: Evaluation of Carcinogenic Risk to Humans: some industrial chemicals. (2000a). Lyon, France, 15-22.

Jiang, Q.Q. (2013). Discovery of potential inhibitors of humane β -tryptase by protein surface recognition, PhD dissertation, University of Duisburg-Essen, Germany.

Kamal, J.K.A., Behere, D.V. (2002). Thermal and conformational stability of seed coat soybean peroxidase, *Biochemistry*, 41: 9034-9042.

Kamal, J.K.A., Behere, D.V. (2003). Activity, stability and conformational flexibility of seed coat soybean peroxidase, *Journal of Inorganic Biochemistry*, 94(3): 236-242.

Kamal, J.K.A., Behere, D.V. (2008). Kinetic stabilities of soybean and horseradish peroxidases, *Biochemical Engineering Journal*, 38(1): 110-114.

Kinsley, C., Nicell, J.A. (2000). Treatment of aqueous phenol with soybean peroxidase in the presence of polyethylene glycol, *Bioresource Technology*, 73: 139-146.

Klibanov, A.M., Alberti, B.N., Morris, E.D., Felshin, L.M. (1980). Enzymatic removal of toxic phenols and anilines from waste waters, *Journal of Applied Biochemistry*, 2: 414-421.

Klibanov, A.M., Alberti, B.N., Morris, E.D., Felshin, L.M. (1980). Enzymatic removal of toxic phenols and anilines from wastewater, *Journal of Applied Biochemistry*, 2: 414-421.

- Liu, Z., Yang, H., Huang, Z., Zhou, P., Liu, S.J. (2002). Degradation of aniline by newly isolated, extremely aniline-tolerant *Delftia sp.* AN3, Applied Microbiology and Biotechnology, 58: 679-682.
- Lizier, T.M., Zanoni, M.V.B. (2012). Effect of ionic liquid on the determination of aromatic amines as contaminants in hair dyes by liquid chromatography coupled to electrochemical detection, Molecules, 17: 7961-7979.
- Lloret, S.M., Legua, C.M., Falco, P.C. (2002). Preconcentration and dansylation of aliphatic amines using C-18 solid-phase packings-Application to the screening analysis in environmental water samples, Journal of Chromatography A, 978: 59-69.
- Lyman, W.J., Reehl W.F., Rosenblatt, D.H. (1990). Handbook of Chemical Property Estimation Methods, American Chemical Society, Washington DC.
- Lyr, H. (1963). Enzymatische detoxifikation chlorierter phenole, Journal of Phytopathology, 47(1): 73-83.
- Mahamuni, N.N., Adewuyi, Y.G. (2010). Advanced oxidation processes (AOPs) involving ultrasound for waste water treatment: A review with emphasis on cost estimation, Ultrasonics Sonochemistry, 17: 990-1003.
- Malik Altahir, B., Feng, W., Jasim, H.H., Taylor, K.E., Biswas, N., Bewtra, J.K., Jasim, S.A.A. (2015). Soybean peroxidase-catalysed removal of benzidines from water, Journal of Environmental Engineering and Science, 10(4): 73-80.
- Mann, M., Wilm, M. (1995). Electrospray mass spectrometry for protein characterization, Trends in Biochemical Science, 20: 219-224.
- Mantha, R., Biswas, N., Taylor, K.E., Bewtra, J.K. (2002). Removal of nitroaromatics from synthetic wastewater using two-step zero-valent iron reduction and peroxidase-catalyzed oxidative polymerization, Water Environment Research, 74: 280-287.

- Matsui, S., Okawa, Y., Ota, R. (1988). Experience of 16 years' operation and maintenance of the Fukushima industrial wastewater treatment plant of the Kashima Petrochemical Complex – II. Biodegradability of 37 organic substances and 28 process wastewaters, *Water Science and Technology*, 20: 201-210.
- Maximum Concentrations at the Workplace, MAK list. (1987). 4,4'-Oxydianiline.
- Webpage:
- <https://onlinelibrary.wiley.com/doi/pdf/10.1002/3527600418.mb10180e0006>.
- Accessed: November 2018.
- Mazloum, S., Mousa Al-Ansari, M., Taylor, K.E., Bewtra, J.K., Biswas N. (2016). Additive effect on soybean peroxidase-catalyzed removal of anilines from water, *Environmental Engineering Science*, 33(2): 133-139.
- McEldoon, J.P., Dordick, J.S. (1996). Unusual thermal stability of soybean peroxidase, *Biotechnology Progress*, 12(4): 555-558.
- McEwen, C.N., McKay, R.G., Larsen, B.S. (2005). Analysis of solids, liquids, and biological tissues using solids probe introduction at atmospheric pressure on commercial LC/MS instruments, *Analytical Chemistry*, 77: 7826-7831.
- McLafferty, F.W. (Ed.) (1983). *Tandem Mass Spectrometry*, John Wiley & Sons Inc., NY, USA.
- McLuckey, S.A. (1988). *Mass Spectrometry/Mass Spectrometry: Techniques and Applications of Tandem Mass Spectrometry*, VCH, NY, USA.
- Meylan, W.M., Howard, P.H. (1991). Bond contribution method for estimating Henry's law constants, *Environmental Toxicology and Chemistry*, 10: 1283-1293.
- Meylan, W.M., Howard, P.H., Boethling, R.S., Aronson, D., Printup, H., Gouchie, S. (1999). Improved method for estimating bioconcentration/bioaccumulation factor

- from octanol/water partition coefficient. *Environmental Toxicology and Chemistry*, 18: 664-672.
- Michaelis, L., Menten, M.L. (1913). Die Kinetik der Invertinwirkung, *Biochemische Zeitschrift*, 49: 333-369.
- Michail, K., Aljuhani, N., Siraki, A.G. (2013). The interaction of diamines and polyamines with the peroxidase-catalyzed metabolism of aromatic amines: a potential mechanism for the modulation of aniline toxicity, *Canadian Journal of Physiology and Pharmacology*, 91: 228-235.
- Michail, K., Baghdasarian, A., Narwaley, M., Aljuhani, N., Siraki, A.G. (2013). Scavenging of free-radical metabolites of aniline xenobiotics and drugs by amino acid derivatives: Toxicological implications of radical-transfer reactions, *Chemical Research in Toxicology*, 26: 1872-1883.
- Michniewicz, A., Ledakowicz, S., Ullrich, R., Hofrichter, M. (2008). Kinetics of the enzymatic decolorization of textile dyes by laccase from *cerrena unicolor*, *Dyes and Pigments*, 77(2): 295-302.
- Mill, T., Mabey, W. (1985). Photodegradation in water, In: *Environmental Exposure from Chemicals*, Eds. Neely, W.R., Blau, G.E., CRC Press, Boca Raton, FL, USA, Vol. 1, pp. 208-211.
- Minard, R.D., Liu, S.Y., Bollag, J.M. (1981). Oligomers and quinones from 2,4-dichlorophenol, *Journal of Agricultural and Food Chemistry*, 29: 250-253.
- Modaressi, K., Taylor, K.E., Bewtra, J.K., Biswas, N. (2005). Laccase-catalyzed removal of bisphenol-A from water: Protective effect of PEG on enzyme activity, *Water Research*, 39(18): 4309-4316.

- Mondal, P.K., Ahmad, R., Usmani S.Q. (2010). Anaerobic biodegradation of triphenylmethane dyes in a hybrid UASFB reactor for wastewater remediation, *Biodegradation*, 21:1041-1047.
- Moore, W.M. (1978). Methylenedianiline, In: Kirk-Othmer Encyclopedia of Chemical Technology, Edition 3, Wiley & Sons, NY, USA, Vol. 2, pp. 338-348.
- Mousa Al-Ansari, M. (2008). Removal of various aromatic compounds from synthetic and refinery wastewater using soybean peroxidase, M.Sc. thesis, University of Windsor, Ontario, Canada.
- Mousa Al-Ansari, M., Saha, B., Mazloun, S., Taylor, K.E., Bewtra, J.K., Biswas, N. (2011). Soybean peroxidase applications in wastewater treatment, In: Soybeans: Cultivation, Uses and Nutrition, Ed. Maxwell, J.E., Nova Science, pp. 189-221.
- Mousa Al-Ansari, M., Steevensz, A., Taylor, K.E., Bewtra, J.K., Biswas, N. (2010). Soybean peroxidase-catalyzed removal of an aromatic thiol, 2-mercaptobenzothiazole, from water, *Water Environment Research*, 82: 2285-2289.
- Mousa Al-Ansari, M.M., Steevensz, A., Al-Aasm, N., Taylor, K.E., Bewtra, J.K., Biswas, N. (2009). Soybean peroxidase-catalyzed removal of phenylenediamines and benzenediols from water, *Enzyme and Microbial Technology*, 45(4): 253-260.
- Munir, I.Z., Dordick, J.S. (2000). Soybean peroxidase as an effective bromination catalyst, *Enzyme and Microbial Technology*, 26: 337-341.
- Nakamoto, S., Machida, N. (1992). Phenol removal from aqueous solutions by peroxidase-catalyzed reaction using additives, *Water Research*, 26: 49-54.
- National Cancer Institute Thesaurus (NCIt), 4,4'-Thiodianiline (2018). Weblink: https://ncit.nci.nih.gov/ncitbrowser/ConceptReport.jsp?dictionary=NCI_Thesaurus&ns=NCI_Thesaurus&code=C44322. Accessed: November 2018.

- National Cancer Institute, NCI. (1979). Carcinogenesis assay of 4-chloro-o-toluidine hydrochloride for possible carcinogenicity (CAS No. 3165-93-3) (Tech. Rep. Series No.165: DHEW Publ. No. NIH 79-1721, Bethesda, MD, USA.
- Nelson, D., Cox, M. (2008). Lehninger Principles of Biochemistry, Edition 5, W.H. Freeman and Company.
- Nicell, J.A. (1991). Enzyme catalyzed polymerization and precipitation of aromatic compounds from waste water, Ph.D. dissertation, University of Windsor, Ontario, Canada.
- Nicell, J.A. (2003). Enzymatic treatment of waters and wastes, In: Chemical Degradation Methods for Wastes and Pollutants: Environmental and Industrial Applications, Ed. Tarr, M.A., Ch.10, CRC Press, USA.
- Nicell, J.A., Al-Kassim, L., Bewtra, J.K., Taylor, K.E. (1993). Wastewater treatment by enzyme catalyzed polymerization and precipitation, Biodeterioration Abstracts, 7: 1-8.
- Nicell, J.A., Bewtra, J.K., Biswas, N., St. Pierre, C.C., Taylor, K.E. (1993). Enzyme catalyzed polymerization and precipitation of aromatic compounds from aqueous solution, Canadian Journal of Civil Engineering, 20(5): 725-735.
- Nicell, J.A., Wright, H. (1997). A model of peroxidase activity with inhibition by hydrogen peroxide, Enzyme and Microbial Technology, 21 (4): 302-310.
- Nisum, M., Schiodt, C.B., Welinder, K.G. (2001). Reactions of soybean peroxidase and hydrogen peroxide pH 2.4-12.0, and veratryl alcohol at pH 2.4, Biochimica et Biophysica Acta (BBA) - Protein Structure and Molecular Enzymology, 1545 (1-2): 339-348.

- Ohnishi, Y., Kinouchi, T., Tsutsu, H., Uejima, M., Nishifuji, K. (1985). Mutagenic nitropyrenes in foods, Princess Takamatsu Symposium, 16: 107-118.
- Oller, I., Malato, S., Sánchez-Pérez, J.A. (2011). Combination of advanced oxidation processes and biological treatments for wastewater decontamination—A review, *The Science of the Total Environment*, 409(20): 4141-4166.
- Ortiz de Montellano, P.R., David, S.K., Ator, M.A., Tew, D. (1988). Mechanism-based inactivation of horseradish peroxidase by sodium azide, Formation of meso-azidoproteoporphyrin IX, *Biochemistry*, 27: 5470-5476.
- Parris, G.E. (1980). Covalent binding of aromatic amines to humates. 1. Reactions with carbonyls and quinones, *Environmental Science and Technology*, 14: 1099-1106.
- Patapas, J., Al-Ansari, M.M., Taylor, K.E., Bewtra, J.K., Biswas, N. (2007). Removal of dinitro-toluenes from water via reduction with iron and peroxidase-catalyzed oxidative polymerization: a comparison between *Arthromyces ramosus* peroxidase and soybean peroxidase, *Chemosphere*, 67: 1485-1491.
- Pereira, L., Mondal, P.K., Alves, M. (2015). Aromatic amines sources, environmental impact and remediation, In: *Pollutants in Buildings, Water and Living Organisms*, Eds. Lichtfouse, E., Schwarzbauer, J., Robert, D. Ch.7, Springer, Switzerland, pp. 302.
- Petucci, C., Diffendal, J. (2008). Atmospheric solids analysis probe: a rapid ionization technique for small molecule drugs, *Journal of Mass Spectrometry*, 43: 1565-1568.
- Pinheiro, H.M., Touraud, E., Thomas, O. (2004). Aromatic amines from azo dye reduction: status review with emphasis on direct UV spectrophotometric detection in textile industry wastewaters, *Dyes and Pigments*, 61: 121-139.
- Pollution inventory - England and Wales. (2003). The Environment Agency.

- Possanzini, M., Palo, V.D. (1990). Improved HPLC determination of Aliphatic-Amines in air by diffusion and derivatization techniques, *Chromatographia*, 29: 151-160.
- Rafii, F., Franklin, W., Heflich, R., Cerniglia, C.E. (1991). Reduction of nitrated compounds by anaerobic bacteria isolated from the human gastrointestinal tract. *Applied and Environmental Microbiology*, 57: 962- 968.
- Raven, E., Dunford, H.B. (2016). Heme Peroxidases, Ch. 1,4,7,8, The Royal Society of Chemistry, Cambridge, UK, pp. 10, 61-98, 133-155, 156-180.
- RCSB-Protein Data Base, category no. 1FHF. Structure of soybean peroxidase (2018). Weblink: <https://www.rcsb.org/structure/1FHF>. Accessed: November 2018.
- Regalado, C., Garcia-Almendarez, B.E., Duarte-Vazquez, M.A. (2004). Biotechnological applications of peroxidases, *Phytochemistry Reviews*, 3(1-2): 243-256.
- Richardson, R.E., Fu, P.P., Cerniglia, C.E. (1988). Metabolism of 1-, 3- and 6-nitrobenzo(a) pyrene by intestinal microflora, *Journal of Toxicology and Environmental Health*, 23: 527-537.
- Rieger, P.G., Meier, H.M., Gerle, M., Vogt, U., Groth, T., Knackmuss, H.J. (2002). Xenobiotics in the environment: present and future strategies to obviate the problem of biological persistence, *Journal of Biotechnology*, 94(1): 101-123.
- Robinson, T., McMullan, G., Marchant, R., Nigam, P. (2001). Remediation of dyes in textile effluent: a critical review on current treatment technologies with a proposed alternative, *Bioresource Technology*, 77: 247-255.
- ROC (Report on Carcinogens), 4,4'-Oxydianiline (ODA), Edition 14. (2018). <https://ntp.niehs.nih.gov/ntp/roc/content/profiles/oxydianiline.pdf>. Accessed: November 2018.

ROC (Report on Carcinogens), *p*-Cresidine. Edition 14. (2018).

<https://ntp.niehs.nih.gov/ntp/roc/content/profiles/cresidine.pdf>. Accessed:

November 2018.

Romanova, L.G., J. Tamuliene, V.S. Vukstich, T.A. Snegurskaya, Papp, A.V., Snegursky, A.V. (2015). Production of similar fragments from the glycine, alanine, and methionine amino acid molecules under low-energy electron impact, *Acta Physica Polonica A*, 128: 15-24.

Rose, D.P. (1972). Aspects of tryptophan metabolism in health and disease: a review, *Journal of Clinical Pathology*, 25: 17-25.

Rosenkranz, H.S., Mermelstein, R. (1983). Mutagenicity and genotoxicity of nitropyrenes. All nitro-containing chemicals were not created equal, *Mutation Research*, 114: 217-267.

Rosenkranz, H.S., Sanders D.R. (1980). Nitropyrenes: isolation, identification, and reduction of mutagenic impurities in carbon black toners, *Science*, 209: 1039-1043.

Ryan, B.J., Carolan, N., O'Fagain, C. (2006). Horseradish and soybean peroxidases: comparable tools for alternative niches?, *Trends in Biotechnology*, 24(8): 355-363.

Saha, B.C., Jordan, D.B., Bothast, R.J. (2009). Enzymes, industrial (overview), In: *Encyclopedia of Microbiology*, Ed. S. Moselio, Edition 3, Academic Press, Oxford, pp. 281-294.

Sánchez, M.D.L., Santos, P.M., Sappó, C.P., Pavón, J.L.P., Cordero, B.M. (2014). Micro extraction by packed bed adsorbent and salting-out-assisted liquid-liquid extraction for the determination of aromatic amines formed from azo dyes in textiles, *Talanta*, 119: 375-384.

- Saunders, B.C., Holmes-Siedle, A.G., Stark, B.P. (1964). Peroxidase: The Properties and Uses of a Versatile Enzyme and of Some Related Catalysts, Butterworths, London.
- Schubert, J., Kappenstein, O., Luch, A., Schulz, T.G. (2011). Analysis of primary aromatic amines in the mainstream waterpipe smoke using liquid chromatography–electrospray ionization tandem mass spectrometry, *Journal of Chromatography A*, 1218: 5628-5637.
- Sessa, D.J., Anderson, R.L. (1981). Soybean peroxidases: purification and some properties, *Journal of Chemical Technology and Biotechnology*, 29(5): 960-965.
- Sidransky, H. (1997). Tryptophan and carcinogenesis: review and update on how tryptophan may act, *Nutrition and Cancer*, 29: 181-194.
- Siewertsen, R., Neumann, H., Buchheim-Stehn, B., Herges, R., Näther, C., Renth, F., Temps, F. (2009). Highly efficient reversible Z-E photoisomerization of a bridged azobenzene with visible light through resolved $S(1)(n\pi^*)$ absorption bands, *Journal of the American Chemical Society*, 131(43): 15594-15595.
- Siewertsen, R., Schönborn, J.B., Hartke, B., Renth, F., Temps, F. (2011). Superior Z→E and E→Z photoswitching dynamics of dihydrodibenzodiazocine, a bridged azobenzene, by $S1(n\pi^*)$ excitation at $\lambda = 387$ and 490 nm, *Physical Chemistry Chemical Physics*, 13(3): 1054-1063.
- Singh, R.K., Kumar, S., Kumar, S., Kumar, A. (2008). Development of parthenium based activated carbon and its utilization for adsorptive removal of *p*-cresol from aqueous solution, *Journal of Hazardous Materials*, 155: 523-535.
- Smith, M.J.P., Cameron N.R., Mosely, J.A. (2012). Evaluating atmospheric pressure solids analysis probe (ASAP) mass spectrometry for the analysis of low molecular weight synthetic polymers, *Analyst*, 137: 4524-4530.

- Smyth, W.F., Brooks, P. (2004). A critical evaluation of high performance liquid chromatography-electrospray ionisation-mass spectrometry and capillary electrophoresis-electrospray-mass spectrometry for the detection and determination of small molecules of significance in clinical and forensic science, *Electrophoresis*, 25: 1413-1446.
- Smyth, W.F., Rodriguez, V. (2007). Recent studies of the electrospray ionisation behaviour of selected drugs and their application in capillary electrophoresis-mass spectrometry and liquid chromatography-mass spectrometry, *Journal of Chromatography, A*, 1159: 159-174.
- Snyderwine, E.G., Sinha, R., Felton, J.S., Ferguson, L.R. (2002). Highlights of the eighth international conference on carcinogenic/mutagenic N-substituted aryl compounds, *Mutation Research*, 506-507: 1-8.
- Soy Canada. (2018). Weblink: <http://soycanada.ca/statistics/at-a-glance/> Accessed: November 2018.
- Stayner, L., Dannenberg, A., Bloom, T., Thun, T., Yearet, M. (1993). Excess hepatobiliary cancer mortality among munition workers exposed to dinitrotoluene, *Journal of Occupational Medicine*, 35(3): 291-296.
- Steevensz, A. (2008). Laccase-catalyzed removal of various aromatic compounds from synthetic and refinery wastewate, PhD dissertation, University of Windsor, Ontario, Canada.
- Steevensz, A., Cordova Villegas, L.G., Feng, W., Taylor, K.E., Bewtra, J.K., Biswas, N. (2014). Soybean peroxidase for industrial wastewater treatment: a mini review, *Journal of Environmental Engineering and Science*, 9(3): 181-186.

- Steevensz, A., Madur, S., Mousa Al-Ansari, M., Taylor, K.E., Bewtra, J.K., Biswas, N. (2013). A simple lab-scale extraction of soybean hull peroxidase shows wide variation among cultivars, *Industrial Crops and Products*, 48: 13-18.
- Steevensz, A., Mousa Al-Ansari, M., Taylor, K.E., Bewtra, J.K., Biswas, N. (2012). Oxidative coupling of various aromatic phenols and anilines in water using a laccase from *Trametes villosa* and insights into the 'PEG effect', *Journal of Chemical Technology and Biotechnology*, 87(1): 21-32.
- Steevensz, A., Mousa Al-Ansari, M., Taylor, K.E., Bewtra, J.K., Biswas, N. (2009). Comparison of soybean peroxidase with laccase in the removal of phenol from synthetic and refinery wastewater samples, *Journal of Chemical Technology and Biotechnology*, 84: 761-769.
- Su, S. (2008). Development and application of non-tapered electrospray emitters for nano-ESI mass spectrometry, PhD dissertation, Queen's University, Ontario, Canada.
- Suarez-Ojeda, E.M., Carrera, J., Metcalfe, I.S., Font, J. (2008). Wet air oxidation (WAO) as a precursor to biological treatment of substituted phenols: Refractory nature of the WAO intermediates, *Chemical Engineering Journal*, 144(2): 205-212.
- Sutiono, S. (2016). Enzyme engineering of a haloacid dehalogenase-like phosphatase from *Thermotoga neopolitana* for optimization of substrate specificity, Master's thesis, Lund University, Sweden.
- Sutthivaiyakit, P., Achatz, S., Lintelmann, J., Aungpradit, T., Chanwirat, R., Chumanee, S., Kettrup, A. (2005). LC-MS/MS method for the confirmatory determination of aromatic amines and its application in textile analysis, *Analytical and Bioanalytical Chemistry*, 381: 268-276.

- Suzuki, J., Hagino, T., Veki, T., Nishi, Y., Suzuki, S. (1983). Formation of mutagens by photolysis of aromatic compounds in water containing nitrite ion, *Environmental Contamination and Toxicology*, 31: 79-84.
- The Merck Index. (1989). *An Encyclopedia of Chemicals, Drugs, and Biologicals*, Ed. Budavari, S. Edition 11, Merck and Co. Inc., Rahway, NJ, USA.
- The Office of Environmental Health Hazard Assessment, OEHHA. (2018). Occurrences and uses of TDA: <https://oehha.ca.gov/chemicals/44-thiodianiline>. Accessed: November 2018.
- Tokiwa, H., Otofji, T., Nakagawa, R., Horikawa, K., Maeda, T., Sano, S., Izumi K., Otsuka, H. (1987). Dinitro derivatives of pyrene and fluoranthrene in diesel emission particulates and their tumorigenicity in mice and rats, *Developments in Toxicology and Environmental Science*, 13: 253-270.
- TOXNET®. (2018). Toxicology Data Network, Accessed: November 2018.
- Trading Economics. United States Inflation Rate, (2017):
<https://tradingeconomics.com/united-states/inflation-cpi>. Accessed: November 2018.
- U.S. Environmental Protection Agency, EPA, 4,4'-Methylenebis(2-chloroaniline), MOCA. (2000). Hazard summary. Weblink:
<https://www.epa.gov/sites/production/files/2016-09/documents/4-4-methylenebis.pdf>. Accessed: November 2018.
- U.S. Environmental Protection Agency, EPA, 4,4'-Methylenedianiline, MDA. (2000). Hazard summary. Weblink: <https://www.epa.gov/sites/production/files/2016-09/documents/4-4-methylenedianiline.pdf>. Accessed: November 2018.

- U.S. Environmental Protection Agency, EPA. (1984). Health and environmental effects profile for 4,4'-methylenbis benzenamine, MDA. EPA/600/x-84/231. Environmental Criteria and Assessment Office, Office of Health and Environmental Assessment, Office of Research and Development, Cincinnati, OH, USA.
- U.S. Environmental Protection Agency, EPA. (2017). TRI list. Weblink:
<https://www.epa.gov/toxics-release-inventory-tri-program/tri-listed-chemicals>.
 Accessed: November 2018.
- United States Department of Agriculture, USDA. (2018). World agricultural supply and demand estimates. Weblink:
<https://www.usda.gov/oce/commodity/wasde/latest.pdf>. Accessed: November 2018.
- van Rantwijk, F., Sheldon, R.A. (2000). Selective oxygen transfer catalysed by heme peroxidases: synthetic and mechanistic aspects, *Current Opinion in Biotechnology*, 11(6): 554-564.
- Wada, S., Ichikawa, H., Tatsumi, K. (1995). Removal of phenols and aromatic amines from wastewater by a combined treatment with tyrosinase and a coagulant, *Biotechnology Bioengineering*, 45: 305-309.
- Wang, L.K., Pereira, N.C., Hung, Y.T. (2009). *Handbook of Environmental Engineering*. Vol.8. Biological Treatment Processes, Humana Press, NY, USA.
- Waters Users Meeting. (2014). Weblink:
https://www.waters.com/webassets/cms/library/docs/local_seminar_presentations/GE_Events/ge_2014_ms%20tech%20days_Xevo%20G2-XS%20QToF_Matthias%20Hofmann.pdf. Accessed: November 2018.
- Welinder, K.G., Larsen, Y.B. (2004). Covalent structure of soybean seed coat peroxidase, *Biochimica et Biophysica Acta (BBA) - Proteins and Proteomics*, 1698: 121-126.

- Westerfeld, W.W., Lowe, C. (1942). The oxidation of *p*-cresol by peroxidase, *Journal of Biological Chemistry*, 145: 463-470.
- Wright, H., Nicell, J.A. (1999). Characterization of soybean peroxidase for the treatment of aqueous phenols, *Bioresource Technology*, 70(1): 69-79.
- Wu, J., Bewtra, J.K., Biswas, N., Taylor, K.E. (1994). Effect of H₂O₂ addition mode on the enzymatic removal of phenol from wastewater in the presence of polyethylene glycol, *Canadian Journal of Chemical Engineering*, 72: 881-886.
- Wu, Y. (1996). Application of additives in horseradish peroxidase-catalyzed removal of phenol derivatives from aqueous solution, PhD dissertation, University of Windsor, Ontario, Canada.
- Wu, Y., Bewtra, J.K., Biswas, N., Taylor, K.E. (1993). Removal of phenol derivatives from aqueous solution by enzymatic reaction with additives, *Proceedings of the 48th Industrial Waste Conference Purdue University, West Lafayette, Indiana, US*, pp. 421-431.
- Wu, Y., Taylor, K.E., Bewtra, J.K., Biswas, N. (1998). A model for the protective effect of additives on the activity of horseradish peroxidase in the removal of phenol, *Enzyme and Microbial Technology*, 22: 315-322.
- Wu, Y., Taylor, K.E., Biswas, N., Bewtra, J.K. (1997). Comparison of additives in the removal of phenolic compounds by peroxidase-catalyzed polymerization, *Water Research*, 31(11): 2699-2704.
- Wu, Y., Taylor, K.E., Biswas, N., Bewtra, J.K. (1998). A model for the protective effect of additives on the reactivity of horseradish peroxidase in the removal of phenol, *Enzyme and Microbial Technology*, 22: 315-322.

- Xu, F. (1997). Effects of redox potential and hydroxide inhibition on the pH activity profile of fungal laccases, *Journal of Biological Chemistry*, 272: 924-928.
- Yamashita, M., Fenn, J.B. (1984). Electrospray ion source. Another variation on the free-jet theme, *The Journal of Physical Chemistry*, 88: 4451-4459.
- Yamashita, M., Fenn, J.B. (1984). Negative ion production with the electrospray ion source, *The Journal of Physical Chemistry*, 88: 4671-4675.
- Yu, J., Taylor, K.E., Zou, H., Biswas, N., Bewtra, J.K. (1994). Phenol conversion and dimeric intermediates in horseradish peroxidase-catalyzed phenol removal from water, *Environmental Science and Technology*, 28(12): 2154-2160.
- Zeleny, J. (1917). Electric discharge from points, *Physical Review A*, 9: 562-563.
- Zepp, R.G., Baughman, G.L., Schlotzhauer, P.F. (1981). Comparison of photochemical behavior of various humic substances in water: I. Sunlight induced reactions of aquatic pollutants photosensitized by humic substances, *Chemosphere*, 10 (1): 109-117.
- Zhu, Y., Shi, Y. (2013). Facile Cu(I)-catalyzed oxidative coupling of anilines to azo compounds and hydrazines with diaziridinone under mild conditions, *Organic Letters*, 15(8): 1942-1945.
- Zuehlke, S., Duennbier, U., Heberer, T. (2007). Investigation of the behavior and metabolism of pharmaceutical residues during purification of contaminated ground water used for drinking water supply, *Chemosphere*, 69: 1673-1680.

APPENDICES

Appendix A: Maximum Wavelength Absorbance Curves in UV-VIS

The absorbance curves for aqueous solutions of the substrates were obtained in UV-VIS spectrophotometer and their maximum wavelength (λ_{\max}) were determined.

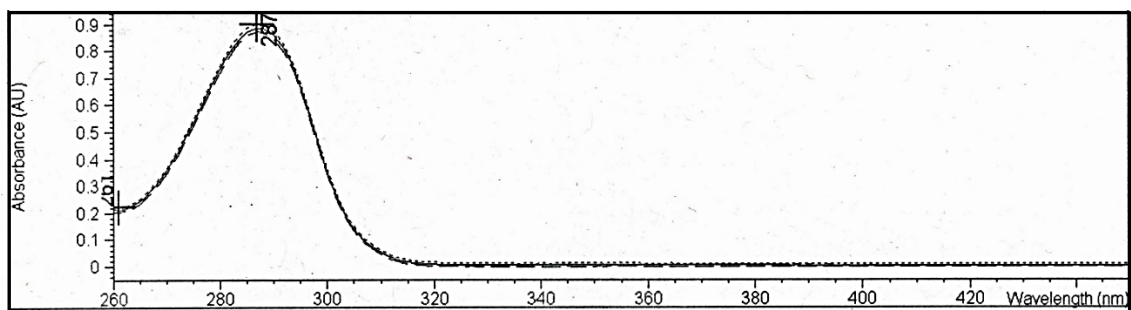


Figure A.1. 0.3 mM *p*-cresidine, approximate extinction coefficient is $2947 \text{ M}^{-1}\text{cm}^{-1}$.

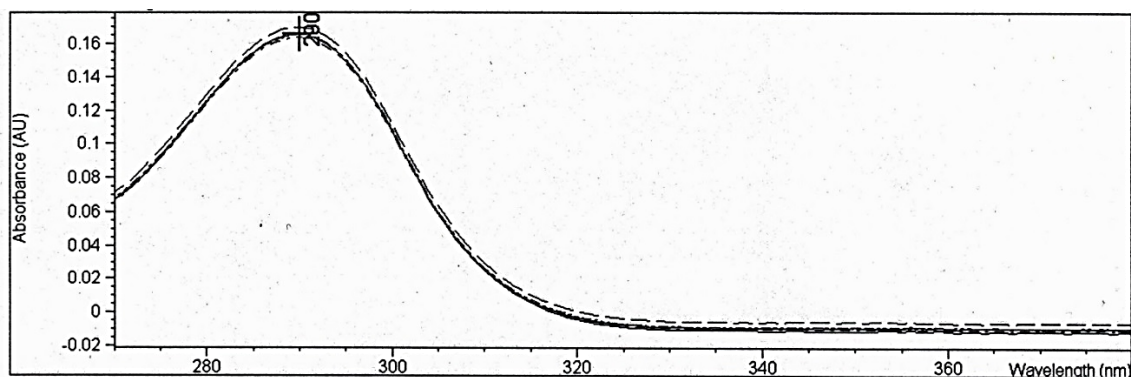


Figure A.2. 0.1 mM 4-COT, approximate extinction coefficient is $1667 \text{ M}^{-1}\text{cm}^{-1}$.

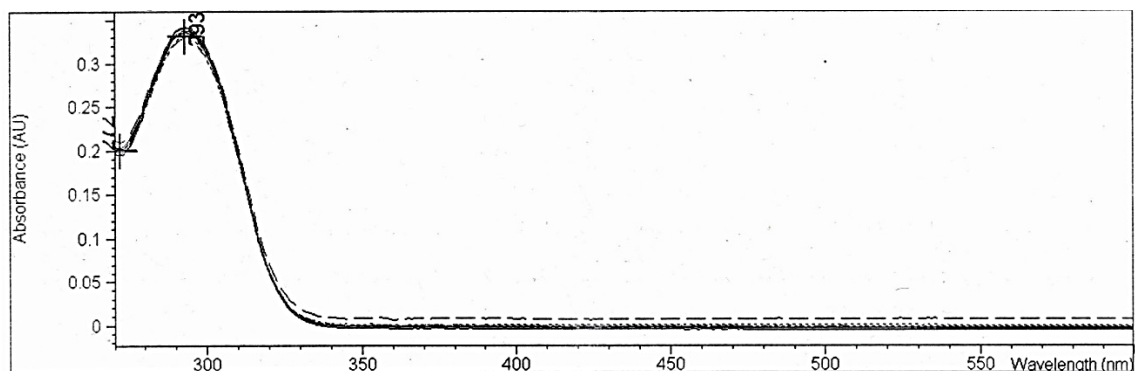


Figure A.3. 0.1 mM ODA, approximate extinction coefficient is $3383 \text{ M}^{-1}\text{cm}^{-1}$.

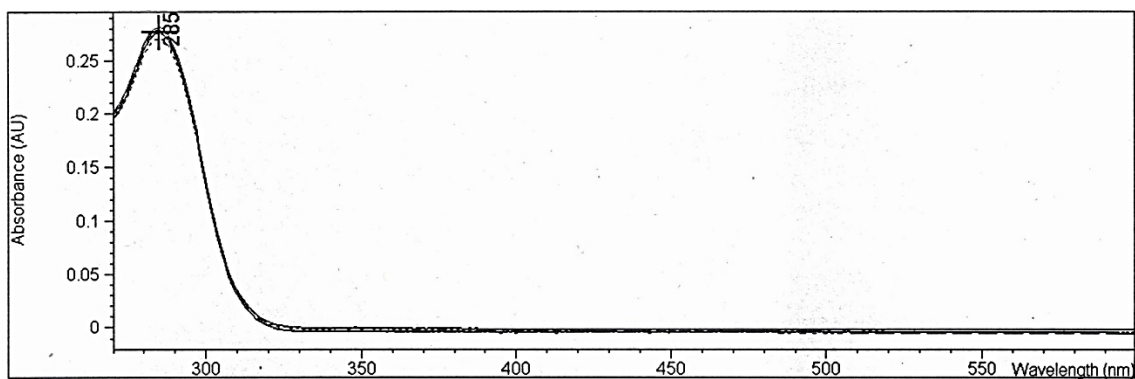


Figure A.4. 0.1 mM MDA, approximate extinction coefficient is $2775 \text{ M}^{-1}\text{cm}^{-1}$.

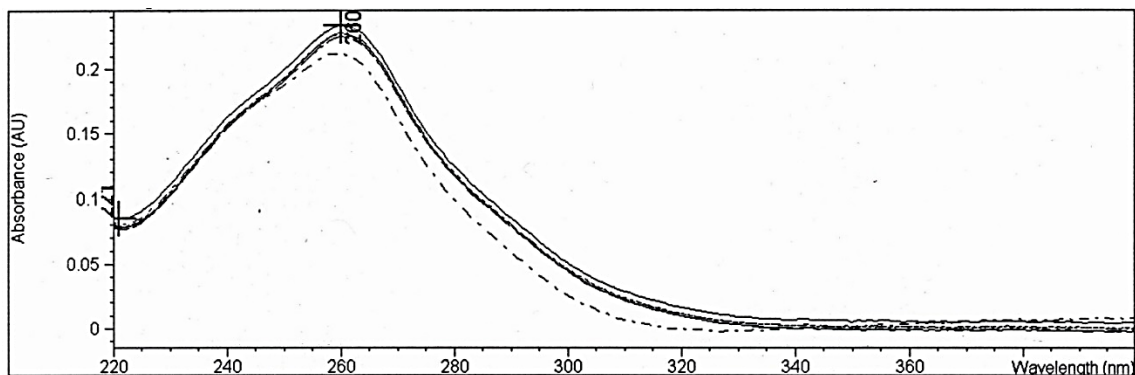


Figure A.5. 0.01 mM TDA, approximate extinction coefficient is $22658 \text{ M}^{-1}\text{cm}^{-1}$.

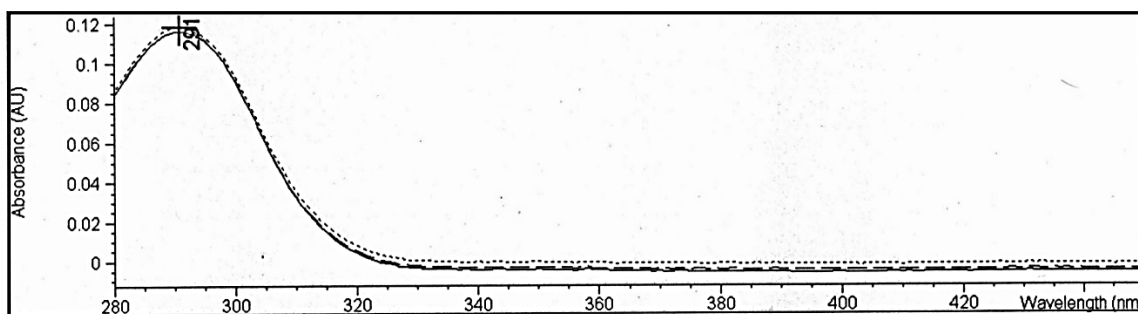


Figure A.6. 0.03 mM MOCA, approximate extinction coefficient is $3875 \text{ M}^{-1}\text{cm}^{-1}$.

Appendix B: Colorimetric Assay for SBP Activity

A colorimetric assay was used to measure the activity of SBP in this study. The principle of the assay is to measure the initial rate of formation of a pink chromophore at 510 nm. The reaction mixture consists of phenol and 4-AAP in the presence of hydrogen peroxide with SBP as catalyst. The product of such reaction produces the pink chromophore. One unit (U) of SBP activity is defined as that amount catalyzing 1 μmol of hydrogen peroxide conversion per minute under the assay conditions.

Test conditions:

- Instrument used: UV-VIS.
- Instrument parameter: The run time was 30 s, cycle time 5 s, zeroth-order process, read at 510 nm.

Assay reagents:

The mixture consists of 100.0 μL of 100.0 mM H_2O_2 , 25.0 mg of 4-AAP and 5.0 mL of 10 \times concentrate (100 mM phenol in 0.5 M phosphate buffer at pH 7.4. Composition: 0.94 g of phenol, 1.3105 g of monobasic sodium phosphate and 3.7479 g of dibasic sodium phosphate in 100 mL with distilled water). The contents were made up in a 50.0 mL volumetric flask with distilled water.

Test procedure: In a 1.0 mL cuvette:

- Blank: 950 μL of assay reagent and 50 μL distilled water
- Test sample: 950 μL of assay reagent and 50 μL diluted SBP. (The SBP dilutions of the standard stock solution were made between 30 \times -50 \times)

Data calculation procedure:

The initial rate was calculated by the change of absorbance over time (the slope of the line) taking into account the dilution factor of reaction and the extinction coefficient of the product. The enzyme activity calculations are summarized as follows:

1. The rate of change in absorbance: $\text{Rate} = \Delta A_{510} / \Delta t = \Delta A_{510}/s$
2. The rate is converted from $\Delta A_{510}/s$ to $\Delta A_{510}/\text{min}$.
3. The change in concentration $A_{510} = \epsilon \Delta c l$
4. $\Delta c = A / \epsilon l$; where, $\epsilon = 6.0 \text{ mM}^{-1}\text{cm}^{-1}$ and path length (l) = 1.0 cm
5. Δc is in mM/min, all this took place in 1.0 mL cuvette.
6. Note: $\text{mM/min.} \times 1.0 \text{ mL} = \mu\text{mol/min.}$; $1.0 \mu\text{mol/min.} = 1.0 \text{ U}$
7. The activity of the enzyme (U/mL) in the source solution was calculated by multiplying the activity of the enzyme in cuvette by the dilution factor.

Procedure:

- First the instrument was blanked with the mixture as stated above.
- The diluted SBP sample, 50 μL was injected it into the cuvette.
- The cuvette was placed into spectrophotometer and the vessel was locked.
- 950 μL of reagent was taken and quickly pushed it into the cuvette.
- The rate of colour formation was monitored on the computer and the SBP activity was calculated.

Appendix C: HPLC Calibration Curves

The standard curves for all the substrates were determined using HPLC. The standard curves were made from the average of triplicates data. The error bars denote respective standard deviations. The error bars are not visible for some of the markers as the latter concealed the bars. All the substrates except *p*-cresidine are made up in 40 mM buffer. Citrate phosphate buffer was used in the *pH* range 2.6-5.0, phosphate buffer was used in *pH* range 6.0-8.0 and in *pH* range 9.2-10.0 carbonate-bicarbonate buffer was used. Table 3.1 summarizes the mobile phase solvents and HPLC conditions.

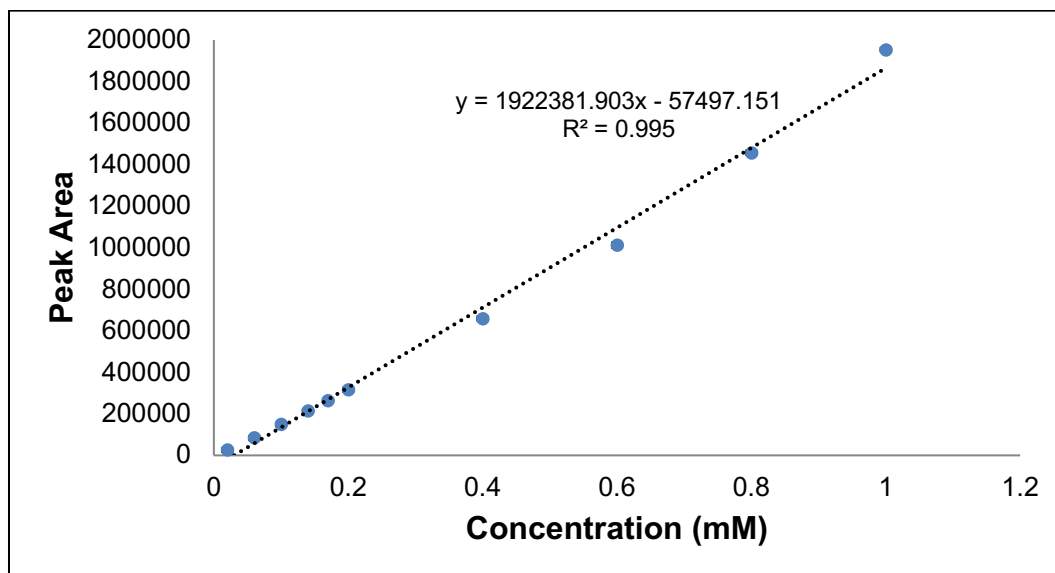


Figure C.1. *p*-Cresidine standard curve at 287 nm.

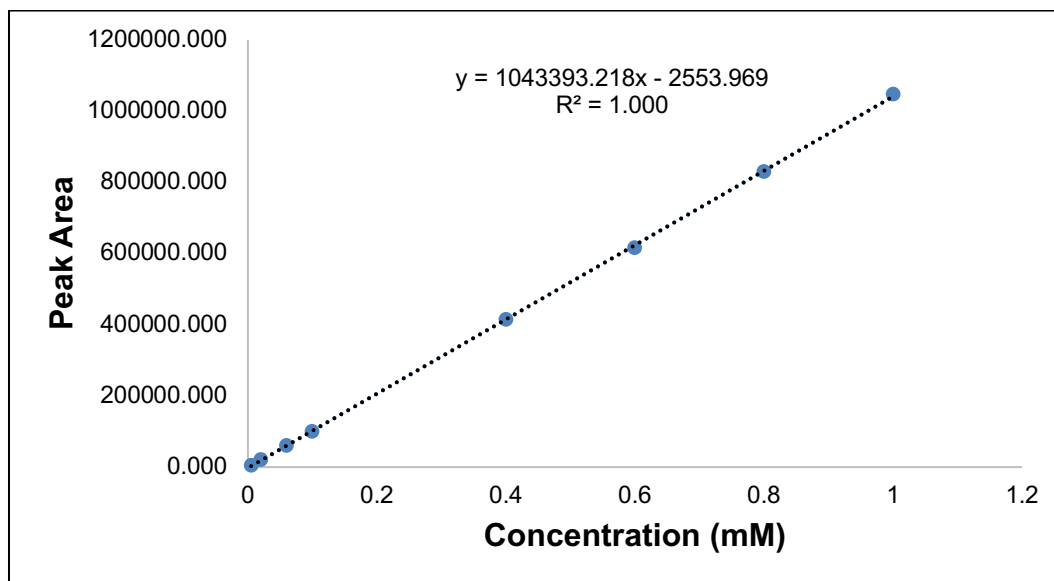


Figure C.2. 4-COT standard curve in pH 2.6 at 290 nm.

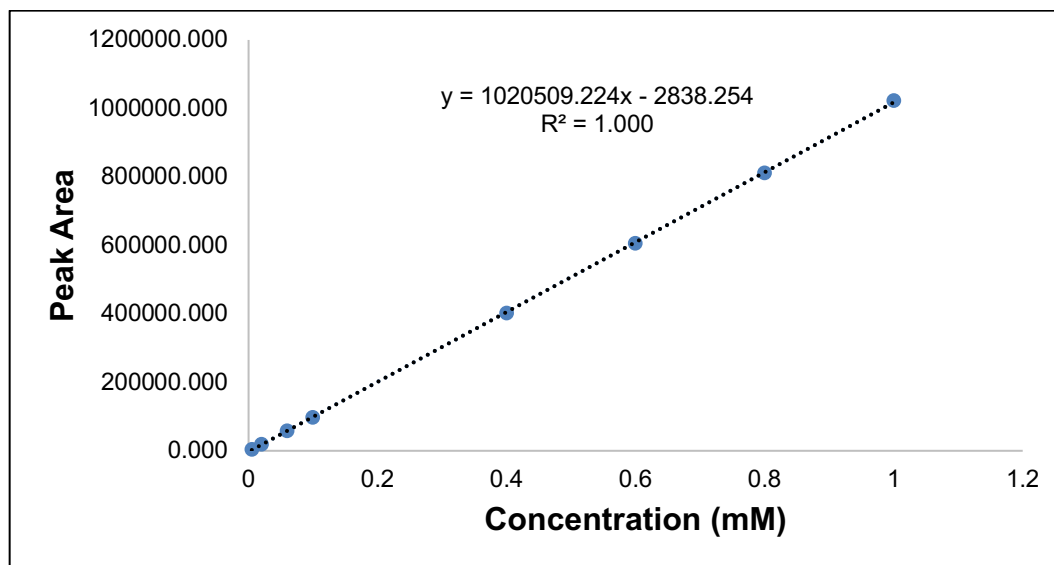


Figure C.3. 4-COT standard curve in pH 3.0 at 290 nm.

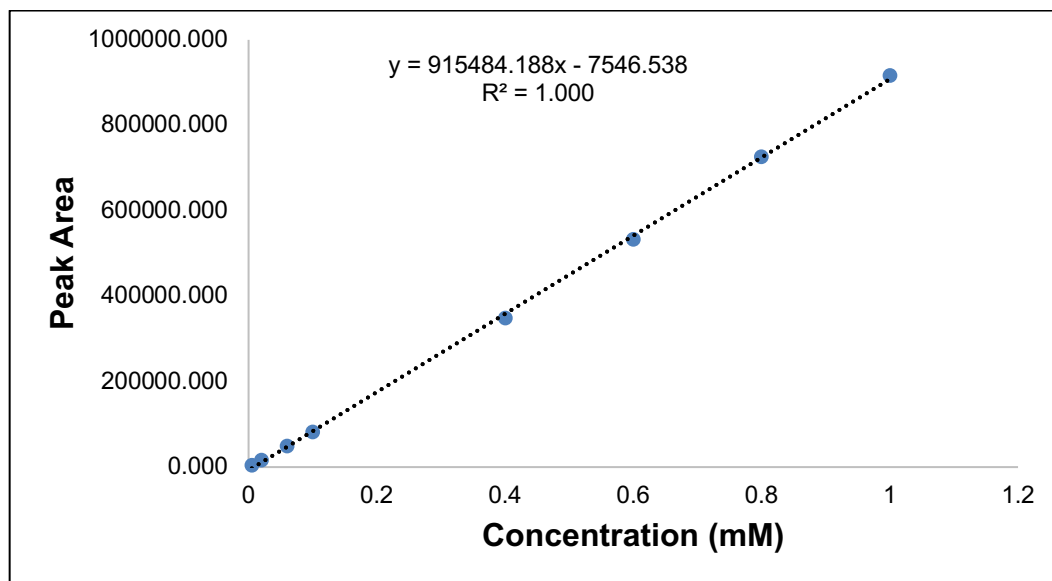


Figure C.4. 4-COT standard curve in pH 4.0 at 290 nm.

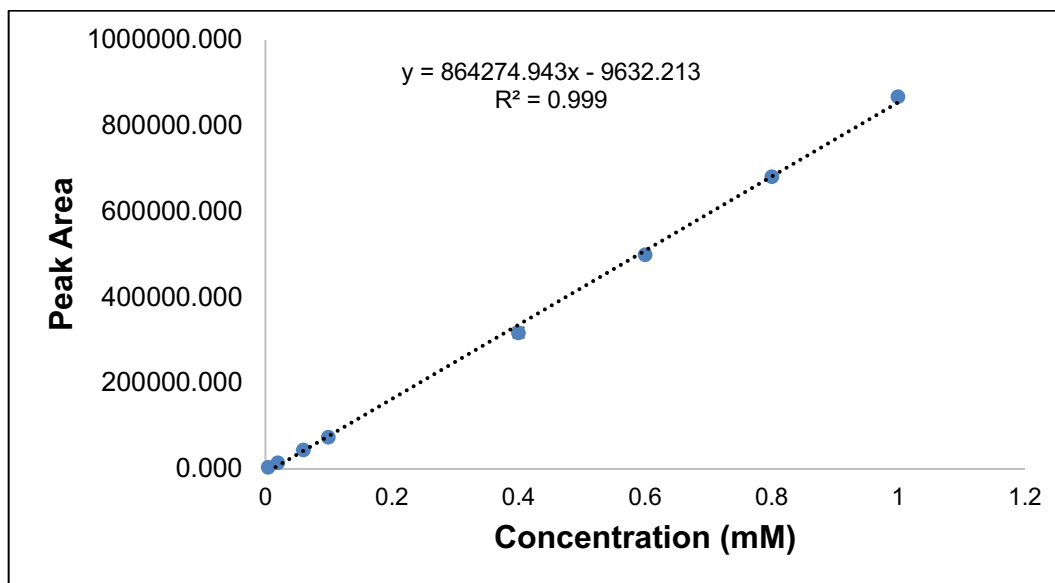


Figure C.5. 4-COT standard curve in pH 5.0 at 290 nm.

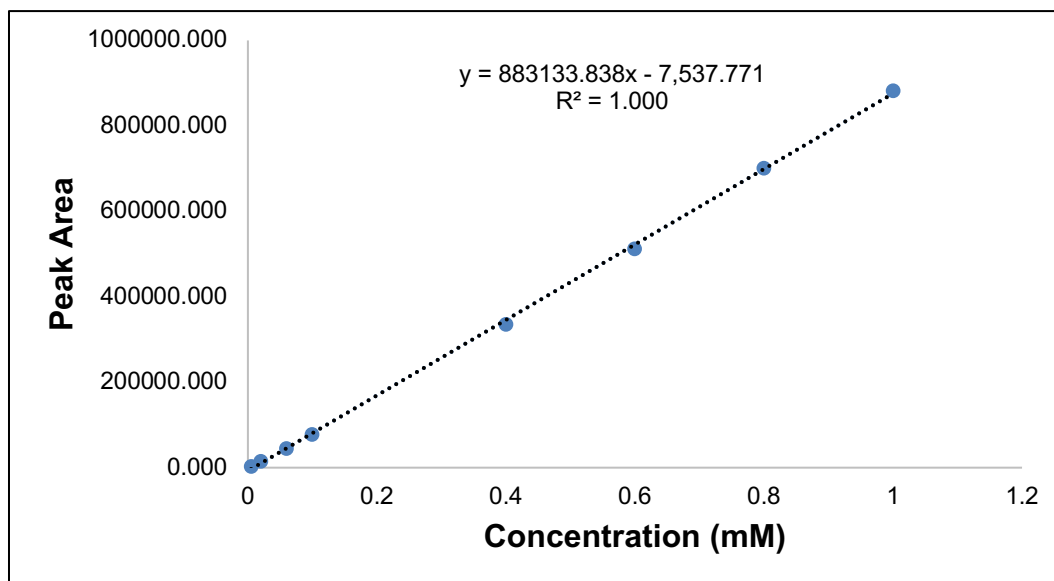


Figure C.6. 4-COT standard curve in pH 7.0 at 290 nm.

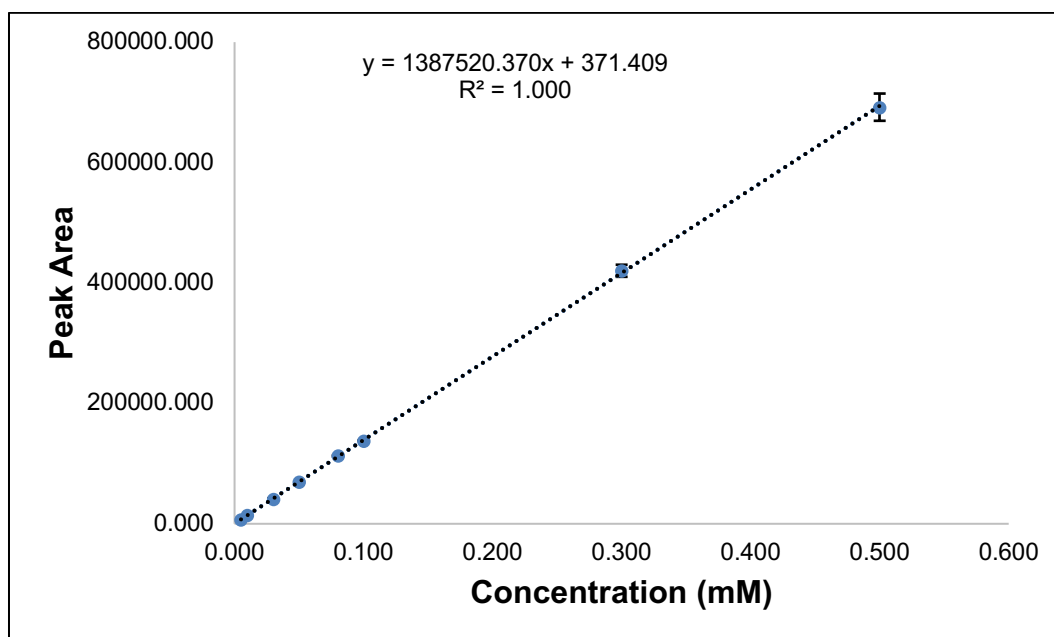


Figure C.7. ODA standard curve in pH 2.6 at 271 nm.

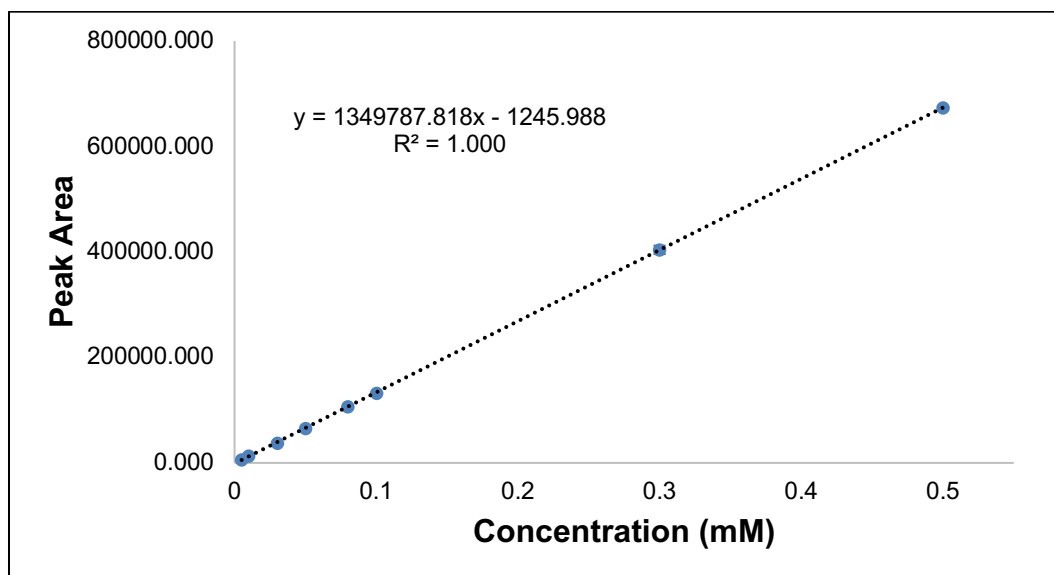


Figure C.8. ODA standard curve in *pH* 4.0 at 271 nm.

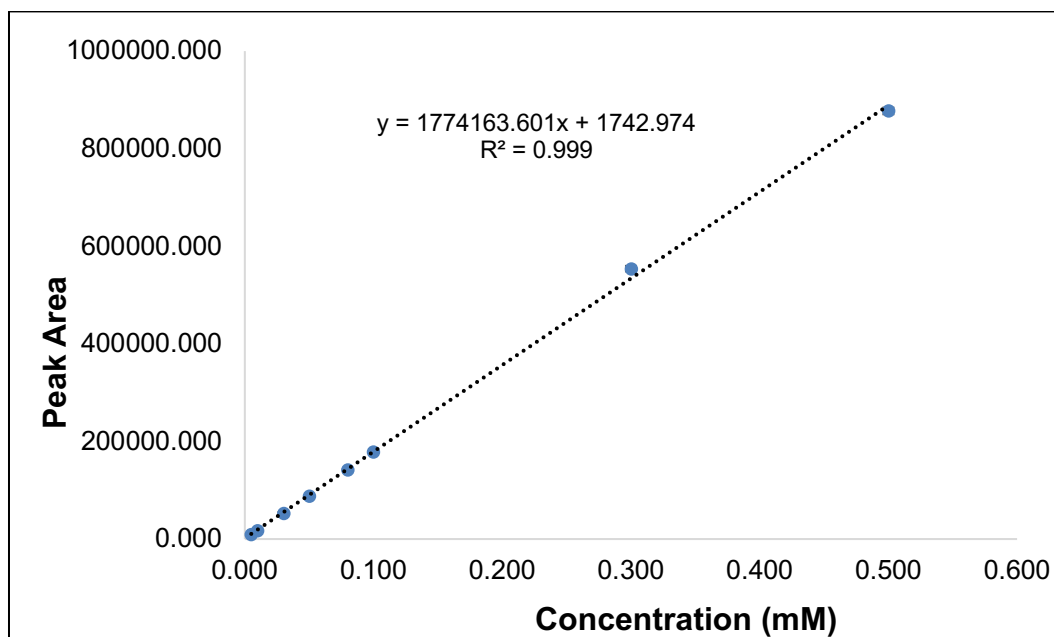


Figure C.9. ODA standard curve in *pH* 7.0 at 293 nm.

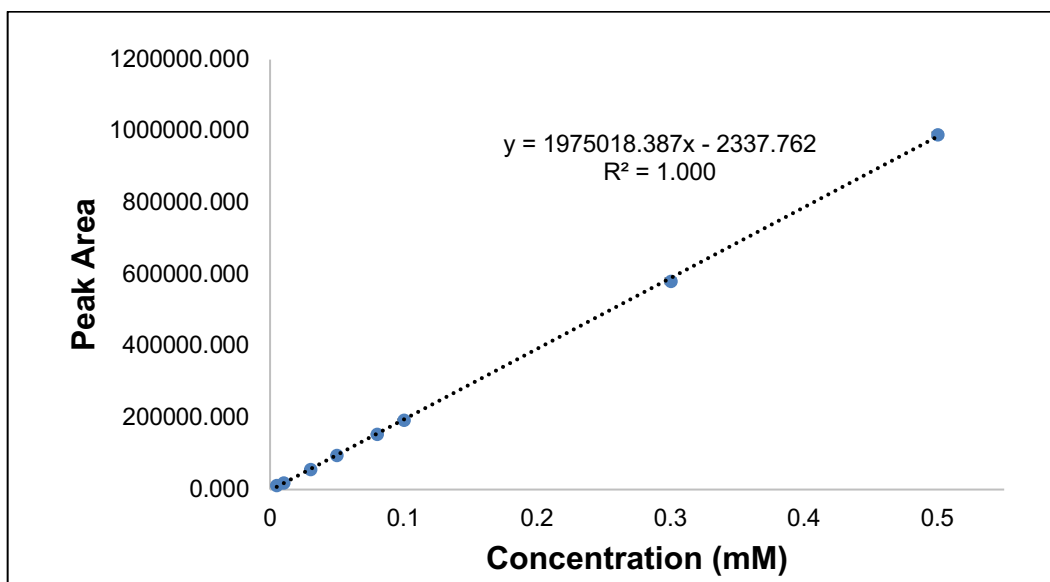


Figure C.10. ODA standard curve in pH 9.2 at 293 nm.

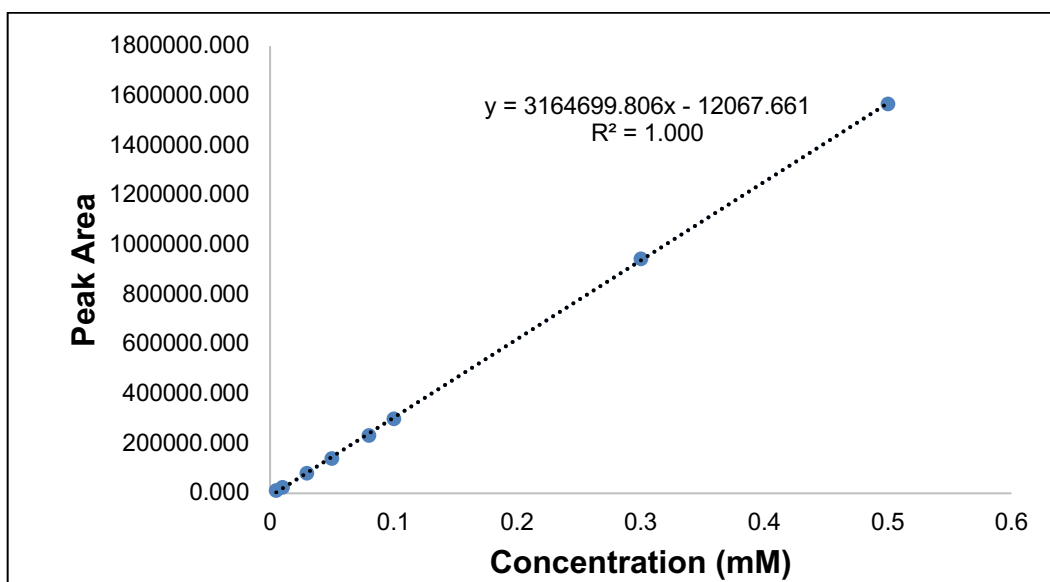


Figure C.11. MDA standard curve in pH 2.6 at 260 nm.

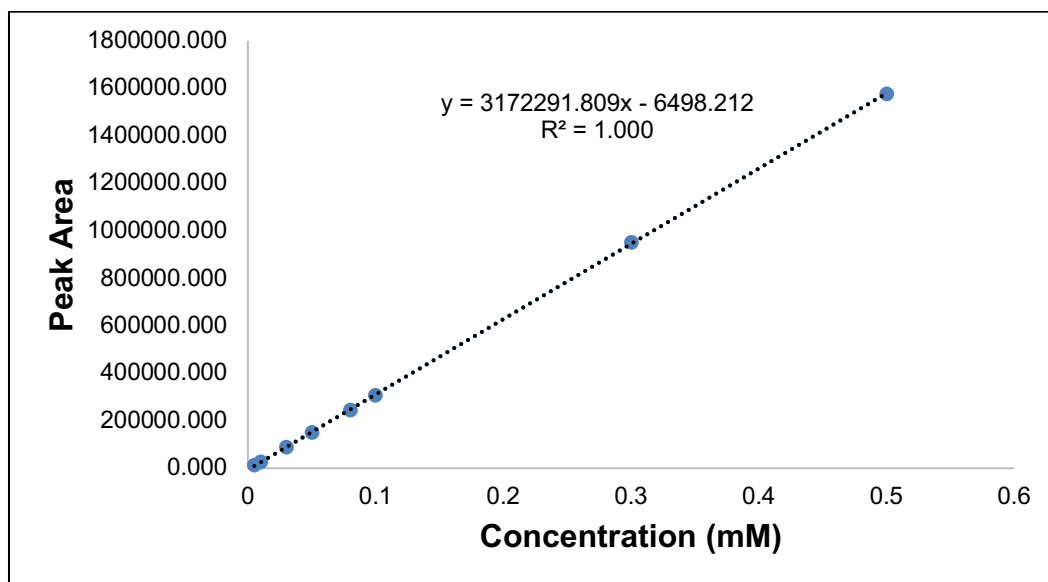


Figure C.12. MDA standard curve in pH 3.0 at 260 nm.

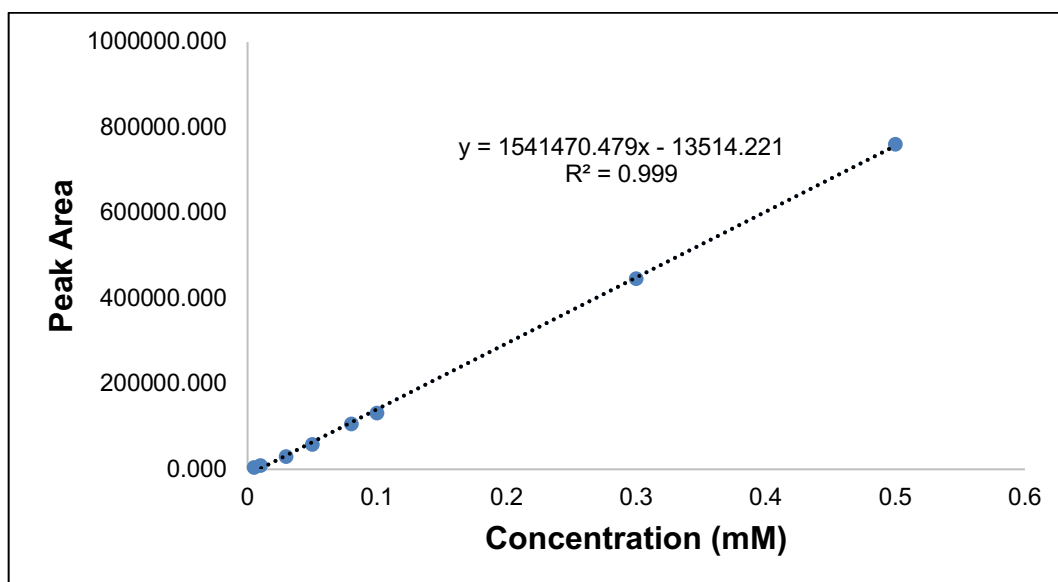


Figure C.13. MDA standard curve in pH 4.0 at 285 nm.

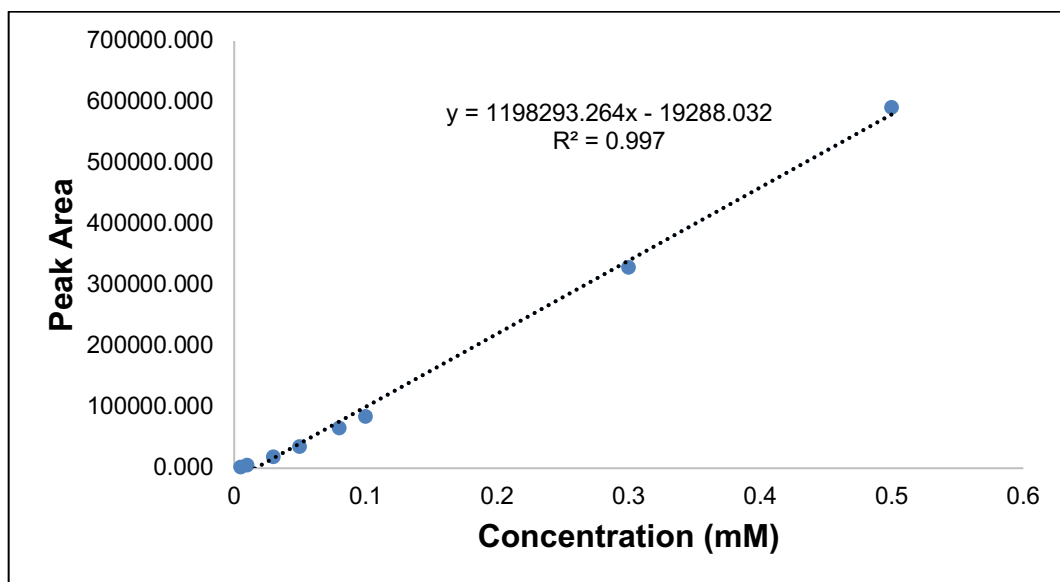


Figure C.14. MDA standard curve in pH 5.0 at 285 nm.

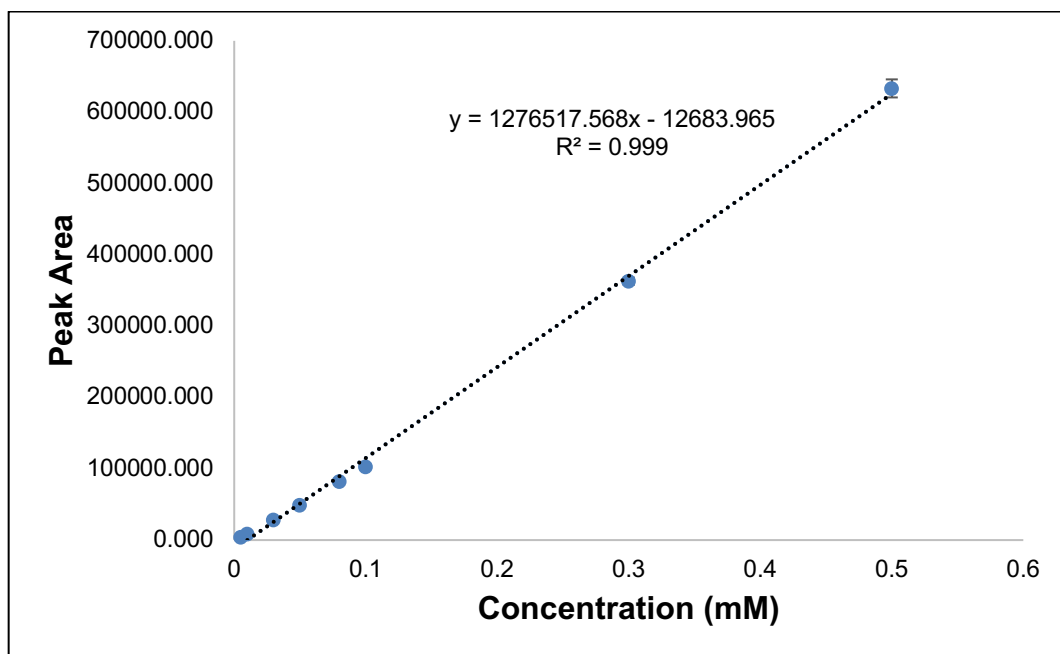


Figure C.15. MDA standard curve in pH 7.0 at 285 nm.

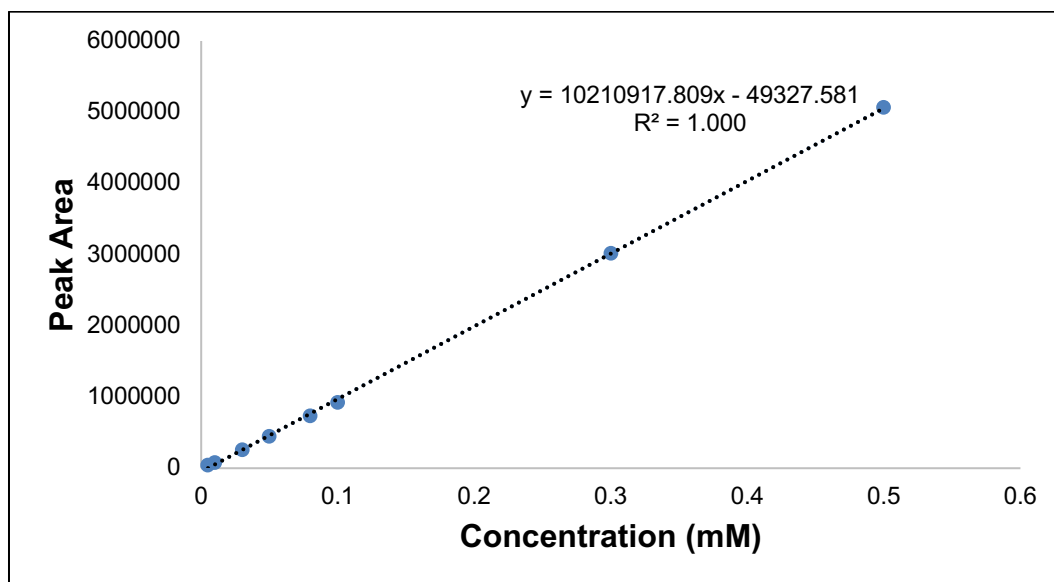


Figure C.16. TDA standard curve in pH 3.0 at 253 nm.

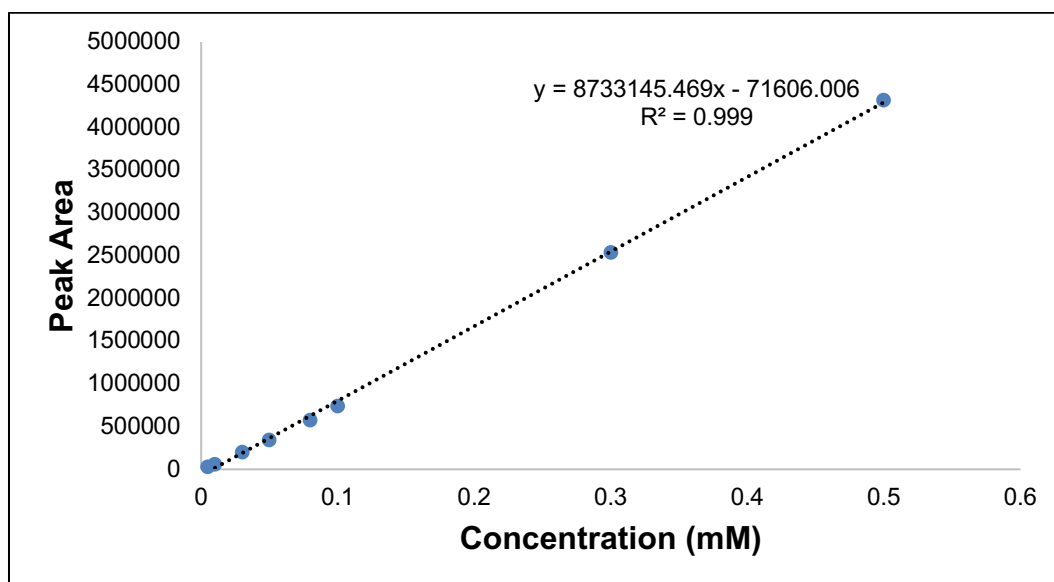


Figure C.17. TDA standard curve in pH 7.0 at 260 nm.

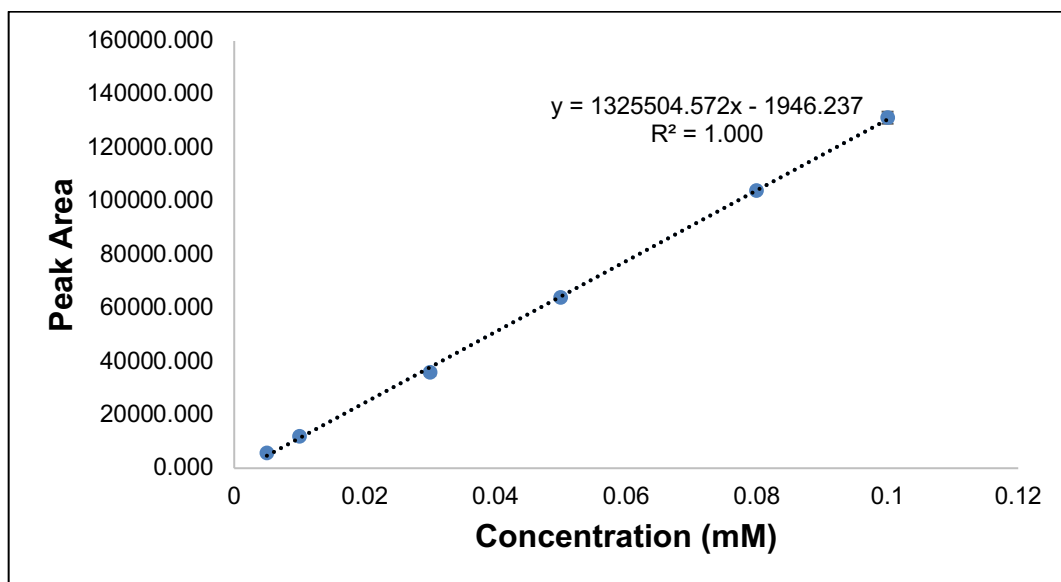


Figure C.18. MOCA standard curve in pH 2.6 at 291 nm.

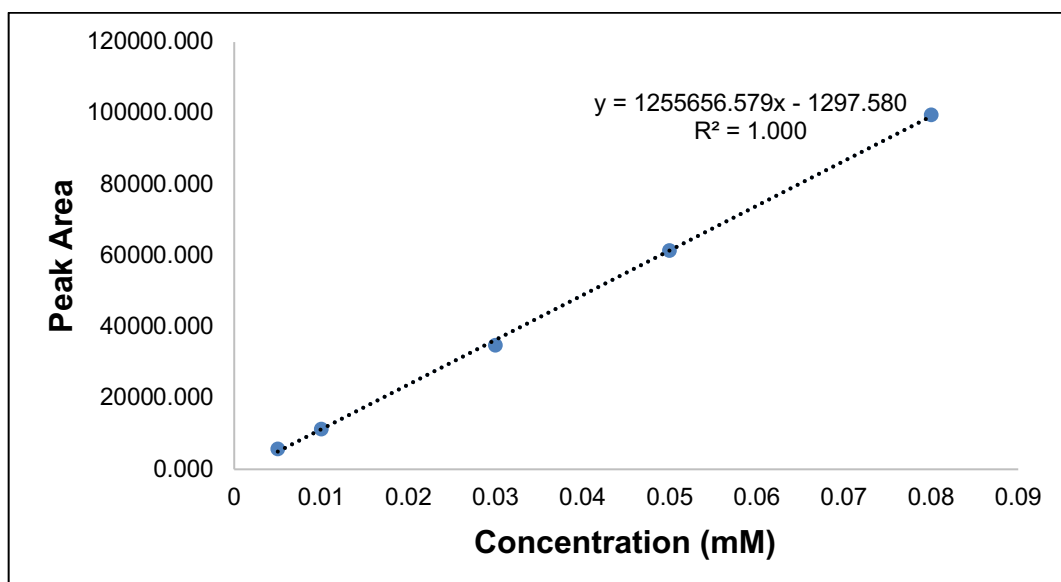


Figure C.19. MOCA standard curve in pH 3.0 at 291 nm.

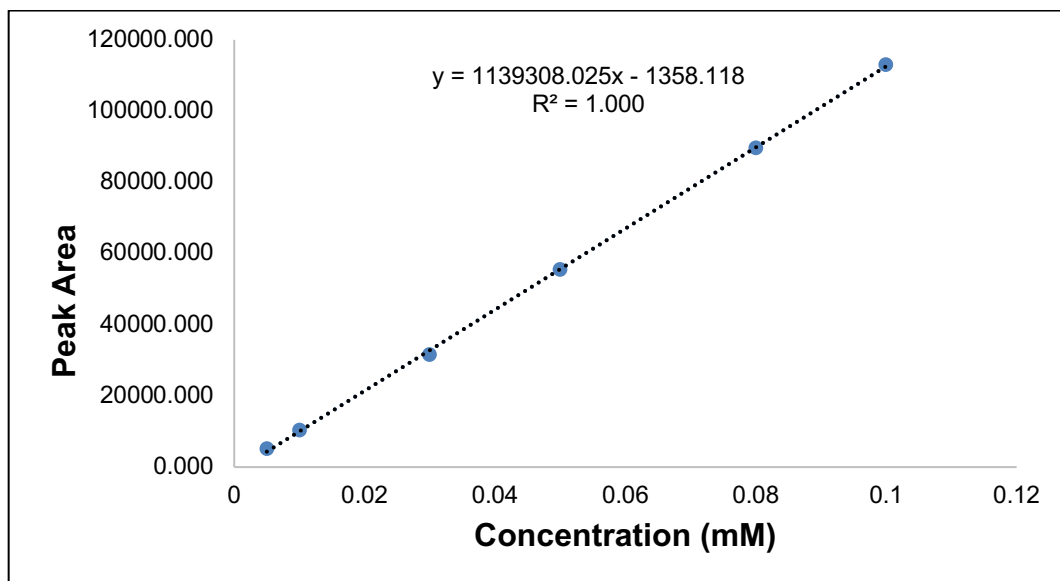


Figure C.20. MOCA standard curve in *pH* 7.0 at 291 nm.

Appendix D: Preparation of SBP and Catalase Stock Solutions

Preparation of SBP stock solution:

The preparation of stock SBP solution is summarized as follows:

1. The crude dry solid SBP, stored at -15°C, was allowed to warm at room temperature approximately 15 min. prior to use.
2. 1.4 g of solid powder of crude SBP was measured and dissolved in 100 mL distilled water. The solution was stirred gently using a magnetic stirrer bars on a stirrer plate for overnight. Vigorous stirring should be avoided to not lose any enzyme activity.
3. The enzyme solution was then centrifuged at 4000-4500 rpm for 20-25 minutes.
4. The supernatant was stored at a temperature of 4°C for future use.

Preparation of catalase stock solution:

1. The dry solid bovine liver catalase stored at -15°C was allowed to warm at room temperature prior to use.
2. 0.5 g of the solid powder was measured and dissolved in 100 mL distilled water.
3. The solution was stirred for at least 3 hours on a magnetic stirrer plate and stored at 4°C for future use.

VITA AUCTORIS

NAME: Debjani Mukherjee

PLACE OF BIRTH: Asansol, West Bengal, India

YEAR OF BIRTH: 1987

EDUCATION: Bharath University, Department of Industrial Biotechnology, B.Tech., India, 2009

Bharath University, Department of Industrial Biotechnology, M.Tech., India, 2011

University of Windsor, Department of Civil and Environmental Engineering, Ph.D., Windsor, ON, 2019

SCHOLARSHIPS: Ontario Graduate Scholarship (OGS), 2016-2019

Sustainable Engineering Faculty Scholarship (Doctoral), 2015-2017

University of Windsor Doctoral (Entrance) Scholarship, 2015

WORK EXPERIENCE:

1. Research and Graduate Assistant, University of Windsor, ON, Canada (2015-2019).
2. Assistant Professor, Lovely Professional University, Punjab, India (2011-2015).

PUBLICATIONS:

1. Mukherjee D., Bhattacharya, S., Taylor K.E., Biswas N. (2019). Enzymatic treatment for removal of hazardous aqueous arylamines, 4,4'-methylenedianiline and 4,4'-thiodianiline. Submitted for publication.
2. Mukherjee D., Taylor K.E., Biswas N. (2018). Soybean Peroxidase-Induced Treatment of Dye-Derived Arylamines in Water. *Water, Air and Soil Pollution*. 229:283-1-13.
3. Cordova Villegas, L.G., Mashhadi, N., Chen, M., Mukherjee D., Taylor K.E., Biswas N. (2016). A Short Review of Techniques for Phenol Removal from Wastewater. *Current Pollution Reports*. 2:157-167.

CONFERENCE PROCEEDINGS:

1. Mukherjee, D., Zhang, X., Taylor, K.E., Biswas, N. (2019). Eco-friendly strategies for treatment of aromatic amines in wastewater: An enzymatic approach. Proceedings for 2019 Water Environment Association of Ontario (WEAO) Technical Symposium. Accepted for publication.
2. Zhang, X., Mukherjee, D., Taylor, K.E., Biswas, N. (2019). Soybean peroxidase (SBP) removal of benzonitrile pesticides. Proceedings for 2019 Water Environment Association of Ontario (WEAO) Technical Symposium. Accepted for publication.
3. Mukherjee D., Cordova Villegas, L.G., Taylor K.E., Biswas N. (2018). An overview of enzymatic treatment of hazardous pollutants in industrial wastewater using soybean peroxidase. Proceedings for Canadian Society for Civil Engineering (CSCE) 2018 Annual Conference. Pages GC128-1-8.
4. Cordova Villegas, L.G., Mukherjee D., Taylor K.E., Biswas N. (2018). Enzymatic treatment with soybean peroxidase of an azo-dye, Direct Black 38, and an azo-dye

- precursor, 4-chloro-*o*-toluidine. Proceedings for Canadian Society for Civil Engineering (CSCE) 2018 Annual Conference. Pages GC127-1-6.
5. Mukherjee D., Taylor K.E., Biswas N. (2018). Sustainable Treatment of a Toxic Aryl-Amine Pollutant, 4,4'-methylenebis(2-chloroaniline), in Water using an Enzyme. Proceedings for 2018 Water Environment Association of Ontario (WEAO) Technical Symposium. Pages 1-8.

CONFERENCE PRESENTATIONS:

1. Mukherjee, D., Cordova Villegas, L.G., Taylor, K.E., Biswas, N. An overview of enzymatic treatment of hazardous pollutants in industrial wastewater using soybean peroxidase. Canadian Society for Civil Engineering (CSCE) 2018 Annual Conference (June 13th-16th), Fredericton, NB, Canada. 15th June 2018. #GC128.
2. Cordova Villegas, L.G., Mukherjee, D., Taylor, K.E., Biswas, N. Enzymatic treatment with soybean peroxidase of an azo-dye, Direct Black 38, and an azo-dye precursor, 4-chloro-*o*-toluidine. Canadian Society for Civil Engineering (CSCE) 2018 Annual Conference (June 13th-16th), Fredericton, NB, Canada. 15th June 2018. #GC127.
3. Mukherjee, D., Taylor, K.E., Biswas, N. Identification of Polymeric Products of a Toxic Arylamine Water Pollutant by Electrospray Ionization Mass Spectrometry (ESI-MS). 101st Canadian Chemistry Conference and Exhibition (May 27th-31st), Edmonton, AB, Canada. 28th May 2018. Abstract ID: CSC181365.
4. Mukherjee, D., Taylor, K.E., Biswas, N. Sustainable Treatment of a Toxic Aryl-Amine Pollutant, 4,4'-methylenebis(2-chloroaniline), in Water using an Enzyme. 2018 Water Environment Association of Ontario (WEAO) Technical Symposium and OPCEA Exhibition (April 15th-17th), London, ON, Canada. 17th April 2018. Control Number 2018-045.

5. Mukherjee, D., Taylor, K.E., Biswas, N. Sustainable Treatment of Toxic 4,4'-thiodianiline in Water using an Enzyme. 255th ACS National Meeting (March 18th - 22nd), New Orleans, LA, USA. 21st March 2018. Paper number ENVR 389.
6. Mukherjee, D., Taylor, K.E., Biswas, N. Treatment of *p*-Cresidine by Soybean Peroxidase-catalysed Oxidative Polymerization in Wastewater. 100th Canadian Chemistry Conference and Exhibition (May 28th -June 1st), Toronto, ON, Canada. 31st May 2017. #02153.
7. Mukherjee, D., Taylor, K.E., Biswas, N. Enzyme-based Treatment of Industrial Wastewater for a Sustainable Environment. World Water Day, University of Windsor, ON, Canada. 22nd March 2017.